A multisystemic approach to investigate the role of polystyrene nanoparticles in neurodegeneration

Inaugural-Dissertation

zur Erlangung des Doktorgrades
der Mathematisch-Naturwissenschaftlichen Fakultät
der Heinrich-Heine-Universität Düsseldorf

vorgelegt von

Laura Schröter
aus Lippstadt

Düsseldorf, August 2023

aus dem Institut für
der Heinrich-Heine-Universität Düsseldorf

Gedruckt mit der Genehmigung der
Mathematisch-Naturwissenschaftlichen Fakultät der
Heinrich-Heine-Universität Düsseldorf

Berichterstatter:

1. Priv. Doz. Dr. Natascia Ventura

2. Prof. Dr. Christine R. Rose

Tag der mündlichen Prüfung: 20. November 2023

Abstract

Over the past 50 years, the exposure to plastic nanoparticles has witnessed a significant increase, with mounting evidence suggesting their absorption by living organisms, their ability to cross the blood-brain barrier and their possible accumulation in the brain. However, a comprehensive understanding of the impact of plastic nanoparticles on organisms, particularly on the nervous system, remains limited.

In my PhD work, I used a multisystemic approach to study the effects of polystyrene nanoparticles (PS and PS-NH_2) in different organisms of particular relevance to neurons under coherent and comparable conditions. First of all, I characterized the particles in terms of their physicochemical characteristics over time and in different exposure media. Subsequently, I investigated the effect of the particles *in vitro* under acute exposure conditions using cytotoxicity measurements in the HEK293 APP695 and SH-SY5Y cell lines, specifically addressing endpoints related to Alzheimer's Disease. In addition, I used differentiated SH-SY5Y cells to mimic a more chronic exposure scenario and to identify the role of PS and PS-NH_2 on further neuronal related readouts. Finally, I analyzed the effect of the particles *in vivo* on the nematode *Caenorhabditis elegans (C. elegans).*

My *in vitro* results demonstrated a particle-, concentration- and time-dependent cytotoxicity, as well as a disruption of mitochondrial membrane potential and apoptotic/necrotic cell death specifically for PS-NH_2. Additionally, I observed a PS-NH_2 dependent increase in the secretion of Amyloid β 1 – 42. Compared to undifferentiated cells, differentiated SH-SY5Y cells not only showed a more sensitive response to PS-NH_2 in terms of cytotoxicity, but also an impaired differentiation along with an altered expression of neuronal marker proteins. Furthermore, the concentration-dependent toxicity of PS-NH_2 was confirmed *in vivo* in *C. elegans*. This was shown by a delayed development, a shortened lifespan, and a slowed movement of the animals. Moreover, PS-NH_2 caused damage to mitochondrial membrane potential in *C. elegans* without an increased production in reactive oxygen species, which is comparable to *in vitro* results. Finally, compared to wild-type animals, a more impaired development was detected in Amyloid β 1 - 42 expressing worms, with synaptic functionality equally affected by PS-NH_2 in both models.

In summary, my work demonstrated a concentration and time dependent toxicity specifically for PS-NH_2, as well as impairment on a neuronal level in different model systems.

Zusammenfassung

In den letzten 50 Jahren hat die Exposition gegenüber Nanopartikeln aus Plastik in unserer Umwelt erheblich zugenommen. Es gibt immer mehr Hinweise darauf, dass die Nanopartikel von lebenden Organismen aufgenommen werden, die Blut-Hirn-Schranke überwinden können und sich möglicherweise im Gehirn anreichern. Die Auswirkungen von Nanopartikeln aus Plastik auf die Organismen, insbesondere auf das Nervensystem, sind jedoch noch nicht vollständig aufgeklärt.

Im Rahmen meiner Doktorarbeit habe ich einen multisystemischen Ansatz verwendet, um die Auswirkungen von Nanopartikeln aus Polystyrene (PS und PS-NH_2) in verschiedenen Organismen und mit neuronalem Bezug unter kohärenten und vergleichbaren Bedingungen zu untersuchen. Zu Beginn der Arbeit wurden die verwendeten Partikel in Bezug auf ihre physikalischen und chemischen Eigenschaften, über einen bestimmten Zeitraum und in unterschiedlichen Expositionsmedien charakterisiert. Im Anschluss habe ich den Effekt der Partikel *in vitro* unter akuten Expositionsbedingungen anhand von Zytotoxizitätsmessungen in den Zelllinien HEK293 APP695 und SH-SY5Y untersucht, wobei insbesondere Endpunkte im Zusammenhang mit der Alzheimer-Krankheit adressiert wurden. Darüber hinaus wurden differenzierte SH-SY5Y Zellen verwendet, um die Wirkung der Partikel über einen längeren Zeitraum und auf weitere neuronale Parameter, wie die neuronale Differenzierung, zu untersuchen. Schließlich wurde der Einfluss der Partikel *in vivo* auf den Fadenwurm *Caenorhabditis elegans (C. elegans*) untersucht.

Meine *in vitro* Ergebnisse haben eine Partikel-, konzentrations-, und zeitabhängige Zytotoxizität sowie eine Störung des mitochondrialen Membranpotentials und einen apoptotisch/nekrotisch bedingten Zelltod speziell für PS-NH_2 gezeigt. Darüber hinaus wurde eine PS-NH_2 abhängige erhöhte Sekretion des potentiell neurotoxischen Amyloids β 1 – 42 gemessen. Im Vergleich zu undifferenzierten Zellen zeigten die differenzierten SH-SY5Y-Zellen nicht nur eine empfindlichere Reaktion auf PS-NH_2 in Bezug auf die Toxizität, sondern auch eine gestörte Differenzierung an sich und eine veränderte Expression von neuronalen Markerproteinen. Weiterhin wurde *in vivo* in dem Modellorganismus *C. elegans* ebenfalls eine konzentrationsabhängige Toxizität für PS-NH_2 verzeichnet. Dies konnte anhand einer verminderten Entwicklung, einer verkürzten Lebensspanne und einer verlangsamten Bewegung der Tiere gemessen werden. Darüber hinaus konnte gezeigt werden, dass PS-NH_2 in *C. elegans* zu einer Schädigung des mitochondrialen Membranpotentials führt, ohne dass die Produktion von reaktiven

Sauerstoffspezies steigt, was mit den *in vitro* Ergebnissen vergleichbar ist. Abschließend konnte, im Vergleich zu Wildtyp Tieren, eine stärker beeinträchtigte Entwicklung in Amyloid β 1 – 42 exprimierenden Würmern gezeigt werden, wobei die synaptische Funktionalität in beiden Modellen gleichermaßen durch PS-NH_2 beeinträchtigt wurde.

Zusammenfassend zeigten meine Ergebnisse in den unterschiedlichen Modellsystemen eine konzentrations- und zeitspezifische Toxizität, sowie eine Beeinträchtigung auf neuronaler Ebene, für PS-NH_2.

.

Table of Contents

List of figures

List of tables

Abbreviations and symbols

AChE	acetylcholinesterase
AD	Alzheimer's Disease
AICD	APP Intracellular Domain
AMA	antimycin A
AMP	adenosine monophosphate
APL	Amyloid Precursor Like protein
APP	Amyloid Precursor Protein
APS	ammonium persulfate
ATP	adenosine triphosphate
ATRA	all-trans retinoic acid
Aβ	Amyloid beta
BBB	blood-brain barrier
BCA	bicinchoninic acid
BDNF	brain derived neurotrophic factor
BGM	Basic Growth Medim
BSA	bovine serum albumin
CAT	catalase
CNS	central nervous system
CO_2	carbon dioxide
CTF	c-terminal fragment
ctrl	control
DAPI	4',6-diamidino-2-phenylindole
DLS	Dynamic Light Scattering
DM	Differentiation Medium
DMEM	dulbecco's modified eagle medium
DMSO	dimethyl sulfoxide
DPBS	dulbecco's modified Phosphate Buffered Saline
DTT	dl-dithiothreitol

ECL	enhanced chemiluminescence
ECM	extracellular Matrix
ELISA	Enzyme-Linked Immunosorbent Assay
EtOH	ethanol
FACS	Fluorescence-Activated Cell Sorting
FBS	fetal bovine serum
FCS	fetal calf serum
FSC	forward scatter
FTIR	Fourier-Transform Infrared Spectroscopy
FUDR	5-fluoro-2-deoxyuridine
GAPDH	glyceraldehyde 3-phosphate dehydrogenase
GPx	gluthatione Peroxidase
H_2DCF-DA	2´,7´-dichlorofluorescin diacetate
H_2O	water
HCl	hydrochloric acid
He	helium
hsp	heat shock protein
IF	immunofluorescence
IL	interleukin
L	liter
LB	Luria Bertani Medium
LDH	lactate dehydrogenase
M	molar
m	milli
mAD	muscle specific Alzheimer's Disease model
MetOH	methanol
MLS	Multiple Light Scattering
MMP	mitochondrial membrane potential
MNPs	micro- and nanoparticles
MP	microparticles

mt	mitochondrial
n	number of replicates
N	number of experiments
N2	Wild Type nematodes
NAC	N-acetyl cysteine
nAD	neuron specific Alzheimer's Disease model
NAFTA	North American Free Trade Agreement
Ne	neon
NGM	Nematode Growth Medium
NLGN	neuroligin
NP	nanoparticles
NSE	neuron specific enolase
OD	optical density
ON	over night
p	probability
PBS	phosphate buffered saline
PCR	Polymerase Chain Reaction
PD	Parkinson's Disease
PDI	Poly Dispersity Index
PE	phycoerythrin (in results)
PE	polyethylene (in introduction)
PET	polyethylene terephthalate
PI	propidium iodide
PP	polypropylene
PS	polystyrene
PS-NH_2	amine modified polystyrene
PS-YG	yellow-green fluorescent polystyrene
PTFE	polytetrafluorethylene
PVC	polyvinyl chloride
PVDF	polyvinylidene fluoride

qPCR	quantitative Polymerase Chain Reaction
RIPA	Radio Immuno Precipitation Assay
ROS	reactive oxygen species
RT	room temperature
SD	standard deviation
SDS PAGE	sodium dodecyl sulfate polyacrylamide gel electrophoresis
SEM	standard error of the mean
SSC	side scatter
SYN	synaptophysin
TEM	Transmission Electron Microscopy
TEMED	tetramethylethylene diamine
TMRE	tetramethyl rhodamine ethyl ester
TUB	tubulin
UV	ultra violet
v	volume
W	watt
w	weight
WB	Western Blot
WST-1	Water-Soluble Tetrazolium-1
WT	Wild Type
x g	times gravity (relative centrifugal force)
β	beta
γ	gamma
ζ	zeta

Clarification of the adoption of public texts

Herewith, I would like to point out that in this work both, text and figures from a review previously published in Small and a manuscript of a research article submitted to Small, recently (not yet accepted) have been taken. This is in line with the *"Promotionsordnung der Mathematisch-Naturwissenschaftlichen Fakultät der Heinrich-Heine-Universität Düsseldorf"* dated 15 June 2018 (§ 6 | 3 Promotionsordnung MNF).[1]

The review **"Nanoplastic Toxicity: Insights and Challenges from Experimental Model Systems"** (*Schröter and Ventura, 2022*) was published in *Small (Wiley)* as open access with Creative Commons license (Attribution-NonCommercial 4.0 International (CC BY-NC 4.0)).[2] According to *Wiley* the authors (Laura Schröter and Natascia Ventura) have the right to reuse the full text of the published article as part of a thesis or dissertation.[3]

The chapter 1 (containing the general introduction to the topic), with sections 1.1 to 1.2 and chapter 5.5 (general discussion) were taken from the review (with minor changes where necessary). This transfer is not further marked, in order not to impair the reading flow unnecessarily. Transferred parts in other chapters were marked as usual.

Authors: Laura Schröter, Natascia Ventura

Title: Nanoplastic Toxicity: Insights and Challenges from Experimental Model Systems

Status: Published in Small 2022, Volume 18, Issue 31

DOI: 10.1002/smll.202201680

Equity ratio: During manuscript preparation, investigation (100 %), visualization (100 %) and original draft writing (100 %) were done by Laura Schröter. Conceptualization, funding acquisition, review and editing of writing were done in collaboration with Natascia Ventura.

The manuscript **"A multisystemic approach revealed aminated polystyrene nanoparticles-induced neurotoxicity"** (*Schröter et al., 2023*) was firstly submitted to *Small* in April 2023 and after major revision resubmitted in July 2023. If this work is published, it will be subject to the same licenses as described above. The data to be published in this thesis describes the results obtained during my PhD and therefore are presented in chapter 4. The results shown in chapter 4 are more detailed and complete

as well as with changes in the figures and text where necessary, compared to the manuscript, however some parts may overlap with the manuscript. The following summary of the experimental part, as well as a short role description of the co-authors shall serve to present my own contribution to the manuscript.

Authors: Laura Schröter, Lena Jentsch, Silvia Maglioni, Amanda Muñoz-Juan, Tina Wahle, Annette Limke, Anna von Mikecz, Anna Laromaine and Natascia Ventura

Title: A multisystemic approach revealed aminated polystyrene nanoparticles-induced neurotoxicity

Status: under revision in *Small*

Equity ratio: During manuscript preparation investigation (100 %), visualization (100 %) and original draft writing (100 %) were done by Laura Schröter. Conceptualization, funding acquisition and editing of writing were done in collaboration with Natascia Ventura. All co-authors initially reviewed the manuscript.

Tina Wahle supervised and supported experiments with HEK293 APP cells. Anna von Mikecz supervised and supported experiments done by Annette Limke in *C. elegans*' lifespan experiments. Anna Laromaine supervised and supported physicochemical characterization of particles done by Laura Schröter in collaboration with Amanda Muñoz-Juan. Natascia Ventura supervised and supported experiments with SH-SY5Y cells done by Laura Schröter. Lena Jentsch, replicated experiments in differentiated SH-SY5Y cells during her master thesis under supervision of Laura Schröter.

Moreover, Natascia Ventura supervised and supported experiments in *C. elegans* performed by Laura Schröter and Silvia Maglioni.

Table 1. Detailed description of the own contribution

Experiment	Concept plan	Experimental part	Data processing	Visualization
Particles characterization	Laura Schröter (50 %), Natascia Ventura (25 %), Anna Laromaine (25 %)	Laura Schröter (95 %), Amanda Munoz-Juan (5 %)	Laura Schröter (100 %)	Laura Schröter (100 %)

Experiment	Concept plan	Experimental part	Data processing	Visualization
***in vitro* analysis in HEK293 APP cells**	Laura Schröter (50 %), Natascia Ventura (25 %), Tina Wahle (25 %)	Laura Schröter (100 %)	Laura Schröter (100 %)	Laura Schröter (100 %)
***in vitro* analysis in SH-SY5Y cells**	Laura Schröter (50 %), Natascia Ventura (50 %)	Laura Schröter (100 %)	Laura Schröter (100 %)	Laura Schröter (100 %)
***in vitro* analysis in differentiated SH-SY5Y cells**	Laura Schröter (50 %), Natascia Ventura (50 %)	Laura Schröter (80 %), Lena Jentsch (20 % (performing replicates))	Laura Schröter (100 %)	Laura Schröter (100 %)
***in vivo* analysis in *C. elegans* on solid plates**	Laura Schröter (50 %), Natascia Ventura (50 %)	Laura Schröter (50 %), Magnitude Biosciences (50 %) (performing movement assay on solid plates))	Laura Schröter (100 %)	Laura Schröter (100 %)
***in vivo* analysis in *C. elegans* in liquid**	Laura Schröter (50 %), Natascia Ventura (50 %)	Laura Schröter (70 %), Annette Limke (5 %, performed lifespan experiments in liquid) Silvia Maglioni (25 % (liquid culture and analysis of ROS)	Laura Schröter (75 %), Silvia Maglioni (25 % (analyzed images acquired during ROS and mitochondrial experiments))	Laura Schröter (100 %)

1 Introduction

1.1 Plastic nanoparticles in our environment

The global plastic production in the world increased from 1.7 million tons in 1950 up to 359 million tons in 2018, whereby 17% can be attributed to Europe, 18% to the North American Free Trade Agreement (NAFTA) and 51% to the Asian continent.[4,5] Approximately 40% of the world's plastic is used for packaging and due to the cheap production and favorable chemical characteristics like lightweight and strong in structure, the single use of plastic packaging became a blessing to our „throw-away society".[3,4] Unfortunately, at least in Europe, only a small amount of plastic packaging waste is collected and used for recycling or energy recovery, but there is still landfill and non-collected waste in form of unauthorized dumping and littering.[4] Once the plastic is released into the environment, it accumulates in water, soil and sediments and their high resistance against biodegradation let it exist for more than 100 years.[6,7]

Nonetheless, external forces like UV radiation, thermodynamic changes and the seawater lead to fragmentation of the plastic particles into smaller pieces like plastic micro- and nanoparticles (MNPs) **(Figure 1).**[7,8]

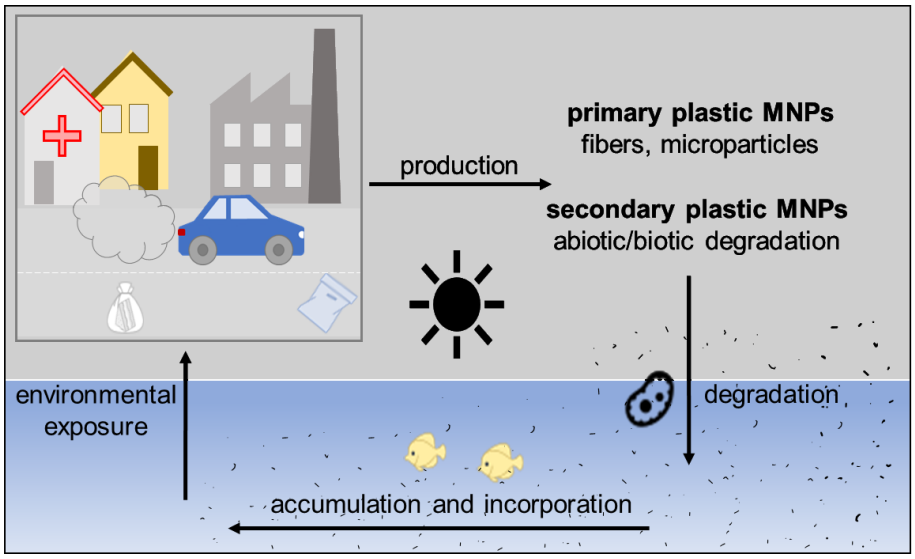

Figure 1. Plastic micro- and nanoparticles (MNPs) in the environment. Formation of primary and secondary MNPs due to industrial manufacturing, degradation of microscopic sized particles and their fate in the environment.

Different types of polymers

In today's world it is impossible to imagine a life without plastic particles. Different types of industrial manufactured plastic particles are major constituents of packaging, foils, medical products like protheses and artificial organs, fibers (e.g. for clothes), furniture, toys, electrochemical components, windows, floorings, office equipment, cables, tubes, pipes, paints, tapes, bottles and much more **(Figure 2)**.[9]

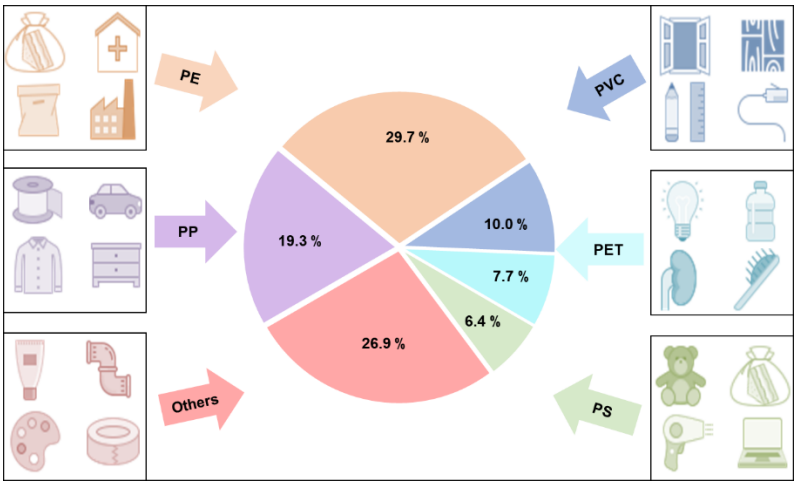

Figure 2. Application and percentual content of the main types of polymers. Polyethylene (PE), polypropylene (PP), polystyrene (PS), polyvinyl chloride (PVC), polyethylene terephthalate (PET).

Single use or abrasion and erosion, followed by abiotic and biotic degradation provide the particles a way into the environment. Particle tracking analysis demonstrated the formation of NPs after 56 days for polystyrene (PS) and morphological changes could be observed for polyethylene (PE) after 8 weeks, when particles have been exposed to artificial sea water.[10,11] So far, plastic MNPs could be detected in terrestrial and maritime environment, including lakes, oceans and also campestral ground like the Antarctica.[12–16] Small organisms like fish, crustacean or nematodes were also shown to accumulate plastic particles after laboratory exposure and developed physiological alterations.[17–19] These organisms can then serve as primary consumers and as the food chain ascends, the content of plastic MNPs can arise and be part of the human diet.[18] Moreover, plastic MNPs have been identified in other food products, the air and even in our drinking water.[20–22]

General aspects of plastic particles

Plastic microparticles (MPs) are defined as plastic particles with a size < 5 mm, whereas plastic particles > 5 mm are classified as meso- and macroparticles.[23] Additionally, the Scientific Committee on Emerging and Newly-Identified Health Risks points out that particles with at least one dimension in a size between 1 and 100 nm are defined as nanoparticles (NPs).[24] Independent from their sizes, the particles can be divided into primary and secondary MNPs.[25] Primary plastic MNPs are manufactured in a microscopic size (microbeads, fibers) to be used, for example, in medical devices or personal care products such as soaps and cosmetics.[25] Instead, secondary plastic MNPs are a result of degradation of larger plastic particles into smaller pieces, which can be detected in several niches of the environment but mainly in oceans.[25,26] According to the World Economic Forum 2016, in the year 2025, for three million tons of fish in the oceans there will be one million tons of plastic and by 2050, we will find more plastic MNPs than fish.[27]

Plastics can be further divided into thermoplastics and thermosets.[28] The plastic resins presented in **Figure 2** are thermoplastics, indicating that their temperature dependent deformation is reversible compared to permanent modifications of thermosets.[28,29] **Figure 2** also shows the percentage distribution of the plastic resin demand in the year 2018. According to this data, PE is the main resin type, followed by polypropylene (PP), polyvinyl chloride (PVC), polyethylene terephthalate (PET), PS and finally other polymers including polytetrafluorethylene (PTFE).[4] In addition to their physical classification, the polymers can be further divided according to their chemical structure .[9,30] Synthetic PE, PS, PP, PET, PVC and PTFE are mainly derived from petroleum hydrocarbons and synthesized by polymerization.[28,31] Some polymers like PE, PP, PS and PVC are characterized by their carbon-carbon backbone, whereas PET has a carbon – oxygen backbone, what is presented in **Table 2**.[30–32] Due to carbons capability to share four electrons with other atoms or even with itself, it enables the building of covalent bonding and therefore the formation of long chains.[32]

Table 2. Overview of structure, modification and backbone characteristics of common plastic resins. PE, PP, PS, PTFE and PVC are grouped by their carbon-carbon backbone and differ due to their different modifications of the side chains. PET possess a carbon-oxygen backbone.[9]

Polymer	Structure	Modification	Backbone
PE (polyethylene)	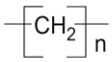		carbon – carbon
PP (polypropylene)	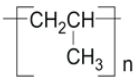	methylated	carbon – carbon
PS (polystyrene)		phenylated	carbon – carbon
PTFE (polytetrafluorethylene)	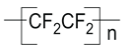	fluorinated	carbon – carbon
PVC (polyvinylcloride)	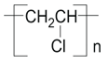	chlorinated	carbon – carbon
PET (polyethylene terephthalate)	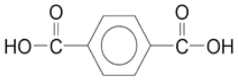	phenylated	carbon – oxygen

PE is the simplest plastic polymer and consists of a long chain of carbon - hydrogen molecule bonding.[9] PP, PS and PVC differ from PE by the addition of a functional group on every other carbon molecule of the backbone chain, whereas PP is methylated, PS is phenylated by adding a benzol ring and PVC is chlorinated.[9] PTFE, better known as Teflon, differentiates from this polymers, because instead of hydrogen, the carbon chain is covalently bounded to flour.[9] In contrast to the carbon-carbon backbone of this five polymers, PETs backbone consist of carbon and oxygen containing functional groups.[9]

Degradation process of plastics

MNPs can differ in their chemical compositions and modifications, their sizes, their physical characteristics and by the incorporation of additives.[33,34] All together, these factors determine their durability and degradation.[8,35] The production of polymers with high durability and stability makes them more resistant to different ways of degradation.[36] The degradation pathways can be divided in biotic and abiotic degradation (**Figure 3**).[37]

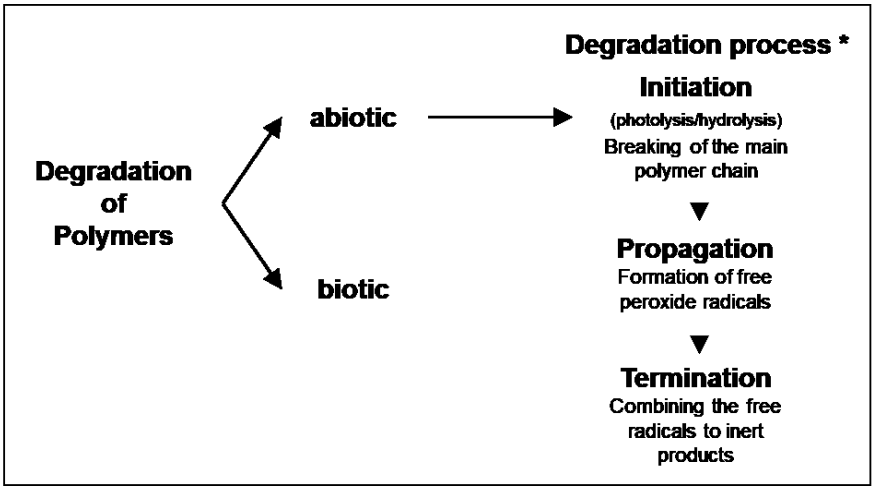

Figure 3. Biotic and abiotic degradation of polymers. Abiotic degradation process of polymers is divided in three steps. Initiation: the main polymer chain is broken by UV radiation (e.g. photolysis) or due to the presence of water (e.g. hydrolysis) and free radicals are formed. Propagation: generation of peroxide radicals due to reaction of radicals and oxygen. Termination: the released radicals are combined together and thereby, inert products occur.[32,37] * only for carbon-carbon backbone polymers.

Biotic biodegradation can be subdivided into aerobic and anaerobic degradation and mainly takes place when the particles are small enough to pass microbial membranes.[37,38] Anaerobic degradation can be found in the absence of oxygen and is characteristic for sediments and landfills, whereas aerobic degradation takes place in the presence of oxygen, for example in the wild nature.[37] The most common forms of abiotic degradation are photodegradation and hydrolysis.[37] Both pathways are based on three steps: initiation, propagation and termination **(Figure 3)**. However, for plastic polymers with a heteroatomic backbone, the degradation is different.[32] As mentioned above, the polymers durability is also dependent on the additives the polymers are treated with and for the case of PE, the stability and durability can be highly increased in this way (e.g. UV absorbers, quenchers).[9,32] In contrast, PP, for example, possesses a lower stability: Due to the fragility of the tertiary carbon, PP is more sensitive to abiotic degradation.[28] Also, PS is prone to abiotic attacks, like UV radiation, while it seems to be the polymer with the highest durability and resistance against biodegradation.[39,40] So far, the highest sensitivity to UV radiation can be found for PVC due to the chlorination.[39,41] Finally, the replacement of a carbon molecule in the main chain of PET leads to an increased thermal stability of the polymer.[42]

1.2 Toxic effects of NPs exposure

Nowadays, we are confronted with plastic NPs every day and the effects on organismal (and especially human) development and health, as well as on the environment, are still largely unknown. Barbosa et al reviewed the exponential growth of studies in the last 10 years investigating the toxicity of plastic NPs: While in 2010 existed more or less 5 publications, in 2019 there were more than 800 papers talking about NPs.[43] This trend continues. Clearly, plastic NPs can have several different biological and/or toxic effects depending on the type and size of the particles as well as the environmental milieu and the affected organism itself.

Figure 4 shows that plastic NPs, once spread in the environment, can enter the organisms by different routes of exposure. Primarily via oral intake, inhalation and dermal exposure, leading to specific effects in the entering tissues and organs.[44]

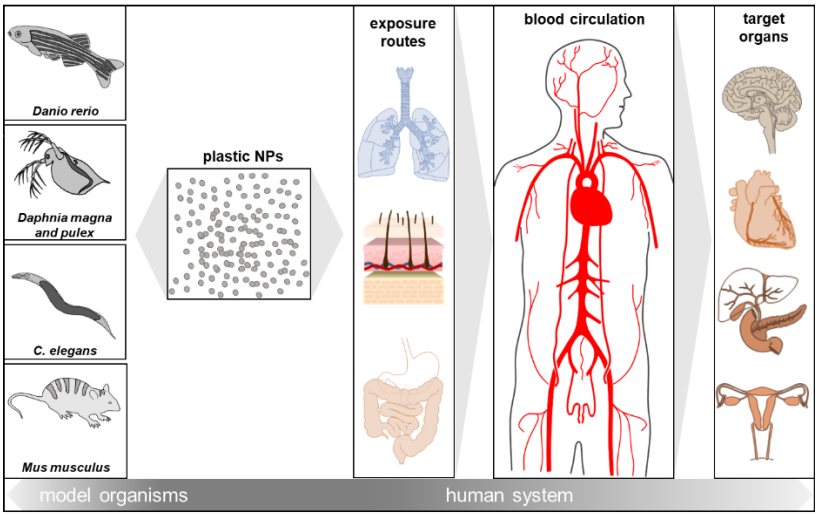

Figure 4. Exposure of plastic NPs to human cells and other organisms. Exposure of plastic NPs takes place by different routes of exposure and by passing biological barriers or entering the blood system. Thereby plastic NPs may be able to reach different target organs like the brain, heart, liver and reproductive organs.

Moreover, different studies investigated the ability of plastic NPs to penetrate biological barriers in order to target additional organs like the brain, liver, heart and even the reproductive system.[17,45–48]

Currently available data on plastic NPs effects on biological systems comes from *in vitro* studies of cellular systems mainly belonging to the gastrointestinal and respiratory tracts, and from *in vivo* studies in model organisms such as aquatic species or the nematode *Caenorhabditis elegans (C. elegans)*. Although a variety of different plastic NPs exist,

due to polystyrene NPs (PS NPs) commercial availability in nanoscale sizes and different modifications as well as their low production costs, most studies have been carried out with PS NPs. Additionally, regarding other plastics like PE and PP, their physical properties make them less usable for toxicity studies on adherent culture cells: Compared to the density of PS (1.04 – 1.06 g/cm³), the density of PE (0.9 – 0.98 g/cm³) and PP (0.84 – 0.91 g/cm³) will let them float on the liquid surface so they will neither distribute homogenous in the media, nor sink to come in contact with the cells.[4,9]

1.2.1 Toxicity induced by PS NPs *in vitro*

Toxicity in cells belonging to the gastro intestinal system

One of the most common route of PS NPs exposure is represented by their direct ingestion through contaminated food sources or indirectly by usage of personal care products like toothpaste.[49,50] Since the stomach and intestines are the first encountered organs, human gastrointestinal cell lines are often used for *in vitro* studies. Once the particles have entered the intestine, the first barrier is given by a layer of viscous mucus, separating the underlying epithelial cells from the lumen.[51,52] To investigate the influence of this protective barrier, Inkielewicz-Stepniak et al. used three different cell lines with a different level of endogenic mucins production. In addition to non-modified PS NPs, they also investigated the effect of carboxylated and aminated PS NPs (~ 60 nm).[52] Experiments with nonmodified, carboxylated and aminated PS NPs could show that independent of the production of mucin, aminated PS NPs decreased cell viability in a concentration dependent manner and more rapidly compared to non-modified and carboxylated particles.[52] These findings are in line with other studies showing that non-modified and carboxylated particles exhibit less cytotoxicity compared to aminated particles.[53,54]

The exposure of aminated PS NPs (44 nm) on human gastric adenocarcinoma cells reduces cell viability, whereas bigger particles (100 nm) increase cell viability.[55] This indicates that the smaller particles are more toxic compared to bigger ones and that these differences might be due to different patterns of internalization.[55] Another study showed that, exposure to 100 nm diameter nonmodified PS NPs does not significantly decrease the general cell viability, but it can inhibit the ATP-binding cassette transporter (ABC transporter) activity and thereby increase arsenic toxicity in Caco-2 after co exposure to arsenic.[56]

In addition to altered cell viability, Forte et al. could show that PS NPs upregulate the expression of pro-inflammation associated genes like IL-6 and IL-8, the latter assumed to be involved in the development of gastric cancer.[55,57]

Toxicity in cells belonging to the respiratory system

The respiratory tract is an additional source of early exposure to PS NPs. Epithelial cells and macrophages build a biological barrier against inhalation of pollutants.[54] Xu et al investigated the effect of nonmodified PS NPs (35 and 70 nm) on human lung adenocarcinoma cells.[58] They found that cell viability is decreased after 24 hours exposure to a concentration of 25 µg mL^{-1} of smaller particles and to a concentration of 160 µg mL_{-1} of bigger particles, again underlying smaller particles are more toxic. The impaired cell viability upon PS NPs exposure was also confirmed by other investigations. A human bronchial epithelial cell line BEAS-2B showed a decreased cell viability after treatment with nonmodified PS NPs in a concentration and time dependent manner.[59,60]

Early investigations from 2008 could also show cell type-dependent effects: a high toxicity for macrophages and human bronchial epithelial cells of aminated PS NPs but not for human cells, mice liver cells or gland cells from rats.[61] In the same study, Xia et al. could show different modalities of cell death for macrophages and bronchial epithelial cells: the former dying through apoptosis, the latter through necrosis.[61]

Toxicity in cells belonging to dermal system and secondary organs

The third primary route of exposure to NPs is the skin. However, there are only a few studies with MPs done on human dermal cell lines. Döge et al. investigated PS particles penetration *ex vivo* across intact human skin barrier by using 20 and 200 nm sized carboxylated PS microspheres for 16 h.[62] The authors could show that the particles mostly remain in the upper part of the stratum corneum, due to the skin barrier function. However, particles could also be identified in deeper sections of the epidermis and particle internalization was proofed with flow cytometry of epidermal cell suspensions.[62] The same particles were used in a previous study, where full-thickness porcine ear skin was used to investigate the transport of particles with confocal laser scanning microscopy after 30 min, 1 h and 2 h.[63] In addition to the results observed from human skin, it was shown that particles accumulate predominantly in follicular regions, with an increased accumulation of 20 nm sized particles compared to 200 nm particles, as well as an increased distribution in a time dependent manner.[63]

Moreover, in addition to cells belonging to organs directly exposed to particles, some investigations were done in cells associated with potential secondary target systems such as the reproductive, neuronal and immune systems.[45,53,64–66] Mouse embryonic cells (NIH 3T3) and human cervix epithelial cells (HeLa) were used to investigate the influence of PS NPs exposure on cell morphology and cell cycle.[64] The results showed that exposure to non-modified, carboxylated or aminated particles affected the interphase and during cell cycle a co-localization between actin microfilaments and the particles could be detected. Time and concentration dependent studies (up to 50 µg mL^{-1}) indicated that carboxylated PS NPs (100 nm) did not influence Hela cells viability but decreased the NIH 3T3 cells viability in a time dependent manner.[64] Instead, after 72 h exposure to aminated PS NPs the highest decrease in cell viability is reached in both cell lines and the increased necrotic cell number and the results of lactate dehydrogenase (LDH) assay indicate that the cellular membrane integrity may be disturbed. Concerning the cell cycle, aminated PS NPs lead to an increased expression of cyclin D, a protein necessary for intact cell cycles, resulting in a prolonged G0/G1 interphase.[64]

Toxicity in cells belonging to the nervous system

Another potential organ targeted by nanoparticles is the brain. However, studies concentrating on how PS NPs may affect the brain and the neuronal system using cell culture models are very limited. PS NPs exposure to glioblastoma cells has no effect on the cell viability but lead to a significant production of ROS when treated for 24 h with 10 µg mL^{-1} of PS particles (40 – 250 nm). [65] Recently, Jung et al. compared the effect of PS NPs (100 nm) in mouse embryonic fibroblasts, in cortical astrocytes and in mixed cells from the embryonic cortex.[67] They observed a reduced cell viability and a defective neuronal viability when the mixed cells were treated for 2 days with unmodified particles (100 – 200 µg mL^{-1}), as well as astrocytosis in astrocytes. However, they found no effect on mouse embryonic fibroblasts, whereby the concentration dependent internalization in these cells was also tested. Similar experiments were done by Murali et al. in 2015, where they compared several mice primary cell lines including neurons, astrocytes and microglial cells while exposed to 45 – 70 nm sized carboxylated PS NPs for 24 h.[68] Internalization studies showed that only microglial cells internalized the particles but neither neurons nor astrocytes do. Interestingly, the authors observed no effect in astrocytes. Additionally, they showed an altered morphology from microglial cells to more macrophage-like type cells due to particle treatment.[68]

1.2.2 Toxicity of PS NPs *in vivo*

In contrast to *in vitro* studies, *in vivo* studies allow the investigation on a whole organism with different tissues and organs. This permits a prolonged particles exposure scenario, exposure at different life-stages (embryonic and post-embryonic development, fertile period, adulthood, senile stage) or even throughout the entire life of the organism, as well as in different genetic backgrounds, thus revealing specific risk groups.[69] Moreover, with chronic exposure of reduced particle concentrations, *in vivo* studies give researchers a better opportunity to mimic the environmental conditions compared to experiments in cell culture systems or other types of 3D systems which can only be treated for a short period of time.[69]

Toxicity in aquatic organisms

Early studies of aquatic organisms pointed out that exposure to PS NPs lead to accumulation of these particles after passing biological barriers and consequently alter organisms behaviors and metabolic activities.[70,71] Clear examples come from studies on the aquatic organism *Danio rerio* (zebrafish). After 5 days exposure of 24 hours post fertilized embryos to PS NPs, particles accumulation in the yolk sac and further migration into the intestines, gallbladder, liver, pancreas, heart and brain could be seen under the microscope.[17] Furthermore, accumulation of PS NPs in the pancreas coincided with decreased glucose levels, increased cortisol secretion and disruption of metabolic homeostasis, which were coupled with disorders in neuronal function leading to altered locomotion activity and exploration behavior.[72–75] Lu et al. also showed the accumulation of PS MPs in fish gill, liver and gut. However, the PS NPs used in the same study were too small for localization purposes.[76] Further accumulation of PS NPs was detected in zebrafish gonads and brain after acute (7 days) and chronic exposure (~7 weeks).[73] Indeed, transportation of PS NPs across the blood-brain barrier (BBB) is a recently discussed topic and Mattsson et al. used hyperspectral microscopy to detect PS NPs in the fishes brain, indicating the transport of PS NPs across the BBB.[18] On the one hand, this helps to understand the development of neuronal toxicity. On the other hand, it supports the hypothesis that nanoparticles are able to cross biological barriers, leading to toxicity in secondary organs, usually protected by biological barriers (e. g. brain, gonads).[18,73] These findings are supported by other studies, who found that PS NPs exposure results in altered neurobehaviors like swimming hypoactivity, decreased locomotion activity, and decreased predator avoidance behavior.[17,72–75]

Chen et al. showed that exposure of zebrafish larvae to non-modified PS NPs increases the activities of catalase (CAT) and glutathione peroxidase (GPx) indicating an increase

in reactive oxygen species (ROS) production, possibly resulting in oxidative stress.[72] The authors hypothesized that oxidative stress via ROS production may lead to damages in the central nervous system (CNS) of zebrafish altering the locomotor activity.[72,77–79] Combined with reduced acetylcholinesterase (AChE) activity, this may lead to altered locomotion activity.[72]

In addition to particle accumulation, neurotoxicity and ROS production, long-term (over 3 weeks) exposure of zebrafish to 2000 µg L^{-1} PS NPs, which is considered as environmental concentration, induced toxic effects like necrosis, infiltration and lipid accumulation in fishes hepatocytes without affecting overall animal mortality.[76] Matsson et al. exposed the organism *Daphnia magna*, a small planktonic crustacea with a lifespan of ~2 months, to aminated particles.[80] In this study, animals died within 13 h after exposure to 75 µg mL^{-1} aminated PS NPs. However, after 24 h exposure to 25 µg mL^{-1} PS NPs all animals were still alive.[18] Chen et al. found that MPs, in contrast to NPs, induce no developmental neurotoxicity in zebrafish larvae. These findings were consistent with results from other studies showing that PS NPs seem to have more toxic effects than PS MPs.[72,73,81] Finally, Mattsson et al. were the first who investigated the ability of PS NPs to be transferred along the food chain. They used *Carassius carassius* (freshwater fish) fed with *Danio rerio* after its exposure to algae treated with PS NPs.[18] The treatment lead to a decreased exploration and feeding behavior of the fishes. This supports the hypothesis, that PS NPs can be transferred along the food chain.[18]

Toxicity in model organism C. elegans

Besides investigation of the PS NPs toxicity on aquatic organism, *C. elegans* has become an important model organism for toxicological studies. Indeed, *C. elegans* small size and transparency, stereotyped behaviors and cell linage, amenability to environmental intervention, in combination with its relatively short life cycle (3-4 days) and lifespan (~ 3 weeks) represents a great model organism for *in vivo* toxicology studies.[82,83] *C. elegans* fed *E. coli* and is primarily cultivated on nematode growth medium solid agar plates but it can also be propagated in defined liquid media supplemented with bacteria. Liquid cultivation facilitates animal exposure to chemicals and materials of different origin and enables internalization not only by ingestion, but also by dermal absorption.

In liquid, 4.5 days exposure, from *C. elegans* larvae to gravid adults, to < 1000 µg L^{-1} PS NPs significantly alter the development of D-type motor neurons.[84,85] Moreover, the increased number of head trashes and body bends of *C. elegans* together with the

significantly decrease of forward movement and increased backward movement upon exposure to concentrations of 100 µg L^{-1} indicate a toxic effect on locomotion.[84,85]

Just as shown in zebrafish, PS NPs can influence lipid metabolism, confirmed by increased expression of two lipid metabolic sensors sbp-1 and transcriptional coregulator mediator-15 (mdt-15) after *C. elegans* was exposed to the particles.[19] In further support of PS NPs neurotoxic effects mdt-15 is also expressed in neurons and mdt-15 mutants are more sensitive to PS NPs-induced decrease in locomotion activity.[19,76,86]

Besides development of neurotoxicity, 4.5 days exposure during development to concentrations higher than 10 µg L^{-1} lead to increased intestinal ROS production and a reduction in brood size, indicating a mitochondrial and reproductive dysfunction.[84] Investigation of particles' localization showed that concentrations above 1 µg L^{-1} facilitate the intestinal permeability and enable the accumulation also in the gonads, which contradicts the findings by Mueller et al. who could detect particles in the intestine but not in the gonads, while reproductive toxicity could be shown as well.[84,87]

Interestingly, Zhao et al. could show that exposure of the parental generation to 100 µg L^{-1} PS NPs, increased ROS production, altered locomotion behavior and also reduced brood size in the F1 generation, not directly confronted with the particles, indicating that PS NPs not only lead to toxicity in the parental generation, but also had transgenerational effects.[84] In addition to an increased ROS production, further mitochondrial toxicity could be revealed via decreased tricarboxylic acid (TCA) cycle intermediate production, resulting in an altered mitochondrial ATP production.[88]

As previously described in *in vitro* studies, autophagy *in vivo* may also be affected by exposure to PS NPs. Concentrations of 10 µg L^{-1} of non-modified PS NPs increase the expression level of lgg-1/GABARAP, lgg-2/LG3, atg-18/WIPI and bec-1/BECN-1, which are associated with autophagy induction, whereby concentrations > 1000 µg L^{-1} suppress their expression. [85,89,90]

Toxicity in mammalian organism

Ethical and moral guidelines limit *in vivo* investigations, especially in mammalian model organisms like mice and rats, however there are some studies pointing out the particles potential for biodistribution and the induction of alterations in a living system. Although early studies are available, they mainly concentrated on the internalization and biodistribution of particles, not on possible toxicity. For instance, in 1990, Jani et al. treated rats daily for 10 days with doses of 125 mg kg^{-1} with 50 nm PS NPs with a gavage and observed a biodistribution by blood into liver, spleen and bone marrow. [91] These

results were confirmed by a similar study from Hillery et al. in 1994.[92] Compared to feeding the rats by gavage, Walczak et al. used an oral exposure scenario to investigate the bioavailability and distribution of different charged PS NPs in rats. They found a higher uptake for negatively charged PS NPs with detectable amounts in kidney, heart, stomach wall and small intestine wall.[93]

Yang et al. examined the permeability of the BBB for PS NPs (20 nm) in rats and several years later, Rafiee et al. investigated the particles effect on behavioral alterations in mice.[94,95] Therefore, the authors treated the mice orally with 1, 3, 6 and 10 mg kg^{-1} of bodyweight per day for 5 weeks with 25 and 50 nm sized PS NPs, however they observed neither an effect on the behavior nor on the bodyweight.

In addition to characterizing, internalization and distribution of the particles, recent studies concentrated on the toxicity in mammals, too. Liang et al. showed that in mice nonmodified PS NPs of 500 and 5000 nm are better internalized when co-exposed with 50 nm sized particles. Moreover, they found that the toxicity of the particles was increased in co-exposure scenarios. [96] The authors conclude that the increased permeability of the intestine and dysfunction of intestinal barriers is based on ROS-mediated epithelial cell apoptosis.

1.3 The role of PS in neurodegenerative diseases

Previously, the effects of PS particles on neuronal readouts *in vitro* and *in vivo* were described, including defects in neuronal viability and alterations in several behavioral assays.[2] Moreover, the particle's ability to cross biological barriers like the BBB and their accumulation in the brain, as described in zebrafish, was recently supported by a publication from Kopatz et al., showing PS particles of 293 nm, but not bigger sized particles, reach the mouse brain 2 h after oral administration.[97] Nonetheless, whether and how exposure to PS NPs concur to the development of neurodegenerative diseases (e.g. Alzheimer's Disease (AD) or Parkinson's Disease (PD)) is still unclear.

Alzheimer's Disease

Although different studies have shown evidence of neuronal alterations and even neuronal toxicity mediated by PS NPs, only a handful of studies have investigated the role of PS NPs in neurodegenerative diseases.

Neurodegenerative diseases present a great challenge our society has to face and the G8 discussed in 2013 that unravelling a therapy against dementia, one of the main

disorder in consequence of neurodegeneration, should be prioritized.[98] Indeed, the neurodegenerative AD is the main cause of dementia with 60 – 80 % and currently there is no curative therapy against.[99,100]

AD was first described in 1906 by Alois Alzheimer, when a 51 years old woman suffered from several symptoms like cognitive disturbance, disorientation and delusions.[101] To date, the diagnostic criteria are regularly revised, most recently in 2018 with the addition of new biomarkers.[101,102] There are two different forms of AD: (1) the genetic autosomal-dominant AD (ADAD), which covers less than 1 % of all AD cases and often manifests in patients younger than 65 years old and (2) the sporadic form (SAD), which is age-related and usually appears after the age of 65.[100]

AD exhibits both structural and functional damage to the nervous system, with the main pathologic characteristics being, on the one hand, extracellular Amyloid β accumulation with subsequent formation of amyloid plaques and, on the other hand, intracellular formation of neurofibrillary tangles due to hyperphosphorylation and accumulation of tau proteins.[100,103,104] While the main cause of AD is controversially discussed, a major theory is the *amyloid cascade hypothesis*.[101]

The *amyloid cascade hypothesis* describes the post-translational processing of a type 1 transmembrane glycoprotein, amyloid precursor protein (APP), as shown in **Figure 5**.[105] In the non-amyloidogenic pathway, APP is processed via α secretase resulting in an extracellular soluble APP (sAPPα) and a 83 amino acids long C-terminal membrane integrated fragment (CTF83).[106] The γ secretase mediated cleavage of CFT83 results in the extracellular P3 peptide and the APP intracellular domain (AICD), which translocates to the nucleus.[107]

In contrast, the amyloidogenic pathway is initiated by β secretase cleavage, defined by processing of a truncated soluble APP (sAPPβ) and a 99 amino acids long C-terminal fragment (CTF99).[108] Subsequent processing by γ secretase produces intracellular C99 as well as extracellular Amyloid β (Aβ).[108] The length of the Aβ peptide is between 37 and 41 amino acids long, however Aβ 1 – 40 and Aβ 1 – 42 are the two main isoforms known to aggregate and form amyloid plaques.[101]

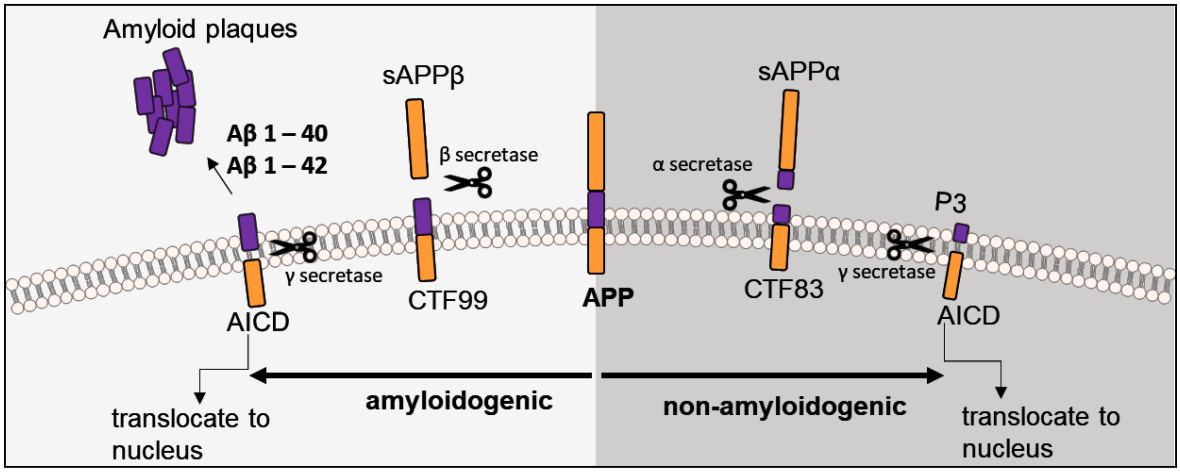

Figure 5. Proteolytic pathway of APP breakdown. Non-amyloidogenic pathway describing the processing of APP via α-secretase resulting in C-terminal fragment CTF83 and soluble sAPP α following γ-secretase mediated breakdown leading to APP intracellular domain (AICD) and extracellular P3 peptide. The amyloidogenic pathway is initiated by β-secretase cleavage of APP into C-terminal fragment CTF99 and sAPPβ and C-terminal fragment CTF99 which is subsequently digested by γ-secretase into AICD and truncated Amyloid β peptides, whereby Aβ 1 – 40 and Aβ 1 – 42 are the two main isoforms known to aggregate and form amyloid plaques.

1.4 Particles and model systems of relevance for my work

1.4.1 Polystyrene nanoparticles (PS NPs)

The evolution of neurodegenerative disorders like AD may be promoted by plastic NPs ability of crossing the BBB and thereby possibly leading to conformational alterations in proteins with subsequent aggregation of misfolded proteins.[109,110] In this context, analytical investigations of Aβ content derived from cerebrospinal fluid samples is altered depending on the material of the reaction tube: While different polymer resins were investigated (e.g. PS, PP and polycarbonate), Aβ peptides exhibited the highest absorption affinity to PS.[111]

In addition, further investigations showed that the polymerization process of Aβ is highly influenced by the presence, and especially the concentration of PS.[112] The authors investigated the kinetic behavior of Aβ 1 – 40 and Aβ 1 – 42 fibrillation while incubated with different concentration of aminated PS NPs (57 nm).[112] They identified two pathways, one describes the fibrillation of free monomers in solution and one the nucleation and further fibrillation at the particles surface, concluding that the general fibrillation rate is mainly dependent on the interplay between both pathways.[112] In particular, 17 and 55 µg mL^{-1} of aminated PS NPs highly promotes the fibrillation of Aβ

1 – 40 by shortening the initial phase of polymerization process (lag phase), resulting in faster polymerization, whereas higher concentrations (>170 µg mL^{-1}) inhibited the fibrillation.[112] A similar trend was observed with Aβ 1 – 42.[112] Finally, a recent study indicates a correlation between PS (6 nm) and a possible stabilizing effect on Aβ oligomers.[109]

In general, PS NPs are not only cheap in production, but they are also commercially available in a wide range of sizes and with several different modifications like coupling to fluorophores or other surface modifications.[2,113–115] Therefore, plain (non-modified) and aminated (amine modified) PS particles are mainly used for the following work.

1.4.2 *In vitro* undifferentiated models

HEK293 APP695

The human embryonic kidney derived cell line was first established in 1977.[116] Due to the adenoviral immortalization, HEK293 cells express several neuronal related proteins.[117] The tumorigenic cell line is characterized by an adherent and clustered growth and their relatively cheap and easy handling, has led to the cells being used for a wide variety of toxicity studies, over the last years, including PS NPs mediated toxicity.[118–120]

The HEK293 cell line used in this work derived from stable transfection with the human wild type APP695 (HEK293 APP695) **(Figure 6)**. As already mentioned, APP plays a major role in the development of AD, hence its processing may lead to the increased formation of neurotoxic of Aβ.[121] The protein itself is transcribed from a single gene, however its post-transcriptional modification leads to many different alternative spliced isoforms of different length: 695, 751 or 770 amino acids long. While APP751 and APP770 are ubiquitiniously expressed in many different cell types, APP695 is only expressed in neuronal cells.[122] Therefore, APP695 overexpressing HEK293 cells can present a great tool to investigate a possible interplay of PS NPs and the development of neurodegeneration and AD on a molecular level. Most notably the amount of cellular production and secretion of APP derived toxic Aβ is often used as an important readout to follow AD pathology.

SH-SY5Y

In addition to HEK293 APP695 cells, the neuroblastoma cell line SH-SY5Y is used. SH-SY5Y is a thrice-cloned subline of the parental cell line SK-N-SH. These cells were derived 1970 from a metastatic bone marrow biopsy of a neuroblastoma developed in a 4-year-old girl.[123,124] To date, SH-SY5Y cells are considered one of the most commonly used cell line when studying neuronal cell processes and especially, neurodegenerative diseases on a molecular level.[123,125] The cells can be distinguished into two populations, one is floating and one is adherent on the bottom of the flask, while the latter is characterized by continuously proliferation, a polygonal shape and short neurite like outgrowths.[126] The adherent cell line can be further divided into epithelial-like (S-type; black arrow) and neuroblast-like (N-type; orange arrow) **(Figure 6)**.[123] Although these cells express immature neuronal proteins, they show neither significant morphological nor biochemical characteristics of mature neurons.[123,125] However, the ability to differentiate SH-SY5Y cells into more neuronal like cells, makes them an interesting tool to study the effect of neurotoxicants on neurodevelopment and neurodegeneration.[123,125]

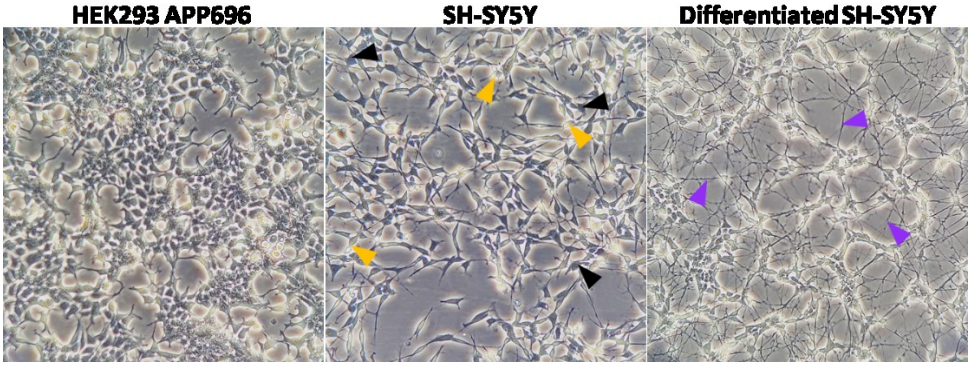

Figure 6. Illustration of *in vitro* models used in this study. HEK293 APP cell growing in clusters, SH-SY5Y cells containing two different populations: epithelial-like (S-type; black arrow) and neuroblast-like (N-type; orange arrow) cells. Differentiated SH-SY5Y show characteristic neuronal outgrowth (purple arrow).

1.4.3 Differentiated SH-SY5Y cells

When using specific differentiation agents like all-trans retinoic acid (ATRA), phorbol esters like 12-O-tetradecanoyl-phorbol-13 acetate (TPA) or dibutyryl cyclic AMP (db cAMP), SH-SY5Y cells can exit the cell cycle and turn from a proliferation state into differentiation.[126,127] Thereby, the cells start to resemble primary neurons morphology of smaller and polarized cells with significantly extended neuronal outgrowth and excitable

membranes.[127–129] One of the most used agent when it comes to SH-SY5Y differentiation is ATRA.[130,131] ATRA is a vitamin A derivate, which is already known to inhibit cell growth and thereby allows the cells initiate differentiation processes.[132] In addition, ATRA mediated differentiation of SH-SY5Y cells leads to activation of phosphatidylinositol 3-kinase/Akt signaling pathway and upregulation of the antiapoptotic Bcl-2 protein.[126,133] ATRA differentiation promotes the development of cholinergic like neurons, which is shown by increased expression levels of the choline acetyltransferase activity (CHAT) as well as of the vesicular monoamine transporter (VMAT).[126,134,135]

In addition to the described morphological changes, ATRA mediated differentiation in SH-SY5Y cells can be detected biochemically via detection of neuronal markers, including neuron specific enolase (NSE), neuronal nuclei (NeuN) or synaptophysin (SYN).[136] Although many studies show the differentiation of SH-SY5Y cells with ATRA only, addition of other compounds like brain derived nutrition factor (BDNF) or B27 may support differentiation as well as the maintenance of differentiated cells.[136–138]

In summary, HEK293 APP695 and undifferentiated SH-SY5Y cells represent a great tool to screen for cytotoxicity induced by different particles, in a time and dose dependent manner as well as to investigate the particles effect at molecular levels. Then, due to their human mature neuronal phenotype, differentiated SH-SY5Y cells allow investigation on more neuronal associated parameters (e.g. neuronal differentiation and degeneration). Moreover, while in proliferating (undifferentiated) cells exposure is limited by the cell cycle length (maximum 24 to 48 h in HEK293 and SH-SY5Y cells), differentiated cells allow a longer exposure time of up to 14 days.

1.4.4 *In vivo* model *Caenorhabditis elegans*

As described above, *in vitro* studies offer a great tool to screen for initial toxicity and to investigate molecular mechanisms, but to understand the effects of nanoplastics particles at tissues/organs as well as on a whole organismal level, *in vivo* studies are mandatory.[2] Using model organism like the nematode *C. elegans* researchers have the opportunity to mimic more relevant environmental conditions like elongated exposure times and several studies pointed out the advantage of nematodes for toxicological screenings, yet still complying with the ethical 3R principles (Replacement, Reduction and Refinement).[2,139,140]

As described above, *C. elegans* is a powerful genetically-tractable model organism for toxicology and aging studies due to its relatively short life cycle and lifespan, combined with a fully sequenced genome, stereotyped (neuro)behaviors and the amenability to

environmental intervention.[141,142] The nervous system of *C. elegans* comprises 302 highly specialized neurons (one third of all *C. elegans* cells), organized in a simple yet with functionally conserved structure.[143] **Figure 7** not only illustrates the structure of an adult animal, including the cuticle, the pharynx, the intestine, the gonads, embryos, the vulva, the body wall muscles and the nervous system. It also shows a fluorescence image done by Chisholm et al., presenting the overall architecture of axon tracts in *C. elegans*.[143]

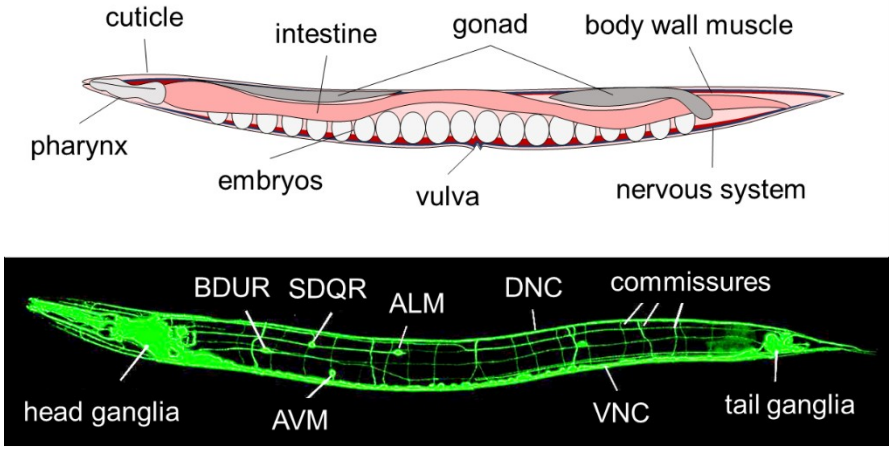

Figure 7. Schematic illustration of an adult nematode as well as fluorescently tagged axonal structures (dorsal nerve cord (DNC), ventral nerve cords (VNC), lateral interneurons (BDUR, SDQR, ALM, AVM)). Adjusted from Chisholm et al.[143]

C. elegans models for AD

In addition to *C. elegans'* nervous system with very well characterized morphology and functions, genetically modified strains are available as disease models, which can be exploited to evaluate particles toxicity in specific risk groups.[2,141,143] This makes *C. elegans* a great model organism to study the neuronal development and degeneration but also to investigate the pathogenesis and possible treatment for different diseases such as AD. *C. elegans* genome contains an ortholog protein to APP, the amyloid precursor like -1 (APL-1) protein, which nonetheless is not processed like in the mammals and therefore does not give rise to any Aβ peptide.[144] Therefore, researchers established transgenic strains by stably transfect with full length Aβ 1 – 42 under the control of different tissue specific promoters. The first AD model line generated expresses toxic Aβ 1 – 42 under the *unc-54* promotor, resulting in body wall muscle cell

specific transgene expression (mAD). [141 A general increase of the metabolic activity via temperature upshift to 25 degrees, results in a time dependent muscle specific accumulation of Aβ 1 – 42.[144] This leads to oligomerization and aggregation of Amyloid plaques, as shown in **Figure 8**, subsequently result in severe, age-progressive paralysis.[144]

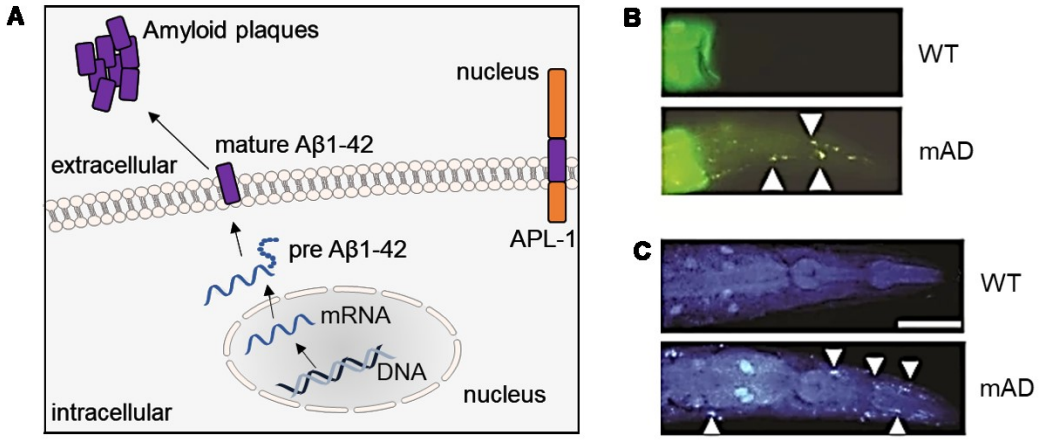

Figure 8. *C. elegans* mAD model expresses full length Aβ 1 – 42. A) Schematic illustration of mAD strain expressing Aβ 1 – 42 peptides after transfection with full length Aβ 1 – 42 under unc-54 promotor. AD specific staining of Aβ 1 – 42 aggregates shows **B)** Thioflavin T positive Aβ aggregates and **C)** X-34 positive Aβ aggregates in mAD strain, but not in WT animals. Adjusted from McColl et al. [144]

In parallel to the strain expressing full-length Aβ 1 – 42 in the muscles, the same sequence was used by Fong et al. to generate a constitutive pan-neuronal Aβ1 – 42 expressing strain under the control of the neuronal specific *unc-119* promoter (nAD).[145] Characterization of this strain could reveal a shortened lifespan, as well as dysfunctions on neuromuscular and behavioral level (e.g. internal hatching, constipation, defects in pharyngeal pumping, abnormal head movements).[145]

To sum up, the usage of the *in vivo* model organism *C. elegans* offers a great system to investigate particles mediated neurodegeneration and even possible interplay with AD pathology. Moreover, *C. elegans* allows to investigate more environmental relevant scenarios, like long-term exposure throughout the whole life cycle and lifespan as well as more physiological investigations, like movement or fertility.[2] Compared to *in vitro* studies, where only one or even a few cell types can be investigated in one scenario, *C. elegans* allows the crosstalk between different cell types and, in particular, investigations on a behavioral level, while still respecting the ethical guidelines and animal welfare protection.[2]

2 Aims

Every day we are exposed to plastic nanoparticles (PS NPs). However, whether and how PS NPs exert neurotoxic effects is largely unknown. Thus, with this work I investigated the detrimental effects of different plastic nanoparticles, but mainly of non-modified PS NPs (PS) and aminated PS NPs (PS-NH_2) in a multisystemic analysis, through three interconnect aims (**Figure 9**):

I) The first aim was to address cytotoxicity in *in vitro* systems, HEK293 APP695 cells, overexpressing wild-type amyloid precursor protein (APP) and undifferentiated SH-SY5Y cells.

II) The second aim was to verify the results shown *in vitro* using *ex vivo* experiments in organoids or premature mouse neurons, but unfortunately due to the COVID19 pandemic, these experiments could not be carried out. Therefore, differentiated SH-SY5Y cells were used as an alternative to investigate the particles effect on chronic exposure scenarios in neuronal like cells.

III) The last aim was to investigate the effect of PS NPs on the nervous system *in vivo* in *C. elegans* to verify the results gained from *in vitro* experiments and to include further morphological and behavioral readouts.

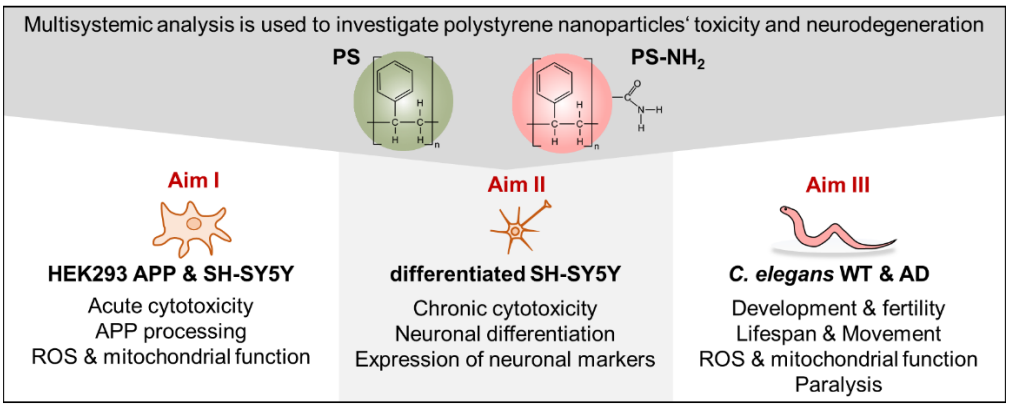

Figure 9. Schematic overview about the multisystemic analysis addressing different readouts dividing in three aims.

3 Material and Methods

A complete list of all used chemicals and solutions (**Table S1**), antibodies and dyes (**Table S2 –Table** S4), kits (**Table S5**) and other devices (**Table S6**), is provided in the appendix.

3.1 Characterization of particles

Preparation of model particles

To investigate the effect of plastic particles on several different parameters *in vitro* and *in vivo*, plain polystyrene particles (PS, 50 nm) (08691-10, Polysciences Inc. (USA)), aminated polystyrene particles (PS-NH_2, 50 nm) (L0780, Merck (USA)), polystyrene particles coupled to a yellow-green fluorophore (PS-YG, 50 nm) (17149-10, Polysciences Inc. (USA)) and polyvinylchloride particles (PVC, > 100 nm) (Werth-Metall (Germany)) were used (**Figure 10**). The particles were purchased in 2.5 % aqueous solution and subsequently stored at 4 °C. PVC powder was kindly provided by Dr. R. Schins and resuspended in sterilized milipore water to a concentration of 4 mg mL^{-1} and sonicated for 10 min using Branson Sonifier 450 at a duty cycle of 0.2 s and an output level of 5.71 (200 W).[146] All particles were diluted to a stock concentration of 4 mg mL^{-1}, prior dilution to respective working concentrations, while using equally amounts of water and exposure media, to a final particle water mixture of 10 %.

The following characterization of the particles was carried out in Dr. Laromaines laboratory at the *Institut de Ciència de Materials de Barcelona, ICMAB-CSIC* in Barcelona.

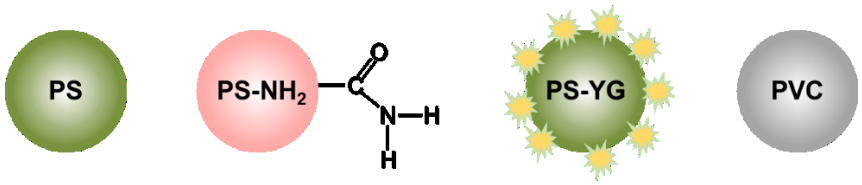

Figure 10. Schematic illustration of particles used in this study. Plain PS particles (PS, 50 nm), aminated PS particles (PS-NH_2, 50 nm), yellow-green fluorescent PS particles (PS-YG, 50 nm) and PVC particles (> 100 nm).

Fourier-Transform Infrared Spectroscopy

The Fourier-Transform Infrared Spectroscopy (FTIR) was done using JASCO FT/IR-4700 to characterize the polystyrene structure. Therefore, the detector was covered with 5 µL of undiluted PS and PS-NH_2 particles (25 mg mL^{-1}). The measurement was started after the particles dried and 500 scans in the range from 4000 to 400 cm^{-1} were measured.

Transmission Electron Microscopy

For Transmission Electron Microscopy (TEM) PS and PS-NH_2 were diluted with sterile H_2O to 10 µg mL^{-2}. Carbon-coated grids were prepared while adding 5 µL of diluted particles, waited until dried and added further particles until 15 µL of diluted particles were dried on the grids. Images were acquired with 120 KV JOEL 1210 and 2.5 x 10^{-4} x magnification at working voltage of 100 kV.

Dynamic Light scattering

Dynamic Light scattering (DLS) was performed to analyze hydrodynamic diameter, polydispersity index and ζ-potential of PS and PS-NH_2. Therefore, the particles were diluted with Millipore water or media of interest to 100 µg mL^{-1} and to identify particles hydrodynamic diameter and PDI, 1 mL of suspension was transferred into micro cuvette without air bubbles. In order to measure the ζ-potential, disposable cuvettes primarily designed to measure ζ-potential were used. These cuvettes are characterized by two closable openings and a partition that is open in the base. To fill the cuvettes, 1 mL of particles solution was filled from one side with a syringe, while any air bubbles had to be avoided. The cuvettes were inserted into Zetasizer Nano ZS (Malvern Instruments Ltd, U.K.) and an He/Ne 633 nm laser measured the samples with ≤ 30 scans per condition at 25 °C and in triplicates each.

Turbiscan analysis

Sedimentation and general stability of the particles was analyzed in media used for *in vitro* experiments, with particles diluted to 100 µg mL^{-1} in a total volume of 25 mL in either BGM or DM in glass reaction vessel and subsequently measured with Turbiscan TURBISCAN LAB (Formulaction, France) for 48 h and 230 scans were taken in total starting with smaller intervals of 5 min to longer timepoints of 15 min. Analysis was done with analyzed with TurbiSoft LAB software 2.2.0.82.

3.2 *In vitro* experiments in undifferentiated cells

Cultivation and maintenance of mammalian cell culture

HEK293 APP695 cells, kindly provided by Prof. Jochen Walter, University of Bonn, were cultivated in RPMI 1640 (31870-025, Thermo Scientific™ (USA)) complemented with 10 % heat inactivated FCS Gold (A11-151, PAA (USA)), 1 % penicillin/streptomycin (P0781, Merck (USA)) and 4 mM L-glutamine (M11-004, PAA (USA)).[147] SH-SY5Y cells were cultivated in BGM (DMEM/F12 *Glutamax* supplement (31331093, Thermo Scientific™ (USA)), 10 % heat inactivated fetal calf serum (FCS) (10082147, Thermo Scientific™ (USA)), 1 % penicillin/streptomycin). For maintenance, cells were grown in T-75 flasks and passaged two times per week when reaching confluence of ~ 70 - 80 %. Therefore, cells were washed once with 10 mL DPBS (D8537, Merck (USA)) prior incubating with 1 mL Trypsin-EDTA solution (0.25/0.02 % (v/v)) (T4049, Merck (USA)) at 37 °C for 2 minutes. To inhibit the reaction 10 mL serum containing medium was added to cells and subsequently cells were transferred to 15 mL reagent tube and centrifuged for 2 min at 1000 x g at RT. Afterwards, the pellet was resuspended in fresh serum containing medium and either partially transferred into new T-75 flask or seeded for experiments. To seed the cells in appropriate concentration, cells were mixed with Trypan blue solution (1:3) (T8154, Merck (USA)) and counted using a *Neubauer* improved hemocytometer. For storage, cells were mixed with 5 % DMSO (D2650, Merck (USA)) and transferred into freezing vial (~ 2 – 5 x 10^6 cells ml^{-1}) and cooled down in freezing container 24 h at -80°C prior transfer into liquid nitrogen.

For experiments Hek293 APP695 cells were used from passage 4 to 25, after selection with Geneticin (G418) (G1279, Merck (USA)) for three passages, while undifferentiated SH-SY5Y from passage 4 to 20 and differentiated SH-SY5Y cells from 4 to 10 were used.

Determining cell growth capacity

The growth capacity of the cells was determined by collecting and counting the cells after 48 and 96 h after seeding at appropriate concentration (6, 10 and 8 x 10^5 cells per dish (10 cm)). The amount of counted cells (N), the number of cells seeded (N_0) and the growth time (t) was used to calculate the proliferation time (maximal age of cells, td) according equation in Sherley, Stadler & Stadler (1) (N: cell number, N_0: initial cell number, td: maximal age of cells, t: growth time).[148]

$$N = N_0 e^{\frac{\ln 2}{td}t} \quad (1)$$

Tetrazolium based cell viability assay – WST-1

Cell viability of Hek293 APP695 and undifferentiated SH-SY5Y cells was measured with a water-soluble tetrazolium-1 (WST-1) (11644807001, Merck (USA)) assay. HEK293 APP695 cells and SH-SY5Y cells were seeded in 96 well plates and treated with 1, 5, 10 and 50 µg cm^{-2} of particles after 24 h. WST-1 assay was done according to Kolling et al. with some adjustments and incubation for 2 h (HEK293 APP695)) or 3 h (SH-SY5Y) at 37 °C, 5 % CO_2 and 95 % humidity before measuring absorbance at 450 nm and 630 nm as (reference) using Multiskan™ GO Microplate Spectrophotometer (Thermo Scientific™).[149]

Resazurin based cell viability assay

Resazurin based assay was used for higher sensitivity. Undifferentiated SH-SY5Y cells were seeded as 1.5 x 10^5 per well in 24 well plates, treated like mentioned above incubated with 10 µM Resazurin (20 mg mL^{-1} in DMSO (w/v)) (37017, Merck (USA)) in BGM without FCS for 4 h. Differentiated SH-SY5Y were seeded at 3.5 x 10^4 cells per well in 24 well plates and treated either with different concentrations of particles for 48 h after differentiated for 6 days or treated with different concentrations of particles for 6 days during differentiation, prior incubation with 10 µM Resazurin in DM without FCS for 24 h. The fluorescence of supernatants of undifferentiated and differentiated cells was measured at 590 nm_{ex}/560 nm_{em} with Infinite® 200 PRO (Tecan).

Detection of Amyloid β in cells supernatant

Secretion of Aβ 1 – 40 and Aβ 1 – 42 in the conditioned media of HEK293 APP695 and SH-SY5Y cells after particle exposure was determined using the Human/Rat β Amyloid ELISA Kit Wako for either Aβ 1 – 40 (294-62501, Fujifilm (Japan)) or Aβ 1 – 42 (292-64501, Fujifilm (Japan)). Cells were seeded on 6 well plates (6 x 10^5 cells/well) and after 24 h treated with PS-NH_2 (0.5 and 1 µg cm^{-1}), PS, PS-YG and PCV (0.5 and 5 µg $cm^{-1)}$ for 24 h as described above. Then, the medium was removed into precooled tubes and centrifuged for 5 min at 4°C and 500 x g. The medium was transferred into fresh tubes, while ~ 20 % was left. The conditioned medium was either stored at -20 °C until usage or subsequently used for Aβ analysis. The Enzyme-Linked Immunosorbent Assay (ELISA) was done as described by manufacturer. In short, the samples were diluted in standard diluent (1:10 for Aβ 1 – 40, 1:5 for Aβ 1 – 42), transferred into antibody coated microtiter plate (BNT77) and incubated at 4°C over night (ON). After incubation, the wells were washed 5 x with washing solution HRP-conjugated antibody solution (Aβ 1 – 40:

BA27 Aβ 1 – 42: BC05) was added for 1 h at 4°C, following further washing steps and final incubation with TMB solution for 30 min at RT and dark conditions. The reaction was stopped with stop solution and the absorbance was measured at 450 nm using Multiskan™ GO Microplate Spectrophotometer (Thermo Scientific™ (USA)). The amount of Aβ protein was determined according the standard curves and normalized on the total protein.

Isolating and measuring of total protein

For protein extraction the cells were washed twice with ice cold DPBS and then exposed to lysis buffer (1 x RIPA buffer (20-188, Merck (USA)), 1 x cOmplete Protease Inhibitor Cocktail (11836170001, Merck (USA)), 1 x Phosphatase Inhibitor Cocktail 2 (P5726, Merck (USA)). The cells were rapidly scraped on ice and cell lysate was centrifuged at 8 000 x g for 10 min at 4 °C to pellet cell debris. The supernatant was transferred into a fresh tube and either used for concentration determination or stored at -80°C for further analysis. The concentration of proteins was determined with BCA Protein assay Kit (23227, Thermo Scientific™ (USA)) according to manufacturer's instruction and measuring the absorbance at 562 nm using Multiskan™ GO Microplate Spectrophotometer (Thermo Scientific™ (USA)).

Cell death analysis

Cell death analysis was addressed via Annexin V-FITC and PI staining (Annexin V-FITC Apoptosis Kit (K101-400, BioVision (USA)). Undifferentiated SH-SY5Y cells were seeded 2 x 10^5 cells in 24 well plates in BGM and after 24 h treated for 1, 2 and 4 hours with 5, 10 and 25 µg cm^{-1} PS and PS-NH_2. Before staining, cells were washed with DPBS, detached with Accutase® (00-4555-56, Thermo Scientific™ (USA)) and transferred into FACS tubes, while collecting all supernatants and cells. Staining was done according to manufacturer's instruction for 10 min at room temperature in the dark. FITC ($502_{ex}/523_{em}$) and PI ($396_{ex}/610_{em}$ nm, phycoerythrin (PE) channel) were acquired with a blue 488 nm laser measured with FACS Canto™ II flow cytometer (BD Biosciences, Heidelberg, Germany) and analyzed with FlowJo software 10.8.1.

ROS and mtROS quantification

General ROS was analyzed by intracellular hydrogen production stained with H_2DCF-DA (2´,7´-Dichlorofluorescin diacetate) (287810, Merck (USA)), whereas mitochondrial

superoxides were stained with MitoSOX™ (M36008, Thermo Scientific™ (USA)) to analyze mitochondrial ROS production according to Alboni et al. with slight modification.[150] Therefore, undifferentiated SH-SY5Y cells were seeded 2 x 10^5 cells in 24 well plates in BGM and after 24 h treated for 1, 2 and 4 hours with 5, 10 and 25 µg cm^{-1} PS and PS-NH_2, with two additional samples treated with 3 µM N-acetyl cysteine (NAC) (A0150000, Merck (USA)) for 18 h before detaching with Accutase®. Supernatant and cells were resuspended in BGM containing 2.5 µM MitoSOX™ and incubated for 20 min at 37°C and 5 % CO_2 together with a control containing 10 µM Antimycin A (AMA, stock: 2 mg ml^{-1} in DMSO (w/v)) (A8674, Merck (USA)) as well as NAC treated sample containing 10 µM AMA, before cells were collected and stained with 200 µM H_2DCF-DA for further 30 min at 37 °C in DPBS. After washing, cells were resuspended in 400 µL DPBS and immediately before FACS analysis 1 µg mL^{-1} of DAPI (MBD0015, Merck (USA)) was added to exclude dead cells. MitoSOX™ was acquired in phycoerythrin (PE) ($396_{ex}/610_{em}$ nm) and H_2DCF-DA in FITC channel (FITC, $502_{ex}/523_{em}$) with a blue 488 nm laser and DAPI was acquired in pacific blue channel ($364_{ex}/454_{em}$) with violet 408 nm laser with FACS Canto™ II flow cytometer (BD Biosciences, Heidelberg, Germany) and analyzed with FlowJo software 10.8.1.

Detection of mitochondrial membrane potential

JC-1 (T3168, Thermo Scientific™ (USA)) is a cationic dye specific for mitochondria and a fluorescence shift from red (aggregates) to green (monomers) indicates a depolarization of the mitochondrial membrane. Therefore, undifferentiated SH-SY5Y cells were seeded 2 x 10^5 cells in 24 well plates in BGM and after 24 h treated for 1, 2 and 4 hours with 5, 10 and 25 µg cm^{-1} PS and PS-NH_2. Before staining, cells were washed with DPBS, detached with Accutase® and transferred into FACS tubes, while collecting all supernatants and cells. Staining was done according to manufacturer's instruction for 30 min at 37 °C in the dark and after washing once, cells were resuspended in 400 µL DPBS. Green (FITC channel, $514_{ex}/529_{em}$) and red signal (PE channel, $585_{ex}/590_{em}$ nm) were acquired with a blue 488 nm laser measured with FACS Canto™ II flow cytometer (BD Biosciences, Heidelberg, Germany) and analyzed with FlowJo software 10.8.1.

3.3 *In vitro* experiments in differentiated cells

Differentiation of SH-SY5Y cells

Cells were seeded in BGM onto MaxGel™ ECM (E0282, Merck (USA)) precoated culture dishes in appropriate concentration and after 24 hours BGM was replaced by freshly prepared and 1 h equilibrated DM (DMEM/F12 *Glutamax* supplement, 1 % heat inactivated fetal calf serum, 1 % penicillin/streptomycin, 10 µM all trans Retinoic acid (R2625, Merck (USA)) (5 mM in 95 % EtOH (w/v), stored at 4 °C for up to 6 weeks according to literature.[136] Cells were differentiated for further 6 days until used for experiments whereby media were replaced one time in between or during particle treatment.

SDS PAGE

Cells were either differentiated for 7 and 14 days or cultured undifferentiated until a confluence of ~ 80 % and the total protein was isolated as described above.

After that, 20 µg of protein were mixed with sample buffer (1x Laemmli Buffer (161-0747, Bio-Rad Laboratories, Inc. (USA)), 3.2 mM DL-dithiothreitol (DTT) (646563, Merck (USA)), denatured for 5 min at 94 °C and after short cool down on ice loaded, together with a PageRuler™ Prestained Protein Ladder (26617, Thermo Scientific™ (USA)) onto Tris-Glycine sodium-dodecyl-sulfate (SDS) polyacrylamide gel run at 70 V through 4 % stacking gel (Acylamide mix Rotiphorese Gel 30 (37.5:1) 17 % (1610158, Bio-Rad Laboratories, Inc. (USA)) , 34 % Tris-HCL buffer (0.5 M, pH 6.8), SDS 1 %, APS 1%, Temed 0.9 M)) and for ~1.5 h at 120 V through 12 % resolving gel (Acylamide mix Rotiphorese Gel 30 (37.5:1) 40 %, 25 % Tris-HCL buffer (1.5 M, pH 8.8) (4855.3, Roth (Germany)), SDS 1 % (8029.3, Roth (Germany)), ammonium persulfate (APS) 1% (17874, Thermo Scientific™ (USA)), TEMED 0.34 M (T9281, Merck(USA)) using Tris-Glycine SDS running buffer (1610772, Bio-RAD Laboratories, Inc. (USA)) in novex® XCell Sure Lock System (Thermo Scientific (USA)).

Western Blot

After electrophoresis, proteins were transferred from gel to polyvinylidene fluoride (PVDF) membrane (0.45 µm pore size) (IPVH00010, Merck (USA)) (after initial membrane activation in methanol for 1 min). Therefore, membrane and gel were covered with filter papers and blotting pads and wet blot transfer was mediated using methanol containing transfer buffer (SDS 0.1 %, Glycin 0.192 M (0079.4, Roth (Germany)), Tris

0.025 M, methanol (20 %) (8388.1, Roth (Germany)) at 25 V and 4 °C for 1 h in novex® XCell Sure Lock System (Thermo Scientific™ (USA)). Subsequently, the protein containing membrane was blocked in freshly prepared blocking solution (TBS pH 7.4, Tween 20 0,1 % (P1379, Merck (USA)), powdered milk 5 % (T145.3, Roth (Germany)) for 1.5 h and stained in respective primary antibody against NSE (Anti-Neuron Specific enolase (monoclonal) (MAB324, Merck(USA))) 1:500; ßIIITUB (Anti ßIII-Tubulin (monoclonal) (T8578, Merck (USA))) 1:2000; in blocking solution over night at 4°C. After that, membrane was washed with TBS containing Tween (0.1%) 3 x 10 minutes prior 1 h incubation in secondary antibody (Mouse IgG HRP Linked Whole AB (GENA931-1ML, Merck (USA))). Finally, membrane was washed again, and Amersham™ ECL™ Prime Western Blotting Detection Reagent (RPN2232, Cytiva (USA)) was used according to manufacturer's instruction. Restore Western blot Stripping Buffer (21059, Thermo Scientific™ (USA)) was used once to strip the membrane according to manufacturer's instruction and to stain with a further antibody. Semi-quantitative analyzes were performed using Image J/Fiji 2.3. while normalizing intensities to housekeeping protein.

Neurite degeneration:

To analyze neurite outgrowths after differentiation, SH-SY5Y cells were seeded on MaxGel™ ECM coated 6 well plates and differentiated as described above. After 6 days DM was refreshed with DM containing PS-NH_2 particles in appropriate concentration. For assessing the particles effect during differentiation, SH-SY5Y cells were seeded on 6 well plates (2.5 x 10^4 cells) in BGM and 24 h after initiating differentiation, DM was refreshed with DM containing PS-NH_2 particles in appropriate concentration. After treatments, the cells were washed with prewarmed DPBS and incubated with 5 µM Hoechst 33342 (H1399, Thermo Scientific™ (USA)) in BGM for 10 min at 37 °C and under dark conditions. Afterwards cells were acquired in brightfield and DAPI channel with Zeiss Axio Vert.A1 and 200 x magnification. Analysis was done with Image J/Fiji 2.3 and NeuriteTracer plugin, according to Pool et al.[151]

Expression of neuronal proteins

SH-SY5Y cells were seeded on MaxGel™ ECM coated glass wells (2.5 x 10^4 cells) in BGM and 24 h after initiating differentiation, DM was refreshed with DM containing PS-NH_2 particles in different concentrations (0.25, 0.5, 1 µg cm^{-2}). After 72 h DM and particles were replaced again and after further 72 h cells were fixed with prewarmed Pierce™ formaldehyde (w/v) solution (28908, Thermo Scientific™ (USA)) (4 % in DPBS,

stock: 16 % formaldehyde solution (w/v)) for 30 min at room temperature and blocked and permeabilized with 3 % BSA (BP9705, ThermoScientific™ (USA)) and 0.1 % Triton X® 100 (3051.3, Roth (Germany)) in DPBS for 1 h. Afterwards, cells were incubated with primary antibody in DPBS containing 1 % BSA (APP (APP/Beta Amyloid antibody (polyclonal) (25524-1AP, Thermo Scientific™ (USA))) 1:100; NSE (Anti-Neuron Specific enolase (monoclonal) (MAB324, Merck (USA)))1:200; SYN (Anti-Synaptophysin antibody [SY38] (monoclonal) (ab8049, Abcam (USA))) 1:50; NLGN1 (Neuroligin 1 antibody (polyclonal) (PA5-786548, Thermo Scientific™ (USA))) 1:250; NLGN3 (Neuroligin 3 antibody (polyclonal) (PA5-78508, Thermo Scientific™ (USA))) 1:100; βIIITUB (Anti βIII-Tubulin (monoclonal) (T8578, Merck (USA))) 1:500; at 4 °C overnight followed by 1 h incubation with secondary antibody (Goat anti-Rabbit IgG (H+L) Highly Cross-Adsorbed Secondary Antibody, Alexa Fluor™ Plus 488 (A11008, Thermo Scientific™ (USA))) and Goat anti-Mouse IgG (H+L) Highly Cross-Adsorbed Secondary Antibody, Alexa Fluor™ Plus 594 (A32742, Thermo Scientific™ (USA))) in DPBS containing 1 % BSA and Fluoroshield™ DAPI (F6057, Merck (USA)) mountain staining. Experiments were done in triplicates and ≥ 15 pictures were acquired per condition with Zeiss Axio Imager M1 microscope (Carl Zeiss Inc., (Germany)), 40 x magnification and ZEN 2 (blue edition) software. Analysis was done with Image J/Fiji 2.3 while normalizing the fluorescence intensity on the number of nuclei and ≥ 10 images were taken and counted per condition and replicate. The used script is provided in Appendix (**Table S7**).

3.4 *In vivo* experiments in *C. elegans*

Maintenance of C. elegans and used strains

Maintenance of *C. elegans* was done under standard nematode culture conditions described previously, while using alive *E. coli* OP50 (*xu363*) bacteria (kindly provided by XU laboratory (University of Michigan).[152] N2 worms were used as wild-type strain, hspSJ4100: *zcIs13[phsp-6::*GFP] and GR2250: *mgIs73[cyp-14A4p::*GFP*::cyp-14A4* 3'UTR + *myo-2p::*mcherry] as mitochondrial stress reporter strains; GMC101 (dvIs100 [*unc-54p::*A-beta-1-42*::unc-54 3'*-UTR + *mtl-2p::*GFP]) as mAD model and AM134 (rmIs126 [unc-54p::Q0::YFP]) as respective control for movement analysis and JGXX2 (*punc-119::*Aβ 1–42*; pmyo-2*::YFP) as nAD model for paralysis in Aldicarb assay and JGXX1 (*pmyo-2::*YFP) as respective control.[144,145,153,154] Unless otherwise described, worms were maintained and cultivated on solid nematode growth medium (NGM) plates spotted with OP50 as food source, as previously described by Stiernagle.[155]

Preparation of bacteria as a food source

In all experiments, OP50 bacteria were used as food source for the nematodes. The bacteria were grown overnight at 37 °C and continuously shaking in LB medium. The ON culture was either spotted on the plates for solid NGM culturing or prepared for liquid culturing. Therefore, the OD_{600} of OP50 ON culture was measured and after centrifugation (10 min at 4 °C and 3 200 x g) the cell pellet was resuspended to a stock solution of 6 x 10^9 cells mL^{-1} (OD_{600} 1 = 5 x 10^8 cells mL^{-1}) in S-Medium containing 50 µg mL^{-1} Streptomycin (S9137, Merck (USA)).[156] Bacteria were stored up to 1 week at 4 °C.

Inactivating OP50 bacteria

For experiments with inactivated OP50 bacteria on solid NGM plates, the OP50 bacteria were spotted on the plates as described above and after 24 h of drying, the plates were exposed to UVB light for 30 min (Waldmann UV 236).

When using inactivated OP50 in liquid culture experiments, OP50 bacteria were prepared as described above and heat inactivated in a heating block for 15 min and 65 °C and vortexing every 5 min before Streptomycin was added.

Age synchronization of C. elegans

Synchronization of nematodes maintained on plates was done via egg lay, while worms synchronized via isolation of eggs with bleaching solution (hypochlorite/NaOH (60 % H_2O, 30 % NaOH (5 M), 10 % hypochlorite (12 % (v/v))) prior to liquid culturing, washed at least four times with S-Basal and incubated on rotating wheel overnight.

C. elegans development and fertility assay on solid plates

In order to investigate the development of the worms after particle exposure, per condition three fresh NGM plates spotted with OP50 were seeded with 25 eggs and treated with 100 µg mL^{-1} PS-NH_2 (diluted with H_2O and added on top, covering the worms and bacterial lawn). After 4 days, development was investigated under stereoscope and worms developed to adult worms were counted. To analyze the fertility of the worms, L4 worms were covered with 100 µL of PS-NH_2 solution (100 µg mL^{-1} in H_2O/S-Basal) and egg lay was done after 24 h with 8 worms per plate and 3 plates per condition for 1 hour.

C. elegans movement assay on solid plates

The movement assays were carried out by Magnitude Bioscience, UK, on solid agar plates (agar at 2%, NaCl at 0.3%, 1 M Magnesium Phosphate at 0.1%, 1 M Potassium Phosphate buffer pH 6 at 2.5%, Cholesterol stock solution (5 mg ml^{-1}, dissolved in ethanol) at 0.1%, Amino-acid Stock solution at 2.03%, Trace metals stock solution at 0.02%, 100 µM Vitamin B12 stock solution at 0.01%, Uracil stock solution (2 mg ml^{-1} dissolved in distilled water and filter sterilized) at 0.2%) containing 10 µM 5-fluoro-2-deoxyuridine (FUDR) and OP50.[157,158] To investigate the post-developmental effect of particles, 100 µL PS and PS-NH_2 solution of 100 µg mL^{-1} in H_2O was added onto the bacterial lawn. Worms were shifted 24 h before movement assays start to 24 °C and afterwards, 30 L4 worms per condition were transferred to plates containing particles and sealed with parafilm. The movement assay was done with Healthspan Machine for 10 days. When analyzing the post-embryonic effect of the particles, egg lay was done on plates containing particles (100 µg mL^{-1}) and after reaching L4, 30 worms were transferred onto fresh plates containing particles (100 µg mL^{-1}). The plates were prepared as described above and movement assay was run for 7 days according to Magnitude Biosciences' automated Healthspan technology.[157] Experiments were done in triplicates using GMC101 worms as an mAD model and AM134 as a control strain.

C. elegans treatment with particles in liquid culture

Liquid culture of *C. elegans* was performed after synchronizing worms via egg isolation as described above and maintaining in S-Medium (containing 1 % BSA, 50 µg mL^{-1} Streptomycin and freshly prepared OP50) according to Petrascheck et al., with slight modifications, unless otherwise described.[156] In short, S-Basal was complemented with potassium citrate solution (citric acid monohydrate 0.1 M (C1909, Merck (USA)), tri-potassium citrate 0.9 M (1049561000, Merck (USA)) pH 6.0), Trace metals solution (Disodium EDTA 4.5 mM (8043.2, Roth (Germany)), $FeSO_4$ • 7 H_2O 4.5 mM (450278, Merck (USA)), $MnCL_2$ • 4 H_2O 1 mM (M-3634, Merck (USA)), $ZnSO_4$ • 7 H_2O 1 mM (Z0251, Merck (USA)), $CuSO_4$ • 5 H_2O 0.1 mM (469130, Merck (USA))), cholesterol solution (5 mg mL^{-1} cholesterol in EtOH 70 % (w/v)), $CaCl_2$ • 2 H_2O solution 1 M (C-3881, Merck (USA)) and $MgSO_4$ • 7 H_2O 1 M (P027.1, Roth (Germany)) and BSA/Streptomycin solution (BSA 10 % in S-Medium (w/v), Streptomycin (100 mg mL^{-1})). Worms (~ 15 per well) were cultivated in 96 well plates in S-Medium and fed with 1 x 10^{9} cells mL^{-1} of OP50 bacteria (total volume of 140 µL) from L1 to adult (~ 4 days) under continuously mild shaking at 20 °C and dark conditions. The particle treatment was done on day 3 for 24 h, unless otherwise described.

C. elegans development during particle exposure in liquid

In order to characterize worm's development during particle exposure, L1 worms were seeded and immediately treated with 10, 50 and 100 µg mL^{-1} of PS-NH_2 and worms were analyzed for 4 days. For measuring the length, either L1, L4 or 1-day old adult worms were seeded and treated with 100 µg mL^{-1} until control worms reached adult state. The development and worm's length were determined in N2 worms. Worms were transferred on NGM plates to determine development and measure body length under a stereoscope.

C. elegans' lifespan during particle exposure in liquid culture

In order to analyze the lifespan of *C. elegans* worms in liquid after PS and PS-NH_2 treatment, synchronized L4 worms (N2) were transferred to S-Medium (containing 50 µg mL^{-1} carbenicillin, 0.1 µg mL^{-1} fungizone, 1.5 mM FUdR, 6 mg mL^{-1} freshly prepared OP50) according to Petrascheck et al., with slight modifications.[156,159,160] Particle exposure was done in 1-day-old adult worms with 1, 10 and 100 µg mL^{-1} of PS and 1, 10, 50 and 100 µg mL^{-1} of PS-NH_2. Experiments were carried out by Dr. Annette Limke and performed in triplicates (63 – 106 worms were used per condition and per experiment). Statistical data was analyzed by myself via OASIS 2 using the Kaplan-Meier estimator and log-rank test to detect differences in the lifespan. Means of average lifetime were compared with unpaired t-tests.

Quantification of body bends per minute in liquid

The number of body bends per min (changes in the body bend at the mid-body point per minute) was counted in liquid for each worm in at least 20 animals in two independent experiments.

Quantification of GFP signal in transgene reporter strains

The GFP signal in the reporter strains *hsp6p*::GFP and *cyp14a4p*::GFP was detected and analyzed as described previously.[161] Briefly, the worms were transferred on microscope glass slides containing S-Basal and levamisole (10 mM), acquired with Zeiss Axio Imager M1 microscope (Carl Zeiss Inc., (Germany)), 40 x magnification and ZEN 2 (blue edition) and analyzed with Image J/Fiji 2.3.

Detection of mitochondrial ROS in vivo

MtROS was detected in living worms using MitoSOX™ Red. To this purpose, nematodes were synchronized, cultivated in liquid culture from L1 and treated with PS-NH_2 for 24 h from L4/young adult as described above. After 24 h, treatment with MitoSOX™ was done according to Chaudhari et al. with slight modifications.[162] Therefore, MitoSOX™ was added to the wells at a final concentration of 10 µM and the plate incubated in the dark at 20 °C with mild shaking. After 24 hours the animals were washed three times with S-Medium and transferred onto solid plates. The worms were incubated on the plates for 20 minutes to let them clean their guts. For imaging, nematodes were mounted on microscopic slides and anesthetized by adding 10 mM levamisole. Images were acquired immediately with a Zeiss Axio Imager M1 microscope (Carl Zeiss Inc., (Germany)) using a 40× objective and a DsRed Filter. Afterwards, the worm head region, specifically the posterior pharyngeal bulb, was manually selected, and the integrated intensity was analyzed with Image J/Fiji 2.3.[163]

Measuring of mitochondrial membrane potential in vivo

In order to determine the mitochondrial membrane potential *in vivo*, nematodes were synchronized, cultivated in liquid culture from L1 and treated with PS-NH_2 for 24 h from L4/young adult as described above. After 24 h, treatment with tetramethyl rhodamine ethyl ester (TMRE) was done according to Kropp et al. with slight modifications.[164]

On the day of the experiment, TMRE (T669, Thermo Scientific™ (USA)) was added to the wells at a final concentration of 200 nM and incubated in the dark for 3 hours. Afterwards animals were washed three times with S-Medium and transferred onto solid plates and let crawl for 20 minutes to clean the guts. For imaging, nematodes were mounted on microscopic slides and anesthetized by adding 10 mM levamisole. Images were acquired immediately with a Zeiss Axio Imager M1 microscope (Carl Zeiss, Inc., Cologne, Germany) using a 10× objective and a DsRed Filter for imaging. The fluorescence intensity in the whole body was quantified using CellProfiler.[165]

Determining the synaptic function in vivo

To assess the synaptic function of WT and AD worms, JGXX2 (*punc-119::*Aβ 1–42*; pmyo-2::*YFP) as nAD model and JGXX1 (*pmyo-2::*YFP) nematodes were synchronized, cultivated in liquid culture from L1 and treated with 10 and 100 µg cm^2 PS-NH_2 for 24 h from L4/young adult as described above. Afterwards, paralysis was induced via aldicarb (33386, Merck (USA)) (inhibitor of acetylcholine esterase) according to Mahoney et al.

with slight modifications.[166] To this purpose, worms were transferred on agar plates by pipetting, and after the liquid drops dried, 25 worms were transferred onto plates containing 0.5 mM aldicarb (33389, Merck (USA)) (w/v) in EtOH (70 %). The number of paralyzed animals (which do not react to gentle touching) was scored every 30 min.

Statistics

Data variances were analyzed using f test and data distribution was evaluated with Shapiro Wilk test. Two tailed Student's t test was used to identify differences between two groups. One-way ANOVA followed by Dunnett's multiple comparison as Post Hoc test were used to compare two or more groups with control group. The statistic was carried out with GraphPad Prims version 8.0.0 for Windows, GraphPad Software, San Diego, California (USA).

Additional Lifespan Analysis was further assessed using Kaplan-Meier estimator and mean lifespan was evaluated using Log-Rank test by comparing two survival functions through overall lifespan using OASIS 2.[167]

4 Results

4.1 Physicochemical characterization of PS NPs

One main challenge to face especially when addressing particles toxicity using different organisms and experimental settings is to adjust the exposure conditions according to the readouts of interest but also in compliance with an artefact-free exposure scenario. For instance, particles tend to agglomerate depending on the suspension media and, in solutions containing serum, a protein corona is formed on the particles surface.[168,169] Therefore, PS and PS-NH_2 were initially characterized for their size, charge and distribution in water but also in the different media which were used in the different exposure scenarios.

Fourier transform infrared spectroscopy revealed chemical structure of particles

Firstly, physicochemical properties of particles, including any changes of their surface functional groups and size in water were characterized (**Figure 11**). Fourier-transform infrared spectroscopy (FTIR) analysis revealed typical bonds for PS particles in both, PS (green) and PS-NH_2 (red) spectra: The aromatic carbon hydrogen (C – H) stretching vibrations (stretching movement of the atoms) at 3024 cm^{-1}, the bending (bending movement of the atoms) and stretching vibrations of the methylene's (CH_2) at 2921 and 2847 cm^{-1}, the carbon-carbon (C – C) stretching vibration within the benzene ring at 1600 cm^{-1} and the asymmetric bending and stretching of the benzene ring at 1494 and 1450 cm^{-1} (C_6H_5) could be observed.[170–173] The peak at 3420 cm^{-1} indicates the amine bending and stretching (NH) and the peak at 1100 cm^{-1} is characteristic for the stretching vibrations of aliphatic amines (C-N).[170,174] Moreover, I observed a peak at 1733 cm^{-1} (PS-NH_2), possibly indicating the carbon oxygen bond (C=O).[175]

An overview with all peaks and respective bindings is summarized in the following table, which is overall compatible with particles chemical structure expected from their manufacturer's description (

Table 3).

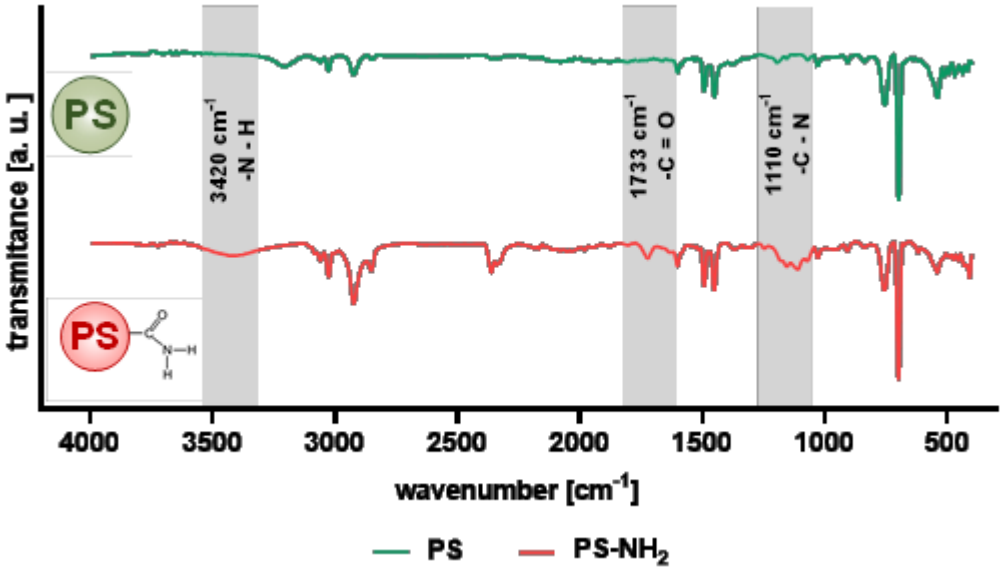

Figure 11. FTIR spectra of PS (green) and PS-NH2 (red) particles. Differences between both particles are highlighted (grey background).

Table 3. Summary of FTIR results. Description and characterization of chemical bonds represented by the peaks in PS and PS-NH_2 spectra.

Peak	Bond	Reference
3420	-N-H bending vibration	[170]
3208	-C-H stretching vibration	[171]
3024	-C-H stretching vibration (aromatic)	[170–172]
2921, 2847	-CH2 bending vibration	[170]
2362	-C-H stretching vibration	[175]
1733	-C=O stretching vibration	[175]
1639	-H-O-H bending vibration	[171]
1600	-C-C stretching vibration (benzene ring)	[170]
1494, 1450	-C6H5 bending and stretching vibration (in plane)	[173]
1110	-C-N stretching vibration (aliphatic amines)	[174]
760, 700	-C-H= stretching and bending vibration (aromatic, in plane)	[172]

TEM analysis confirms size of PS and PS-NH_2 in nanoscale

The size and shape of the particles were analyzed by Transmission Electron Microscopy (TEM), after diluting in sterile Millipore water, and revealed a size of 60 ± 5 nm for PS **(Figure 12 A)** and 48 ± 5 nm for PS-NH_2 (**Figure 12 B**) comparable to manufacturer's information.

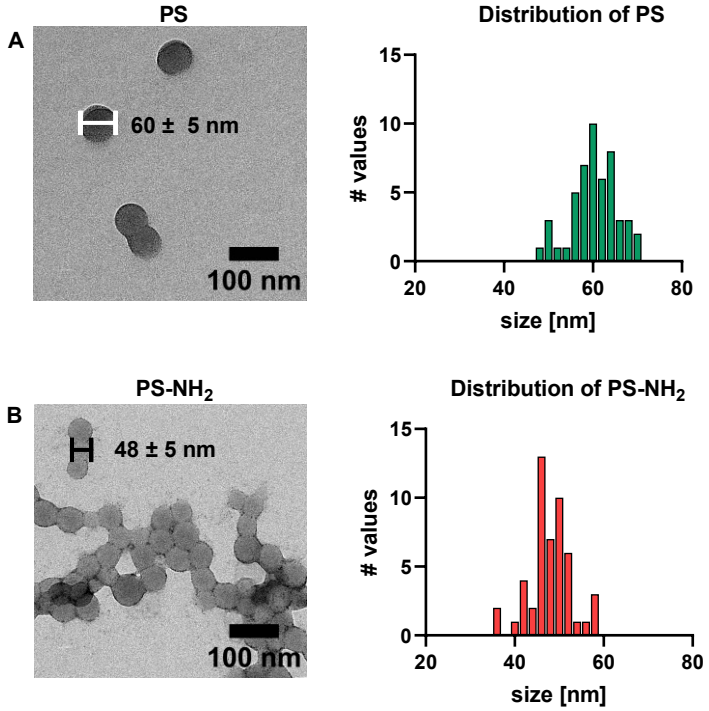

Figure 12. TEM analysis of PS and PS-NH_2. TEM images (25 000 x) in millipore water (10 µg mL^{-1}) of **(A)** PS and **(B)** PS-NH_2 with respective size distribution. Shown are mean values calculated from at least 50 particles (n = 50) ± SD.

DLS analysis reveals changes of particles size, size distribution and charge depending on the exposure media

Dynamic light scattering (DLS) was performed to characterize PS and PS-NH_2 in the different media used for different exposure scenarios and to identify changes in size (hydrodynamic diameter, Z-Average), in size distribution (Poly Dispersity Index, PDI) and in particles' charge (ζ-potential).

As shortly described in chapter 3, SH-SY5Y cells were maintained in Basic Growth Medium (BGM) composed of DMEM/F12 (media), 1 % Penicillin/Streptomycin mixture and 10 % of heat inactivated and filtered fetal calf serum (FCS). Differentiation Medium (DM) contained a reduced amount of serum (1 % FCS) and 10 µM All-trans Retinoic acid

and was used for neuronal differentiation. The results show an intensity weighted mean hydrodynamic diameter (Z-Average) of 61.7 ± 0.1 nm (PDI = 0.02 ± 0.01) for PS and 50.5 ± 0.4 nm (PDI = 0.03 ± 0.0.1) for PS-NH_2 in media, comparable to the TEM results **(Figure 13 A, C)**. Moreover, the low PDI is characteristic of a homogeneously distributed particle population, which is revealed by the number of peaks (in this case only one) in **Figure 13**.

Both particles show an increased size when adding proteins: PS increases from 61.7 ± 0.1 nm in medium only to 83.7 ± 0.2 (PDI = 0.10 ± 0.01) nm in BGM (10 % FCS) or to 107.6 ± 1.1 nm (PDI = 0.10 ± 0.01) in DM (1 % FCS), whereas PS-NH_2 from 50.5 ± 0.4 nm in medium only to 103.1 ± 0.8 nm (PDI = 0.262 ± 0.007) in BGM (10 % FCS) or 273 ± 5 nm (PDI = 0.29 ± 0.03) in DM (1 % FCS) **(Figure 13 A, C; Figure 15 A, C)**. In addition, PS and PS-NH_2 in S-Medium containing OP50 bacteria (*E. coli* bacteria used as food source for the nematodes) built agglomerates around 1081 ± 282 nm (PDI = 0.5 ± 0.1) for PS and 4505 ± 859 nm (PDI = 0.2 ± 0.2) for PS-NH_2 **(Figure 13 B, D)**.

This effect, especially for PS-NH_2, was already observed by eye: S-Medium with OP50 bacteria mixed with PS-NH_2 appeared agglomerated and very blurred under the stereoscope, however adding BSA (1 %) to this mixture, removed the clumps and made the suspension clear again **(Figure 14)**. The decreased particle size in S-Medium containing OP50 and BSA (1 %) of 140.2 ± 0.9 nm (PDI = 0.80 ± 0.01) for PS and 423 ± 43 (PDI = 1) for PS-NH_2 nm, compared to particles in S-Medium containing OP50 only, confirmed this phenomenon **(Figure 13 B, D)**. In S-Medium containing OP50, both particles showed an increased PDI while addition of BSA (1 %) is further increasing the PDI.

Overall, TEM and DLS analysis revealed particle size, shape and dispersity according to the characteristics described by the manufacturer and confirmed a change in size and PDI depending on media composition.

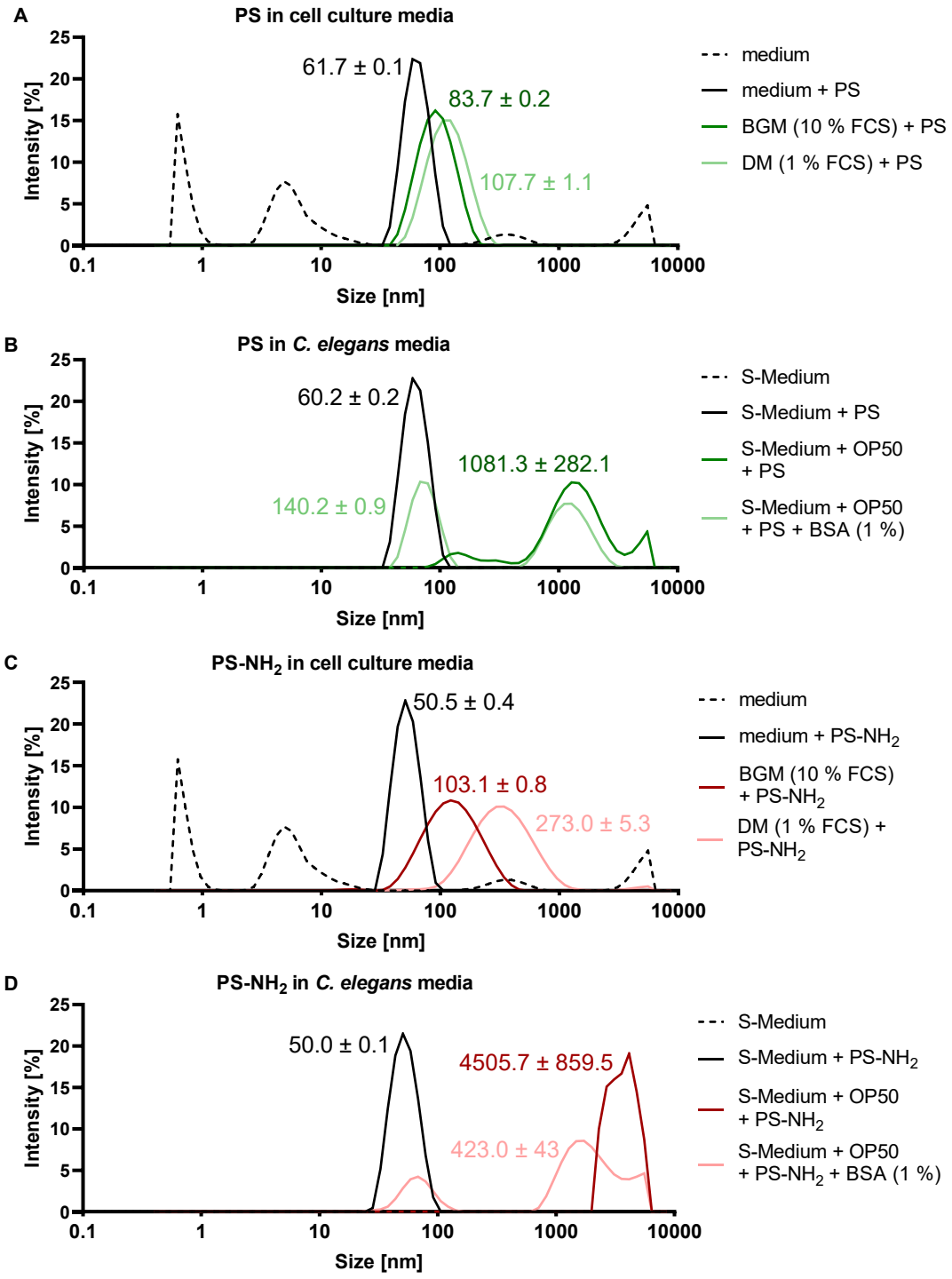

Figure 13. DLS analysis of PS and PS-NH_2 revealed different particle populations. Different peaks in Z-Average of PS and PS-NH_2 under cell culture media **(A, C)** or *C. elegans* growing media S-Medium **(B, D)** shows different population intensities (Y axis) depending on particle sizes in nm (X axis). Dotted lines represent the medium only without any particles added. Characterization of OP50 in S-Medium (with and without BSA) is provided in **Figure S1**. Data shows the average of three replicates per treatment (n=3) and the respective mean of the hydrodynamic diameters.

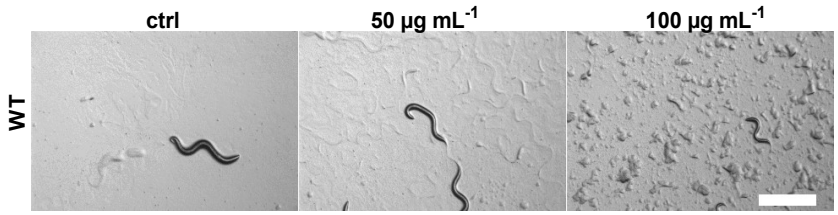

Figure 14. Representative images of 4 days old WT worms after PS-NH_2 treatment from L1 in liquid. Images show a concentration dependent effect on the developmental timing, whereby concentrations higher 100 µg ml^{-1} inhibits animal development at the L1/L2 larval stage. Adding high concentrations (100 µg mL^{-1}) of PS-NH_2 under liquid culture conditions without adding 1 % BSA leads to accumulation of particles and thereby disturbing further analysis.

The ζ-potential describes the electro kinetic potential of a nanoparticle in solution. PS particles present a negative ζ-potential in both, cell culture medium and S-Medium (-36 ± 1 mV in medium; - 60 ± 1 mV in S-Medium), while the potential is less negative in BGM (-15 ± 2 mV) and DM (-14 ± 1 mV) as well as in S-Medium with OP50 containing BSA (1 %) (-16 ± 1) or without BSA (-17.7 ± 0.4 mV) **(Figure 15 A – C,** dashed bars**)**. In contrast, PS-NH_2 particles initial ζ-potential in medium and S-Medium is positive (19 ± 2 mV in media; 46 ± 4 mV in S-Medium) but turned negative in media containing proteins or OP50 (-11 ± 1 mV in BGM; -9.6 ± 0.4 mV in DM; -5.1 ± 0.5 mV S-Medium + OP50; -10 ± 1 mV in S-Medium + OP50 + BSA (1 %) **(Figure 15 C – D).** The exposure of particles to different media can lead to changes in their properties, for example through the formation of a protein corona or other physical forces. In addition, different exposure times are to be investigated, which is why the particles were characterized after 4 and 24 h in the respective medium. **Figure 15** shows no significant change of Z-Average (bars), PDI (dots) or ζ-potential (dashed bars) over time.

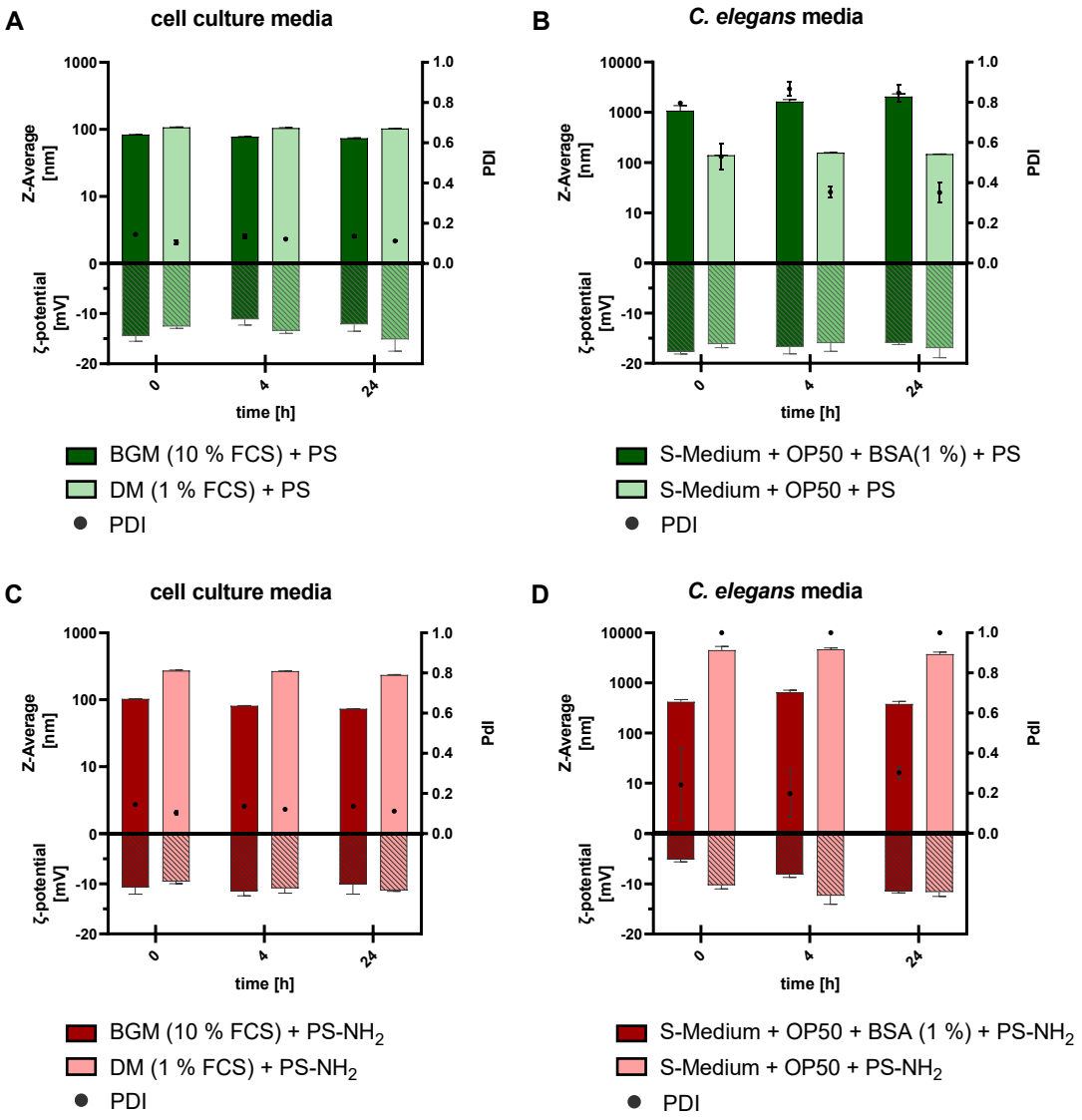

Figure 15. DLS analysis of PS and PS-NH₂. Characterization of particles in mammalian cell culture conditions of SH-SY5Y cells **(A, C)** and *C. elegans* liquid culture conditions **(B, D)** to identify the Z-Average, PDI and ζ-potential. Regarding different timepoints (X axis; 0, 4 and 24 h), the positive range on the Y axis shows the size in nm (left) and the size distribution (right), while the negative range shows the charge in mV. Data shows the average of three measurements per treatment (N=3).

The following table summarizes all the results regarding the Z-Average, PDI and ζ-potential achieved with DLS analysis under SH-SY5Y cell culture conditions and *C. elegans* liquid media as well as with PS and PS-NH_2 particles.

Table 4. Summary of DLS analysis of PS and PS-NH_2. Physicochemical characterization of PS and PS-NH_2 in millipore water, mammalian cell culture conditions and *C. elegans* liquid culture conditions. Data shows the average ± SD of three replicates per treatment (n=3).

	PS		
	Z-Average [nm]	**PDI**	**ζ-potential [mV]**
Water	61 ± 1	0.01 ± 0.01	-52 ± 1
Medium (DMEM/F12) [a)]	61.7 ± 0.1	0.02 ± 0.01	-36 ± 1
BGM (10 % FCS) [a)]	83.7 ± 0.2	0.10 ± 0.01	-15 ± 2
DM (1 % FCS) [a)]	108 ± 1	0.10 ± 0.01	-14 ± 1
S-Medium [b)]	61.8 ± 0.4	0.02 ±0.01	- 60 ± 1
S-Medium (OP50) [b)]	1081 ± 282	0.5 ± 0.1	-17.7 ± 0.4
S-Medium (OP50, 1 % BSA) [b)]	140.2 ± 0.9	0.80 ± 0.01	-16 ± 1
	PS-NH_2		
	Z-Average [nm]	**PDI**	**ζ-potential [mV]**
Water	51 ± 1	0.04 ± 0.0	49 ± 1
Medium (DMEM/F12) [a)]	50.5 ± 0.4	0.03 ± 0.01	19 ± 2
BGM (10 % FCS) [a)]	103 ± 1	0.262 ± 0.007	-11 ± 1
DM (1 % FCS) [a)]	273 ± 5	0.29 ± 0.03	-9.6 ± 0.4
S-Medium [b)]	50.4 ± 0.2	0.037 ± 0.003	46 ± 4
S-Medium (OP50) [b)]	4506 ± 860	0.2 ± 0.2	-5.1 ± 0.5
S-Medium (OP50, 1 % BSA) [b)]	423 ± 43	1	-10 ± 1

[a)] Mammalian cell culture condition; [b)] *C. elegans* condition

Turbiscan analysis reveals no sedimentation of PS and PS-NH_2 under cell culture conditions

The sedimentation capacity of the particles in BGM and DM was evaluated using Turbiscan analysis. To this extent, the particles were prepared in either BGM or DM and after upright placing the machine multiple light scattering (MLS) was used to send photons through the sample and to detect the back scattering. The back scatter is directly

related to the particle size and therefore an indicator for size and stability related alterations in the sample.

While treating the worms in liquid, the particles were under continuously shaking compared to the static exposure in cell culture conditions. Therefore, the sedimentation capacity of the particles was only evaluated in BGM and DM. The results shown in **Figure 16** presents the mean back scatter in percent of **(A)** PS in BGM or DM and **(B)** PS-NH_2 in BGM or DM. The X axes present the height of the reaction tube, beginning at the bottom (from left to right – bottom to top). Different timepoints were measured, while it was started with smaller intervals of 5 min to longer timepoints of 15 min. In total, 230 scans were taken per 48 h measurement, which is the longest timepoint used for initial cytotoxicity testing.

In summary, the Turbiscan analysis revealed that neither PS nor PS-NH_2 sediment nor flocculate over time **(Figure 16)**.

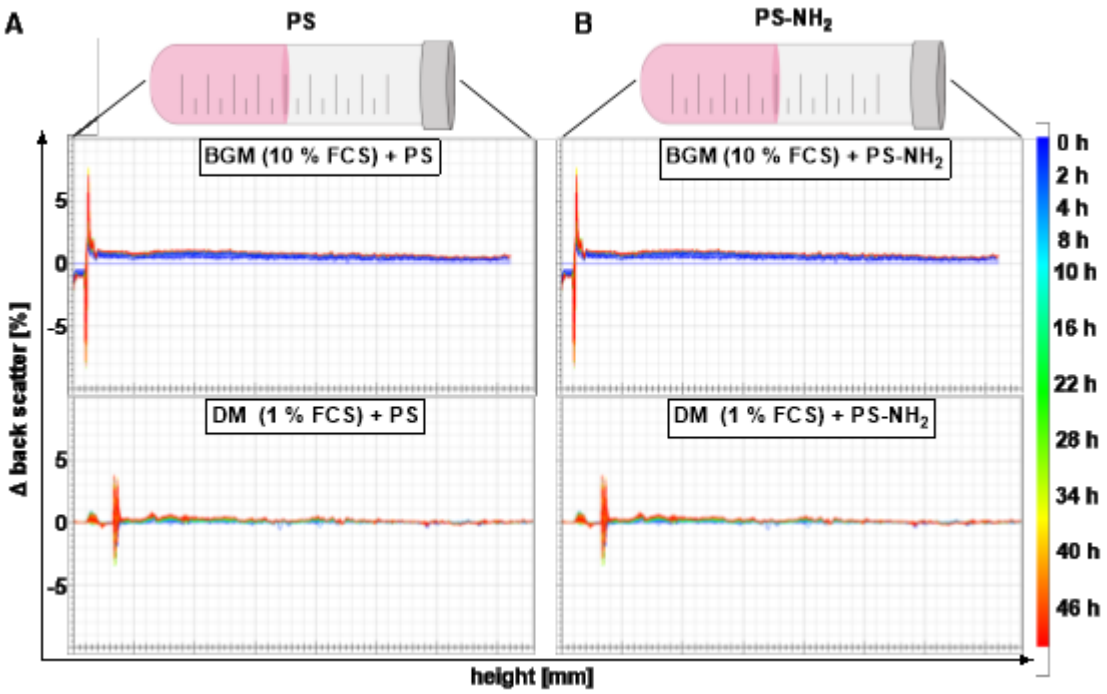

Figure 16. Sedimentation analysis of PS and PS-NH_2 in cell culture media. A) PS in BGM or DM, **B)** PS-NH_2 in BGM or DM. Analysis confirms that particles do not sediment within 48 hours. Analysis was done with TURBISCAN LAB (Formulaction, France) and analyzed with TurbiSoft LAB software 2.2.0.82.

4.2 *In vitro* analysis of PS NPs in undifferentiated cells

PS-NH_2 particles decreases cell viability in HEK293 APP695 cells

To investigate the effects of the particles *in vitro* and on acute toxicity, HEK293 cells stably overexpressing APP695 were used. This cell line is widely used for toxicology studies and due to APP overexpression it is also suitable to unravel alterations relevant for AD pathology.[176] Cells were treated with different concentrations of PS, PS-NH_2), yellow-green fluorescent PS (PS-YG; 50 nm) and PVC (> 100 nm; included as additional plastic resin) particles for 24 hours and a tetrazolium based cell viability assay (WST-1 assay) was done. In this assay, the mitochondrial dehydrogenase catalyzes the reduction of the light red tetrazolium salt to dark red formazan, which is revealed through colorimetric measurement. The determined metabolic activity of the cells is proportional to the number of viable cells (metabolically active cells).[177]

The results show a concentration dependent decrease of cell viability after 24 h treatment with PS-NH_2 but not with PS, PS-YG or PVC **(Figure 17)**.

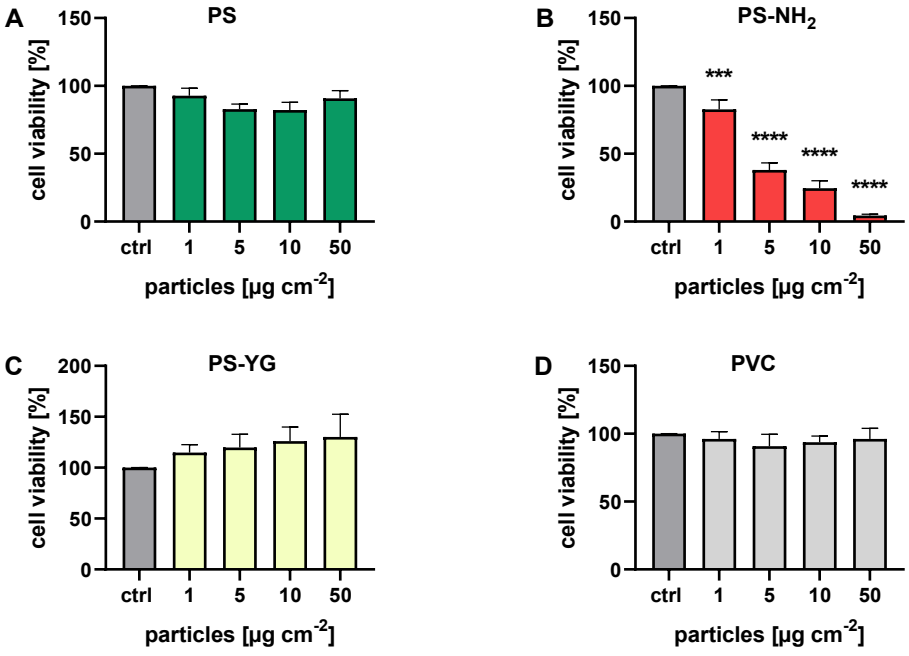

Figure 17. PS-NH_2 induce cytotoxicity after 24 h treatment in HEK293 APP695. Cells were exposed to **A)** plain PS NPs (PS), **B)** aminated PS NPs (PS-NH_2), **C)** fluorescent PS NPs (PS-YG) and **D)** PVC NPs (PVC) for 24 h and a WST-1 assay was carried out to measure particle toxicity. The data shows mean of three independent experiments (N=3) performed in 4 replicates (n=4) + SEM and values are normalized on control (w/o treatment), ordinary one-way ANOVA indicates differences between treatment and ctrl (*** $p < 0.001$, **** $p < 0.0001$).

To further investigate more disease-specific neuronal parameters and specifically Aβ production after acute particle treatments, an ELISA assay was done. Increased production of Aβ is indeed one of the main pathogenetic markers of AD, which can lead to accumulation of intracellular toxic oligomers and the development of extracellular senile plaques ultimately leading to neuronal dysfunction and death. The APP is processed by the secretases β and γ, resulting in Amyloid β 1 – 40 and Amyloid β 1 – 42, whereby the Amyloid β 1 – 42 is more often found in early stages and Amyloid β 1 – 40 in late stages of the disease.[101,178] Therefore, in order to investigate if PS NPs can also promote the formation of Aβ peptides, the supernatant of cells exposed to non-lethal concentrations of particles was used to quantify Aβ peptides by ELISA. The results in **Figure 18** show the percentage of Aβ secretion in the conditioned medium normalized to the cell's total protein and untreated control. The data indicates no significant alteration in the secretion of Aβ 1 – 40 or Aβ 1 – 42 in the conditioned medium of HEK293 APP695 cells in any tested condition, with a slightly increased secretion of Aβ 1 – 42 upon PS-NH_2 treatment.

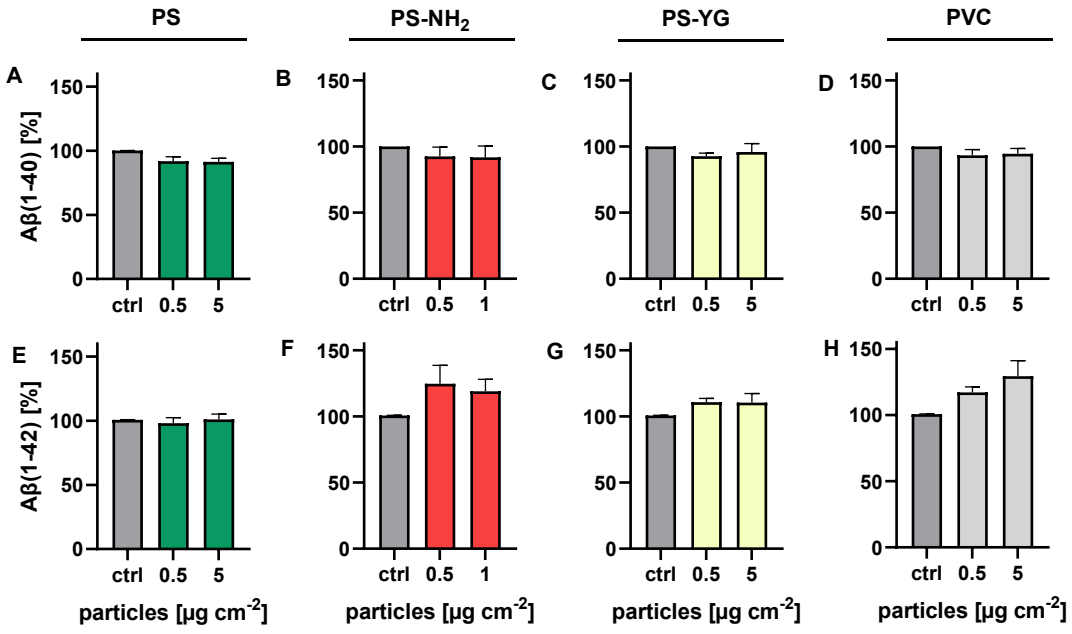

Figure 18. Plastic NPs exposure did not alter Aβ 1 – 40 or Aβ 1 – 42 secretion in the conditioned medium of HEK293 APP695. Cells were treated with **A, E)** PS, **B, F)** PS-NH_2, **C, G)** PS-YG and **D, H)** PVC for 24 h and the supernatant was used for ELISA assays against Aβ 1 – 40 **(A – D)** and Aβ 1 – 42 **(E – H).** The data shows mean of three independent experiments (N=3) performed with 4 replicates (n=4) + SEM. Values are normalized on whole protein lysates and relative to control (w/o treatment), ordinary one-way ANOVA indicates no differences between treatment and ctrl.

PS-NH_2 particles decreases cell viability and promote Aβ 1 – 42 secretion in neuroblastoma SH-SY5Y cells

To further investigate particle acute toxicity, a neuroblastoma cell line SH-SY5Y was used. This cell line is one of the most common cell lines in the field of neuronal cell biology and presents a great tool when it comes to neurotoxicology.[123] Similar to the effect observed in HEK293 APP695 cells, only aminated particles reduced the cell viability in a dose-dependent manner **(Figure 19)**. Thereby, treatment with 1 µg cm^{-2} reduces the cell viability less than 10 %, while treatment with 50 µg cm^{-2} killed almost 100 % of the cells.

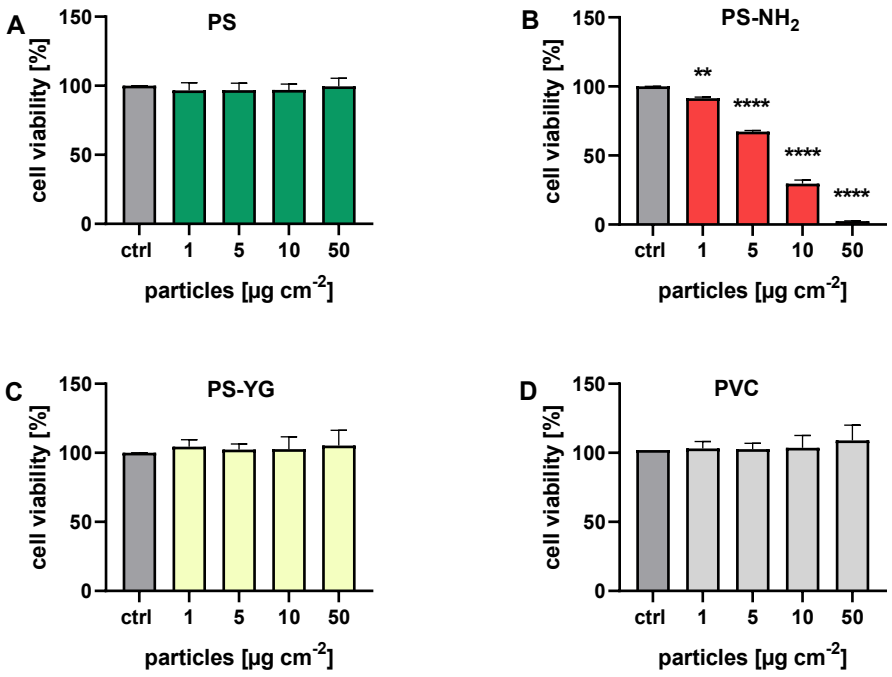

Figure 19. PS-NH_2 induced cytotoxicity after 24 h treatment in SH-SY5Y cells. Cells were seeded in 96-well plates and exposed to **A)** PS, **B)** PS-NH_2, **C)** PS-YG and **D)** PVC for 24 h and a WST-1 assay was carried out to measure particle toxicity. The data shows mean of three independent experiments (N=3) performed in 4 replicates (n=4) + SEM and values are normalized on control (w/o treatment), ordinary one-way ANOVA indicates differences between treatment and ctrl (** $p < 0.01$, **** $p < 0.0001$).

SH-SY5Y cells endogenously express all three major isoforms of APP including APP_{770}, APP_{751} and APP_{695}.[179] Therefore, also SH-SY5Y cells were used to investigate the effect of plastic NPs on APP processing and secretion via ELISA assay. **Figure 20** shows a significant increased secretion of Aβ 1 – 42 in the conditioned medium after PS-NH_2 exposure (0.5 and 1 µg cm^{-2}) only.

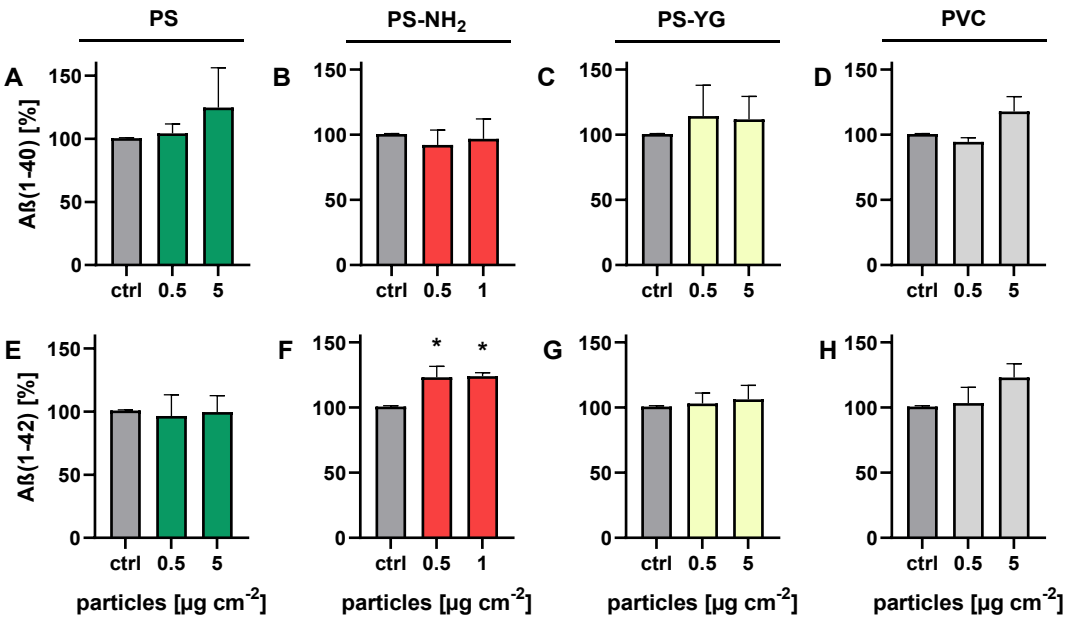

Figure 20. PS-NH_2 treatment increases Aβ 1-42 secretion in the conditioned medium of SH-SY5Y cells. SH-SY5Y cells were treated with **A, E)** PS, **B, F)** PS-NH_2, **C, G)** PS-YG and **D, H)** PVC for 24 h and the supernatant was used for ELISA assays to quantify Aβ 1 – 40 (A – D) and Aβ 1 – 42 (E – H) secretion. The data shows mean of three independent experiments (N=3) performed with 4 replicates (n=4) + SEM. Values are normalized on whole protein lysates and relative to control (w/o treatment), ordinary one-way ANOVA indicates differences between treatment and ctrl (* $p < 0.05$).

Besides dose-response, time-course experiments were carried out to check particle effects on cell viability at earlier and later time points, namely 1, 2, 4, 24 and 48 hours after particle treatment. The latest time point was chosen since SH-SY5Y cells show a significant longer duplication time of ~ 35 h compared to HEK293 cells (~ 23 h), as shown in **Figure 21**. Additionally, an intermediate concentration of 25 µg cm^{-2} was included when checking early time points. Most importantly, I was planning to check cell viability also in differentiated, less metabolically active cells. Therefore, I decided to validate results from WST-1 assay, with a more sensitive cell viability assay, the Resazurin assay.

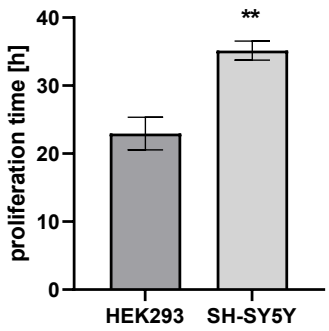

Figure 21. Proliferation time of HEK293 and SH-SY5Y cells. Cells were maintained in media containing 10 % FCS and proliferation time was estimated within different time points and seeding concentrations. The data shows mean of three independent experiments (N=3) performed in 4 replicates (n=3) + SEM. Unpaired and two-tailed t-test indicates differences between both cell lines (** $p < 0.01$).

In contrast to the previously used WST-1 assay, the mitochondrial dehydrogenase catalyzes the reduction of the blue colored Resazurin salt to the pinkish Resorufin. Due to the great colorimetric spectra from blue to pink (compared to WST-1 assay: light red to dark red) and a fluorescence emission, this cell viability assay is very sensitive and enables the usage in even less metabolic active cells (e.g. differentiated cells). **Figure 22 A, C E, G** and **I** show that PS particles do not influence the cell viability in SH-SY5Y cells, neither with increasing concentrations, nor over time. Contrary, treatment of the cells with PS-NH_2 for 1 h leads to a significant decrease of cell viability with concentrations higher 25 µg cm^{-2} **(Figure 22 B)**. In addition to the concentration dependent effect, PS-NH_2 exposure for 2 and 4 h resulted in a time dependent decrease of cell viability: While treatment with 25 µg cm^{-2} for 1 h decreased the cell viability up to 50 %, almost all cells were dead after 4 h treatment. The results gained from the Resazurin assay after 24 h treatment of PS and PS-NH_2 are comparable to the results gained from WST-1 assay and clearly show the concertation dependent decreased cell viability for PS-NH_2, only. Finally, treatment for 48 hours shows a time-dependent decreased cell viability, especially after treatment with 5 µg cm^{-2}: While after 24 h the cell viability is decreased up to ~ 75 %, after 48 h treatment almost 50 % of the cells died **(Figure 22 H, J)**.

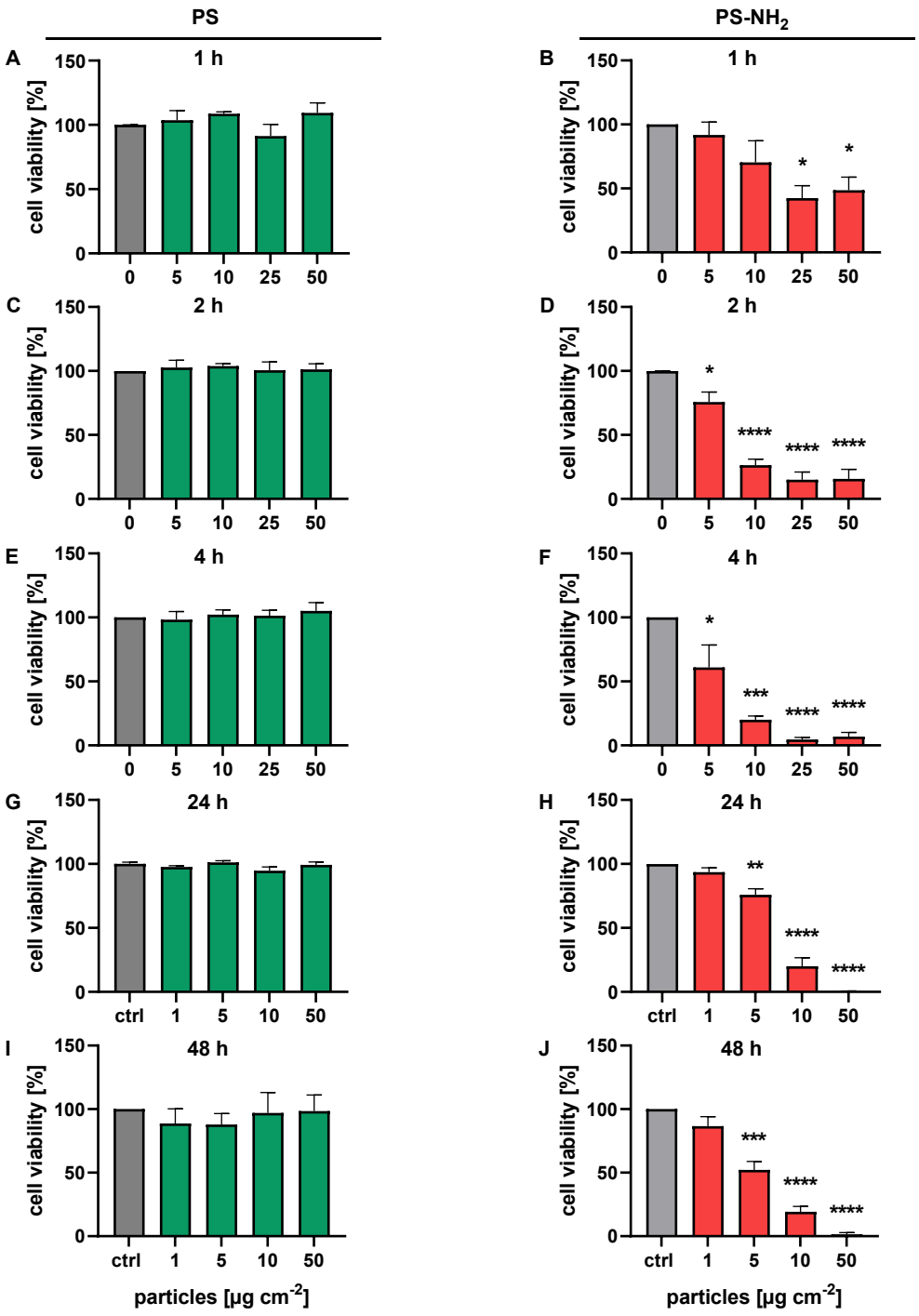

Figure 22. PS-NH_2 treatment decreased cell viability in SH-SY5Y cells in a concentration and time-dependent manner. Resazurin based assay in undifferentiated SH-SY5Y cells treated with PS **(A, C, E, G and I)** and PS-NH_2 **(B, D, F, H and J)** for 1, 2, 4, 24 and 48 h. Data show the mean of (n=36) replicates in (N=3) independent experiments + SEM and values are normalized on control (w/o treatment), ordinary one-way ANOVA indicates differences between treatment and ctrl (*p < 0.05, ** p < 0.01, *** p < 0.001, **** p < 0.0001).

PS-NH_2 induces late apoptotic/necrotic cell death

To start investigating possible molecular mechanisms behind particles-induced toxicity, different flow cytometry-based assays were utilized to specifically assess their effects on cell death and mitochondrial damage. To this extent, undifferentiated SH-SY5Y cells were treated with different concentrations of PS and PS-NH_2 for 1, 2 and 4 hours, and were stained with Annexin V coupled to fluorescein isothiocyanate (FITC) and Propidium Iodide (PI). Annexin V is a phospholipid binding protein with a high affinity for the protein phosphatidylserine, which is located in the intracellular membrane surface.[180] During apoptosis, the phosphatidylserine is repositioned to the extracellular space due to membrane shifting and able to be bind by Annexin V. PI is instead a DNA-binding dye that only penetrates cells with nonintact membranes, thereby only necrotic or late apoptotic cells can be positive for PI. Cells undergoing apoptosis can thereby be detected with Annexin V coupled to a fluorophore.

While preparing the cell suspensions for measuring, all cells (including floating cells as well as cells still attached to the well plates) were collected. Moreover, to ensure that apoptotic and other nonviable cells were not excluded from flow cytometer analysis, the gating was adjusted with unstained/untreated cells and stained/treated cells. **Figure 23** shows the gating strategy in unstained and untreated **(A)** and stained and treated cells **(B)**, whereby debris was excluded in forward scatter area (FSC-A) against sideward scatter area (SSC), including the populations of apoptotic/necrotic cells (red) and viable cells (blue). Singlets (blue) and doublets (orange) were detected in FSC area versus height and the gate was set including viable singlets and apoptotic/necrotic cells (red). Finally, stained cells were distributed in dot plots showing FITC signal (X axis) and phycoerythrin (PE) signal (Y- axis), while viable cells remain unstained (blue) and apoptotic/necrotic cells stained positive for PE and FITC.

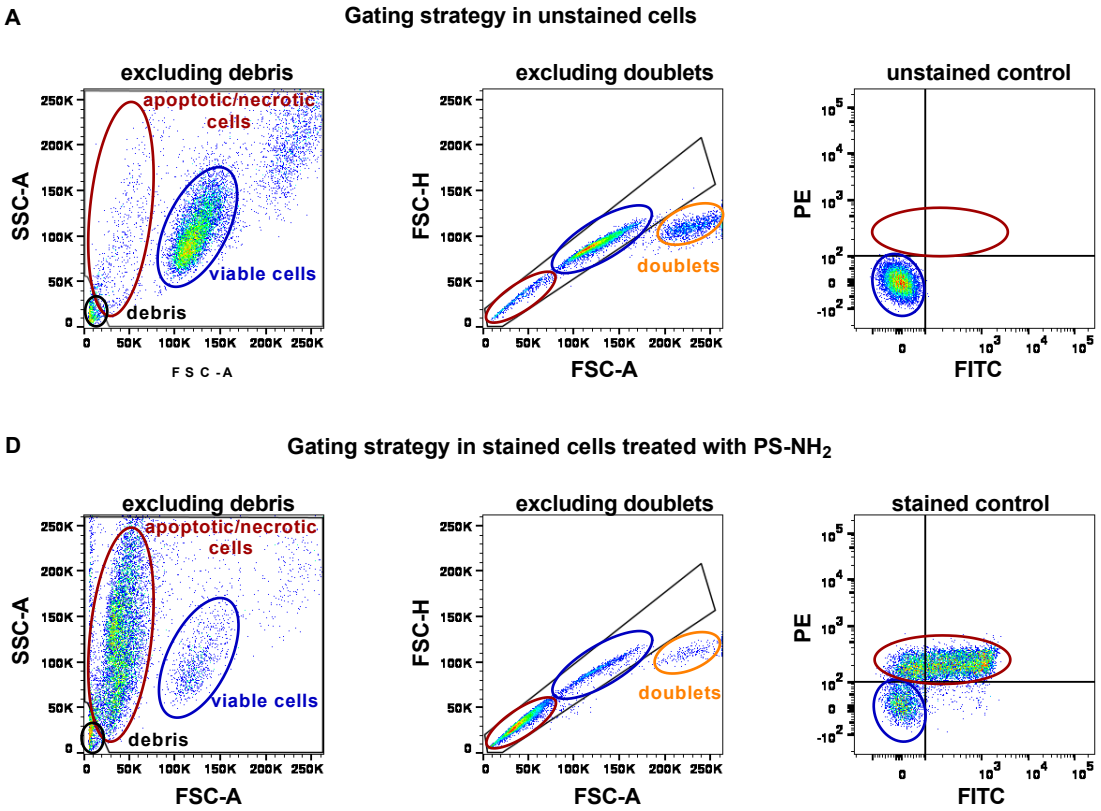

Figure 23. Gating strategy for flow cytometry analysis. A) Representative images in of unstained and untreated cells with big viable population (blue) and single apoptotic/necrotic events (red). Debris (black) and doublets (orange) were excluded. **B)** Stained and treated (25 µg cm^{-2} $PS\text{-}NH_2$ for 4 h) cells in with small viable population (blue) and big population of apoptotic/necrotic events (red). Debris (black) in FSC-A vs SSC-A and doublets (orange) in FSC-A vs. FSC-H were excluded.

Due to the fact that Annexin V is coupled to FITC and counterstaining of necrotic and late apoptotic cells was done with Propidium Iodide (PI), slight compensation was necessary. **Figure 24** shows the compensated (black) and uncompensated (cyan) events in the stained control (A) and in stained and treated sample (B; 25 µg cm^{-2} $PS\text{-}NH_2$ for 4 h).

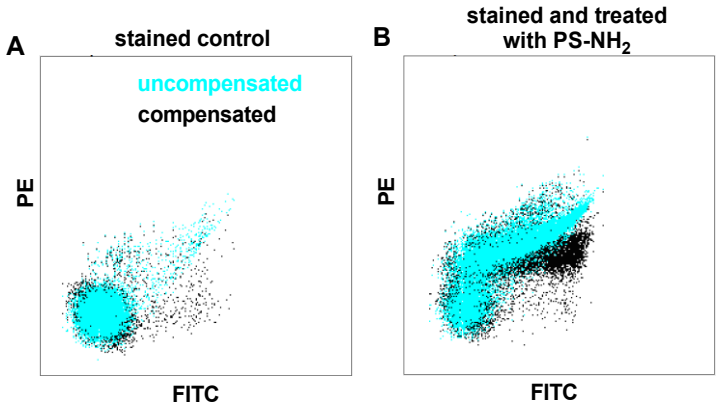

Figure 24. Compensation of Annexin V-FITC and PI. A) compensated (black) and uncompensated (cyan) events in **A)** the stained control and in stained and **B)** treated sample (25 µg cm^{-2} $PS\text{-}NH_2$ for 4 h). Compensation in PE channel – 35 % FITC.

After setting the gates and establishing a compensation matrix, different controls were used to divide the different populations in the respective quadrants of the dot plot.

Single stainings in untreated cells (**Figure 25 A,** upper panels) with PI and Annexin V-FITC were done and measured in FITC and Phycoerythrin (PE) channel. As mentioned above, viable cells, like unstained cells, remain in the unstained population because they are neither stained with Annexin V-FITC nor PI (FITC-/PE-) (bottom left quadrant of the dot plots). In a normal, untreated cell culture, most cells are therefore FITC and PE negative (FITC-/PE-). However, in a running cell culture a small number of cells is always either early apoptotic (FITC+/PE-) (bottom right) or even late apoptotic or necrotic (FITC+/PE+ and FITC-/PE+) (top) like in the single Annexin V-FITC and PI staining in **Figure 25 A.**

Four controls, hydrogen peroxide (H_2O_2), ethanol (EtOH), antiFAS antibody and Staurosporine were used, all known inducers of cell death.[181–183] Treatment for 24 h of 250 µM H_2O_2 impairs almost the whole population and shifted from viable cells to apoptotic cells (FITC+/PE-) and a majority to late apoptotic/necrotic cells (FITC+/PE+). Ethanol (EtOH) as well as the antiFAS antibody slightly induced cell death with an increase in apoptotic as well as in late apoptotic/necrotic dell death and Staurosporine treatment resulted in a mixed population of viable, early apoptotic and late apoptotic/necrotic cells (**Figure 25)**.

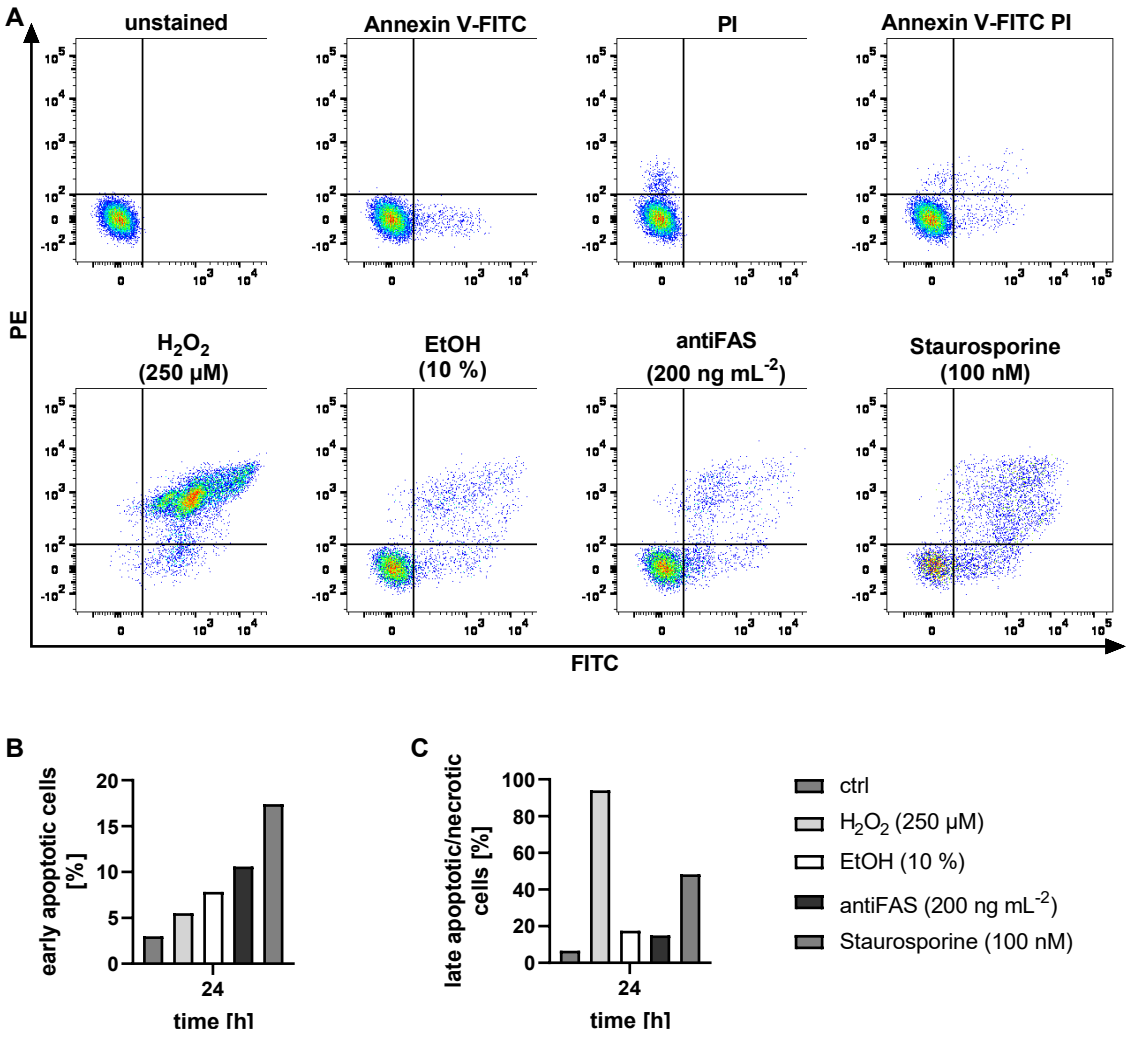

Figure 25. Hydrogen Peroxide, ethanol, antiFAS antibody and Staurosporine induce cell death. A) Representative FACS dotplots of untreated cells stained, unstained, stained with Annexin V-FITC, stained with FITC or double stained with Annexin V-FITC and PI, as well as stained cells treated with different controls (Hydrogen Peroxide, Ethanol, anti FAS Antibody and Staurosporine). Cells were acquired in FITC (X axis) channel PE (Y axis) channel. Calculation of **B)** early apoptotic cells or **C)** late apoptotic/necrotic cells in different controls treatments in percent over time.

Based on the results gained from cell viability assays, cells were treated with 50 µg cm^{-2} PS for 1, 2 or 4 h to investigate if there might be some early events of apoptosis or necrosis, which could not be detected with cell viability assays before. **Figure 26** shows representative **(A)** and the calculated percentages ((**B**) and (**C**)) of the cell population clearly indicating no cell death at any time point.

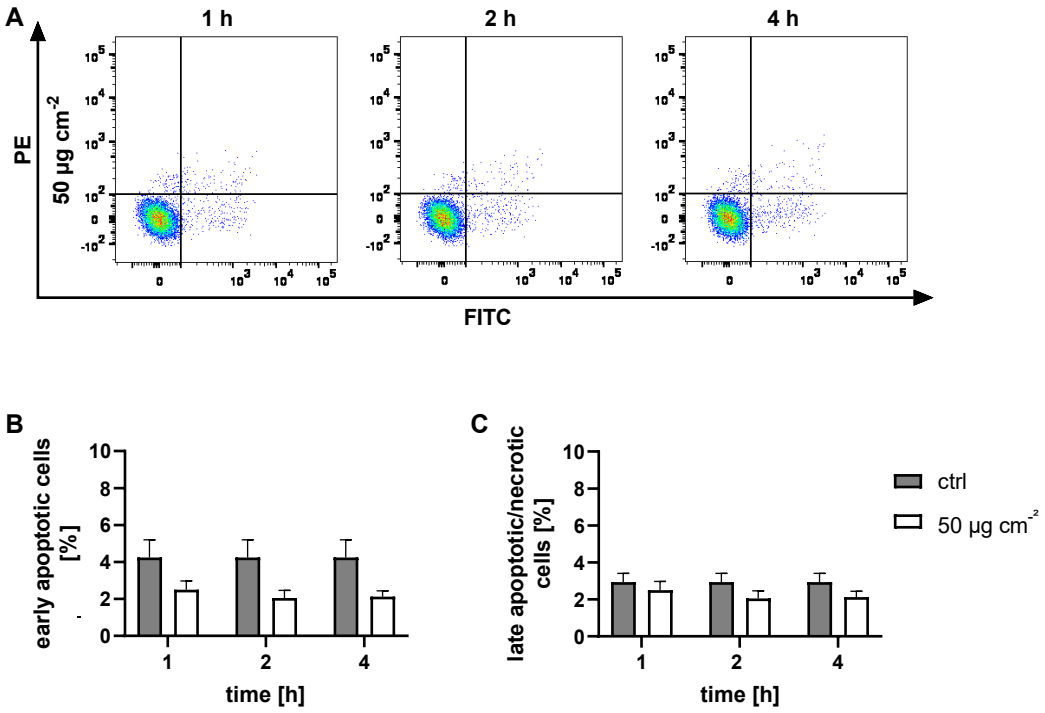

Figure 26. PS does not induce cell death. A) Representative FACS dot plots of cells treated with 50 µg cm^{-2} PS for 1, 2 and 4 h acquired in FITC (Y axis) and PE (Y axis) channel. **B)** Percentage of early apoptotic cells after PS treatment and **C)** percentage of late apoptotic/necrotic cells after PS treatment over time. Data show the mean of three (N=3) independent experiments + SEM and ordinary one-way ANOVA indicates no differences between treatment and ctrl.

In parallel, SH-SY5Y cells were treated with 5, 10 and 25 µg cm^{-2} PS-NH_2 for 1, 2 and 4 hours. PS-NH_2 induced cell death in a dose and time dependent manner, while a concentration of 25 µg cm^{-2} killed more than a third of the cells already after only 2 hours (**Figure 27).** In addition to the time and concentration dependent decrease of viable cells**,** **Figure 27 B** and **C** clearly indicate that PS-NH_2 do not change the amount of early apoptotic cells but late apoptotic/necrotic cells, significantly.

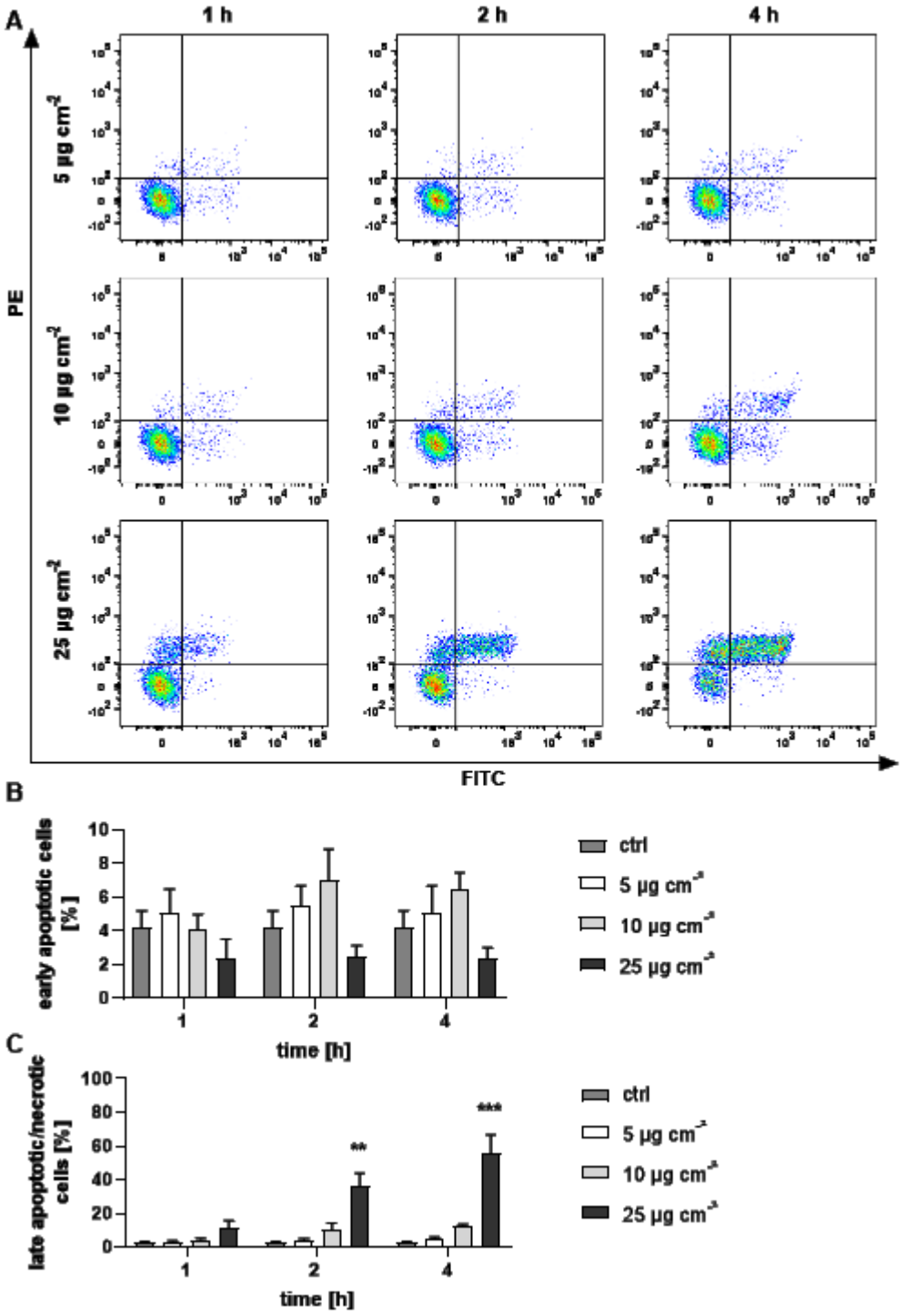

Figure 27. PS-NH_2 induces cell death in time and concentration dependent manner. A) Representative FACS dot plots of cells treated with 5, 10 and 25 µg cm^{-2} PS-NH_2 for 1, 2 and 4 h acquired in FITC (X axis) and PE (Y axis) channel. **B)** Percentage of early apoptotic cells after PS-NH_2 treatment and **C)** percentage of late apoptotic/necrotic cells after PS-NH_2 treatment over time. Data show the mean of three (N=3) independent experiments + SEM and ordinary one-way ANOVA indicates differences between treatment and ctrl. (** $p < 0.01$, *** $p < 0.001$).

When the cells were instead treated with 1, 5 and 25 µg cm^{-2} for 24 h no increase in early apoptotic cell death could be detected (**Figure 28.)**. However, consistent with results gained from cell viability assays, the amount of late apoptotic and necrotic cells is increased up to 20 % after treatment with 5 µg cm^{-2}.

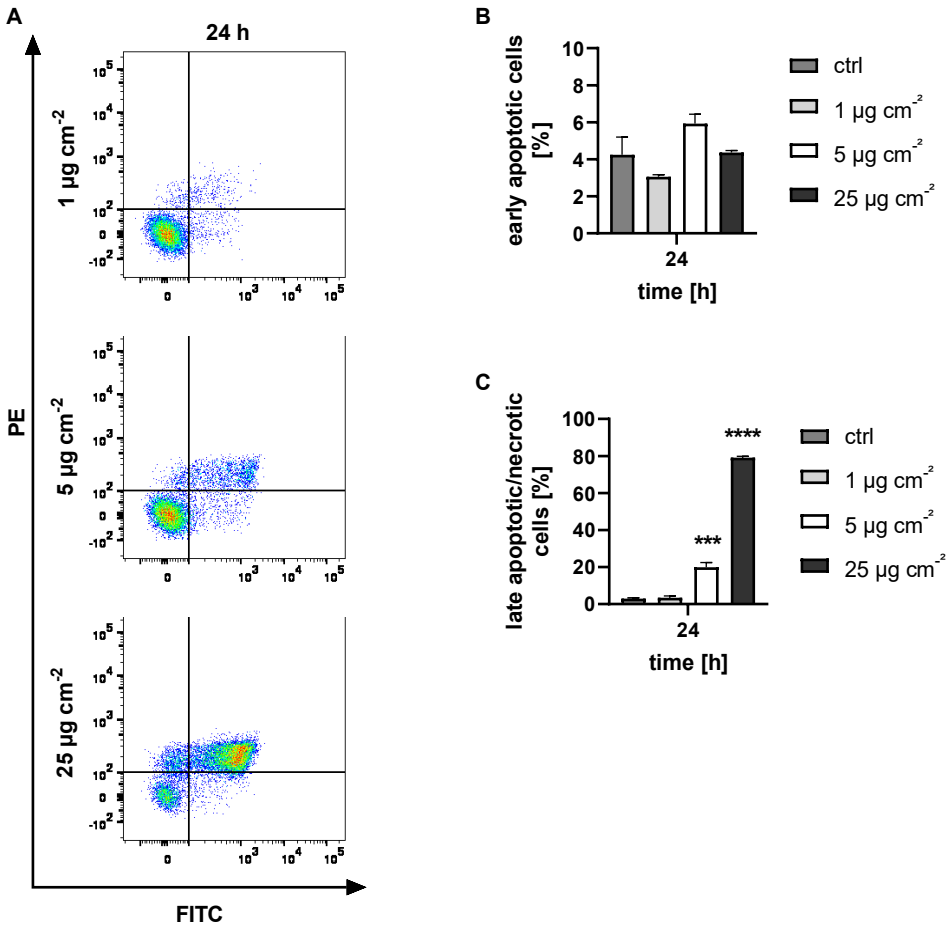

Figure 28. $PS\text{-}NH_2$ induces cell death in concentration dependent manner. A) Representative FACS dot plots of cells treated with 1, 5 and 25 µg cm^{-2} $PS\text{-}NH_2$ for 1, 2 and 4 h acquired in FITC (X axis) and PE (Y axis) channel. **B)** Percentage of early apoptotic cells after $PS\text{-}NH_2$ treatment and **C)** percentage of late apoptotic/necrotic cells after $PS\text{-}NH_2$ treatment over time. Data show the mean of three (N=3) independent experiments + SEM and ordinary one-way ANOVA indicates differences between treatment and ctrl. (*** $p < 0.001$, **** $p < 0.0001$).

PS and $PS\text{-}NH_2$ do not increase production of ROS and mitochondrial ROS

Cytotoxicity and death could be ascribed by particle-inducing mitochondrial damage and production of reactive oxygen species (general and mitochondrial ROS).

ROS (e.g. superoxide anion or hydrogen peroxide) are indeed involved in different physiological processes and it is only when they accumulate in large quantities that the cell can no longer process that stress occurs.[184,185] So far, it is known that the brain is susceptible to increased ROS production and especially oxidative stress plays a key role in age-related neurodegenerative diseases like AD.[186]

To identify increased levels of general ROS, 2',7'-dichlorodihydrofluorescein diacetate (H_2DCF-DA) was used, while mitochondrial ROS (mtROS) was detected with MitoSOX™, both in combination with DAPI staining. The cell permeable H_2DCF-DA enters the cells after esterase cleaves off acetyl groups and DCFH gets oxidized by ROS to DCF resulting in a green fluorescence measured in FITC channel.[185]

In parallel to H_2DCF-DA staining, cells were double stained with mitohydroethidine, better known as MitoSOX™.[187] Contrary to H_2DCF-DA, mitohydroethidine specifically localizes to mitochondria and is oxidized by superoxide to mito-2-hydroxyethidium, exhibiting a red fluorescence.[187,188] The mitochondrial selectivity is based on MitoSOX™ positive charge and the electrochemical potential. This in turn means, that MitoSOX™ staining in cells with depolarized mitochondrial membrane potential (e.g. apoptotic cells) cannot be considered as mitochondrial or superoxide specific.[187] Therefore, DAPI staining was used to exclude dead cells according to Alboni et al. since those would not only interfere with the MitoSOX™ staining but also decrease the DCF signal independently from ROS production.[150]

To establish the staining with DAPI, MitoSOX™ and H_2DCF-DA single stainings were done and acquired in Pacific Blue (**A**), PE (**B**) and FITC (**C**) channels respectively **(Figure 29).**

In **Figure 29 A** DAPI (blue), MitoSOX™ (red) and H_2DCF-DA (green) staining of untreated control cells was analyzed in the DAPI channel. The first blue peak around 0 covering the peak of the unstained control (grey filling), shows that a majority of the cells remained unstained is viable and only a small peak between 10^3 and 10^4 refers to dead cells. The red histogram accurately overlays with the unstained control (grey) indicating no unspecific staining of MitoSOX™ and no need for compensation in the DAPI channel. The same effect can be observed from the green histogram of H_2DCF-DA stained cells acquired in DAPI channel.

Figure 29 B shows the single staining in the PE channel. DAPI staining shows no signal when acquired in PE channel, as well as MitoSOX™ staining. Due to the fact, that under basal conditions no increased mtROS is detected (as expected) a positive control for MitoSOX™ staining was used in the actual experimental setting.

Moreover, no signal should be detected with H_2DCF-DA staining in the PE channel, but the green histogram clearly shows a shifted population indicating H_2DCF-DA signal also in the PE channel and compensation was necessary (**Figure 29 B**). Finally, **Figure 29 C** shows a peak for H_2DCF-DA in the FITC channel at 10^3, indicating a positive staining for H_2DCF-DA, but no interference of DAPI or MitoSOX™ staining.

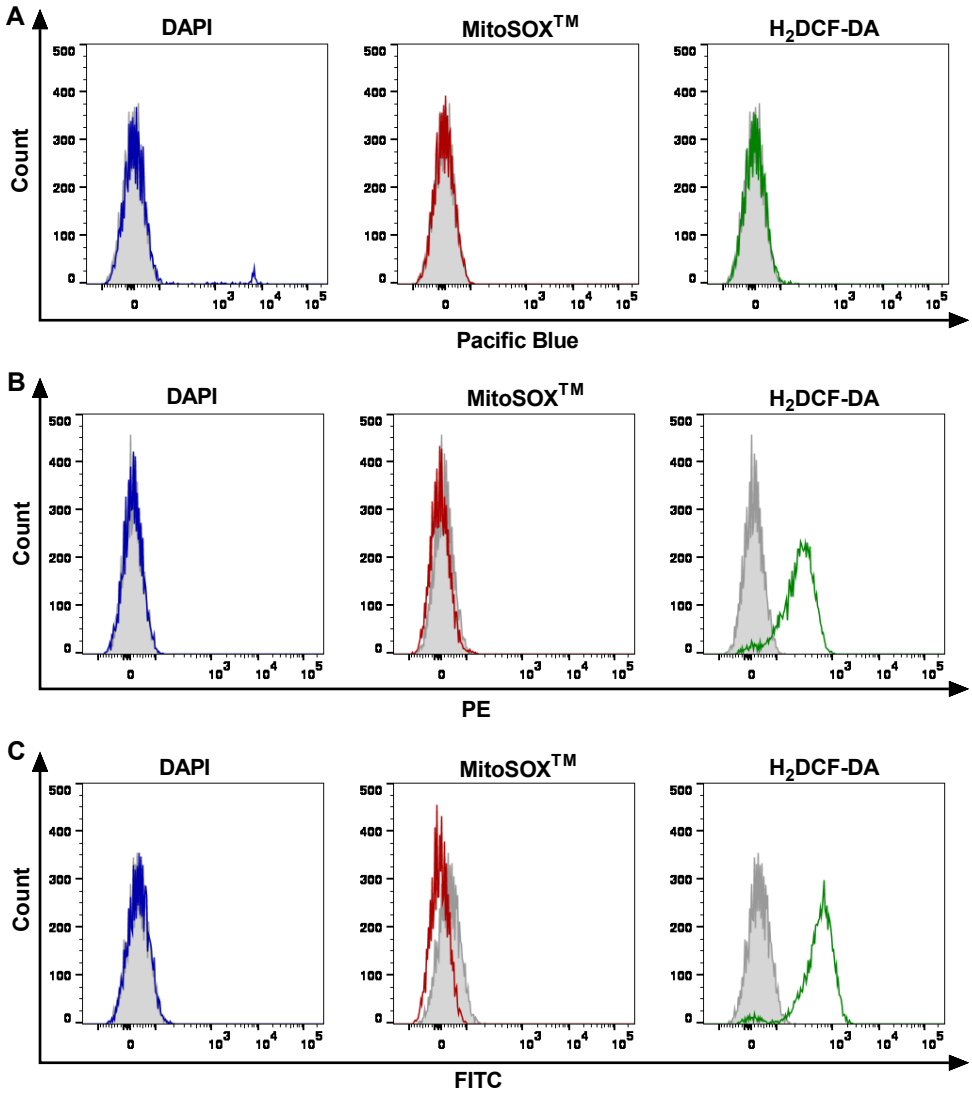

Figure 29. Representative histogram of single staining of DAPI, MitoSOX™ and H_2DCF-DA in **A)** Pacific Blue, **B)** PE and **C)** FITC channel.

Figure 30 shows the compensated (black) versus the uncompensated (cyan) histogram of triple staining with DAPI, MitoSOX™ and H_2DCF-DA. In **Figure 30 A** and **C** it can be seen, that no compensation was necessary in Pacific Blue and FITC channel, but due to the fact that H_2DCF-DA could be also acquired in the PE channel, PE and FITC detection had to be compensated (PE – 42 % FITC).

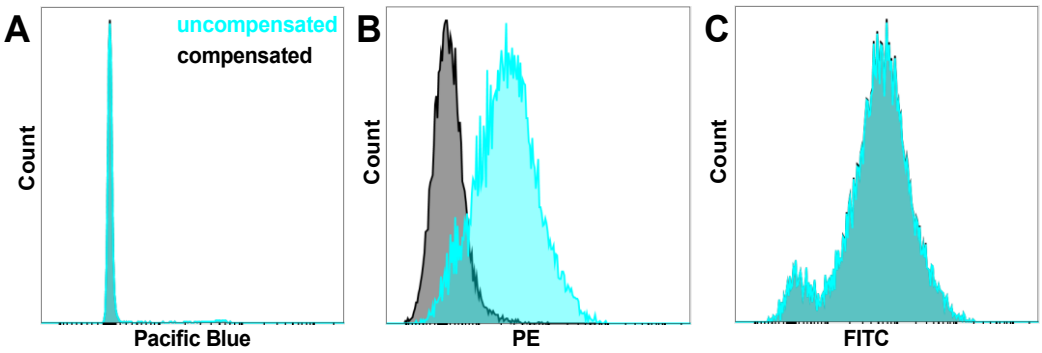

Figure 30. Representative histogram of compensated triple staining with DAPI, MitoSOX™ and H_2DCF-DA in **A)** Pacific Blue, **B)** PE and **C)** FITC channel.

After establishing the single and triple staining in untreated cells (**Figure 29**), ROS production was assessed upon 10, 25 and 50 ug cm^{-2} PS at early time points (2 and 4 hours). The data in **Figure 31** shows the intensity (**A**) and geo mean (**B, C**) in the FITC channel after excluding all cells previously acquired in the DAPI channel to avoid unspecific staining and non-reliable results. Although the bar graphs presenting the geo mean reveals a significant concentration dependent increase in ROS after 2 h exposure, the histogram shows no shift of the peak **(Figure 31 A)**.

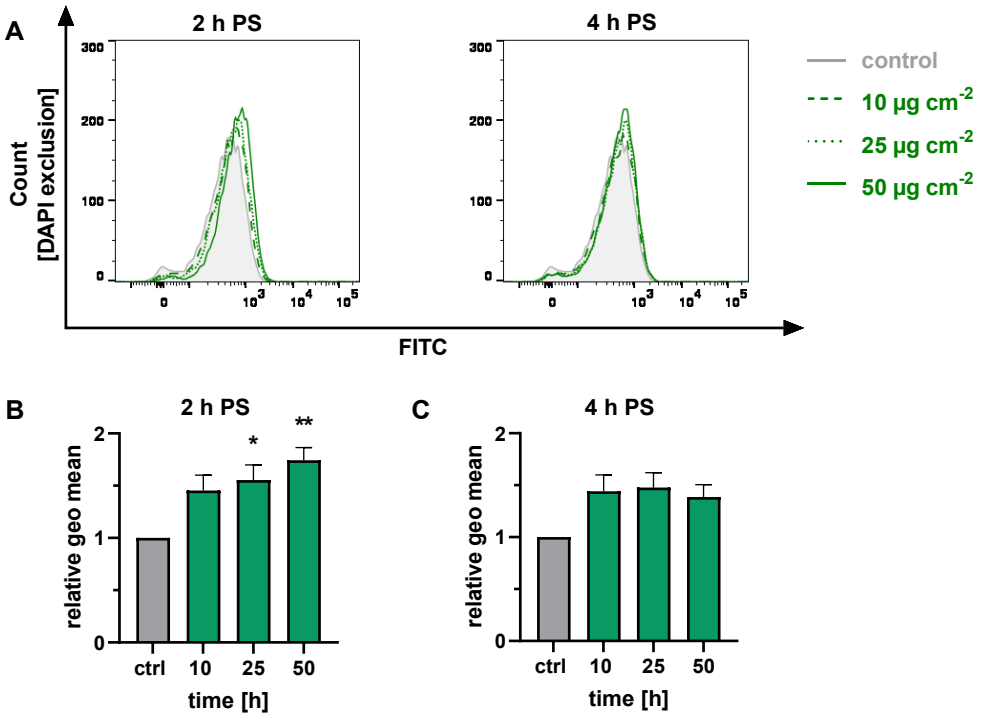

Figure 31. PS slightly increases ROS production in SH-SY5Y cells. A) Representative histogram of triple stained cells treated with 10, 25 and 50 µg cm^{-2} PS for 2 and 4 h acquired in

FITC (X axis) channel after exclusion of DAPI positive events. **B)** Relative geo mean of cells after PS treatment for 2 h and **C)** 4 h acquired in FITC channel and after exclusion of DAPI positive events over time. Data show the mean of three (N=3) independent experiments + SEM and ordinary one-way ANOVA indicates differences between treatment and ctrl. (* $p < 0.05$, ** $p < 0.01$).

In addition to treatment with PS, cells were treated with 5, 10 and 25 µg cm^{-2} PS-NH_2 for 2 and 4 hours, which presumably precede cell death. Similar to PS, **Figure 32 A** shows no significant shift of the peaks, neither after 2 nor after 4 h treatment. However, in **Figure 32 B** a slight but significant increased geo mean after 2 hours exposure to 25 µg cm^{-2} can be seen. Overall, these data indicate a slight increase in general ROS production with both PS and PS-NH_2, thus likely not being responsible for PS-NH_2 induced cytotoxicity.

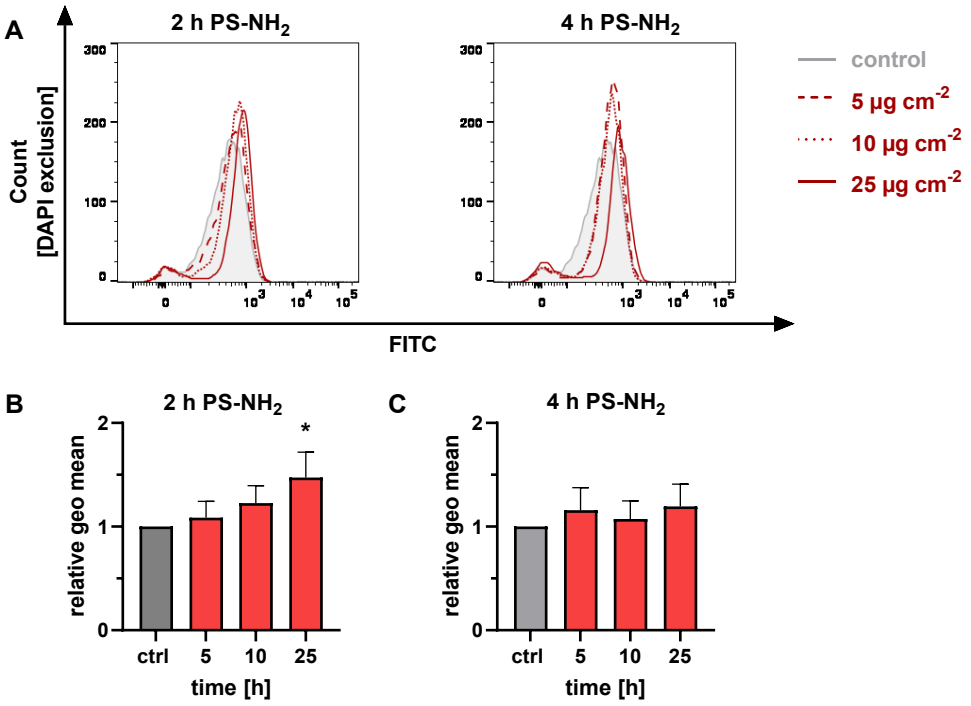

Figure 32. **PS-NH_2 slightly increases ROS production in SH-SY5Y cells. A)** Representative histogram of triple stained cells treated with 5, 10 and 25 µg cm^{-2} PS-NH_2 for 2 and 4 h acquired in FITC (X axis) channel after exclusion of DAPI positive events. **B)** Relative geo mean of cells after PS-NH_2 treatment for 2 h and **C)** 4 h acquired in FITC channel and after exclusion of DAPI positive events over time. Data show the mean of three (N=3) independent experiments + SEM and ordinary one-way ANOVA indicates differences between treatment and ctrl. (* $p < 0.05$).

In parallel to ROS measurement, the induction of mtROS was investigated. The cells were treated as described above and acquired in the PE channel. Differently from

H_2DCF-DA, which staining could be clearly detected compared to unstained cells, the endogenous level of detected MitoSOX™ in SH-SY5Y cells was quite low and could not be distinguished by the unstained control cells. Therefore, **Figure 33** B illustrates the effect of 30 min treatment with 10 µM Antimycin A (AMA), an antibiotic known to bind to mitochondrial complex III in turn blocking the electron transport chain and increasing mtROS production and used as a positive control for the staining.[189] To further proof that the detected signal is not based on cell death but specific of oxidative stress, DAPI staining was again used to exclude dead cells and pretreatment for 18 h N-acetylcysteine (NAC) was done prior treatment with AMA. NAC is a well-known antioxidant and the pretreatment with 5 µM of NAC for 18 h could prevent the generation of mtROS, what is indicated by the peaks shifted from AMA treatment (dotted) to AMA+NAC treatment (black), which is almost similar to the control (grey).[190]

Figure 33 B, C and **D** show the results of SH-SY5Y cells exposed to 10, 25 and 50 µg cm^{-2} PS for 2 and 4 hours. Compared to the significant difference of AMA to the control as well as AMA to double treatment with NAC **(Figure 33 C – D)**, no effect could be observed after PS exposure.

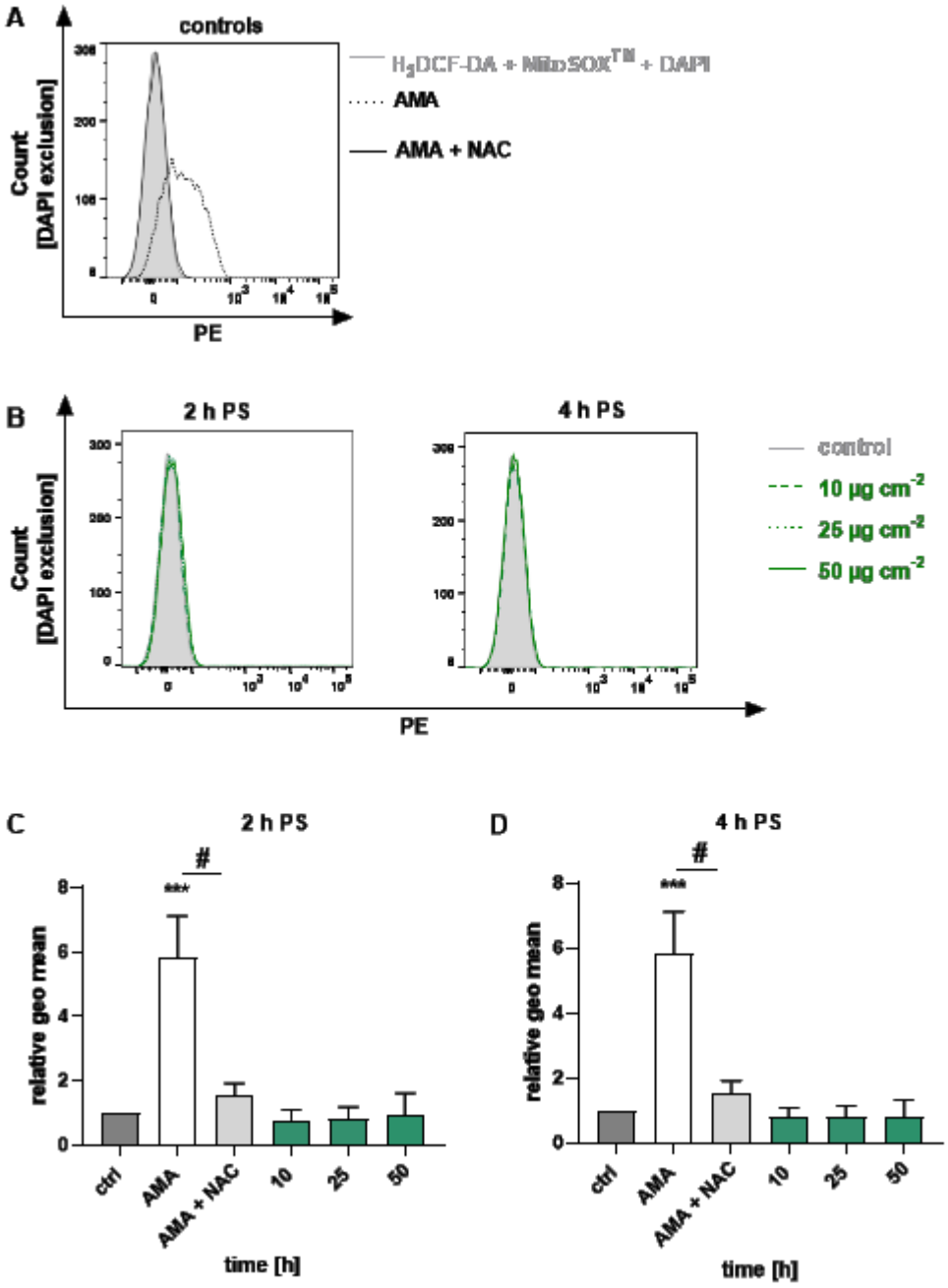

Figure 33. PS did not increase mtROS production in SH-SY5Y cells. A) Representative histogram of triple stained cells (H_2DCF-DA, MitoSOX™ and DAPI), in untreated control cells (grey), AMA (Antimycin A; 30 min 10 µM) treated cells (dotted) and cells pretreated with NAC (N-acetylcysteine; 18 h 3 µM) and acute AMA treatment (black) after exclusion of DAPI positive events acquired with PE (X axis) channel. **B)** Representative histogram of cells treated with 10, 25 and 50 µg cm^{-2} PS for 2 and 4 h acquired in PE (X axis) channel after exclusion of DAPI positive events. **C)** Relative geo mean of cells after PS treatment for 2 h and **D)** 4 h acquired in PE channel and after exclusion of DAPI positive events over time. Data show the mean of three (N=3) independent experiments + SEM and ordinary one-way ANOVA indicates differences between treatment and ctrl. (*** $p < 0.001$) while unpaired t-test indicates difference between AMA and AMA + NAC treatment (# $p < 0.05$).

Finally, after PS-NH_2 treatment the histograms in **Figure 34 A** show a small decrease in the peak's height, which is most likely based on a reduction of viable cells. This, together with the graphs shown in **Figure 34 B** and **C** indicates that no production of mitochondrial ROS could be observed after PS-NH_2 treatment, too.

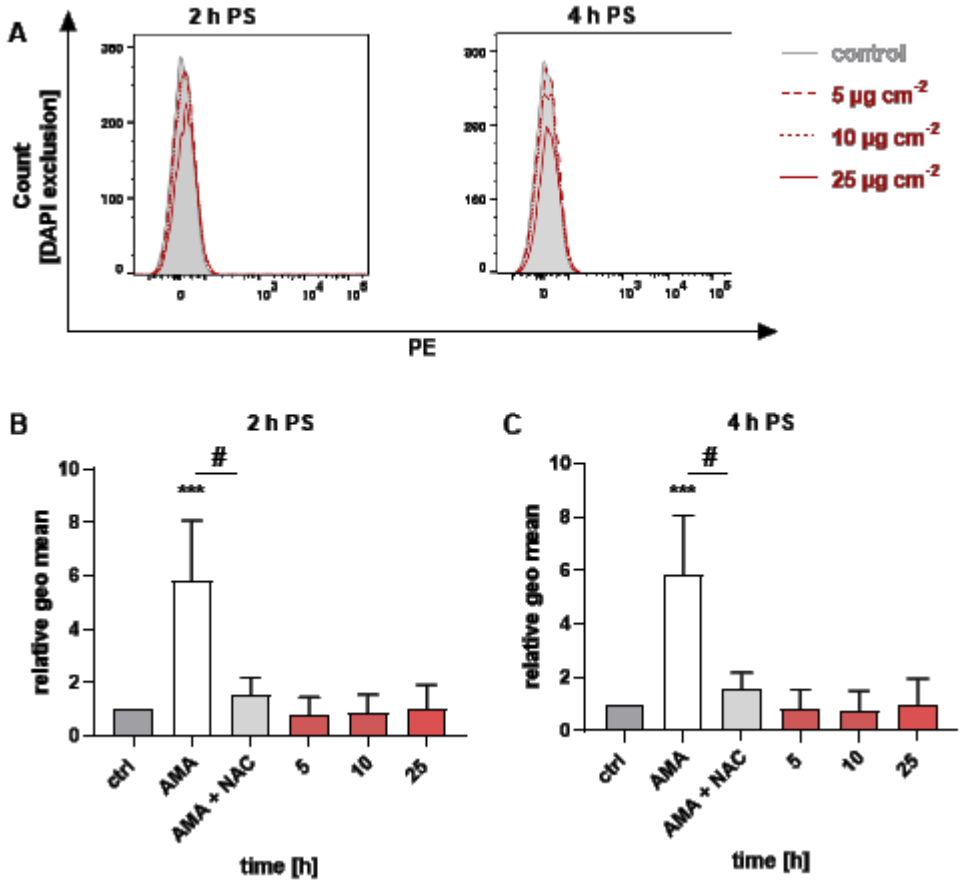

Figure 34. PS-NH_2 does not increases mtROS production in SH-SY5Y cells. A) Representative histogram of cells treated with 5, 10 and 25 µg cm^{-2} PS-NH_2 for 2 and 4 h acquired in PE (X axis) channel after exclusion of DAPI positive events. **B)** Relative geo mean of cells after PS-NH_2 treatment for 2 h and **C)** 4 h acquired in PE channel and after exclusion of DAPI positive events over time. Data show the mean of three (N=3) independent experiments + SEM and ordinary one-way ANOVA indicates differences between treatment and ctrl (*** $p < 0.001$) while unpaired t-test indicates difference between AMA and AMA + NAC treatment (# $p < 0.05$).

PS-NH_2 decreases mitochondrial membrane potential

Given the possibility that particles affect cellular membranes, although no mitochondrial oxidative stress could be observed after PS and PS-NH_2 treatment, the effect of the particles on the mitochondrial membrane potential (MMP) was investigated. Therefore,

the cells were treated as described above and a JC-1 staining was done. JC-1 is a membrane permeable dye identifying disruption of active mitochondria including changes in the MMP. When the MMP is high (e.g. in intact cells) the dye accumulates in the mitochondria forming red fluorescent aggregates which can be detected in the PE channel (red). When the MMP is disturbed, the staining is diffuse and the monomeric form can be detected in the FITC channel (green). Due to the fact, that FITC and PE signals may overlap in the PE channel, a slight compensation was necessary **(Figure 35 A**). Viable cells were positively stained with JC-1 and could be acquired in the PE channel and the mitochondria uncoupler CCCP was used as positive control for reduction of MMP to set the gates properly for the FITC channel (**Figure 35 B**). Moreover, cells with depolarized mitochondrial membrane often overlap with apoptotic cells. Therefore, the same gating strategy explained for Annexin V-FITC and PI treatment was used.

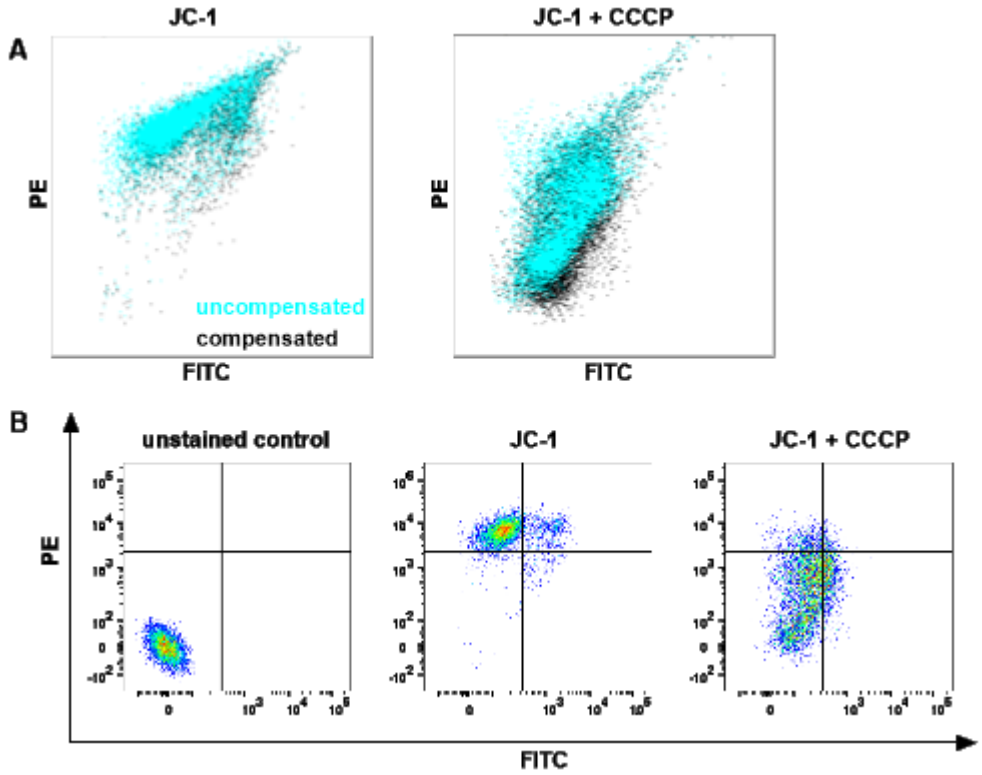

Figure 35. Establishing JC-1 staining in SH-SY5Y cells. A) compensated (black) and uncompensated (cyan) events in the stained control (JC-1) and in stained and treated sample (JC-1 + CCCP). Compensation in PE channel – 52 % FITC. **B)** Representative dot plots of unstained control, untreated JC-1 stained cells (JC-1) and CCCP treated and JC-1 stained cells (JC-1 + CCCP) acquired in FITC (X axis) and PE (Y axis) channel.

Cells were treated with 50 µg cm^{-2} PS for 1, 2 and 4 hours. However, neither the representative dot plots, nor the ratio of aggregates (PE positive cells) and monomers

(FITC positive cells) show any significant effect of PS, differently from the CCCP control treatment (**Figure 36).**

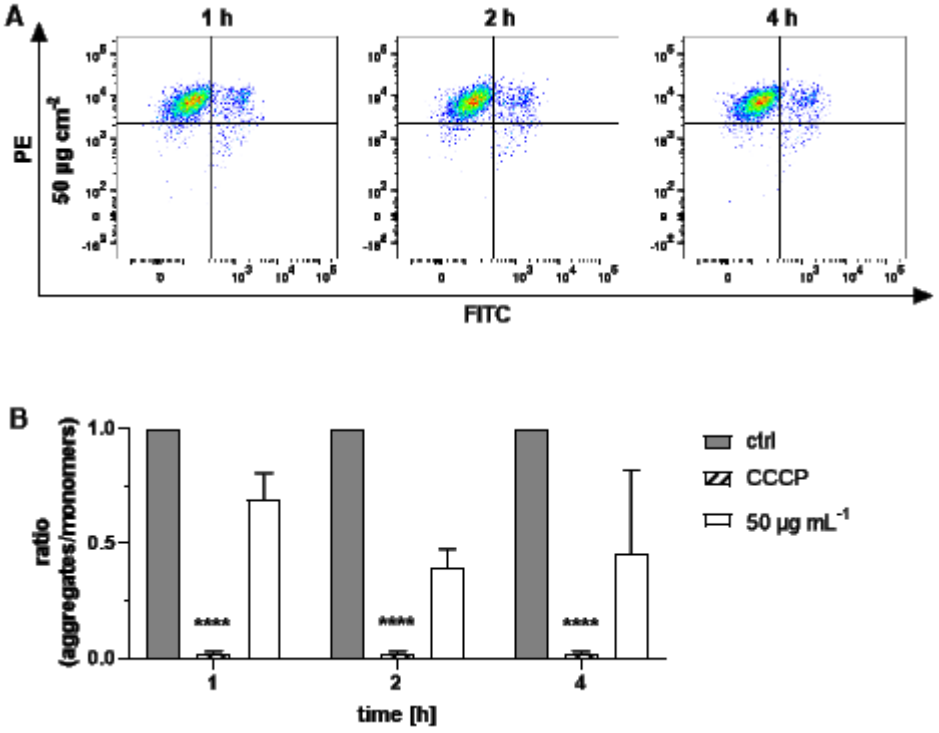

Figure 36. **PS has no effects on mitochondrial membrane potential. A)** Representative FACS dot plots of cells treated with 50 µg cm-2 PS for 1, 2 and 4 h and stained with JC-1 acquired in FITC (X axis) and PE (Y axis) channel. **B)** Ratio of PE positive cells (aggregates) to PE negative/FITC positive cells (monomers) relative to control after PS treatment over time. Data show the mean of three (N=3) independent experiments + SEM and ordinary one-way ANOVA indicates no differences between treatment and ctrl (**** $p < 0.0001$).

Instead, cells treated with the same concentrations of PS-NH_2 as used for cell death analysis (5, 10 and 25 µg cm^{-2}) for 1, 2 and 4 hours show a time and concentration dependent shift from PE positive cells (aggregates) to FITC positive cells (monomers) (**Figure 37 A)**. In addition, the calculated ratio of aggregates and monomers analyzed in **Figure 37 B** proofs a significant decrease of MMP after treatment with 25 µg cm-2 even after 1 h of exposure. Overall, FACS analysis indicated that despite no increase in ROS production was observed, treatment with PS-NH_2 particles affect the mitochondrial membrane potential.

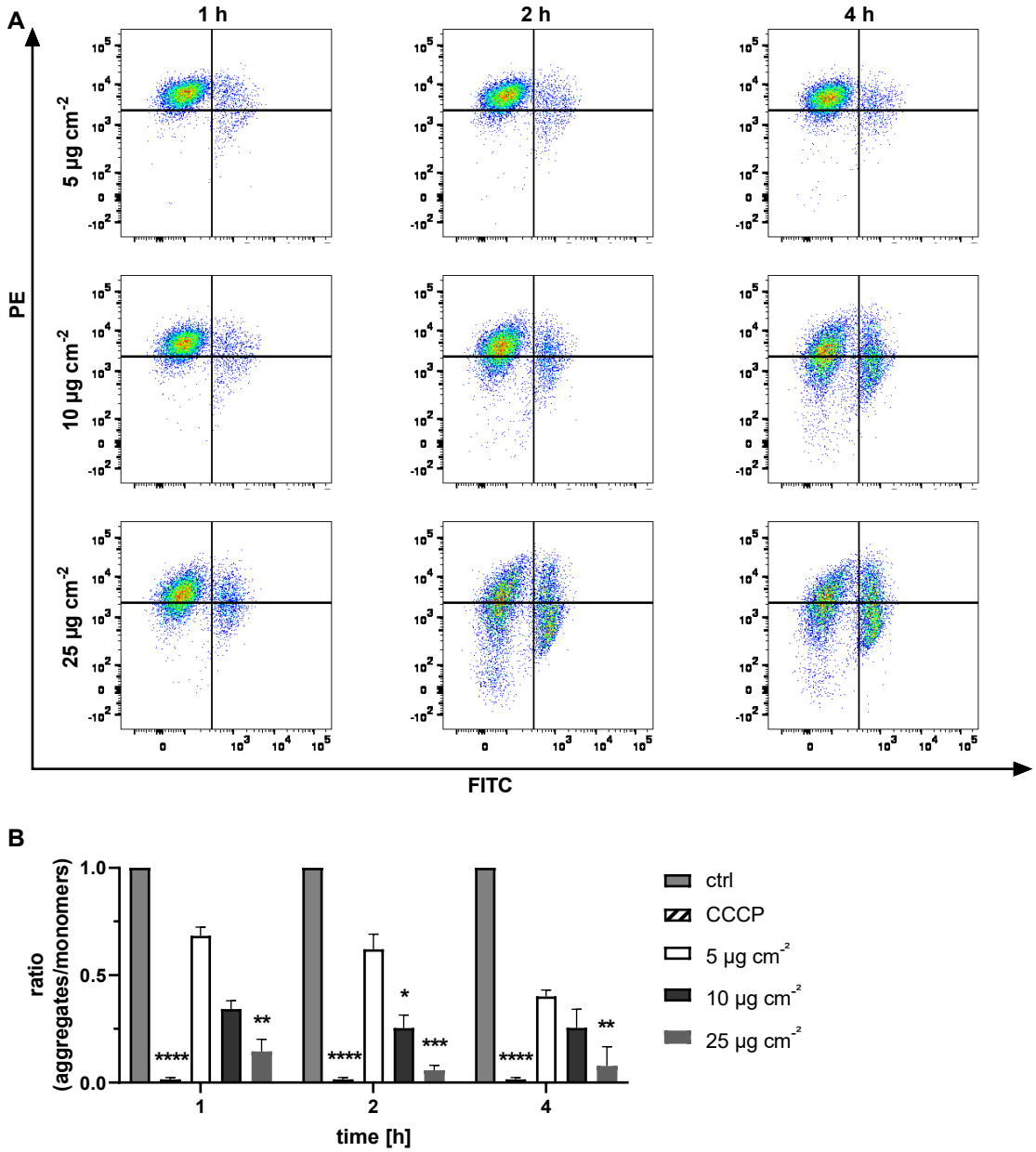

Figure 37. PS-NH_2 depolarized mitochondrial membrane in a concentration and time-dependent manner. A) Representative FACS dot plots of cells treated with 5, 10 and 25 µg cm^{-2} PS-NH_2 for 1, 2 and 4 h acquired in FITC (X axis) and PE (Y axis) channel after JC-1 staining. **B)** Ratio of PE positive cells (aggregates) to PE negative/FITC positive cells (monomers) relative to control after PS-NH_2 treatment over time. Data show the mean of three (N=3) independent experiments + SEM and ordinary one-way ANOVA indicates differences between treatment and ctrl. (* $p < 0.05$, ** $p < 0.01$, *** $p < 0.001$, **** $p < 0.0001$).

4.3 *In vitro* analysis of PS NPs in differentiated cells

Immortalized cell lines like HEK293 and SH-SY5Y cells are great tools to screen for toxicants under several different conditions (e.g. duration, concentration) and to unravel the molecular mechanisms of toxicity.[191] Especially SH-SY5Y cells is one of the most common used cell lines for neuronal cell biology studies and therefore it offers a good opportunity to investigate neurotoxicity on the immature nervous system.[191]

Although these cells display some neuronal associations such as short neurite outgrowth processes and neuroblast-like cell bodies, they do not cover the full morphology and biochemistry of mature neurons.[191] Moreover, their cell cycle of around 35 hours (as shown in **Figure 21)** limits the duration of chronic and more realistic exposure scenarios. In order to extend the time of exposure and to investigate the effect of PS and PS-NH_2 particles in a more neuronal-like system, SH-SY5Y cells were differentiated into cholinergic neurons through serum deprivation and all-trans retinoic acid (ATRA) treatment.

A variety of different differentiation protocols have been described using ATRA alone or in combination with other agents such as brain-derived neurotrophic factor (BDNF) and ATRA is by far the most used one when it comes to differentiation of SH-SY5Y cells into a more cholinergic like phenotype.[131]

During this process, SH-SY5Y cells escaped from a ~35 h cell cycle by shifting from a proliferation state into differentiating model, including polarized smaller cell bodies with extended neurite outgrowths and excitable membranes.[128,129,191,192]

Establishment of differentiation protocol for SH-SY5Y cells

Shipley et al. provided a very comprehensive protocol regarding the SH-SY5Y differentiation with ATRA and BDNF using three different media.[136] To investigate which differentiation protocol is the most suitable one for studying the effects of PS and PS-NH_2 on more neuronal related readouts and over time, two different differentiation protocols were applied in parallel. The protocol provided by Shipley et al. aims to obtain a homogeneous population of fully differentiated cholinergic neurons after 3 weeks, whereas other differentiation protocols, which are often used in the literature, lead to a large population of neuronal like cells after only 7 days.[136,193]

Figure 38 shows an overview of the two differentiation protocols, which I tried in my study: The first one involves the use of ATRA and the cells could be used from day 7, although they were still viable up to day 14 (or even longer). This protocol is considered

the short differentiation protocol that is often used in the literature.[192,194] The other, long protocol, is based on Shipley et al. with minor changes and includes 3 different media and one splitting step.[136]

Due to the fact that the long protocol required a lot of time and results in completely differentiated single cells, instead of a whole cell population, the decision was made in favor of the short protocol (**Figure 38**). The advantages are that several different time points could be investigated (e.g. 7 days vs 14 days) and the yield of cells was large enough that previously used assays, such as the resazurin assay, could also be used in differentiated cells.

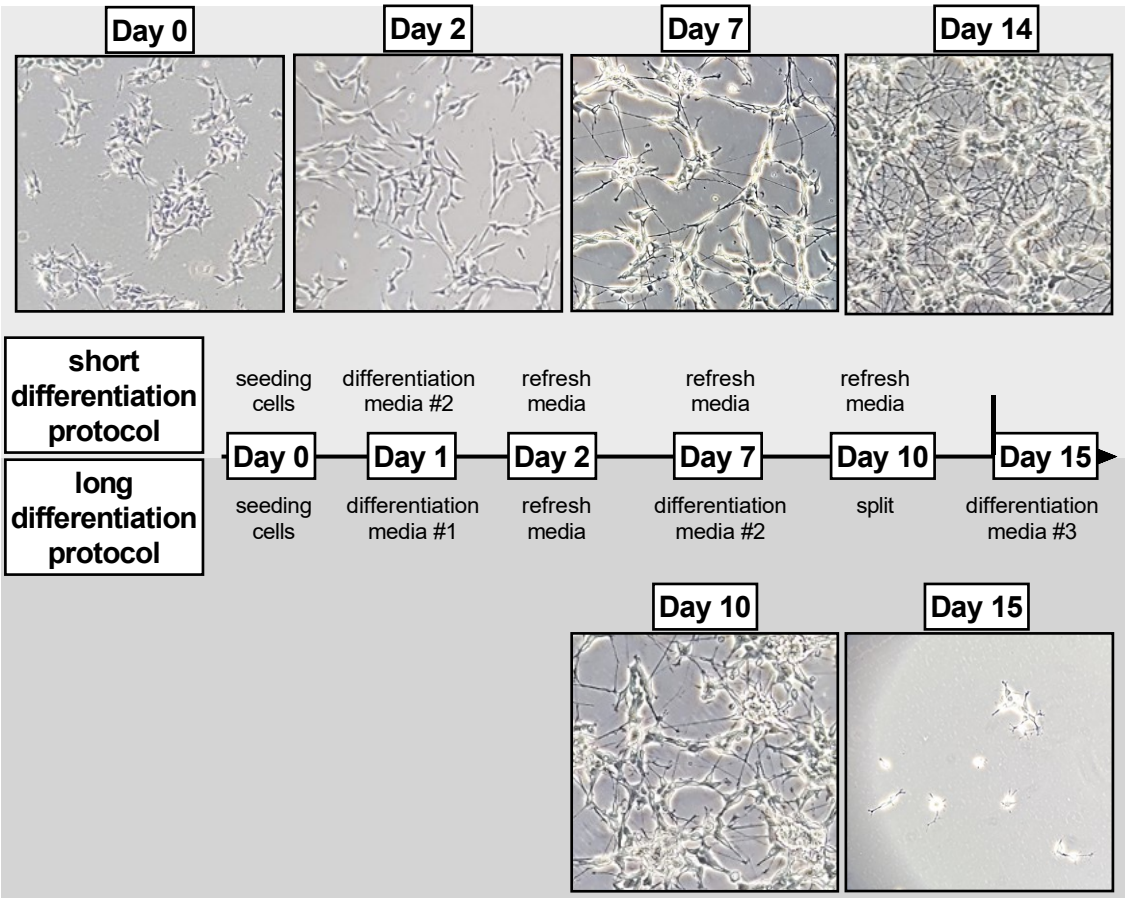

Figure 38. Scheme for short and long differentiation protocols. The *short differentiation protocol* starts from Day 1 with serum deprivation and ATRA supplementation and after 7 days, cells were differentiated and still viable up to 14 days. The *long differentiation protocol* starts from day 1 and includes 3 differentiation media. At day 15, the final differentiation media (#3) is used and after recovering of the cells, they can be used for experiments.

ATRA is usually resuspended in 95 % EtOH (v/v) and stored under dark conditions at 4 °C up to 4 to 6 weeks. Once the ATRA is resuspended, the amount is sufficient for

numerous differentiations, but the throughput is not high enough to consume it all. Since ATRA can also be dissolved in 100 % DMSO, which could be stored at - 20°C for long-term storage, the cells were treated with ATRA dissolved either in DMSO or in EtOH. Following 7 or 14 days of differentiation, the neurite outgrowths were measured and total protein was isolated to study the expression of Neuron Specific Enolase (NSE), a marker often used for neurons and neuronal differentiation.[195]

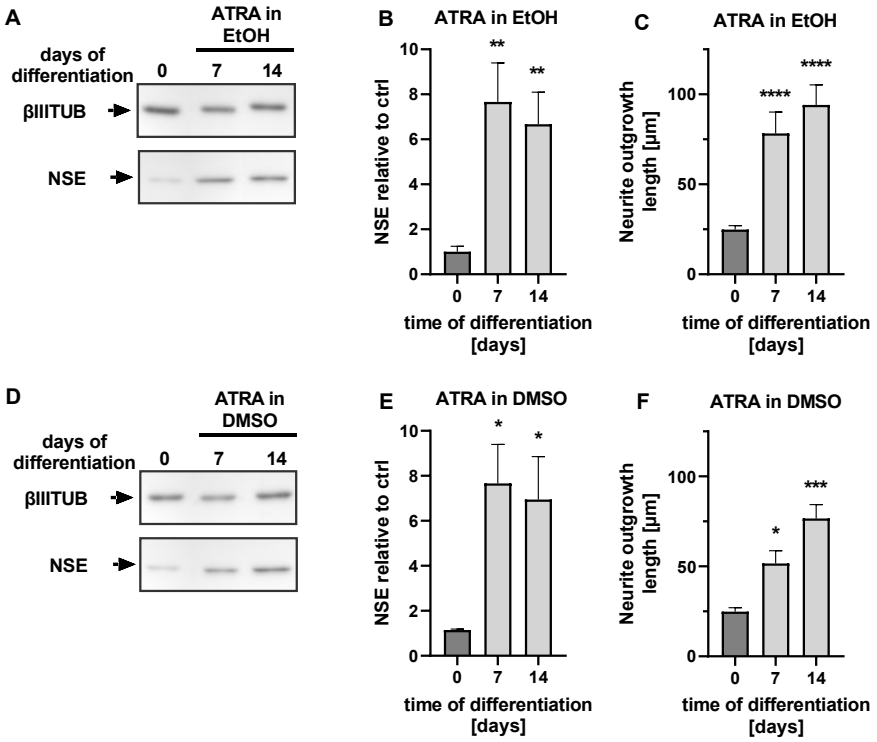

Figure 39. Differentiation of SH-SY5Y cells for 7 and 14 days with ATRA dissolved in either EtOH or DMSO. Shown are representative Western Blots stained with ß Tubulin and NSE primary antibodies and the calculated NSE intensity normalized to ßIIITUB and relative to control after cells were differentiated with ATRA dissolved in EtOH **(A – C)** or DMSO **(D – F)**. Data show the mean of (n=3) replicates in (N=3) independent experiments + SEM. Raw images of Western Blot analysis from all replicates are provided in Figure S2 - Figure S3. Ordinary one-way ANOVA indicates differences between treatment and ctrl (*p < 0.05; **p < 0.01; ***p < 0.001; ****p < 0.0001).

Figure 40 shows the cells after 7 days differentiation (A) and 14 days differentiation (B) in Ethanol and especially the neurite outgrowth could be easily identified after 7 as well as after 14 days of differentiation.

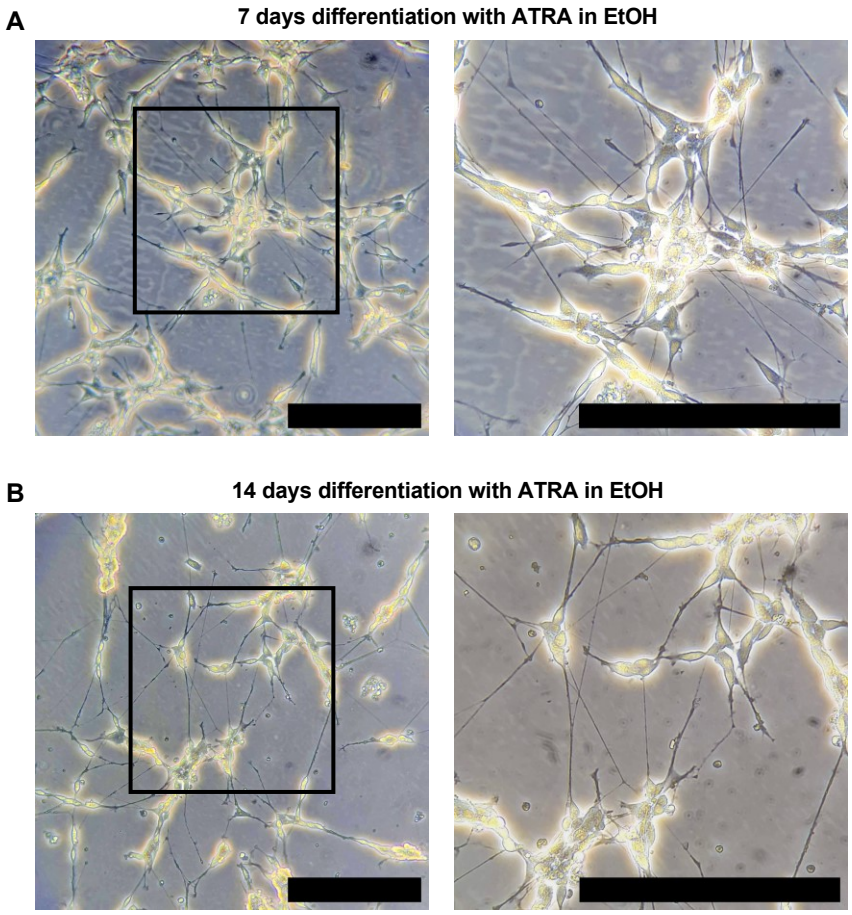

Figure 40. SH-SY5Y differentiated for with ATRA in dissolved in Ethanol. Representative images of **A)** cells differentiated for 7 days and **B)** cells differentiated for 14 days. 10x and 40x magnification; bar graphs = 250 µm.

PS-NH_2 decreases cell viability in differentiated SH-SY5Y cells

In parallel to the exposure scenarios in undifferentiated SH-SY5Y cells, 7 days differentiated cells were treated with PS and PS-NH_2 for 48 h after 7 days of differentiation (**Figure 41 A – B**). Moreover, to further investigate particles toxicity on additional neuronal parameters, the viability of SH-SY5Y upon chronic (6 days, starting from day 2 of differentiation) exposure to PS and PS-NH_2 during cell differentiation was assessed (**Figure 41 C – D**). This offered to use neuronal-like differentiated cells while prolonging the exposure time up to 6 days. Consistent with results gained from undifferentiated (proliferating) cells, treatment of differentiated cells (**Figure 41 B**) or during differentiation (**Figure 41 D**) again revealed a dose- and time-dependent toxicity only for aminated particles in both exposure scenarios. The long-term treatment of 6 days is killing almost 90 % of the cells already after treating with 5 µg cm^{-2} and almost all

cells died after treatment with 10 µg cm^{-2}, indicating a more severe effect compared to an acute exposure of 48 hours (or an increased resistance of fully differentiated cells).

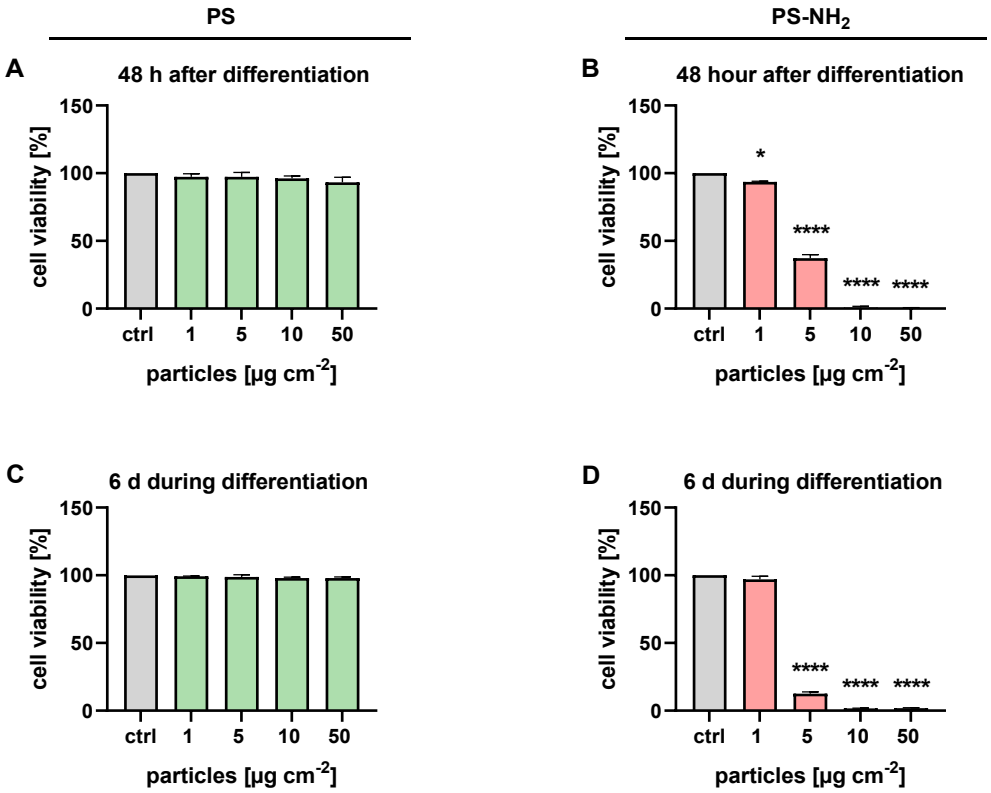

Figure 41. PS-NH$_2$ treatment decreases cell viability in differentiated SH-SY5Y cells. Differentiated SH-SY5Y cells were treated with PS and PS-NH$_2$ for 48 h after 7 days of differentiation **(A, B)** or for 6 d during differentiation from day 2 **(C, D)**. Data show the mean of (n=12) replicates in (N=3) independent experiments + SEM. Ordinary one-way ANOVA indicates differences between treatment and ctrl (*p < 0.05; **p < 0.01; ***p < 0.001; ****p < 0.0001).

PS-NH$_2$ decreases neuronal outgrowth length and affect expression of neuronal markers

To further assess particles neurotoxicity, the effect of PS and PS-NH$_2$ on structures and markers of cell differentiation upon acute (48 h) and chronic (6 days) exposure was assessed. Cells were treated with lower concentrations of particles, which had no or just a slight effect on the cell's viability. In fact, in order to measure neurite-like structures after chronic PS-NH$_2$ treatment, it was necessary to even further reduce particles concentrations due to cell loss **(Figure 42 A – B)**. After treatments, the length of neurite outgrowth was measured and, consistent with the cytotoxicity results, only cells treated with PS-NH$_2$ show a decreased length at concentrations ≥ 1 µg cm^{-2} both upon acute and chronic exposure (**Figure 42 E – F**). Compared to the 48 h PS treatment, where no

effect could be seen for the PS treatment, not even at very high concentrations, long term treatment of 6 days during differentiation resulted in a significantly decreased length of neurite outgrowth up to ~ 25 %, for all concentrations (**Figure 42 D).**

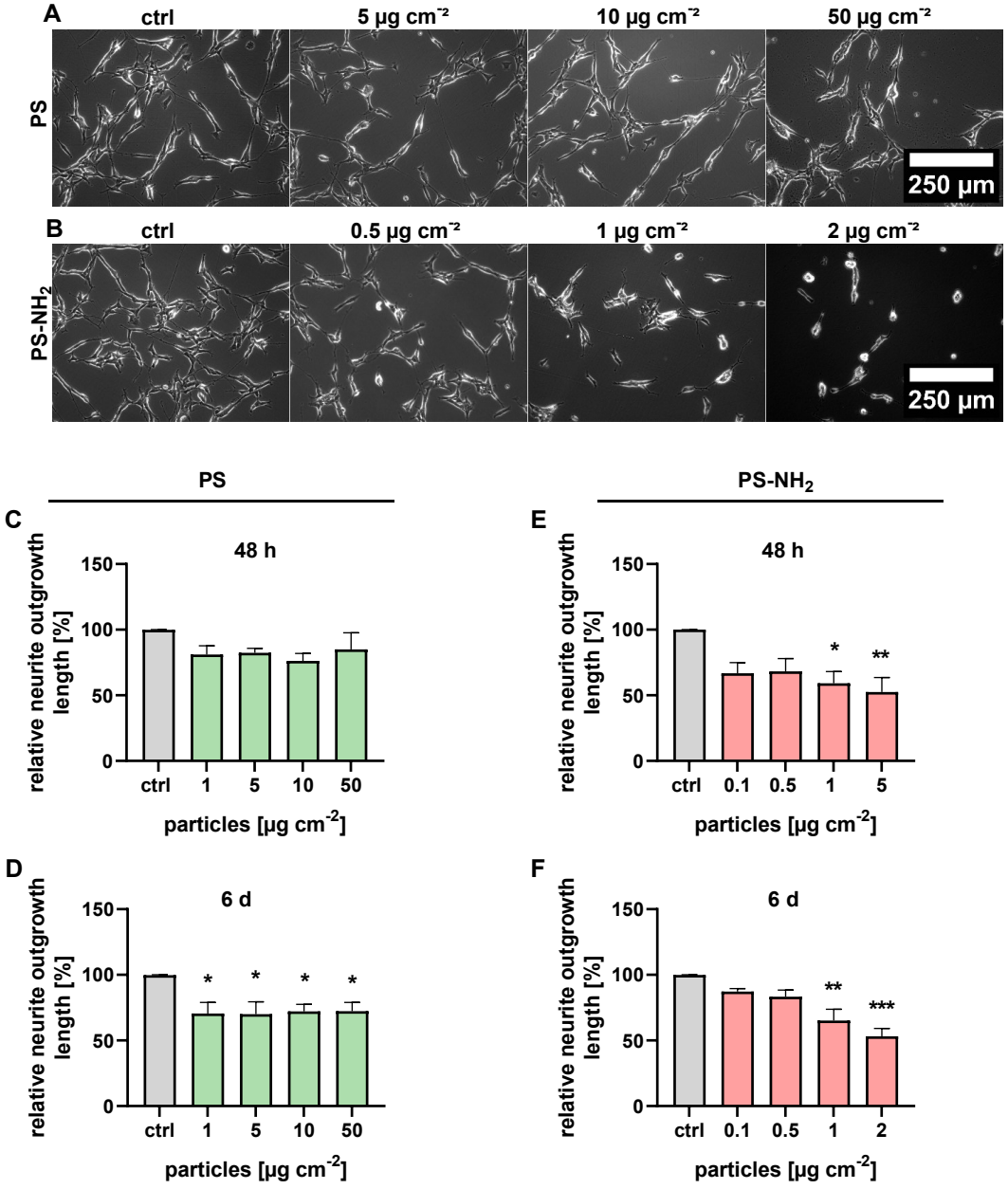

Figure 42. PS-NH_2 affect SH-SY5Y differentiation into neuronal-like cells. A-B) Representative brightfield images with 200 x magnification of 7 day differentiated SH-SY5Y cells treated with different concentration of PS and PS-NH_2 particles for 6 days during differentiation, scale bar = 250 µm. **C-F)** Neurite outgrowth quantification in differentiated SH-SY5Y cells after 48 h treatment with PS **(C)** or PS-NH_2 **(E)** or after treatment during differentiation for 6 days with PS **(D)** and PS-NH_2 **(F)**. Data show the mean of (n ≥ 15) replicates in (N=3) independent experiments + SEM and one-way ANOVA indicates differences between treatment and ctrl (* $p < 0.05$, ** $p < 0.01$, *** $p < 0.001$).

Furthermore, the expression of different neuronal markers after 6 days of PS-NH_2 particle treatment during differentiation, specifically Neuron Specific Enolase (NSE), Synaptophysin (SYN), Amyloid Precursor Protein (APP), Neuroligin 1 (NLGN1), Neuroligin 3 (NLGN3) and βIII Tubulin (βIIITub) was analyzed. The cells were treated with 0.25, 0.5 and 1 µg cm^{-2} of PS-NH_2. **Figure 43** shows immunofluorescence images after treatment, fixation with paraformaldehyde and staining with respective antibodies of untreated cells and cells treated for 6 days with 1 µg cm^{-2} of PS-NH_2.

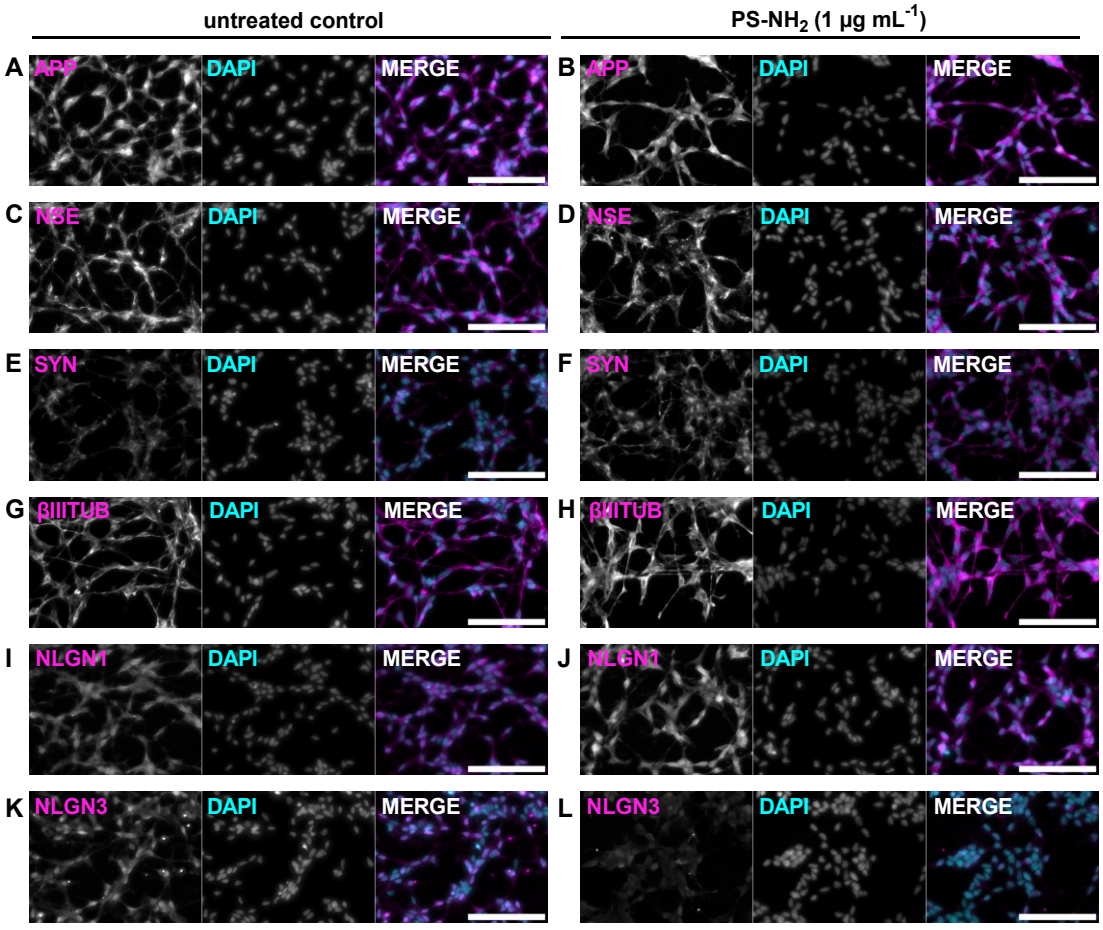

Figure 43. Altered immunofluorescence of neuronal marker proteins APP (**A, B**), NSE (**C, D**), SYN (**E, F**), ßIIITUB (**G, H**), NLGN1 (**I, J**) and NLGN3 (**K, L**) in differentiated SH-SY5Y cells after 6 days exposure to 1 µg cm_{-2} PS-NH_2. Fixed cells were stained with the respective antibody and secondary antibody coupled to Alexa488 or Alexa594 and mountain stained with DAPI. Images are representative images with 400 x magnification and graphs show results of 3 independent experiments (N=3) with at least 30 images per condition + SEM. Scale bar = 100 µm.

Interestingly, analysis of the fluorescence intensity indicates that the expression of APP, NSE, βIIITUB and SYN was increased after treatment with 1 µg cm^{-2} and decreased for NLGN3 **(Figure 44).**

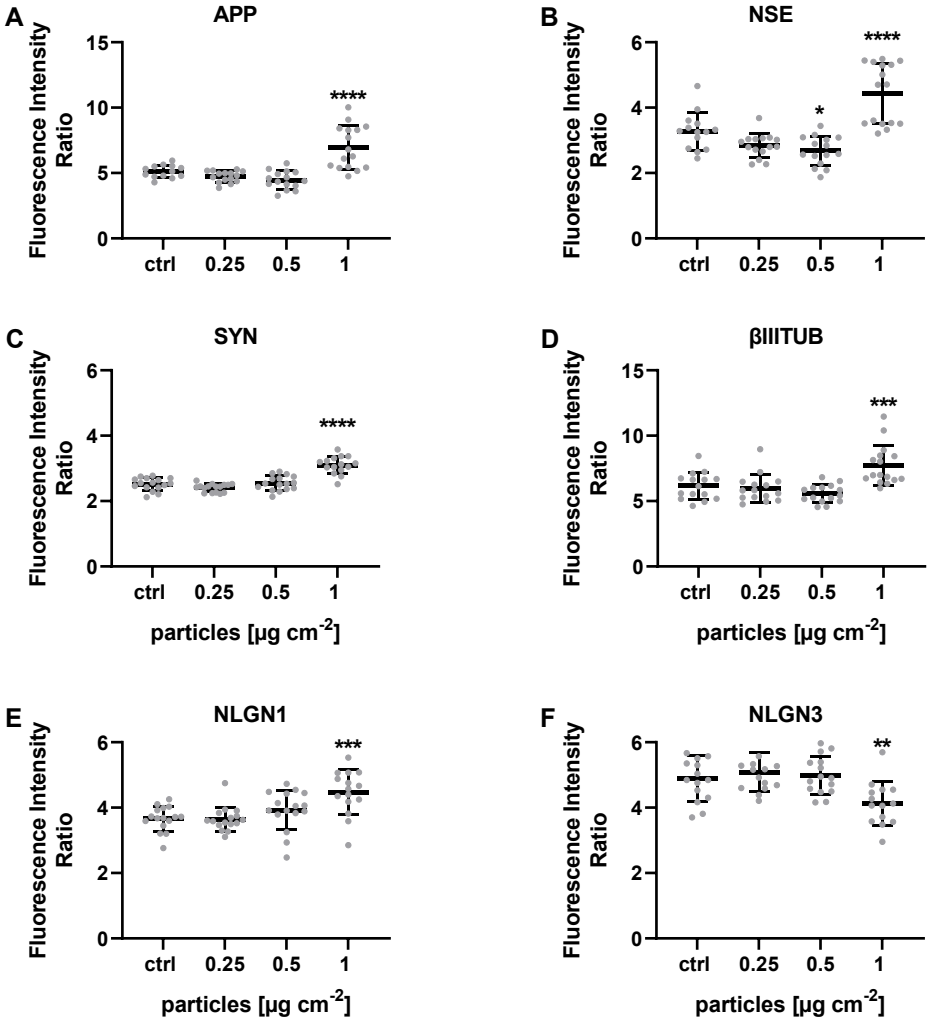

Figure 44. PS-NH$_2$ affect SH-SY5Y expression of neuronal marker proteins. Quantification of indicated neuronal marker proteins **A)** APP, **B)** NSE, **C)** SYN, **D)** βIIITUB, **E)** NLGN1 and **F)** NLGN3 expression from immunofluorescence staining in differentiated SH-SY5Y cells after 6 d PS-NH$_2$ exposure during differentiation. Data show the mean of (n ≥ 30) replicates in (N=3) independent experiments + SEM. Script used to analyze images is provided in **Table S7.** One-way ANOVA indicates differences between treatment and ctrl (* $p < 0.05$, ** $p < 0.01$, *** $p < 0.001$, **** $p < 0.0001$).

4.4 *In vivo* analysis in the nematode *C. elegans*

To investigate the potential neurotoxic effects of PS particles upon different exposure scenarios *in vivo*, I used the nematode *C. elegans,* a powerful model organism for toxicology studies.[2,142] In contrast to *in vitro* studies, *in vivo* studies allow the investigation on a whole organism with different tissues and organs and permit prolonged particles exposure scenarios, as well as exposure at different life-stages (from development, to adulthood and senile stages). Moreover, *C. elegans* can be cultivated in liquid media (S-Medium) or on solid nematode growth medium (NGM) agar plates and together with its relatively short life cycle (3-4 days) and lifespan (~ 3 weeks) as well as its stereotyped and widely characterized behaviors, it offers a great multicellular model organism for *in vivo* investigation of chronic effects and life-long exposure to different kind of interventions. [82,83,141,161].

No effects of PS and PS-NH_2 on C. elegans were observed in solid agar plates

In our laboratory, most of the work with *C. elegans* is done by feeding the worm in nematode grown medium supplemented with *E. coli* on solid agar plates. Thus, the effect of PS-NH_2 particles in *C. elegans* was initially evaluated by exposing wild type (WT) animals in solid agar plates and during animals' development in order to rule out particles' toxicity as well as neurodevelopmental effects. To establish the optimal experimental settings many different experimental conditions were initially tested, like different number of bacteria, alive versus killed bacteria, treatment from embryos/L1 (first larval stage) to L4 or adults, different methods of adding particles to the worms and of course different concentration of particles. Due to the fact, that previous *in vitro* data showed no effect of PS particles and also initial *in vivo* experiments (e.g. survival analysis, length measurement, fertility and fecundity assays) did not show any effect, for most experiments only PS-NH_2 particles were used.

Figure 45 A shows that 100 µg mL^{-1} of PS-NH_2 did not alter the development of the worms fed alive bacteria and 100 % of treated larvae developed to adult within 96 h. In contrast, **Figure 45 B** clearly indicates that particles did not alter animals' development, yet using inactivated bacteria delayed the development and almost 40 % of the worms did not develop into adult within 96 h.

The treated worms were then used for a fecundity assay and after egg lay, the number of eggs laid per worm within one hour was calculated (**Figure 45 C – D**). The results indicate no significant differences neither within the particle treatment nor within the bacterial conditions. Afterwards, the fertility was assessed by counting the hatched

larvae, which also indicated no effect of PS-NH_2 treatment or using inactivated bacteria (**Figure 45 A – F**).

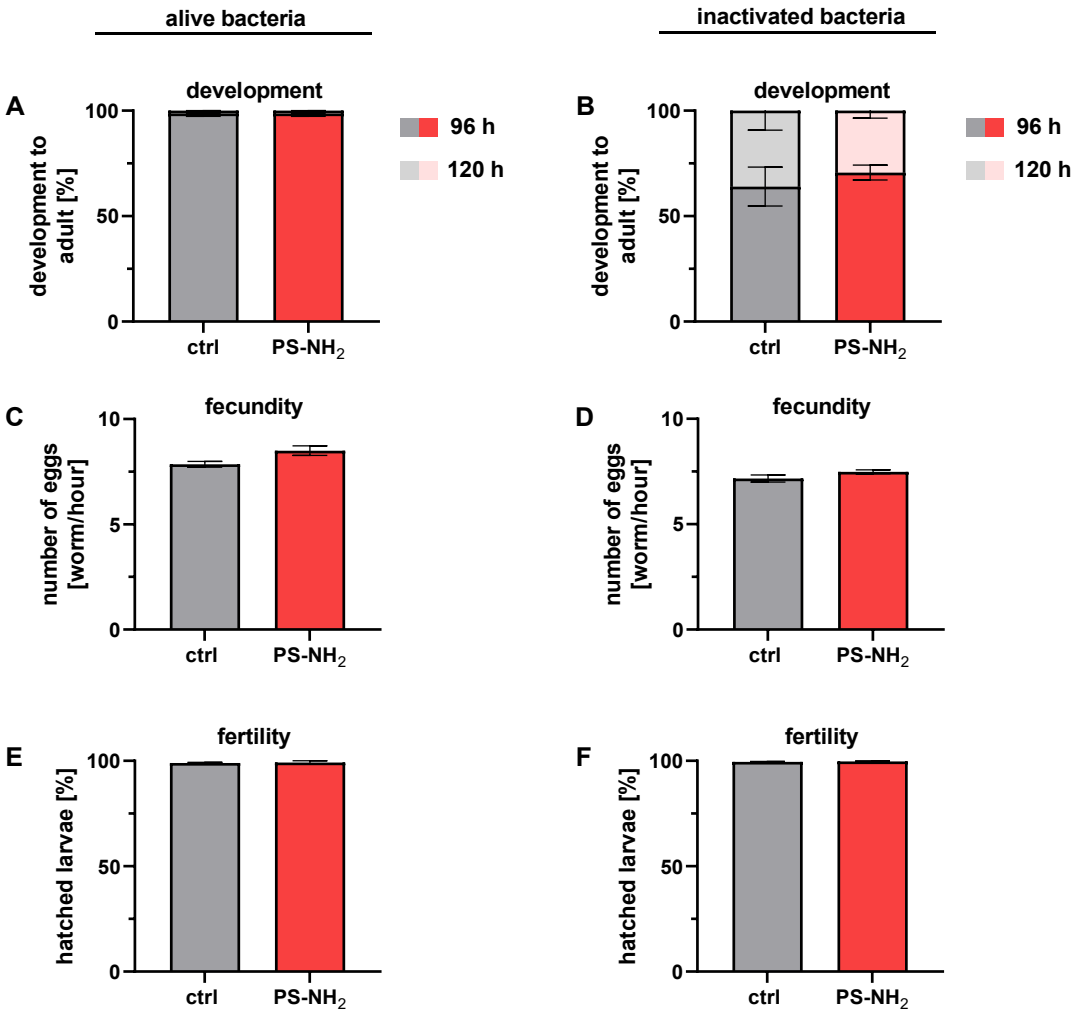

Figure 45. Development, fecundity and fertility of WT worms after PS-NH_2 exposure on solid medium with alive (A, C, D) or inactivated bacteria (B, D, F). Eggs were treated with 100 µg mL^{-1} PS-NH_2 until L4 on NGM plates and **A-B)** development was checked on day 4 (96 h) and day 5 (120 h) after egg lay. **C-D)** Adults were then used for fecundity (number of eggs) and **E-F)** fertility assay (hatched larvae). Experiments were done in triplicates per each condition. The data show mean of triplicates (n=75) within three independent experiments (N=3) + SEM. A table comparing used concentrations *in vitro* and *in vivo* is provided in **Table S8**.

To evaluate possible particle toxicity in a longer exposure scenario, and to specifically investigate neuronal toxicity, the particles effects on *C. elegans* locomotion decline (a typical age-associated phenotype) was evaluated in WT as well as in a widely established AD model, namely a strain expressing the human Aβ 1 – 42 peptide under a muscle specific promoter (mAD).[144] These experiments were carried out by Magnitude

Bioscience, a company in UK, which developed an automatic platform to quantify worm's motility. In order to make sure that we did not miss any relevant information, the automated assay was used to test PS in parallel. To this extent, 30 L4 worms per plate were transferred onto agar plates containing alive OP50 bacteria covered with 100 µg mL^{-1} PS or PS-NH_2 and motility was quantified up to 10 days during particle treatment (without refreshing the particles). The imaging technology measured worms moving above a certain threshold distance in a 160 second window, and repeated every 5 minutes. In general, the mean number of worms moving at any timepoint is analogous to survival metrics in a lifespan assay, while the fraction of worms moving, the mean speed of the worms and the mean speed of worms in relation to the fraction of worms moving were used to analyze the outcome. The results of a post-developmental treatment of PS and PS-NH_2 clearly show a difference in worms' motility (i.e. fraction of worm moving and mean speed) between WT and mAD strains in untreated as well as treated animals (**Figure 46).** While WT animals show movement over 10 days, the fraction of AD animals moving is decreasing from day 1 and at day 5 almost all animals are paralyzed **(Figure 46 A – B**). Regarding the mean speed, WT animals achieve their maximum between day two and day five, however mAD animals decrease already after some hours (**Figure 46 C – D**). The mean speed of animals moving is around 20 µm s^{-1} for WT worms and 15 µm s^{-1} for mAD worms (**Figure 46 E – F**).

Neither PS nor PS-NH_2 show a significant difference in WT or mAD worms. However, the fraction of worms moving as well as the mean speed is slightly increased after PS exposure.

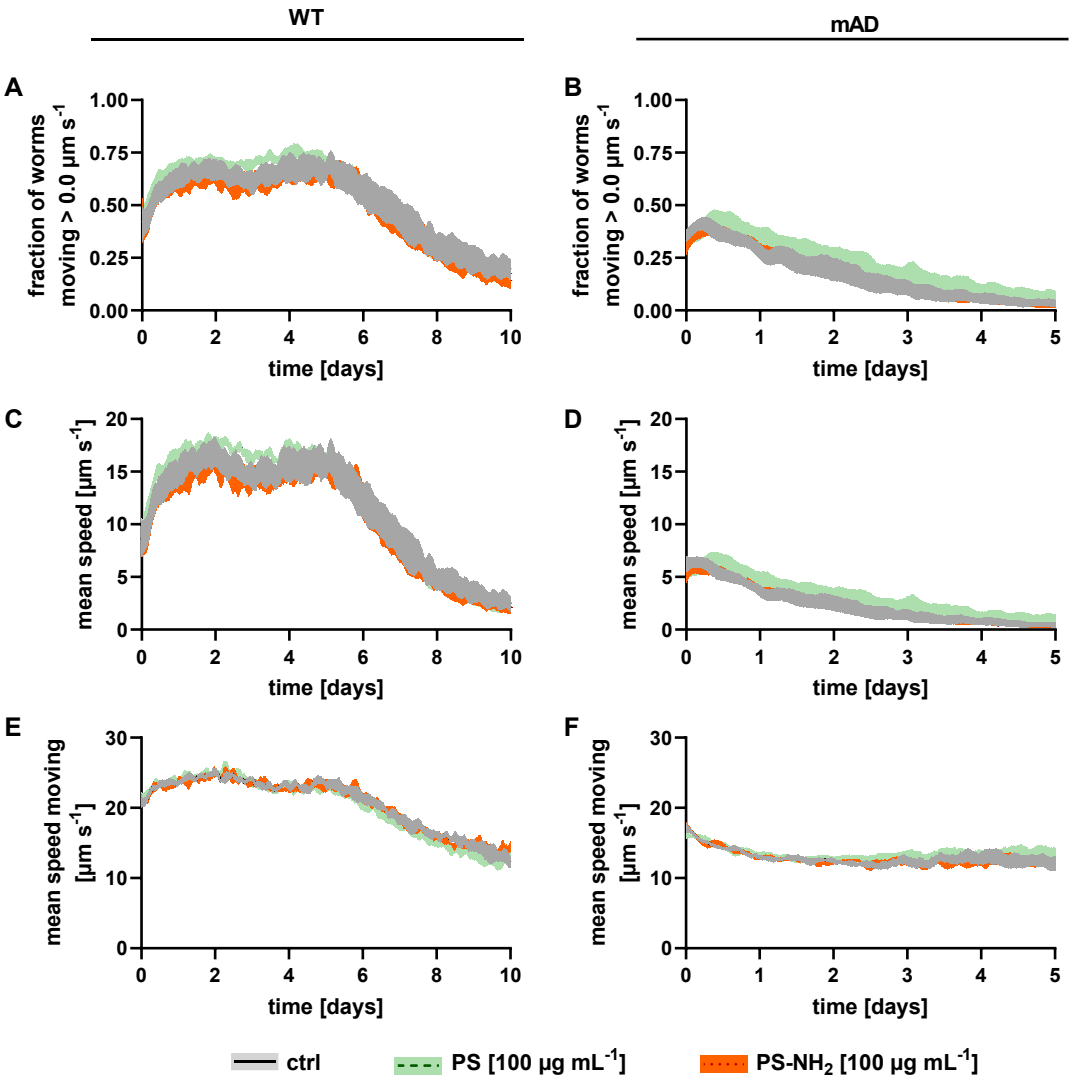

Figure 46. Movement assessment of WT and mAD worms exposed to control (water only) (black lines) PS (green lines) or PS-NH_2 (red lines) on solid NGM plates starting from L4 developmental stage. A) fraction of WT worms moving (150 animals in 5 replicates in ctrl (n=150; N=5); PS (n=180; N=6); PS-NH_2 (n=150, N=5)); **B)** fraction of mAD worms moving (ctrl (n=180; N=6); PS (n=180, N=6); PS-NH_2 (n=180, N=6)) **C)** the mean speed of WT worms, **D)** mean speed of mAD worms, **E)** mean speed of moving WT worms and **F)** mean speed of moving mAD worms ± SEM.

Due to the fact that no differences in the movement after post developmental PS and PS-NH_2 exposure could be detected and that no developmental toxicity was observed in initial experiments, the particles' effect on movement was then investigated after worms were exposed to the particles also throughout development. To this extent, the egg lay was performed on plates containing either 100 µg mL^{-1} PS or PS-NH_2 and after 4 days 30 L4 worms were transferred onto fresh plates containing the same concentration of particles.

Figure 47 confirms the difference between mAD and WT models, with mAD worms showing a smaller fraction of moving animals and a lower mean speed. Moreover, the results indicate a small decrease of moving animals as well as in the mean speed after treatment with 100 µg mL^{-1} PS-NH_2 in both models, although the difference is not significant.

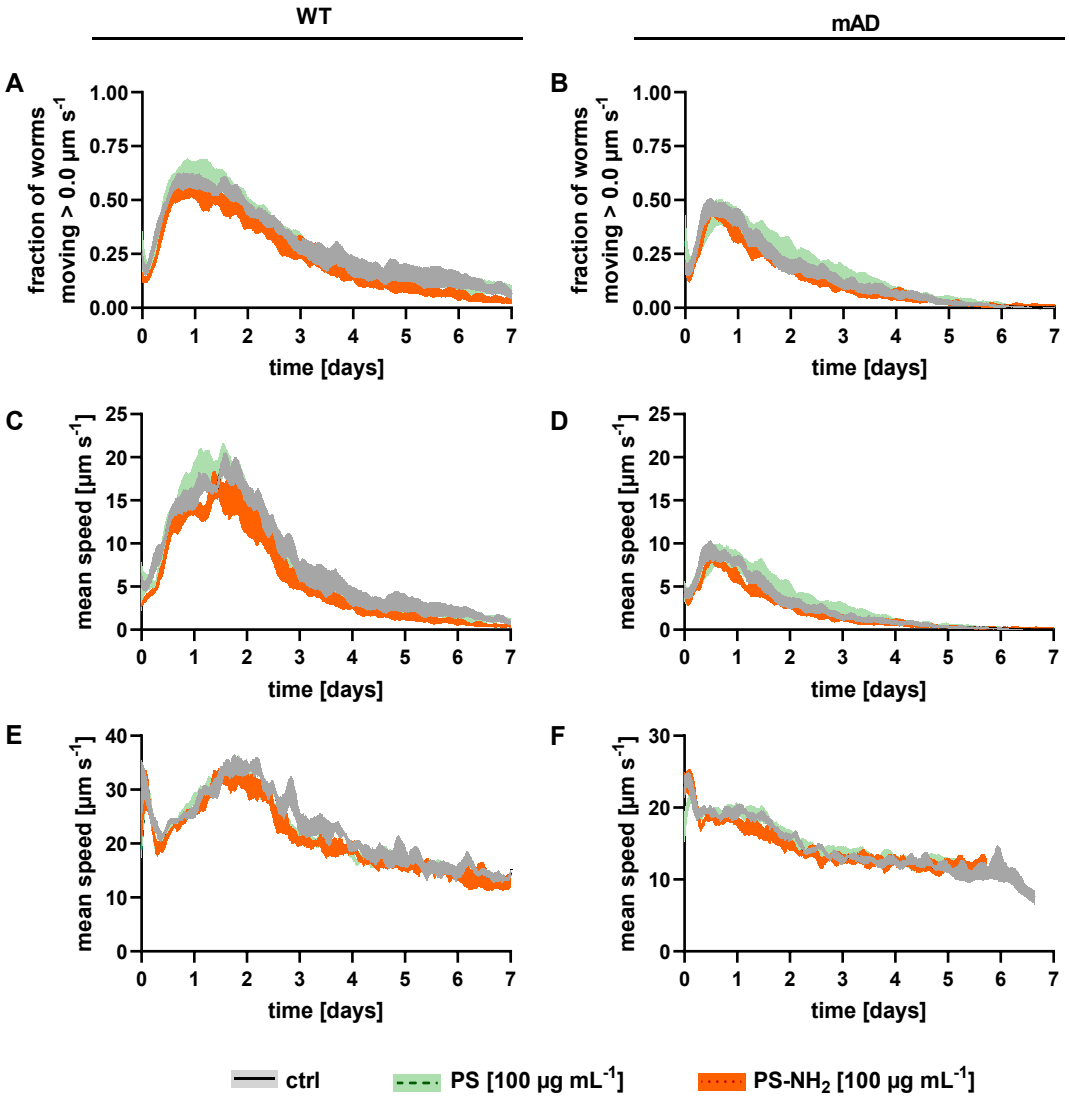

Figure 47. Movement assessment of WT and mAD worms exposed to control (water only) (black lines) PS (green lines) or PS-NH_2 (red lines) on solid NGM solid plates starting from embryos. A) fraction of WT worms moving (150 animals in 5 replicates in ctrl (n=150; N=5); PS (n=180; N=6); PS-NH_2 (n=120, N=4)); **B)** fraction of AD worms moving (ctrl (n=180; N=6); PS (n=180, N=6); PS-NH_2 (n=150, N=5)) **C)** the mean speed of WT worms, **D)** mean speed of mAD worms, **E)** mean speed of moving WT worms and **F)** mean speed of moving mAD worms ± SEM.

PS-NH_2 in liquid culture inhibits C. elegans development and movement

No significant differences could be detected between untreated and treated worms when experiments were carried out solid agar plates, but the literature indicates that PS and PS-NH_2 indeed may influence the worms.[2]

Therefore, the worms were exposed to the particles in liquid media as this may improve particles uptake via different routes.[196] Again, I first tested different exposure scenarios and looked at the effect of different concentrations of PS and PS-NH_2 particles on animals' development (length) and viability while treating them from L1 (for 3 days), from L4 (for 24 h) or from adults (for 24 h). According to previous findings, there was no effect for PS in any condition. Therefore, most experiments were performed only with PS-NH_2.

Figure 48 A shows the effect of different concentrations (10, 50 and 100 µg mL^{-1}) of PS-NH_2 on the development after treatment of WT and mAD L1 worms for 3 days in liquid. WT and mAD animals both exhibit a concentration dependent negative effect on animals' growth and arrested animals' development at the highest concentration 100 µg mL^{-1}, with the Aβ expressing animals clearly being more sensitive than WT.

The effect of the particles on development and movement is quantified in WT animals treated in different life stages and different time points (**Figure 48).** A significant reduction of worm's development (length ~ 50 %) after treating L1 worms with 50 µg mL^{-1} PS-NH_2 for 3 days (**Figure 48 B**) as well as a reduction of~ 10 to 20 percent after treatment of L4 worms with 100 µg mL^{-1} PS-NH_2 for 24 h day (**Figure 48 C**) and young adult worms with 100 µg mL^{-1} PS-NH_2 for 24 h day (**Figure 48 D**).

In order to compare results gained from movement assays on solid agar plates, movement of animals in liquid was quantified via manual counting of animals' body bends (trashing assay) in 4-day-old WT animals after PS-NH_2 treatment with either 50 µg mL^{-1} for 3 days from L1 animals, 100 µg mL^{-1} for 24 h from L4 or 100 µg mL^{-1} for 24 h from young adult animals. Contrary to what was observed from experiments done on solid plates, where PS-NH_2 did not alter the movement at all, the number of body bends in one minute is significantly decreased in liquid and under all conditions in (**Figure 48 E - G)**.

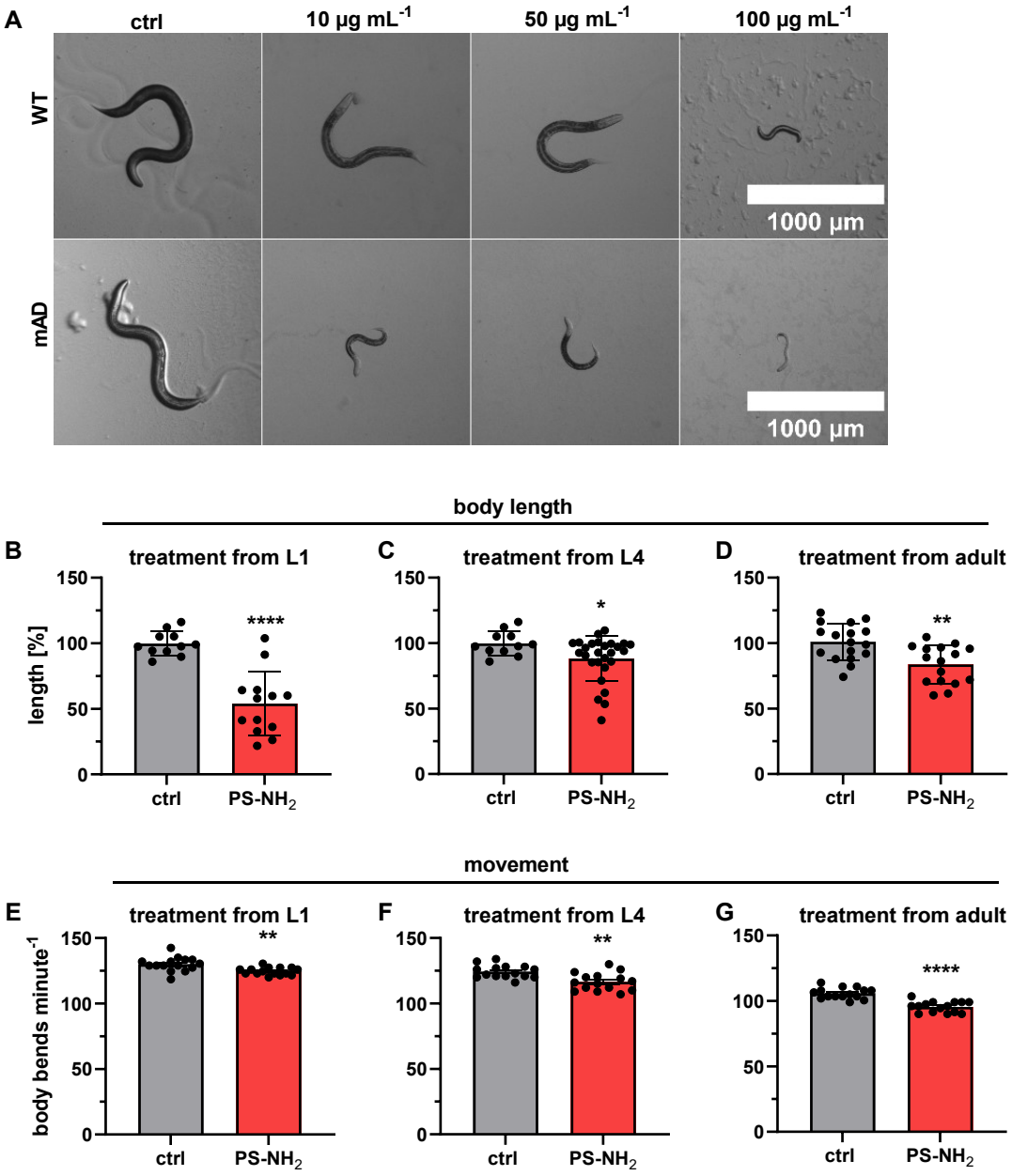

Figure 48. PS-NH_2 particles affected animals' development and movement. A) Representative images of 4 days old WT and mAD worms after PS-NH_2 treatment from L1 (for 3 days) in liquid. **B – D)** Length of 4 d old WT animals after treatment with **B)** 50 µg ml^{-1} PS-NH_2 for 3 days from L1 (N=2, n=18), **C)** with 100 µg mL^{-1} for 24 hours from L4 animals (N=2, n=43), **D)** and for 24 hours from young adult (N=2, n=22). For movement analysis Frequency of body bends in liquid medium (trashing) was quantified for one minute in 4 d old WT animals after treatment with **E)** 50 µg mL^{-1} PS-NH_2 for 3 days from L1 animals and (N=2, n=30) **F)** 100 µg mL^{-1} PS-NH_2 for 24 h from L4 animals (N=2, n=45) and **G)** 100 µg mL^{-1} PS-NH_2 for 24 h from adult animals (N=2, n=30). Data show the mean ± SEM and unpaired T-test indicates differences between treatment and control, ctrl (* $p < 0.05$, ** $p < 0.01$, **** $p < 0.0001$).

PS-NH$_2$ in liquid culture shortens C. elegans lifespan and affects synaptic function

To further investigate the particles chronic effects, the lifespan of the animals upon continuous treatment with different concentrations was analyzed **(Figure 49)**. In order to avoid confounding effects of developmental toxicity, the lifespan analysis started from adult worms and lasted the whole lifespan. While treatment with PS had a slight effect on the lifespan, survival analysis revealed a dose-dependent detrimental effect of PS-NH$_2$ treatment: The mean lifespan of animals exposed from day 1 adult to PS-NH$_2$ particles (100 µg mL^{-1}) was significantly reduced from 27 days in untreated control to 22 days **(Figure 49 C – D)**.

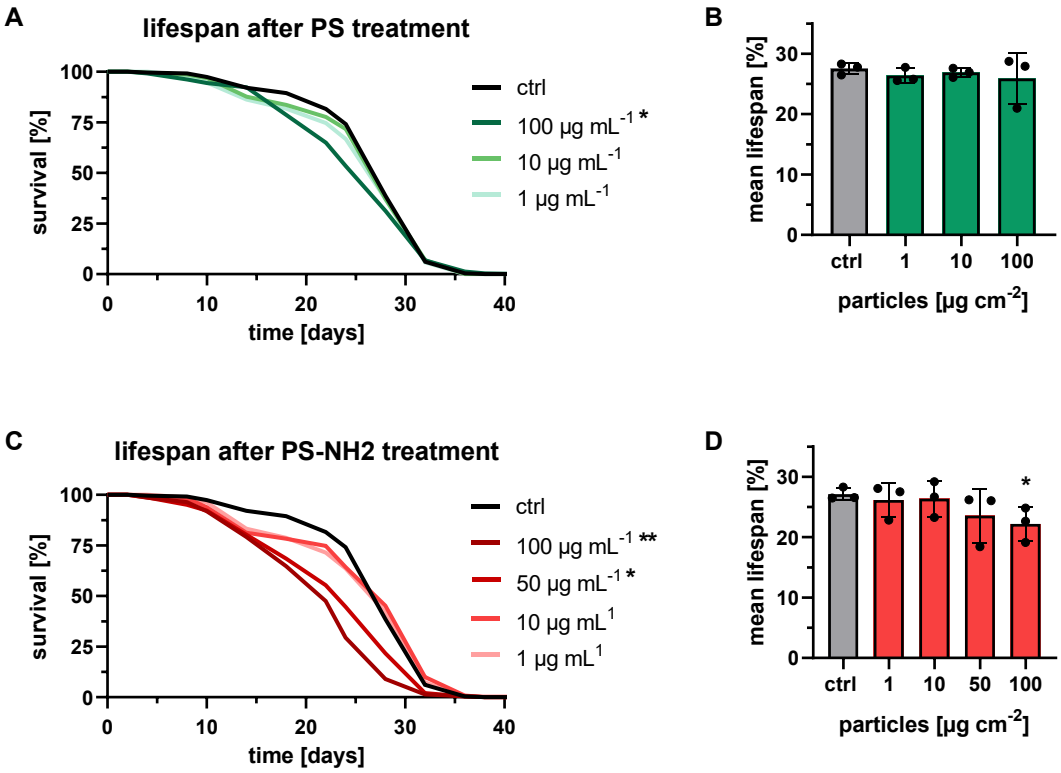

Figure 49. PS-NH$_2$ particles affect animals' lifespan. Survival analysis **(A, C)** and mean lifespan **(B, D)** of WT animals treated with the indicated concentration of PS **(A, B)** or PS-NH$_2$ **(C, D)** from day 1 old adult in liquid. Shown are data from three independent experiments (N=3, n=63 - 106) mean ± SD and unpaired T-test indicates differences between treatment and control (* $p < 0.05$, ** $p < 0.01$, **** $p < 0.0001$). Summary of statistics is provided in **Table S9.**

In parallel to *in vitro* analysis, I used the concentrations that significantly affected worms' lifespan to study the effect of the particles on a neuronal level while specifically addressing AD pathology.

To this extent, the synaptic function in animals constitutively expressing the human Aβ 1 – 42 peptide under a pan-neuronal promoter (nAD), which are known to display neuromuscular defects, was investigated.[145] When exposing *C. elegans* to plates containing aldicarb, an acetylcholine esterase inhibitor, an accumulation of acetylcholine in the synaptic cleft leads to time-dependent muscle contraction followed by complete paralysis of the worms.[166] In **Figure 50** it can be seen, that paralysis of the nAD model strain starts earlier compared to the WT animals. However, 100 µg mL^{-1} PS-NH_2 particles accelerated the paralysis in both strains.

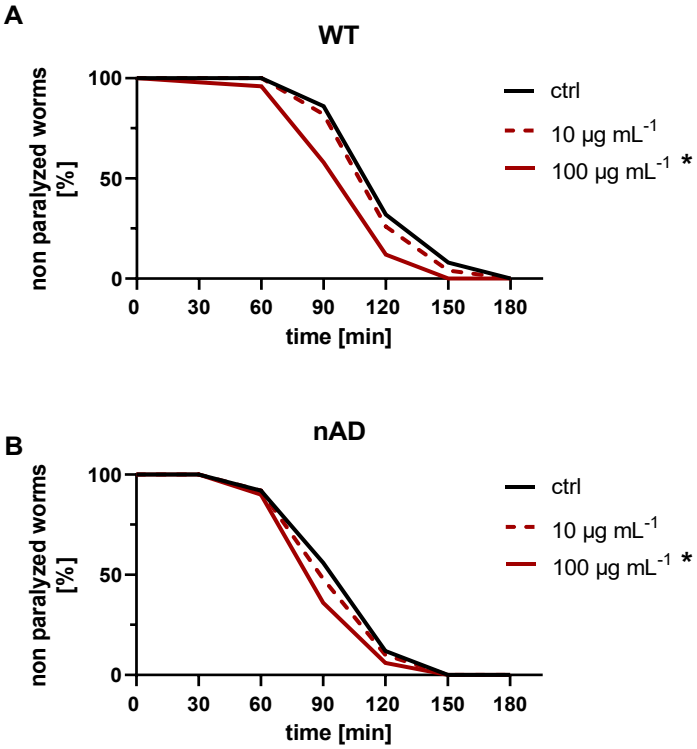

Figure 50. Aldicarb Assay showed PS-NH_2 mediated paralysis in WT and nAD animals. A) WT and **B)** nAD worms were treated as L4/YA with 10 and 100 µg mL^{-1} PS-NH_2 for 24 h. and afterwards 25 worms per condition were transferred to fresh Aldicarb plates to measure paralysis of the worms (every 30 min). Shown are data from two independent experiments (N=2, n=50 and Log-Rank test shows a statistically significant difference between ctrl and PS-NH_2 in WT [100 µg mL^{-1} (X^2 = 13; Bonferroni * P-value = 0.002) and nAD animals (X^2 = 13; Bonferroni *P-value = 0.007)].

PS-NH_2 in liquid culture alters mitochondrial related parameters

Different degrees of mitochondrial stress in *C. elegans* differentially impact animals' development/size and lifespan.[141,197–199] Thus, similar to *in vitro* experiments, the

hypothesis that PS-NH_2 particles may induce mitochondrial damage in *C. elegans* was investigated. To this end, two transgenic strains were employed: One expressing a transcriptional reporter for a cytochrome *p450* gene *cyp14a4p::gfp* and one expressing a reporter for mitochondrial unfolded protein *hsp6p::gfp*, which are both known to be induced upon mitochondrial stress.[154,200] No increase in the GFP expression could be detected after treating the *hsp6p::gfp* strain from either L1 for 3 days with 50 µg mL^{-1}, or from L4 or adult worms for 24 h with 100 µg mL^{-1} PS-NH_2 **(Figure 51 A – C)**. Similarly, the GFP signal in 3-day-old *cyp14a4p::gfp* animals treated from L4 was acquired, showing no difference between 100 µg mL^{-1} PS-NH_2 treatment and control **(Figure 51 D).**

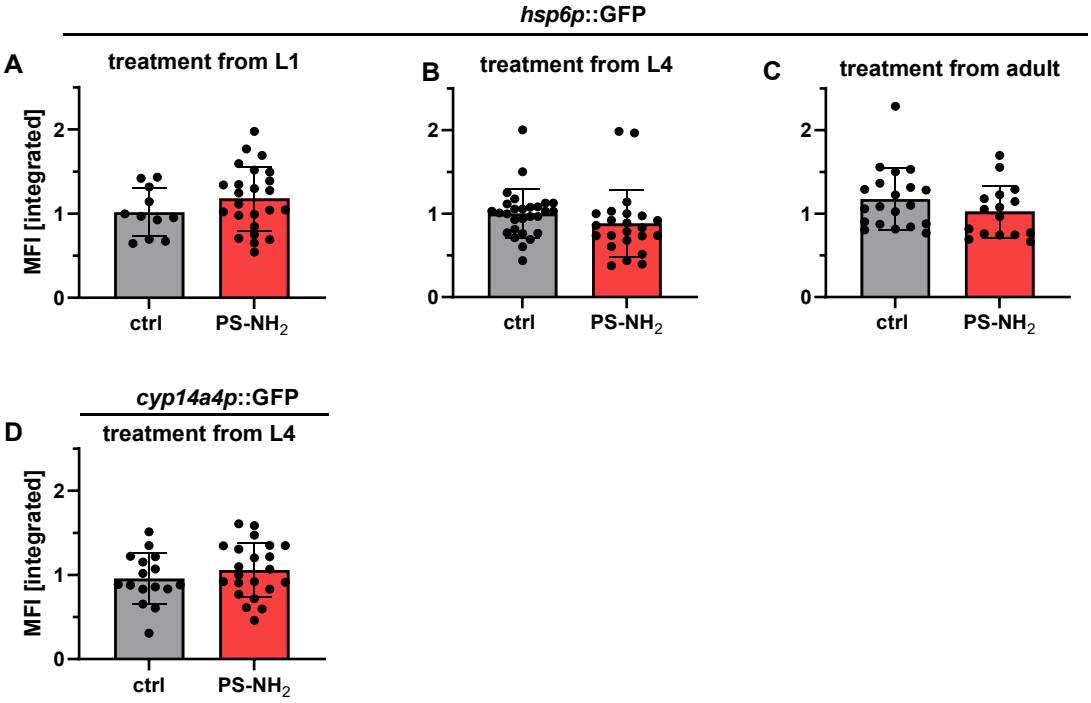

Figure 51. No induction of mitochondrial stress response genes after treatment with PS-NH_2. A-C) Integrated mean fluorescence intensity (MFI) of 4 d old *hsp6p*::GFP animals after treatment with 50 µg ml^{-1} PS-NH_2 for 3 days from L1 (N=2, n=38) **(A)**, 100 µg ml^{-1} PS-NH_2 for 24 hours from L4 animals (N=2, n=45) **(B)**, and 100 µg ml^{-1} PS-NH_2 for 24 hours from young adult (N=3, n=29) **(C)**. **D)** Integrated mean fluorescence intensity (MFI) of 4 d old *cyp14a4p*::GFP animals (N=2, n=38), treated from L4 with 100 µg mL^{-1} for 48 h in liquid culture. GFP intensity and size where quantified after transferring on NGM plates with a fluorescence microscope 200 x magnification in the FITC channel. Data show the mean ± SEM and unpaired T-test indicates no differences.

To further address possible alterations in mitochondrial functions, a similar readout previously investigated *in vitro* in SH-SY5Y cells, was used to measure a possible

increase in mtROS. **Figure 52 A** shows representative images after treating L4 worms for 24 h with 100 µg mL^{-1} of PS-NH_2 and subsequent staining with MitoSOX™ for 24 h. Compared to the control (untreated and stained), treatment with the pesticide paraquat significantly increased the mtROS production. Paraquat is a well-known inducer of mitochondrial stress, due to its complex I and III mediated reduction into the a radical inside the mitochondrial matrix.[201,202] However, no increase in mtROS could be detected after 24 h treatment with 100 µg mL^{-1} PS-NH_2. In fact, the calculated MFI in **Figure 52 C** exhibits even a significant reduction of mtROS after PS-NH_2 treatment. In parallel, tetramethylrhodamine ethyl esther (TMRE) staining and rotenone treatment were used to unravel the particles effect on the mitochondrial membrane potential. Rotenone is another pesticide and like paraquat, exposure leads to a decreased mitochondrial membrane potential due to its direct inhibition of mitochondrial complex I.[203] This effect is recognizable by a significant decreased MFI in **Figure 52 B** and **D**. Of note, treatment with PS-NH_2 shows a significantly reduced MFI, indicating a decrease in the mitochondrial membrane potential which is consistent with results observed from *in vitro* experiments in cells.

Overall, my *in vivo* data indicate that PS-NH_2 treatment affects animals' development, motility and lifespan, together with alterations in synaptic and mitochondrial function.

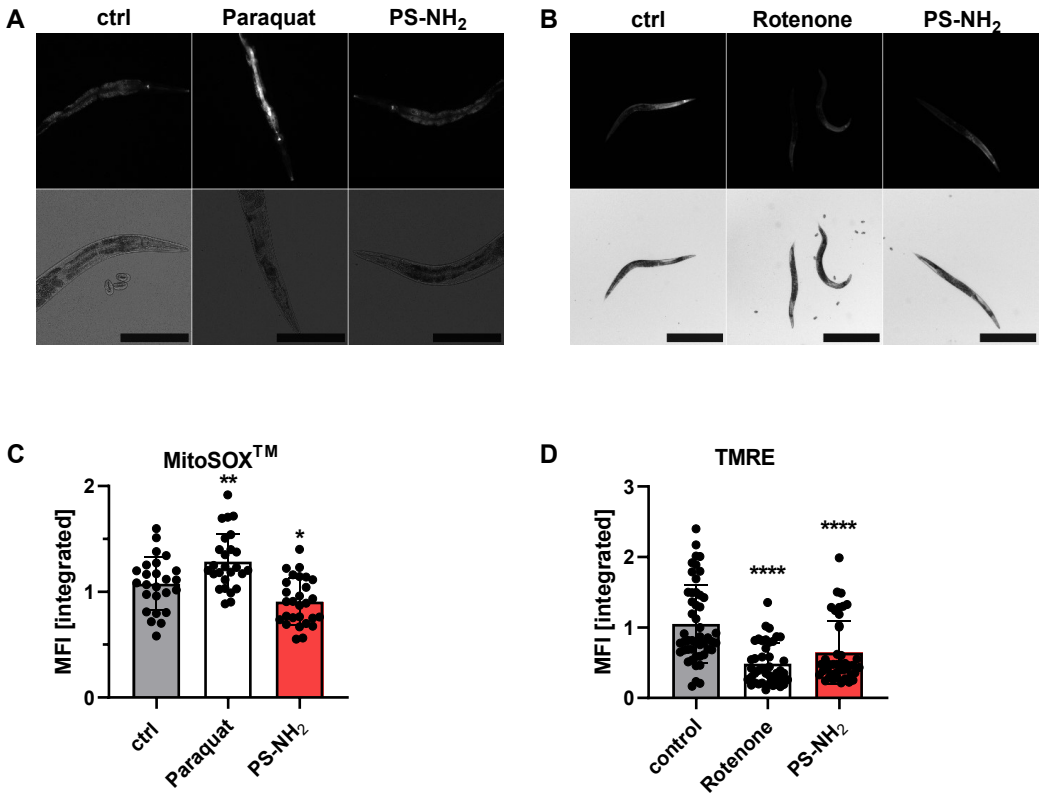

Figure 52. $PS\text{-}NH_2$ decreases mitochondrial membrane potential without increase in mitochondrial ROS. Representative fluorescence images of adult WT worms treated with **A)** paraquat as control and 100 µg mL^{-1} $PS\text{-}NH_2$ from L4 worms for 24 h previous MitoSOX™ staining for 24 h in liquid (scale bar = 250 µm) or **B)** rotenone as control and 100 µg mL^{-1} $PS\text{-}NH_2$ from L4 worms for 24 h previous TMRE staining for 3 h in liquid (scale bar = 1 000 µm). **C)** Integrated MFI of MitoSOX™ stained adult worms without (ctrl (N=3, n=38) and after treatment with paraquat (N=3, n=39) or 100 µg mL^{-1} $PS\text{-}NH_2$ (N=3, n=41) for 24 h. **D)** Integrated MFI of TMRE stained adult worms without (ctrl (N=3, n=48)) and after treatment with rotenone (N=3, n=40) or 100 µg mL^{-1} $PS\text{-}NH_2$ (N=3, n=42) for 24 h. Shown are data from three independent experiments (N=3, n=63 - 106) ± SEM and unpaired T-test indicates differences between treatment and control (* $p < 0.05$, ** $p < 0.01$, **** $p < 0.0001$).

5 Discussion

5.1 Particles physicochemical characteristics changed depending on respective exposure media

In order to study the role of PS and PS-NH_2 *in vitro* and *in vivo*, it is important to analyze the initial physico chemical characteristics of the particles as well as their possible changes during the different experimental settings. To this extent, during a short stay in Dr. Laromaines laboratory at the *Institut de Ciència de Materials de Barcelona, ICMAB-CSIC* in Barcelona, I employed FTIR, TEM, DLS and Turbiscan analysis to characterize PS and PS-NH_2.

FTIR analysis confirmed expected chemical bindings for PS and PS-NH_2

The chemical bindings were analyzed via FTIR to confirm the polystyrene identity as well as differences between PS and PS-NH_2 (comparison in chapter 4.1). According to the described results, it could be shown that the particles are both polystyrene nanoparticles, one of which has been amine modified (PS-NH_2). However, the molecular structure of PS-NH_2 cannot be clearly identified: The observed peak at 1733 cm^{-1} in the PS-NH_2, which is ascribed to a possible carbon oxygen bond (C=O), might be part of the amine surface modification when it is bound to the styrene backbone.[175]

This would be in line with the manufacturer's description but also with findings by Sun et al. They analyzed PS particles after amination treatment and one of their representative peaks for amines is in line with peaks in our PS-NH_2 spectra (e.g. 3420 cm^{-1}). Moreover, the authors concluded that the amine substitution takes place at the PS benzene, which in their spectra is supported by a missing peak at 1830 cm^{-1} in the aminated spectra, compared to the naked particles, what could not be observed in my analysis.[170] This can be further evidence that the amination is tied to the styrene backbone rather than the benzene.

DLS analysis revealed particle size depending on the exposure media composition

In addition to the chemical structure analysis, the measurement of the particle size via TEM and DLS showed that the particles were uniformly round and the size described by the manufacturer of ~50 nm was confirmed, when measured dry (TEM) or in water (DLS). As soon as the particles got in contact with different exposure media, the hydrodynamic

diameter (Z-Average), the PDI and the ζ-potential changed. In general, PS and PS-NH_2 were very stable in both cell culture media conditions regarding the size and the PDI, although the hydrodynamic diameter was slightly increased in BGM and DM compared to medium only (**Figure 13**).

These results might indicate that serum proteins (from FCS and BSA) induced alterations on the particle surfaces like building a corona on the particles.[2] This in turn could affect the route of internalization, which was previously shown in SH-SY5Y cells.[2,204–206] Ruenraroengsak and Tetley could further show that Z-average, PDI and the ζ-potential also differ depending on the suspension medium of the particles, which agrees with my measurements. [2,207]

Although the particles' size increased after adding proteins, the ratio of particle and protein might play an important part when it comes to particles' stability: A higher amount of protein (like in BGM) seems to stabilize the particles, implicating that protein corona formation leads to less agglomeration and a smaller size of particles.[2] This might explain the smaller particle size in BGM compared to DM.[2]

A similar effect was also observed for *C. elegans* media between S-Medium containing OP50 and BSA (1 %) and S-Medium containing OP50 but without BSA. However, these results show a much higher size range, up to ~1 µm for PS and 4.5 µm for PS-NH_2. *E. coli* bacteria usually have a size between 1 – 2 µm and a possible internalization or other interaction with the bacteria cannot be excluded, due to the fact that alive OP50 bacteria were used as a food source.[208] Although the particles, especially PS-NH_2 tend to agglomerate and coronate, adding BSA seems to reduce the particles mean Z-average significantly: It is not only reducing the actual size of the particles in general, but it helps to regain the original particle size. This effect becomes obvious from the histogram presenting the intensity dependent from the size in chapter 4.1, where two different populations of particles could be detected: one of the original size and a bigger one at the end of the range, which is most likely interacting with the OP50 bacteria (~ 1 500 nm, shown **Figure S1**) **(Figure 13)**. Furthermore, this phenomenon is schematically demonstrated in **Figure 53**, as there are still bigger aggregates of particles, but also a population with smaller and singled particles.

The analysis of the PDI supported the hypothesis of different sized particle populations. The PDI is a dimensionless indication for the quality of a particles solution regarding to their size distribution, where smaller values (<0.05) are assumed to be highly monodispersed and higher values (>0.7) exhibit a very polydisperse particle solution.[209]

My data show that the PDI under cell culture conditions for PS and PS-NH_2 exhibited values under 0.3 and could be described as a heterogeneous size distribution. However,

the particles in the *C. elegans* liquid media were well above this range and showed multiple particle populations of different sized particles (**Figure 15**).[209]

Previous results from the literature showed that toxicity is strongly influenced by particle size and that uptake of big particles (500 and 5000 nm) improved when co-exposed with small particles (50 nm) resulting in an increased toxicity.[96] This implicates that the observed toxicity in *C. elegans* exposed to particles in liquid compared to no detectable effects when treated on solid plates, might be partly due to the presence of PS-NH_2 particles of bigger and different sizes.

The particles' electrochemical stability was decreased in exposure media

A further indicator of stability is the ζ-potential, that mainly refers to the electrochemical stability. Analysis of the ζ-potential showed that both particles have a decreased ζ-potential when proteins or bacteria were added compared to initial conditions indicating a decreased stability of PS and PS-NH_2 in all exposure media (**Figure 15**). Interestingly, initially positively charged PS-NH_2 particles exhibit a negative charge under all tested experimental settings, that is again, most likely due to a protein corona formed by negatively charged proteins in the exposure media.

Particles' stability was not affected over time

None of the above discussed characterizations could reveal an effect on the physicochemical properties over time, implicating that the particles remain stable over time (**Figure 15**). In addition, the sedimentation capacity of the particles under cell culture conditions was also investigated via Turbiscan analysis. Compared to *C. elegans* culture conditions, where the worms are maintained under continuously mild shaking, the cells are exposed to particles under static conditions. Initially, due to the density of PS (1.04 – 1.06 g cm^{-3}), one would assume that the particles sediment under static conditions and over time.[9] Previously, Busch et al. calculated the estimated dose of PS and PS-NH_2 sedimenting onto the cells over time using an *In vitro* Sedimentation, Diffusion and Dosimetry model (ISDD).[146] The simulations revealed that after 24 h, from initially added 50 µg cm^{-2}, 8 µg of PS (50 nm, Polysciences (Germany)) and 5 µg of PS-NH_2 (50 nm, Merck (USA)) reached the cells.[146] Indeed, the results gained from Turbiscan analysis indicated that neither PS nor PS-NH_2 sediment or flocculate at all within 48 hours (**Figure 16**).This may affect the actual final concentration the cells are exposed to and therefore the actual concentration inducing toxic effects.

In summary, it was shown that the physical chemical state of the particles depends on the exposure medium and the settings. In the presence of proteins or bacteria in the exposure medium, the particles enlarge and the stability decreases (altered ζ-potential and PDI), but the state does not change over time **(Figure 53)**.

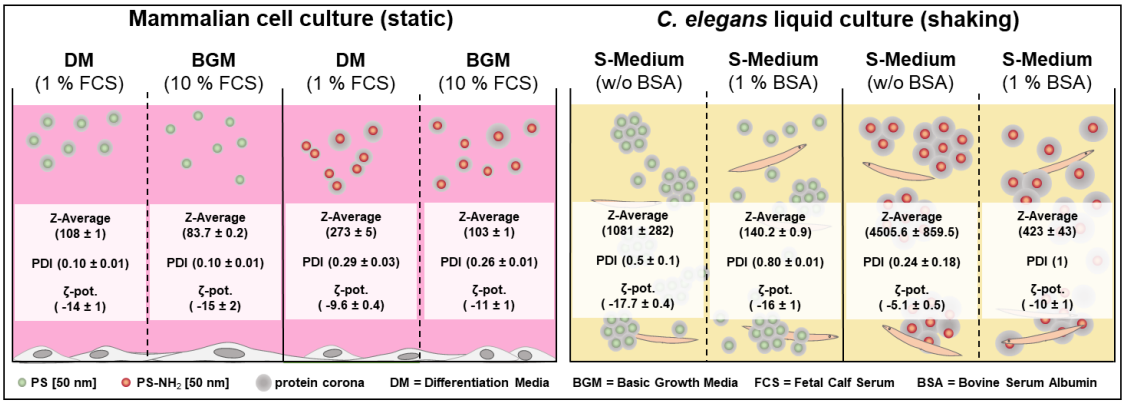

Figure 53. Summary of physicochemical characterization of PS and PS-NH_2. Image shows schematic illustration of particles changes in size (Z-average), poly dispersity index (PDI) and the ζ potential in BGM (10 % FCS) and DM (1 % FCS) and in *C. elegans* S-Medium with (1 % BSA) and without BSA (w/o BSA) compared to medium and S-Medium only (at t_0 = 15 min and room temperature).

5.2 PS-NH_2 but not PS induced toxicity *in vitro* and *in vivo*

In this work, numerous different endpoints and models were addressed to unravel cytotoxicity of PS and PS-NH_2 particles. A common feature that stood out both *in vitro* and *in vivo* was the significant toxicity induced only by PS-NH_2.

Acute PS-NH_2 exposure induced toxicity in vitro

Cell viability assays *in vitro* in HEK293 APP695 cells initially revealed a concentration dependent decrease of cell viability only for PS-NH_2, but not for PS, PS-YG or PVC. In this setting, a concentration of 1 µg cm^{-2} for 24 h significantly reduced the cell viability while concentrations of 50 µg cm^{-2} killed or less all cells (**Figure 17**). Similar results could be observed in SH-SY5Y cells thus excluding a cell type specific effect as well as a toxicity based on APP overexpression (**Figure 19**).

Due to the cell duplication time of ~ 35 h in SH-SY5Y cells, the cells were also treated with PS and PS-NH_2 particles for 48 h. This, together with the earlier time points of 1,2 and 4 h confirms not only a concentration-dependent effect but also reveals a time

dependency, since 48 h treatment with 5 µg cm^{-2} of PS-NH_2 led to higher cytotoxicity compared to 1, 2, 4 and 24 h treatment with the same concentration (**Figure 22**).

The results gained from cell viability analysis in HEK293 APP and SH-SY5Y cells are in line with findings by others, confirming the acute toxicity of PS-NH_2 particles.[146,210,211] Anguissola et al. could for instance already show a concentration-dependent toxicity mediated by PS-NH_2, but not by PS or carboxylated PS in undifferentiated SH-SY5Y, while using the same particles and comparable particle concentrations to the ones used in this study.[211]

In contrast, there are also studies showing increased toxicity for PS particles in SH-SY5Y cells. For example, Ban et al. present a slightly reduced cell viability after exposing differentiated SH-SY5Y cells to 138 & 690 µg of PS (50nm, NANO-MIR Co. (Japan)) for 24 h, while 138 µg used in their study is equivalent to 50 µg cm^{-2} used in my cell viability assays (**Table S8.** Treatment concentrations of particles **in "*in vitro* concentrations" (µg cm-2) used for *in vivo* (µg mL-1). Frequently used concentrations *in vitro* are 1, 10, 50 and 100 µg mL-1.** summarized different particle concentrations in different units).[212] The discrepancy between the studies could be ascribed to different experimental settings: Firstly, different assays were used to analyze particle toxicity (Live/Dead Cell Staining Kit II vs Resazurin Assay). Secondly, different exposure media were used (DMEM/F12 with ATRA and 1 % FCS vs Neurobasal with ATRA and B-27), which, based on our particle's characterization, may have a significant influence on particle physicochemical feature.

Acute and chronic PS-NH_2 induced toxicity in differentiated SH-SY5Y cells

I also observed that differentiated cells seemed to be more sensitive to PS-NH_2 treatment compared to proliferating SH-SY5Y cells when analyzing cell viability after 48 h treatment (**Figure 41**). In addition, the long-term treatment of 6 days killed almost 90 % of the cells already after treating with 5 µg cm^{-2} and all the cells after treatment with 10 µg cm^{-2}, indicating a more severe effect compared to an acute exposure (**Figure 41**). Interestingly, ATRA induced differentiation of SH-SY5Y cells was shown to induce a more resistant phenotype when it comes to neurotoxicity: For instance, Cheung et al. showed a decreased sensitivity of differentiated SH-SY5Y cells to the neurotoxicant 6-hydroxydopamine (6-OHDA) compared to undifferentiated cells.[192] The authors hypothesize that in line with another study, up-regulating of the survival kinases *Akt* may lead to neuroprotection. [192,213]

The fact that differentiated cells were more sensitive to PS-NH_2 exposure, could be ascribed to the different cell states or to particles specific characteristics in the differentiation media. Changes of SH-SY5Y cells undergoing neuronal-like differentiation may sensitize the cells to particle toxicity, for instance by morphological changes, such as increased neuronal outgrowths. These are indeed characteristics of the differentiation process and lead to an increased cell surface, which, if the toxic effects of PS-NH_2 are due to damage in cellular membranes, may thus increase cell vulnerability compared to undifferentiated cells.

In conclusion, my *in vitro* data revealed a cytotoxicity after cells were exposed to concentrations of PS-NH_2 particles > 5 µg cm^{-2} under all tested conditions, whereby toxicity was increased in a time- dose- and cell state-dependent manner and a higher sensitivity in differentiated cells.

PS-NH_2 affected development and lifespan in vivo

In line with the observations from *in vitro* experiments, *in vivo* studies with *C. elegans* revealed a toxicity mainly mediated by PS-NH_2 although it was highly dependent on the experimental settings. As already mentioned, *C. elegans* can be cultivated in liquid media or on solid NGM agar plates, therefore the effect of PS and PS-NH_2 particles was compared under both scenarios, while an effect could be observed only in animals exposed to PS-NH_2 in liquid.

For instance, no decrease in movement, development or fertility could be detected when worms were cultivated and treated on solid plates, neither in WT nor in the mAD (Aβ 1 – 42 peptide overexpressing) strain (**Figure 45 –Figure 47)**. However, using the same concentration range (1 – 100 µg mL^{-1}) in liquid S-Medium a concentration- and stage-dependent toxic effect was observed only with PS-NH_2, which is in line with the *in vitro* data. Specifically, treatment of WT animals for 4 days from the L1 stage reduced animals' length in a dose-dependent manner and arrested animals' development at the highest concentration 100 µg mL^{-1}. In addition, similar results could be observed while investigating the movement in liquid (**Figure 48**).

Finally, treatment of young adult worms with 100 µg mL^{-1} significantly shorten the lifespan of worms from 27 to 22 days, proving that chronic exposure can have a far-reaching impact on animals' lifespan (**Figure 49**). A number of studies investigating the effect of PS and PS-NH_2 in *C. elegans* can be found in the literature, most of which were also conducted in liquid culture whereby the results are only in part comparable to those of my work.

The effect of the particles on animals' development clearly indicated PS-NH_2 dose-, time and stage-dependency and are in line with a previous study, which showed the decrease in body length, too, however also after PS treatment.[214] The literature also showed a reduced fertility and general reproductive toxicity mediated by both PS (23 nm, no manufacturer mentioned) and PS-NH_2 (23 nm, no manufacturer mentioned), whereby results gained from PS-NH_2 were more severe.[215] Thus, similar to what was previously discussed for *in vitro* findings, there is also evidence of an induced toxicity with PS particles, although no influence of PS could be observed under any tested condition in my work. For instance, it was shown by Qu et al. that PS (100 nm, Janus New-Materials Co. (China)) exposure from L1 to L4 to 0.001 – 1 µg mL^{-1} altered movement and decreased head trash and body bends.[85]

Observing toxicity mediated by PS is in contrast to results gained in my work. The concentration used in studies that revealed PS (100 nm, Janus New-Materials Co. (Nanjing, China)) toxicity in *C. elegans* were often much lower (0.001 – 1 µg mL^{-1}) compared to concentrations used in my experiments (1 – 100 µg mL^{-1}).[19,84,85,216] Although, the particles used in these studies were slightly bigger (100 nm) this might not explain the controversial results, as it was previously shown by Mueller et al., that the induced toxicity in *C. elegans* is higher in smaller PS particles (e.g. 50 nm) and is more likely due to other particle specific characteristics.[87]

Since neither the concentration nor particles' size seem to be responsible for the differences, it seems likely that the contrasting results are either due to differences in the experimental design, which is not described in detail, or to the condition of the particles itself (e.g. specific stabilizers in the stock solution), since again no information is available from the manufacturer.

Overall, results in *C. elegans* indicate that particles toxicity *in vivo* strongly depends on the experimental settings. Thus, the same particles at the identical concentrations, which in solid culture medium showed no effect, could instead inhibit development, reduce worm length and significantly shorten lifespan when the worms were treated in liquid culture. It can be hypothesized that this effect is based on the fact that the worms cannot escape from the particles when cultured in liquid compared to solid culturing and they are constantly surrounded by the particles. Moreover, liquid culturing may improve particles uptake via different routes and not only by ingestion.[196]

5.3 Mode of toxicity

To unravel the possible mechanisms behind PS, and especially PS-NH_2 dependent toxicity, the underlying forms of cell death, the alterations of mitochondria potential as well as the production of ROS and mtROS were investigated.

PS-NH_2 induced late apoptosis and necrotic cell death

Cell death analysis was carried out with Annexin V-FITC and PI staining in undifferentiated SH-SY5Y cells under acute exposure scenario of PS and PS-NH_2 treatment with 5, 10 and 25 µg cm^{-2} for 1, 2, 4 and 24 h.

According to cell viability and cell death assays, no toxic effect of PS at any tested concentration could be observed (**Figure 26**). Instead, in line with the cell viability assays, treatment with PS-NH_2 induced cell death in a dose and time dependent manner (**Figure 27Figure 28**). Moreover, these findings are in line with the literature, showing only PS-NH_2 induces cell death, in different types of cells, yet, again with some contradicting findings showing toxicity for PS, too.[66,207] Specifically in SH-SY5Y cells, Tang et al. hypothesized that as revealed by an increased release of cytochrome c, combined with an overexpression of apoptotic related proteins like protease activating factor-1 (Apaf-1), cysteinyl aspartate specific proteinase-3 (caspase-3), and caspase-9, apoptosis may play a major role in PS induced toxicity (concentrations >10 µg) (50 nm; Janus New-Materials (China)).[190] In addition, Xia et al. could show different modalities of cell death induced by PS-NH_2 (60 nm; Bangs Laboratory (Fishers, US)) for macrophages and bronchial epithelial cells: the former dying through apoptosis, the latter through necrosis. Although this study did not address cell death *in vivo*, few studies could also identify a form of apoptotic cell death in zebrafish and in mice.[48,96]

To sum up, in my study PS-NH_2 seems to induce severe apoptosis or even necrotic cell death, because independent from exposure time or concentration, as soon as cell death is induced, the population is positive for both FITC staining of Annexin V, a typical marker for apoptosis as well as for PI staining nuclei of dead cells and therefore a typical marker of necrotic cells.

PS-NH_2 had no significant effect on ROS production but depolarized mitochondrial membrane potential

In addition to cell death analysis, the production of ROS was investigated, which depending on the amount, can interfere with different forms of cell death.[184] Cells were

stained with H_2DCF-DA and DAPI was used to exclude dead cells and to avoid unspecific staining. While FACS analysis showed neither PS nor PS-NH_2 significantly increased ROS production (**Figure 31 – Figure 32**).

In parallel with the results gained from ROS analysis *in vitro*, neither PS nor PS-NH_2 induced mtROS under any of the tested conditions (**Figure 33 –Figure 34**). Interestingly, while PS-NH_2 treatment did not significantly impact ROS and mtROS production, it instead reduced the mitochondrial membrane potential (MMP) already at concentrations where no significant cell death was detected (25 µg cm^{-2} PS-NH_2 for 1 h) (**Figure 37**).

Previous work on SH-SY5Y cells showed an increased ROS production after treatment with PS particles (50 nm, Janus New-Materials (China)) but have in fact used higher particles concentrations (up to 5 x).[190] Similar concentrations to my experiments were used by Nie et al., which resulted in increased oxidative stress in SH-SY5Y cells after exposure to PS (60 nm, Bangs Laboratory (USA)).[217] Interestingly, the authors used SH-SY5Y cells up to 6 months after thawing, which may lead up to passage 48 when passaging at least 2 times per week (which is recommended).[136] In my experiments I used SH-SY5Y cells until passage 20. The literature points out that SH-SY5Y cells may not only lose their ability to differentiate after passage 15 to 20, but are also attributed with '*a rough, unhealthy appearance'* as well as increased cell death, when culturing in high passages (20 – 50) what might explain the PS induced increase in oxidative stress observed by the authors.[136]

In addition, in T98G and Hela cells, ROS production was increased after PS exposure, too. However, in cells of the respiratory tract, ROS and mitochondrial damage could be detected, comparable to our study, upon treatment with PS-NH_2 only.[60,61,218]

Importantly, the results gained from *in vivo* experiments in *C. elegans* support my *in vitro* findings. Similar to *in vitro* experiments, the possible induction of oxidative and mitochondrial damage in *C. elegans* mediated by PS-NH_2 particles was investigated. Of note, two transgenic reporter strains for mitochondrial stress (*cyp14a4p::gfp* and *hsp-6p::gfp)* were used, indicating no altered expression (**Figure 51**).[154,200] Additionally, mtROS production was measured through MitoSOX™ staining in *C. elegans* after PS-NH_2 exposure, which in line with *in vitro* results, did not lead to a significant alteration (**Figure 52**).

However, when investigating the effect of PS-NH_2 on the MMP *in vivo* with TMRE, a significant reduction in the signal could be observed indicating a depolarization of the mitochondrial membrane comparable to the results gained from JC-1 staining in SH-SY5Y cells (**Figure 52**).

The mechanism underlying PS-NH_2 mediated toxicity might be based on cell membrane disturbance

Up to now, it has often been reported in the literature that the aminated particles exhibit high cytotoxicity, including ROS production, mitochondrial membrane disturbance and cell death, compared to other particles.[2] However, it has not yet been demonstrated on which particle property this toxicity is based on and which mechanism underlies it. Previously, the physicochemical differences between PS and PS-NH_2 under different experimental systems were discussed and one of the main differences between the particles is their initial charge. While PS particles exhibit a slight anionic charge, most likely from sulfate esters, PS-NH_2 have, due to their amine groups, a cationic surface charge.[219] The different charge may affect the mechanisms of particles' uptake, which could then influence their toxicity. Indeed, there are reports showing both, particle-dependent and cell type-dependent internalization of particles, although the results are contradictory: Yacobi et al. pointed out that PS are internalized via non-endocytic pathways, possibly by interaction with the lipid bilayer of the plasma membranes and they further demonstrate that the uptake of positively charged PS-NH_2 is much higher compared to negatively charged particles.[2,220] In contrast to Yacobi et al., Jiang et al. described the uptake of positively charged PS-NH_2 via clathrin-mediated endocytosis, whereas experiments with plain PS indicated internalization by micropinocytosis. [2,221,222] Furthermore, Nie et al. could show that 60 nm sized anionic PS particles enter SH-SY5Y cells via caveolae-mediated endocytosis.[2,217]

Walczak et al. further investigted the translocation of negatively and positively charged PS-NH_2 (50 nm, Merck) *in vitro* in co-culture experiments (Caco-2 and HT29-MTX) concluding a charge dependent translocation of the particles. However, when comparing non-modified (PS) and carboxy-modified particles, both of which have an anionic charge, the authors found a 30-fold difference in translocation, and suspected this was ascribed to modifications rather than to their charge.[223] The physicochemical characterization could further show, that independent from the initial charge, both particles had a similar negative ζ-potential in all different exposure media, most likely due to coronation with negatively charged proteins, which may support the hypothesis that the particles fate is destinated by the cationic group itself instead of the charge. Indeed, it is already known that amine groups on NPs can make material permeable to water.[224] In particular, in the study by Hong et al. it was shown that amine groups can form holes in lipid membranes, leading to enzyme leakage and increased membrane permeability, which could underlie the molecular structure in addition to the cationic charge.[225] Finally, it was shown that PS-NH_2 (50 nm, Sigma) initiated nanosized holes in the membrane of alveolar epithelial cells and the authors hypothesized a possible electrostatic attraction between amino

surface grouops and phospholipids of cell membrane and thereby a transformation of lipid bilayer.[226]

Altogether, findings from the literature together with the fact that PS-NH_2 affect the mitochondrial membrane potential but does not induce a gradual transition from early (Annexin V + / PI -) to late (Annexin V + / PI +) apoptosis/necrosis, suggest that PS-NH_2 particles' toxicity is likely induced by direct damage to cellular membranes.

5.4 Toxicity in neuronal related readouts

My data show that PS-NH_2 not only have cytotoxic effects, but also affect neuronal differentiation. Therefore, further neuronal readouts such as the elongation of neuronal outgrowths, the expression of neuronal marker proteins as well as APP processing and Aβ secretion, specifically addressing the ADs pathology, were investigated.

PS-NH_2 increased Aβ 1 – 42 secretion, decreased neuronal outgrowth and altered expression of neuronal marker proteins in SH-SY5Y cells

Firstly, comparable analysis in HEK293 APP695 and SH-SY5Y exhibit a concentration dependent decrease in cell viability mediated by PS-NH_2 particles, what is in line with findings by others and confirmed the acute toxicity of PS-NH_2 particles and excluded an APP overexpressing specific effect.[146,210,211]

Moreover, in both cell lines the secretion of Aβ peptides Aβ 1 – 40 and Aβ 1 – 42 was analyzed in the conditioned media. In general, Aβ is known to form extracellular plaques, whereby Aβ 1 – 42 is assumed to be more prone to aggregate and to initiate Aβ deposition.[227] A slight increase in Aβ 1 – 42 could be observed in both cell lines, while only SH-SY5Y cells exhibit a significant difference (**Figure 18 –Figure 20**). These results indicate, that the PS-NH_2 mediated induced cytotoxicity was not necessarily based on increased Aβ secretion. However, PS-NH_2 might promote the formation of pathogenic Aβ 1 – 42 under acute exposure to even low concentrations.

An important characteristic of neurons and differentiated SH-SY5Y cells is the extension of neurite outgrowths. In this study, the effect of PS and PS-NH_2 on the neurite outgrowths of differentiated cells, as well as during differentiation, was investigated. Particle treatment of 48 h after 7 days of differentiation showed a concentration dependent decrease in neurite outgrowth length only for PS-NH_2 treatment (> 1 µg cm^{-2}) (**Figure 42**). Similar results could be observed when cells were more chronically treated during the differentiation for 6 days, however the cells were more sensitive during

differentiation. Interestingly, while an acute exposure of PS did not influence the neurite outgrowth length, chronic PS exposure (> 1 µg cm^{-2}) decreased the neurite outgrowth length in all conditions independently from concentrations up to ~70 %. These results are in accordance with findings from Ban et al., showing that PS (50 nm , NANO-MIR Co. (Japan)) decreases the neurite outgrowth in SH-SY5Y cells.[212] However, due to the fact that an acute PS treatment in differentiated SH-SY5Y did not alter neurite outgrowth length, chronic exposure during differentiation may inhibit the neurite outgrowth possibly via mechanical pathways like covering the cells surface.

In addition to investigating the particles effect on the morphology of differentiated SH-SY5Y cells, the expression of different neuronal marker proteins (APP, NSE, βIIITUB, SYN, NLGN1 and NLGN3) was analyzed via fluorescence microscopy. Interestingly, the expression of APP, NSE, βIIITUB, SYN and NLGN1 was increased after treatment with 1 µg cm^{-2} (**Figure 43 –Figure 44**). It could be hypothesized that the observed increased expression of the different proteins could be a cellular reaction to stress. NSE is indeed an isoenzyme of the glycolytic enzyme enolase and an often used marker for neurons and neuronal differentiation.[195] However, it is also a marker for neuronal injury as it is upregulated when cells undergo stress and can support the degradation of the extra cellular matrix, actin remodeling and facilitate neuronal cell death.[228,229] The integral membrane protein SYN, prominent in presynaptic vesicles is instead not only a marker for neuronal differentiation, but a marker for axonal damage as well.[230,231] Furthermore, SYN colocalizes with APP, which is an important protein in AD's pathology and another marker for axonal damage.[230] NLGN1 and NLGN3 also play important roles in synaptic structure and function as cell adhesion and neuronal intercellular communication proteins as well as in neuronal morphology.[232] NLGN1 is an additional potential binding partner of APP derived proteins like Aβ and therefore it is conceivable that an increased Aβ content is in line with an increase of its binding partner NLGN1.[233]

Altogether, my results gained from experiments addressing neuronal related readouts *in vitro* show that PS-NH_2 not only have a cytotoxic effect but also effect neuronal differentiation and the secretion of neurotoxic Aβ 1 – 42.

PS-NH_2 affected C. elegans' movement and synaptic function

Compared to *in vitro* experiments, *C. elegans* reporter strains expressing Aβ 1 – 42 (in muscles (mAD) or neurons (nAD)) were used to investigate the particles effect on AD related readouts. Analysis of worms' movement on NGM agar plates, revealed (as expected) that mAD worms paralyze faster and have a decreased speed compared to

WT animals. However, no effect of the particles could be observed (**Figure 46 –Figure 47**).

Only after investigating the development in liquid culture, it became clear, that mAD worms exhibit a higher sensitivity to particles thus hypothesizing that the Aβ 1 – 42 worsen the PS-NH_2 particles' impact on the animal's development (**Figure 48**). Finally, the synaptic function of WT and nAD worms was analyzed via aldicarb assay. Exposure to aldicarb, an acetylcholine esterase inhibitor, leads to an accumulation of acetylcholine in the synaptic cleft, subsequently leading to muscle overactivation followed by paralysis of the worms.[166] The results showed that PS-NH_2 particles (100 µg mL^{-1}) lead to a significantly faster paralysis compared to control worms. Moreover, nAD worms seemed to be more sensitive to aldicarb itself, compared to WT animals, whereby the particles similarly affected WT and nAD strains. Interestingly, a previous study investigating worms' sensitivity to Aldicarb while comparing WT worms and worms expressing Aβ 1 – 42 in the muscles, has shown that acetylcholine transmission was inhibited in the mAD model.[234]

To summarize, my results showed that the used nAD strain seemed to suffer from an increased acetylcholine transmission, compared to WT worms, but PS-NH_2 exposure showed no significant difference between WT and nAD worms. However, my results indicate that the development of mAD worms is significantly stronger impaired by PS-NH_2 treatment than the WT animals what supports the *in vitro* displayed connection between PS-NH_2 exposure and Aβ 1 – 42 neurotoxicity.

5.5 Advantages and limitations of the study

Diversity of plastic particles

All particles used in this study belong to the primary and engineered NPs. Especially PS NPs are commercially available in a wide range of sizes and with different modifications and are used in a wide spectrum of application from medical drug delivery to ingredients of daily care products.[114,235,236]

These engineered particles differ from secondary particles mainly by their monodisperse and homogeneous size, but also due to their purity: During the manufacturing of bigger plastic products, a lot of different additives are used to modify the final product in order to improve the polymers performance and avoid early degradation.[9] These additives include fillers, plasticizers, dyes, lubricants and much more, and some of these chemicals are already known to have hazardous potential.[237]

In addition to additives, which are intentionally added to the products during production, Campanale et al. described chemicals, derived from environmental depositions, as a second form of chemical absorbance, taking place mainly during the formation of secondary particles and not for engineered particles.[237] Thus, engineered monodispersed particles mainly produced for experimental approaches could give heterogeneous results, which often cannot directly be compared to our environmental conditions since secondary particles derived from different types of plastic products consist of much more chemicals than only the plastic resins.[238] Therefore, one main challenge in the NPs field is to shift from the use of engineered particles to more environmental relevant and diverse particles.

Determining environmental concentrations

Moreover, the literature often points out a lack of information concerning the environmental concentration of plastic NPs since there are currently no calculations available to reflect the actual situation of plastic NPs in the environment.[35] Therefore, studies can lead to different results, because of the wide range of used concentrations for toxicity studies. For example, the study from Chiu et al. showed that non-modified or carboxylated particles inducing no toxicity at concentrations of 40 µg mL^{-1} but are toxic at higher concentrations (> 100 µg mL^{-1}).[58,59,239] Therefore, it is important to find suitable analytical methods to identify plastic NPs, their structure and their concentrations in the environment.[34,240] The current state of research enables the identification and characterization of micro sized particles by usage of techniques like X-ray photoelectron spectroscopy, Fourier transform infrared spectroscopy and Raman spectroscopy.[34,241–244] However, there are limitations to identify and analyze plastic NPs and thereby impede the realization of the particles' concentration we are exposed to in our environment.[34] So far, extrapolation studies assume environmental concentrations in a range of 0.1 to 1 µg L^{-1} or lower, but there are no clear evidences to support this hypothesis.[245–247]

Although, these concentrations are much lower compared to the ones I used in my study, it should be kept in mind that under experimental conditions the exposure time is very limited whereby under environmental conditions living beings are exposed to these amounts on a daily basis for years.

Advantage of SH-SY5Y cells and C. elegans as model systems

As described above, the wide range of different particles together with a relatively unknown environmental concentration, can go far beyond the scope of a study. Although,

many studies investigating the effect of PS NPs exist, the number of researches specifically addressing neuronal degeneration or the development of neurodegenerative diseases is still limited. One main challenge is to find a suitable model organism. For instance, experiments with mice could be useful for individual investigations, but do not allow extensive screening of many particles, concentrations or time points in order to protect animal welfare. Moreover, human stem cells can have a high risk for mutations and together with human 3D cell culture or organoids, it is time and cost consuming and therefore not recommended for high throughput analysis.[125] Finally, when deciding for immortalized human cell lines, they often lack of neuronal morphologies as well as metabolism.[125] In this study, SH-SY5Y were used for initial analysis of toxic parameters like concentrations, as well as, molecular mechanisms, whereby differentiated SH-SY5Y cells also allow to investigate more neuronal parameters. To further overcome the problem of moral and ethical guidelines, *C. elegans*, a powerful 3R complying model organism for toxicology studies was used. It allows to mimic different scenarios, like using different exposure settings (solid vs. liquid) or doing chronic lifetime and lifespan characterizations. Compared to *in vitro* studies, where only one or even a few cell types can be investigated in one scenario, *C. elegans* can give several different readouts especially on a behavioral level, by staying in line with ethical guidelines and animal protection. Ultimately, my multisystemic study allowed me to investigate dose, time and stage/cell dependent toxicity of the particles on different parameters (many of neuronal relevance), which could not be carried out using only one system.

Limits of my study

Nevertheless, to confirm findings of *in vitro* and *in vivo* studies, human studies might be useful, which are nonetheless still limited or missing. Recently, Cox et al. recalculated the amount of yearly uptake of MP, including ingestion and inhalation, to 94 283 MPs for adult females and 113 743 MPs for adult males.[248] This is in line with a WWF study carried out by the University of Newcastle, Australia, suggesting an amount of 2000 tiny pieces of plastic per week.[249] Moreover, a very current issue was discussed on 17 August 2020 in an online conference of the American Chemical Society (ACS), where researchers of the Arizona State University identified plastic particles in human brain and other tissues.[250] They analyzed the samples with flow cytometry, µ-Raman spectrometry and mass spectrometry and in addition to plastic monomers, the researchers could find the plastic constituent Bisphenol A in all human samples.

6 Conclusion

To sum up, after a systematic characterization of PS and PS-NH_2 physicochemical properties, treatment of undifferentiated as well as differentiated neuroblastoma cells clearly indicates a cytotoxic effect, a decrease in neuronal differentiation and an increase in secretion of Aβ primarily for aminated particles. Although the exact mechanism underlying the toxicity of aminated particles remains to be fully clarified, my cell death and mitochondrial membrane potential investigations suggest a possible early membrane damage. Finally, chronic particle treatment *in vivo* confirms a selective toxicity of aminated particles, with detrimental effects on *C. elegans* lifespan, motility and development, the latter even more affected in a *C. elegans* strain expressing human toxic Aβ. Overall, my multisystemic approach reveals a toxic effect induced by aminated polystyrene nanoparticles, especially in terms of neuronal parameters, which is consistent in *in vitro* as well as in *in vivo* models.

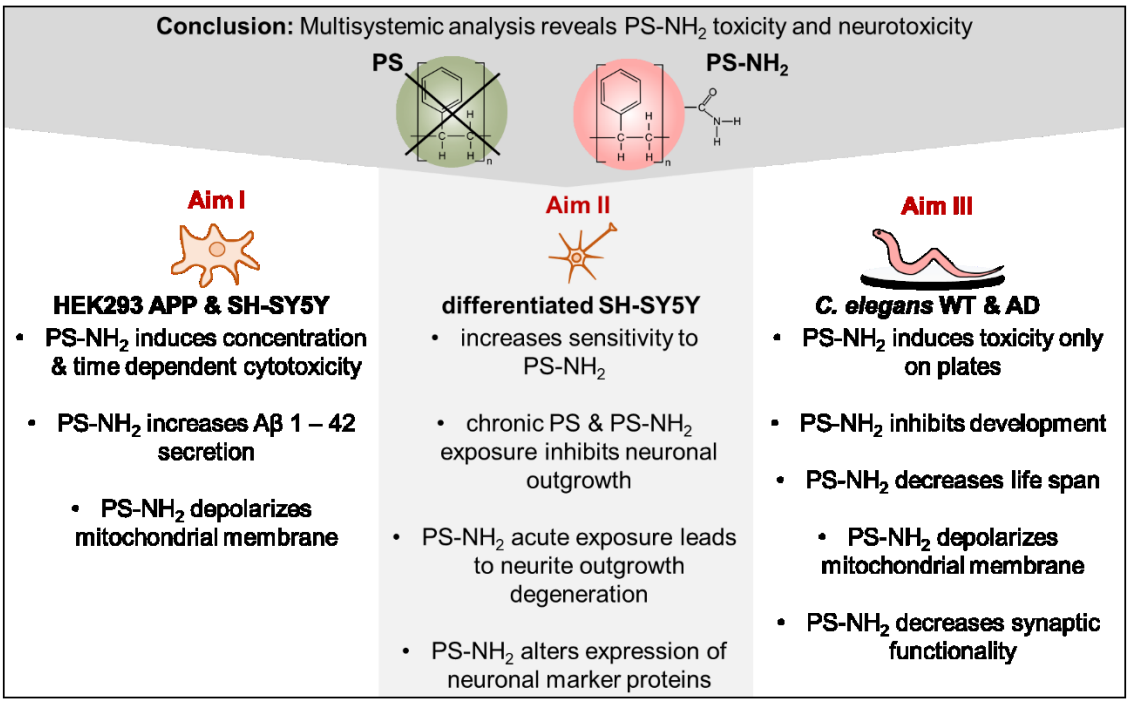

Figure 54. Summary of results. Compared to PS, PS-NH_2 leads to increased cytotoxicity, membrane damage, inhibited development and differentiation, as well as alterations in movement and synaptic functions in the respective model organism.

7 Bibliography

(1) Rektorin der Heinrich-Heine-Universität Düsseldorf; Justitiariat, R. S. *Promotionsordnung MNF*. https://www.math-nat-fak.hhu.de/fileadmin/redaktion/Oeffentliche_Medien/Fakultaeten/Mathematisch-Naturwissenschaftliche_Fakultaet/Dekanat/Promotion/PO/Promotionsordnung_MNF_Aenderung_2018_06_15.pdf (accessed 2023-08-03).

(2) Schröter, L.; Ventura, N. Nanoplastic Toxicity: Insights and Challenges from Experimental Model Systems. *Small* **2022**, *18* (31). https://doi.org/10.1002/smll.202201680.

(3) Alaani, L. (Senior M. M. *How to Clear Permissions for a Thesis or Dissertation*. The Wiley Network. https://www.wiley.com/en-us/network/publishing/research-publishing/trending-stories/how-to-clear-permissions-for-a-thesis-or-dissertation (accessed 2023-05-30).

(4) Plastics Europe. *Plastics - The Facts 2019: An analysis of European plastics production, demand and waste data*. https://plasticseurope.org/de/knowledge-hub/plastics-the-facts-2019/ (accessed 2023-08-03).

(5) Plastics Europe. *Plastics - The Facts 2012: An analysis of European latest plastics production, demand and waste data for 2011*. Association of Plastics & Manufacturers. https://plasticseurope.org/knowledge-hub/plastics-the-facts-2012/ (accessed 2023-08-03).

(6) Barnes, D. K. A.; Galgani, F.; Thompson, R. C.; Barlaz, M. Accumulation and Fragmentation of Plastic Debris in Global Environments. *Phil. Trans. R. Soc. B* **2009**, *364* (1526), 1985–1998. https://doi.org/10.1098/rstb.2008.0205.

(7) Kik, K.; Bukowska, B.; Sicińska, P. Polystyrene Nanoparticles: Sources, Occurrence in the Environment, Distribution in Tissues, Accumulation and Toxicity to Various Organisms. *Environ. Pollut.* **2020**, *262*. https://doi.org/10.1016/j.envpol.2020.114297.

(8) Moore, C. J. Synthetic Polymers in the Marine Environment: A Rapidly Increasing, Long-Term Threat. *Environ. Res.* **2008**, *108* (2), 131–139. https://doi.org/10.1016/j.envres.2008.07.025.

(9) Wypych, G. *Handbook of Polymers*; Elsevier, 2012. https://doi.org/10.1016/C2011-0-04631-8.

(10) Lambert, S.; Wagner, M. Characterisation of Nanoplastics during the Degradation of Polystyrene. *Chemosphere* **2016**, *145*, 265–268. https://doi.org/10.1016/j.chemosphere.2015.11.078.

(11) Da Costa, J. P.; Nunes, A. R.; Santos, P. S. M.; Girão, A. V.; Duarte, A. C.; Rocha-Santos, T. Degradation of Polyethylene Microplastics in Seawater: Insights into the Environmental Degradation of Polymers. *J. Environ. Sci. Heal. - Part A Toxic/Hazardous Subst. Environ. Eng.* **2018**, *53* (9), 866–875. https://doi.org/10.1080/10934529.2018.1455381.

(12) Zhang, G. S.; Liu, Y. F. The Distribution of Microplastics in Soil Aggregate Fractions in Southwestern China. *Sci. Total Environ.* **2018**, *642*, 12–20. https://doi.org/10.1016/j.scitotenv.2018.06.004.

(13) Wen, X.; Du, C.; Xu, P.; Zeng, G.; Huang, D.; Yin, L.; Yin, Q.; Hu, L.; Wan, J.; Zhang, J.; Tan, S.; Deng, R. Microplastic Pollution in Surface Sediments of Urban Water Areas in Changsha, China: Abundance, Composition, Surface Textures. *Mar. Pollut. Bull.* **2018**, *136* (June), 414–423. https://doi.org/10.1016/j.marpolbul.2018.09.043.

(14) Xiong, X.; Zhang, K.; Chen, X.; Shi, H.; Luo, Z.; Wu, C. Sources and Distribution of Microplastics in China's Largest Inland Lake – Qinghai Lake. *Environ. Pollut.* **2018**, *235*, 899–906. https://doi.org/10.1016/j.envpol.2017.12.081.

(15) Browne, M. A.; Crump, P.; Niven, S. J.; Teuten, E.; Tonkin, A.; Galloway, T.; Thompson, R. Accumulation of Microplastic on Shorelines Woldwide: Sources and Sinks. *Environ. Sci. Technol.* **2011**, *45* (21), 9175–9179. https://doi.org/10.1021/es201811s.

(16) Munari, C.; Infantini, V.; Scoponi, M.; Rastelli, E.; Corinaldesi, C.; Mistri, M. Microplastics in the Sediments of Terra Nova Bay (Ross Sea, Antarctica). *Mar. Pollut. Bull.* **2017**, *122*

(1–2), 161–165. https://doi.org/10.1016/j.marpolbul.2017.06.039.

(17) Pitt, J. A.; Kozal, J. S.; Jayasundara, N.; Massarsky, A.; Trevisan, R.; Geitner, N.; Wiesner, M.; Levin, E. D.; Di Giulio, R. T. Uptake, Tissue Distribution, and Toxicity of Polystyrene Nanoparticles in Developing Zebrafish (Danio Rerio). *Aquat. Toxicol.* **2018**, *194* (1), 185–194. https://doi.org/10.1016/j.aquatox.2017.11.017.

(18) Mattsson, K.; Johnson, E. V.; Malmendal, A.; Linse, S.; Hansson, L. A.; Cedervall, T. Brain Damage and Behavioural Disorders in Fish Induced by Plastic Nanoparticles Delivered through the Food Chain. *Sci. Rep.* **2017**, *7* (1), 1–7. https://doi.org/10.1038/s41598-017-10813-0.

(19) Yang, Y.; Shao, H.; Wu, Q.; Wang, D. Lipid Metabolic Response to Polystyrene Particles in Nematode Caenorhabditis Elegans. *Environ. Pollut.* **2019**, 113439. https://doi.org/10.1016/j.envpol.2019.113439.

(20) Cox, K. D.; Covernton, G. A.; Davies, H. L.; Dower, J. F.; Juanes, F.; Dudas, S. E. Human Consumption of Microplastics. *Environ. Sci. Technol.* **2019**, *53* (12), 7068–7074. https://doi.org/10.1021/acs.est.9b01517.

(21) Gasperi, J.; Wright, S. L.; Dris, R.; Collard, F.; Mandin, C.; Guerrouache, M.; Langlois, V.; Kelly, F. J.; Tassin, B. Microplastics in Air: Are We Breathing It In? *Curr. Opin. Environ. Sci. Heal.* **2018**, *1*, 1–5. https://doi.org/10.1016/j.coesh.2017.10.002.

(22) Kosuth, M.; Mason, S. A.; Wattenberg, E. V. Anthropogenic Contamination of Tap Water, Beer, and Sea Salt. *PLoS One* **2018**, *13* (4), 1–18. https://doi.org/10.1371/journal.pone.0194970.

(23) Fuhr, L.; Franklin, M. *The PLASTIC ATLAS 2019*. Heinrich Böll Foundation, Break Free From Plastic. https://www.boell.de/sites/default/files/2019-11/Plastic Atlas 2019.pdf (accessed 2023-08-01).

(24) EFSA. *The appropriateness of the risk assessment methodology in accordance with the Technical Guidance Documents for new and existing substances for assessing the risks of nanomaterials*. Environment. http://ec.europa.eu/health/ph_risk/risk_en.htm.

(25) Auta, H. S.; Emenike, C. U.; Fauziah, S. H. Distribution and Importance of Microplastics in the Marine EnvironmentA Review of the Sources, Fate, Effects, and Potential Solutions. *Environ. Int.* **2017**, *102*, 165–176. https://doi.org/10.1016/j.envint.2017.02.013.

(26) Andrady, A. L. Microplastics in the Marine Environment. *Mar. Pollut. Bull.* **2011**, *62* (8), 1596–1605. https://doi.org/10.1016/j.marpolbul.2011.05.030.

(27) World Economic Forum. *The New Plastics Economy: Rethinking the future of plastics*. Ellen MacArthur Foundation. http://www3.weforum.org/docs/WEF_The_New_Plastics_Economy.pdf (accessed 2023-08-03).

(28) Rane, A. V.; Kathalewar, M.; Jamdar, V.; .Abitha, V. K.; Sabnis, A. Sustainability by Converting Waste Polyurethane Foam into Superior Polyurethane Urea Coatings. *OALib* **2015**, *02* (05), 1–8. https://doi.org/10.4236/oalib.1101533.

(29) Reddy, A. B.; Reddy, G. S. M.; Jayaramudu, J.; Sudhakar, K.; Manjula, B.; Ray, S. S.; Sadiku, E. R. Polyethylene Terephthalate-Based Blends: Natural Rubber and Synthetic Rubber. *Poly(Ethylene Terephthalate) Based Blends, Compos. Nanocomposites* **2015**, 75–98. https://doi.org/10.1016/B978-0-323-31306-3.00005-1.

(30) Singh, B.; Sharma, N. Mechanistic Implications of Plastic Degradation. *Polym. Degrad. Stab.* **2008**, *93* (3), 561–584. https://doi.org/10.1016/j.polymdegradstab.2007.11.008.

(31) Singh, A. A.; Afrin, S.; Karim, Z. Green Composites: Versatile Material for Future. *Green Energy Technol.* **2017**, No. 9783319493817, 29–44. https://doi.org/10.1007/978-3-319-49382-4_2.

(32) Gewert, B.; Plassmann, M. M.; Macleod, M. Pathways for Degradation of Plastic Polymers Floating in the Marine Environment. *Environ. Sci. Process. Impacts* **2015**, *17* (9), 1513–1521. https://doi.org/10.1039/c5em00207a.

(33) Marturano, V.; Cerruti, P.; Ambrogi, V. Polymer Additives. *Phys. Sci. Rev.* **2019**, *2* (6), 1–

22. https://doi.org/10.1515/psr-2016-0130.

(34) Sobhani, Z.; Zhang, X.; Gibson, C.; Naidu, R.; Megharaj, M.; Fang, C. Identification and Visualisation of Microplastics/Nanoplastics by Raman Imaging (i): Down to 100 Nm. *Water Res.* **2020**, *174* (i), 115658. https://doi.org/10.1016/j.watres.2020.115658.

(35) Mattsson, K.; Hansson, L. A.; Cedervall, T. Nano-Plastics in the Aquatic Environment. *Environ. Sci. Process. Impacts* **2015**, *17* (10), 1712–1721. https://doi.org/DOI: 10.1039/c5em00227c.

(36) Nagalakshmaiah, M.; Afrin, S.; Malladi, R. P.; Elkoun, S.; Robert, M.; Ansari, M. A.; Svedberg, A.; Karim, Z. Biocomposites: Present Trends and Challenges for the Future. *Green Compos. Automot. Appl.* **2018**, 197–215. https://doi.org/10.1016/B978-0-08-102177-4.00009-4.

(37) Luyt, A. S.; Malik, S. S. Can Biodegradable Plastics Solve Plastic Solid Waste Accumulation? *Plast. to Energy Fuel, Chem. Sustain. Implic.* **2018**, 403–423. https://doi.org/10.1016/B978-0-12-813140-4.00016-9.

(38) Shah, A. A.; Hasan, F.; Hameed, A.; Ahmed, S. Biological Degradation of Plastics: A Comprehensive Review. *Biotechnol. Adv.* **2008**, *26* (3), 246–265. https://doi.org/10.1016/j.biotechadv.2007.12.005.

(39) Yousif, E.; Haddad, R. Photodegradation and Photostabilization of Polymers, Especially Polystyrene: Review. *Springerplus* **2013**, *2* (1), 1–32. https://doi.org/10.1186/2193-1801-2-398.

(40) Worzakowska, M. Thermal and Mechanical Properties of Polystyrene Modified with Esters Derivatives of 3-Phenylprop-2-En-1-Ol. *J. Therm. Anal. Calorim.* **2015**, *121* (1), 235–243. https://doi.org/10.1007/s10973-015-4547-7.

(41) González, A.; Pastor, J. M.; De Saja, J. A. Monitoring the UV Degradation of PVC Window Frames by Microhardness Analysis. *J. Appl. Polym. Sci.* **1989**, *38* (10), 1879–1882. https://doi.org/10.1002/app.1989.070381009.

(42) Venkatachalam, S.; G., S.; V., J.; R., P.; Rao, K.; K., A. Degradation and Recyclability of Poly (Ethylene Terephthalate). *Polyester* **2012**. https://doi.org/10.5772/48612.

(43) Barbosa, F.; Adeyemi, J. A.; Bocato, M. Z.; Comas, A.; Campiglia, A. A Critical Viewpoint on Current Issues, Limitations, and Future Research Needs on Micro- and Nanoplastic Studies: From the Detection to the Toxicological Assessment. *Environ. Res.* **2020**, *182*, 109089. https://doi.org/10.1016/j.envres.2019.109089.

(44) Chang, X.; Xue, Y.; Li, J.; Zou, L.; Tang, M. Potential Health Impact of Environmental Micro- and Nanoplastics Pollution. *J. Appl. Toxicol.* **2019**, *2015* (September), 1–12. https://doi.org/10.1002/jat.3915.

(45) Monti, D. M.; Guarnieri, D.; Napolitano, G.; Piccoli, R.; Netti, P.; Fusco, S.; Arciello, A. Biocompatibility, Uptake and Endocytosis Pathways of Polystyrene Nanoparticles in Primary Human Renal Epithelial Cells. *J. Biotechnol.* **2015**, *193*, 3–10. https://doi.org/10.1016/j.jbiotec.2014.11.004.

(46) Hesler, M.; Aengenheister, L.; Ellinger, B.; Drexel, R.; Straskraba, S.; Jost, C.; Wagner, S.; Meier, F.; von Briesen, H.; Büchel, C.; Wick, P.; Buerki-Thurnherr, T.; Kohl, Y. Multi-Endpoint Toxicological Assessment of Polystyrene Nano- and Microparticles in Different Biological Models in Vitro. *Toxicol. Vitr.* **2019**, *61* (May), 104610. https://doi.org/10.1016/j.tiv.2019.104610.

(47) Mattsson, K.; Ekvall, M. T.; Hansson, L.-A.; Linse, S.; Malmendal, A.; Cedervall, T. Altered Behavior, Physiology, and Metabolism in Fish Exposed to Polystyrene Nanoparticles. *Environ. Sci. Technol.* **2015**, *49* (1), 553–561. https://doi.org/10.1021/es5053655.

(48) Sökmen, T. Ö.; Sulukan, E.; Türkoğlu, M.; Baran, A.; Özkaraca, M.; Ceyhun, S. B. Polystyrene Nanoplastics (20 Nm) Are Able to Bioaccumulate and Cause Oxidative DNA Damages in the Brain Tissue of Zebrafish Embryo (Danio Rerio). *Neurotoxicology* **2020**, *77*, 51–59. https://doi.org/10.1016/j.neuro.2019.12.010.

(49) Revel, M.; Châtel, A.; Mouneyrac, C. Micro(Nano)Plastics: A Threat to Human Health? *Curr. Opin. Environ. Sci. Heal.* **2018**, *1*, 17–23.

https://doi.org/10.1016/j.coesh.2017.10.003.

(50) Hoet, P. H. M.; Brüske-Hohlfeld, I.; Salata, O. V. Nanoparticles - Known and Unknown Health Risks. *J. Nanobiotechnology* **2004**, *2*, 1–15. https://doi.org/10.1186/1477-3155-2-12.

(51) Atuma, C.; Strugala, V.; Allen, A.; Holm, L. The Adherent Gastrointestinal Mucus Gel Layer: Thickness and Physical State in Vivo. *Am. J. Physiol. - Gastrointest. Liver Physiol.* **2001**, *280* (5 43-5), 922–929. https://doi.org/10.1152/ajpgi.2001.280.5.g922.

(52) Inkielewicz-Stepniak, I.; Tajber, L.; Behan, G.; Zhang, H.; Radomski, M. W.; Medina, C.; Santos-Martinez, M. J. The Role of Mucin in the Toxicological Impact of Polystyrene Nanoparticles. *Materials (Basel).* **2018**, *11* (5), 1–12. https://doi.org/10.3390/ma11050724.

(53) Fuchs, A. K.; Syrovets, T.; Haas, K. A.; Loos, C.; Musyanovych, A.; Mailänder, V.; Landfester, K.; Simmet, T. Carboxyl- and Amino-Functionalized Polystyrene Nanoparticles Differentially Affect the Polarization Profile of M1 and M2 Macrophage Subsets. *Biomaterials* **2016**, *85*, 78–87. https://doi.org/10.1016/j.biomaterials.2016.01.064.

(54) Paget, V.; Dekali, S.; Kortulewski, T.; Grall, R.; Gamez, C.; Blazy, K.; Aguerre-Chariol, O.; Chevillard, S.; Braun, A.; Rat, P.; Lacroix, G. Specific Uptake and Genotoxicity Induced by Polystyrene Nanobeads with Distinct Surface Chemistry on Human Lung Epithelial Cells and Macrophages. *PLoS One* **2015**, *10* (4), 1–20. https://doi.org/10.1371/journal.pone.0123297.

(55) Forte, M.; Iachetta, G.; Tussellino, M.; Carotenuto, R.; Prisco, M.; De Falco, M.; Laforgia, V.; Valiante, S. Polystyrene Nanoparticles Internalization in Human Gastric Adenocarcinoma Cells. *Toxicol. Vitr.* **2016**, *31*, 126–136. https://doi.org/10.1016/j.tiv.2015.11.006.

(56) Wu, B.; Wu, X.; Liu, S.; Wang, Z.; Chen, L. Size-Dependent Effects of Polystyrene Microplastics on Cytotoxicity and Efflux Pump Inhibition in Human Caco-2 cells. *Chemosphere* **2019**, *221*, 333–341. https://doi.org/10.1016/j.chemosphere.2019.01.056.

(57) Asfaha, S.; Dubeykovskiy, A. N.; Tomita, H.; Yang, X.; Stokes, S.; Shibata, W.; Friedman, R. A.; Ariyama, H.; Dubeykovskaya, Z. A.; Muthupalani, S.; Ericksen, R.; Frucht, H.; Fox, J. G.; Wang, T. C. Mice That Express Human Interleukin-8 Have Increased Mobilization of Immature Myeloid Cells, Which Exacerbates Inflammation and Accelerates Colon Carcinogenesis. *Gastroenterology* **2013**, *144* (1), 155–166. https://doi.org/10.1053/j.gastro.2012.09.057.

(58) Xu, M.; Halimu, G.; Zhang, Q.; Song, Y.; Fu, X.; Li, Y.; Li, Y.; Zhang, H. Internalization and Toxicity: A Preliminary Study of Effects of Nanoplastic Particles on Human Lung Epithelial Cell. *Sci. Total Environ.* **2019**, *694*, 133794. https://doi.org/10.1016/j.scitotenv.2019.133794.

(59) Lim, S. L.; Ng, C. T.; Zou, L.; Lu, Y.; Chen, J.; Bay, B. H.; Shen, H. M.; Ong, C. N. Targeted Metabolomics Reveals Differential Biological Effects of Nanoplastics and NanoZnO in Human Lung Cells. *Nanotoxicology* **2019**, *13* (8), 1117–1132. https://doi.org/10.1080/17435390.2019.1640913.

(60) Chiu, H. W.; Xia, T.; Lee, Y. H.; Chen, C. W.; Tsai, J. C.; Wang, Y. J. Cationic Polystyrene Nanospheres Induce Autophagic Cell Death through the Induction of Endoplasmic Reticulum Stress. *Nanoscale* **2015**, *7* (2), 736–746. https://doi.org/10.1039/c4nr05509h.

(61) Xia, T.; Kovochich, M.; Liong, M.; Zink, J. I.; Nel, A. E. Cationic Polystyrene Nanosphere. *ACS Nano* **2008**, *2* (1), 85–96.

(62) Döge, N.; Hadam, S.; Volz, P.; Wolf, A.; Schönborn, K. H.; Blume-Peytavi, U.; Alexiev, U.; Vogt, A. Identification of Polystyrene Nanoparticle Penetration across Intact Skin Barrier as Rare Event at Sites of Focal Particle Aggregations. *J. Biophotonics* **2018**, *11* (4), 1–10. https://doi.org/10.1002/jbio.201700169.

(63) Alvarez-Román, R.; Naik, A.; Kalia, Y. N.; Guy, R. H.; Fessi, H. Skin Penetration and Distribution of Polymeric Nanoparticles. *J. Control. Release* **2004**, *99* (1), 53–62. https://doi.org/10.1016/j.jconrel.2004.06.015.

(64) Liu, Y.; Li, W.; Lao, F.; Liu, Y.; Wang, L.; Bai, R.; Zhao, Y.; Chen, C. Intracellular Dynamics of Cationic and Anionic Polystyrene Nanoparticles without Direct Interaction with Mitotic Spindle and Chromosomes. *Biomaterials* **2011**, *32* (32), 8291–8303. https://doi.org/10.1016/j.biomaterials.2011.07.037.

(65) Schirinzi, G. F.; Pérez-Pomeda, I.; Sanchís, J.; Rossini, C.; Farré, M.; Barceló, D. Cytotoxic Effects of Commonly Used Nanomaterials and Microplastics on Cerebral and Epithelial Human Cells. *Environ. Res.* **2017**, *159* (June), 579–587. https://doi.org/10.1016/j.envres.2017.08.043.

(66) Heinlaan, M.; Kasemets, K.; Aruoja, V.; Blinova, I.; Bondarenko, O.; Lukjanova, A.; Khosrovyan, A.; Kurvet, I.; Pullerits, M.; Sihtmäe, M.; Vasiliev, G.; Vija, H.; Kahru, A. Hazard Evaluation of Polystyrene Nanoplastic with Nine Bioassays Did Not Show Particle-Specific Acute Toxicity. *Sci. Total Environ.* **2020**, *707*, 136073. https://doi.org/10.1016/j.scitotenv.2019.136073.

(67) Jung, B. K.; Han, S. W.; Park, S. H.; Bae, J. S.; Choi, J.; Ryu, K. Y. Neurotoxic Potential of Polystyrene Nanoplastics in Primary Cells Originating from Mouse Brain. *Neurotoxicology* **2020**, *81* (September), 189–196. https://doi.org/10.1016/j.neuro.2020.10.008.

(68) Murali, K.; Kenesei, K.; Li, Y.; Demeter, K.; Környei, Z.; Madarász, E. Uptake and Bio-Reactivity of Polystyrene Nanoparticles Is Affected by Surface Modifications, Ageing and LPS Adsorption: In Vitro Studies on Neural Tissue Cells. *Nanoscale* **2015**, *7* (9), 4199–4210. https://doi.org/10.1039/c4nr06849a.

(69) Rubio, L.; Marcos, R.; Hernández, A. Potential Adverse Health Effects of Ingested Micro- and Nanoplastics on Humans. Lessons Learned from in Vivo and in Vitro Mammalian Models. *J. Toxicol. Environ. Heal. - Part B Crit. Rev.* **2019**, *00* (00), 1–18. https://doi.org/10.1080/10937404.2019.1700598.

(70) Cedervall, T.; Hansson, L. A.; Lard, M.; Frohm, B.; Linse, S. Food Chain Transport of Nanoparticles Affects Behaviour and Fat Metabolism in Fish. *PLoS One* **2012**, *7* (2), 1–6. https://doi.org/10.1371/journal.pone.0032254.

(71) Kashiwada, S. Distribution of Nanoparticles in the See-through Medaka (Oryzias Latipes). *Environ. Health Perspect.* **2006**, *114* (11), 1697–1702. https://doi.org/10.1289/ehp.9209.

(72) Chen, Q.; Gundlach, M.; Yang, S.; Jiang, J.; Velki, M.; Yin, D.; Hollert, H. Quantitative Investigation of the Mechanisms of Microplastics and Nanoplastics toward Zebrafish Larvae Locomotor Activity. *Sci. Total Environ.* **2017**, *584–585*, 1022–1031. https://doi.org/10.1016/j.scitotenv.2017.01.156.

(73) Sarasamma, S.; Audira, G.; Siregar, P.; Malhotra, N.; Lai, Y. H.; Liang, S. T.; Chen, J. R.; Chen, K. H. C.; Hsiao, C. Der. Nanoplastics Cause Neurobehavioral Impairments, Reproductive and Oxidative Damages, and Biomarker Responses in Zebrafish: Throwing up Alarms of Wide Spread Health Risk of Exposure. *Int. J. Mol. Sci.* **2020**, *21* (4), 1–29. https://doi.org/10.3390/ijms21041410.

(74) Brun, N. R.; Koch, B. E. V.; Varela, M.; Peijnenburg, W. J. G. M.; Spaink, H. P.; Vijver, M. G. Nanoparticles Induce Dermal and Intestinal Innate Immune System Responses in Zebrafish Embryos. *Environ. Sci. Nano* **2018**, *5* (4), 904–916. https://doi.org/10.1039/c8en00002f.

(75) Brun, N. R.; van Hage, P.; Hunting, E. R.; Haramis, A. P. G.; Vink, S. C.; Vijver, M. G.; Schaaf, M. J. M.; Tudorache, C. Polystyrene Nanoplastics Disrupt Glucose Metabolism and Cortisol Levels with a Possible Link to Behavioural Changes in Larval Zebrafish. *Commun. Biol.* **2019**, *2* (1). https://doi.org/10.1038/s42003-019-0629-6.

(76) Lu, Y.; Zhang, Y.; Deng, Y.; Jiang, W.; Zhao, Y.; Geng, J.; Ding, L.; Ren, H. Uptake and Accumulation of Polystyrene Microplastics in Zebrafish (Danio Rerio) and Toxic Effects in Liver. *Environ. Sci. Technol.* **2016**, *50* (7), 4054–4060. https://doi.org/10.1021/acs.est.6b00183.

(77) Nielsen, A. L.; Jørgensen, A. L. Structural and Functional Characterization of the Zebrafish Gene for Glial Fibrillary Acidic Protein, GFAP. *Gene* **2003**, *310* (1–2), 123–132. https://doi.org/10.1016/S0378-1119(03)00526-2.

(78) Fausett, B. V.; Goldman, D. A Role for Alpha1 Tubulin-Expressing Müller Glia in Regeneration of the Injured Zebrafish Retina. *J. Neurosci.* **2006**, *26* (23), 6303–6313. https://doi.org/10.1523/JNEUROSCI.0332-06.2006.

(79) McGrath, P.; Li, C. Q. Zebrafish: A Predictive Model for Assessing Drug-Induced Toxicity. *Drug Discov. Today* **2008**, *13* (9–10), 394–401. https://doi.org/10.1016/j.drudis.2008.03.002.

(80) Pietrzak, B.; Bednarska, A.; Grzesiuk, M. Longevity of Daphnia Magna Males and Females. *Hydrobiologia* **2010**, *643* (1), 71–75. https://doi.org/10.1007/s10750-010-0138-6.

(81) Lee, W. S.; Cho, H. J.; Kim, E.; Huh, Y. H.; Kim, H. J.; Kim, B.; Kang, T.; Lee, J. S.; Jeong, J. Bioaccumulation of Polystyrene Nanoplastics and Their Effect on the Toxicity of Au Ions in Zebrafish Embryos. *Nanoscale* **2019**, *11* (7), 3200–3207. https://doi.org/10.1039/c8nr09321k.

(82) Weinhouse, C.; Truong, L.; Meyer, J. N.; Allard, P. Caenorhabditis Elegans as an Emerging Model System in Environmental Epigenetics. *Environ. Mol. Mutagen.* **2018**, *59* (7), 560–575. https://doi.org/10.1002/em.22203.

(83) Ruszkiewicz, J. A.; Pinkas, A.; Miah, M. R.; Weitz, R. L.; Lawes, M. J. A.; Akinyemi, A. J.; Ijomone, O. M.; Aschner, M. C. Elegans as a Model in Developmental Neurotoxicology. *Toxicol. Appl. Pharmacol.* **2018**, *354* (1), 126–135. https://doi.org/10.1016/j.taap.2018.03.016.

(84) Zhao, L.; Qu, M.; Wong, G.; Wang, D. Transgenerational Toxicity of Nanopolystyrene Particles in the Range of Mg L-1 in the Nematode: Caenorhabditis Elegans. *Environ. Sci. Nano* **2017**, *4* (12), 2356–2366. https://doi.org/10.1039/c7en00707h.

(85) Qu, M.; Kong, Y.; Yuan, Y.; Wang, D. Neuronal Damage Induced by Nanopolystyrene Particles in Nematode: Caenorhabditis Elegans. *Environ. Sci. Nano* **2019**, *6* (8), 2591–2601. https://doi.org/10.1039/c9en00473d.

(86) Taubert, S.; Van Gilst, M. R.; Hansen, M.; Yamamoto, K. R. A Mediator Subunit, MDT-15, Integrates Regulation of Fatty Acid Metabolism by NHR-49-Dependent and -Independent Pathways in C. Elegans. *Genes Dev.* **2006**, *20* (9), 1137–1149. https://doi.org/10.1101/gad.1395406.

(87) Mueller, M. T.; Fueser, H.; Trac, L. N.; Mayer, P.; Traunspurger, W.; Höss, S. Surface-Related Toxicity of Polystyrene Beads to Nematodes and the Role of Food Availability. *Environ. Sci. Technol.* **2020**, *54* (3), 1790–1798. https://doi.org/10.1021/acs.est.9b06583.

(88) Kim, H. M.; Lee, D. K.; Long, N. P.; Kwon, S. W.; Park, J. H. Uptake of Nanopolystyrene Particles Induces Distinct Metabolic Profiles and Toxic Effects in Caenorhabditis Elegans. *Environ. Pollut.* **2019**, *246*, 578–586. https://doi.org/10.1016/j.envpol.2018.12.043.

(89) Alberti, A.; Michelet, X.; Djeddi, A.; Legouis, R. The Autophagosomal Protein LGG-2 Acts Synergistically with LGG-1 in Dauer Formation and Longevity in C. Elegans. *Autophagy* **2010**, *6* (5), 622–633. https://doi.org/10.4161/auto.6.5.12252.

(90) Ruck, A.; Attonito, J.; Garces, K. T.; Núnez, L.; Palmisano, N. J.; Rubel, Z.; Bai, Z.; Nguyen, K. C. Q.; Sun, L.; Grant, B. D.; Hall, D. H.; Meléndez, A. The Atg6/Vps30/Beclin 1 Ortholog BEC-1 Mediates Endocytic Retrograde Transport in Addition to Autophagy in C. Elegans. *Autophagy* **2011**, *7* (4), 386–400. https://doi.org/10.4161/auto.7.4.14391.

(91) JANI, P.; HALBERT, G. W.; LANGRIDGE, J.; FLORENCE, A. T. Nanoparticle Uptake by the Rat Gastrointestinal Mucosa: Quantitation and Particle Size Dependency. *J. Pharm. Pharmacol.* **1990**, *42* (12), 821–826. https://doi.org/10.1111/j.2042-7158.1990.tb07033.x.

(92) Hillery, A. M.; Jan, P. U.; Florence, A. T. Comparative, Quantitative Study of Lymphoid and Non-Lymphoid Uptake of 60 Nm Polystyrene Particles. *J. Drug Target.* **1994**, *2* (2), 151–156. https://doi.org/10.3109/10611869409015904.

(93) Walczak, A. P.; Hendriksen, P. J. M.; Woutersen, R. A.; van der Zande, M.; Undas, A. K.; Helsdingen, R.; van den Berg, H. H. J.; Rietjens, I. M. C. M.; Bouwmeester, H. Bioavailability and Biodistribution of Differently Charged Polystyrene Nanoparticles upon Oral Exposure in Rats. *J. Nanoparticle Res.* **2015**, *17* (5), 231.

https://doi.org/10.1007/s11051-015-3029-y.

(94) Yang, C. S.; Chang, C. H.; Tsai, P. J.; Chen, W. Y.; Tseng, F. G.; Lo, L. W. Nanoparticle-Based in Vivo Investigation on Blood-Brain Barrier Permeability Following Ischemia and Reperfusion. *Anal. Chem.* **2004**, *76* (15), 4465–4471. https://doi.org/10.1021/ac035491v.

(95) Rafiee, M.; Dargahi, L.; Eslami, A.; Beirami, E.; Jahangiri-rad, M.; Sabour, S.; Amereh, F. Neurobehavioral Assessment of Rats Exposed to Pristine Polystyrene Nanoplastics upon Oral Exposure. *Chemosphere* **2018**, *193*, 745–753. https://doi.org/10.1016/j.chemosphere.2017.11.076.

(96) Liang, B.; Zhong, Y.; Huang, Y.; Lin, X.; Liu, J.; Lin, L.; Hu, M.; Jiang, J.; Dai, M.; Wang, B.; Zhang, B.; Meng, H.; Lelaka, J. J. J.; Sui, H.; Yang, X.; Huang, Z. Underestimated Health Risks: Polystyrene Micro- and Nanoplastics Jointly Induce Intestinal Barrier Dysfunction by ROS-Mediated Epithelial Cell Apoptosis. *Part. Fibre Toxicol.* **2021**, *18* (1), 1–19. https://doi.org/10.1186/s12989-021-00414-1.

(97) Kopatz, V.; Wen, K.; Kovács, T.; Keimowitz, A. S.; Pichler, V.; Widder, J.; Vethaak, A. D.; Hollóczki, O.; Kenner, L. Micro- and Nanoplastics Breach the Blood–Brain Barrier (BBB): Biomolecular Corona's Role Revealed. *Nanomaterials* **2023**, *13* (8), 1–10. https://doi.org/10.3390/nano13081404.

(98) Scheltens, P.; Blennow, K.; Breteler, M. M. B.; de Strooper, B.; Frisoni, G. B.; Salloway, S.; Van der Flier, W. M. Alzheimer's Disease. *Lancet* **2016**, *388* (10043), 505–517. https://doi.org/10.1016/S0140-6736(15)01124-1.

(99) Livingston, G.; Huntley, J.; Sommerlad, A.; Ames, D.; Ballard, C.; Banerjee, S.; Brayne, C.; Burns, A.; Cohen-Mansfield, J.; Cooper, C.; Costafreda, S. G.; Dias, A.; Fox, N.; Gitlin, L. N.; Howard, R.; Kales, H. C.; Kivimäki, M.; Larson, E. B.; Ogunniyi, A.; Orgeta, V.; Ritchie, K.; Rockwood, K.; Sampson, E. L.; Samus, Q.; Schneider, L. S.; Selbæk, G.; Teri, L.; Mukadam, N. Dementia Prevention, Intervention, and Care: 2020 Report of the Lancet Commission. *Lancet* **2020**, *396* (10248), 413–446. https://doi.org/10.1016/S0140-6736(20)30367-6.

(100) Passeri, E.; Elkhoury, K.; Morsink, M.; Broersen, K.; Linder, M.; Tamayol, A.; Malaplate, C.; Yen, F. T.; Arab-Tehrany, E. Alzheimer's Disease: Treatment Strategies and Their Limitations. *Int. J. Mol. Sci.* **2022**, *23* (22). https://doi.org/10.3390/ijms232213954.

(101) Soria Lopez, J. A.; González, H. M.; Léger, G. C. Alzheimer's Disease. *Handb. Clin. Neurol.* **2019**, *167*, 231–255. https://doi.org/10.1016/B978-0-12-804766-8.00013-3.

(102) Jack, C. R.; Bernstein, M. A.; Fox, N. C.; Thompson, P.; Alexander, G.; Harvey, D.; Borowski, B.; Britson, P. J.; L. Whitwell, J.; Ward, C.; Dale, A. M.; Felmlee, J. P.; Gunter, J. L.; Hill, D. L. G.; Killiany, R.; Schuff, N.; Fox-Bosetti, S.; Lin, C.; Studholme, C.; DeCarli, C. S.; Gunnar Krueger; Ward, H. A.; Metzger, G. J.; Scott, K. T.; Mallozzi, R.; Blezek, D.; Levy, J.; Debbins, J. P.; Fleisher, A. S.; Albert, M.; Green, R.; Bartzokis, G.; Glover, G.; Mugler, J.; Weiner, M. W. The Alzheimer's Disease Neuroimaging Initiative (ADNI): MRI Methods. *J. Magn. Reson. Imaging* **2008**, *27* (4), 685–691. https://doi.org/10.1002/jmri.21049.

(103) Querfurth, H. W.; LaFerla, F. M. Alzheimer's Disease. *N. Engl. J. Med.* **2010**, *362* (4), 329–344. https://doi.org/10.1056/NEJMra0909142.

(104) Thal, D. R.; Rüb, U.; Orantes, M.; Braak, H. Phases of Aβ-Deposition in the Human Brain and Its Relevance for the Development of AD. *Neurology* **2002**, *58* (12), 1791–1800. https://doi.org/10.1212/WNL.58.12.1791.

(105) da Rocha, J. F.; da Cruz e Silva, O. A. B.; Vieira, S. I. Analysis of the Amyloid Precursor Protein Role in Neuritogenesis Reveals a Biphasic SH-SY5Y Neuronal Cell Differentiation Model. *J. Neurochem.* **2015**, *134* (2), 288–301. https://doi.org/10.1111/jnc.13133.

(106) Kojro, E.; Fahrenholz, F. The Non-Amyloidogenic Pathway: Structure and Function of α-Secretases. *Subcell Biochem.* **2005**, *38*, 105–127. https://doi.org/10.1007/0-387-23226-5_5.

(107) Haass, C.; Hung, A. Y.; Schlossmacher, M. G.; Teplow, D. B.; Selkoe, D. J. Beta-Amyloid Peptide and a 3-KDa Fragment Are Derived by Distinct Cellular Mechanisms. *J. Biol. Chem.* **1993**, *268* (5), 3021–3024. https://doi.org/10.1016/S0021-9258(18)53650-4.

(108) Vassar, R.; Bennett, B. D.; Babu-Khan, S.; Kahn, S.; Mendiaz, E. A.; Denis, P.; Teplow, D. B.; Ross, S.; Amarante, P.; Loeloff, R.; Luo, Y.; Fisher, S.; Fuller, J.; Edenson, S.; Lile, J.; Jarosinski, M. A.; Biere, A. L.; Curran, E.; Burgess, T.; Louis, J.; Collins, F.; Treanor, J.; Rogers, G.; Citron, M. β-Secretase Cleavage of Alzheimer's Amyloid Precursor Protein by the Transmembrane Aspartic Protease BACE. *Science (80-.).* **1999**, *286* (5440), 735–741. https://doi.org/10.1126/science.286.5440.735.

(109) Gabbrielli, S.; Colnaghi, L.; Mazzuoli-Weber, G.; Redaelli, A. C. L.; Gautieri, A. In Silico Analysis of Nanoplastics' and β-Amyloid Fibrils' Interactions. *Molecules* **2023**, *28* (1), 388. https://doi.org/10.3390/molecules28010388.

(110) Windheim, J.; Colombo, L.; Battajni, N. C.; Russo, L.; Cagnotto, A.; Diomede, L.; Bigini, P.; Vismara, E.; Fiumara, F.; Gabbrielli, S.; Gautieri, A.; Mazzuoli-Weber, G.; Salmona, M.; Colnaghi, L. Micro- and Nanoplastics' Effects on Protein Folding and Amyloidosis. *Int. J. Mol. Sci.* **2022**, *23* (18), 1–13. https://doi.org/10.3390/ijms231810329.

(111) Lewczuk, P.; Beck, G.; Esselmann, H.; Bruckmoser, R.; Zimmermann, R.; Fiszer, M.; Bibl, M.; Maler, J. M.; Kornhuber, J.; Wiltfang, J. Effect of Sample Collection Tubes on Cerebrospinal Fluid Concentrations of Tau Proteins and Amyloid β Peptides. *Clin. Chem.* **2006**, *52* (2), 332–334. https://doi.org/10.1373/clinchem.2005.058776.

(112) Cabaleiro-Lago, C.; Quinlan-Pluck, F.; Lynch, I.; Dawson, K. A.; Linse, S. Dual Effect of Amino Modified Polystyrene Nanoparticles on Amyloid β Protein Fibrillation. *ACS Chem. Neurosci.* **2010**, *1* (4), 279–287. https://doi.org/10.1021/cn900027u.

(113) Lunov, O.; Syrovets, T.; Loos, C.; Beil, J.; Delacher, M.; Tron, K.; Nienhaus, G. U.; Musyanovych, A.; Mailänder, V.; Landfester, K.; Simmet, T. Differential Uptake of Functionalized Polystyrene Nanoparticles by Human Macrophages and a Monocytic Cell Line. *ACS Nano* **2011**, *5* (3), 1657–1669. https://doi.org/10.1021/nn2000756.

(114) Holzapfel, V.; Musyanovych, A.; Landfester, K.; Lorenz, M. R.; Mailänder, V. Preparation of Fluorescent Carboxyl and Amino Functionalized Polystyrene Particles by Miniemulsion Polymerization as Markers for Cells. *Macromol. Chem. Phys.* **2005**, *206* (24), 2440–2449. https://doi.org/10.1002/macp.200500372.

(115) Musyanovych, A.; Rossmanith, R.; Tontsch, C.; Landfester, K. Effect of Hydrophilic Comonomer and Surfactant Type on the Colloidal Stability and Size Distribution of Carboxyl- And Amino-Functionalized Polystyrene Particles Prepared by Miniemulsion Polymerization. *Langmuir* **2007**, *23* (10), 5367–5376. https://doi.org/10.1021/la0635193.

(116) Graham, F. L.; Smiley, J.; Russell, W. C.; Nairn, R. Characteristics of a Human Cell Line Transformed by DNA from Human Adenovirus Type 5. *J. Gen. Virol.* **1977**, *36* (1), 59–72. https://doi.org/10.1099/0022-1317-36-1-59.

(117) Inada, M.; Izawa, G.; Kobayashi, W.; Ozawa, M. 293 Cells Express Both Epithelial As Well As Mesenchymal Cell Adhesion Molecules. *Int. J. Mol. Med.* **2016**, *37* (6), 1521–1527. https://doi.org/10.3892/ijmm.2016.2568.

(118) Almeer, R. S.; Ali, D.; Alarifi, S.; Alkahtani, S.; Almansour, M. Green Platinum Nanoparticles Interaction With HEK293 Cells: Cellular Toxicity, Apoptosis, and Genetic Damage. *Dose-Response* **2018**, *16* (4), 1–11. https://doi.org/10.1177/1559325818807382.

(119) Chou, C. C.; Riviere, J. E.; Monteiro-Riviere, N. A. The Cytotoxicity of Jet Fuel Aromatic Hydrocarbons and Dose-Related Interleukin-8 Release from Human Epidermal Keratinocytes. *Arch. Toxicol.* **2003**, *77* (7), 384–391. https://doi.org/10.1007/s00204-003-0461-z.

(120) Kang, T.; Park, C.; Lee, B. J. Investigation of Biomimetic Shear Stress on Cellular Uptake and Mechanism of Polystyrene Nanoparticles in Various Cancer Cell Lines. *Arch. Pharm. Res.* **2016**, *39* (12), 1663–1670. https://doi.org/10.1007/s12272-016-0847-0.

(121) Lopez Sanchez, M. I. G.; Waugh, H. S.; Tsatsanis, A.; Wong, B. X.; Crowston, J. G.; Duce, J. A.; Trounce, I. A. Amyloid Precursor Protein Drives Down-Regulation of Mitochondrial Oxidative Phosphorylation Independent of Amyloid Beta. *Sci. Rep.* **2017**, *7* (1), 1–10. https://doi.org/10.1038/s41598-017-10233-0.

(122) Uberti, D.; Cenini, G.; Olivari, L.; Ferrari-Toninelli, G.; Porrello, E.; Cecchi, C.; Pensafini,

A.; Liguri, G.; Govoni, S.; Racchi, M.; Maurizio, M. Over-Expression of Amyloid Precursor Protein in HEK Cells Alters P53 Conformational State and Protects against Doxorubicin. *J. Neurochem.* **2007**, *103* (1), 322–333. https://doi.org/10.1111/j.1471-4159.2007.04757.x.

(123) Lopez-Suarez, L.; Awabdh, S. Al; Coumoul, X.; Chauvet, C. The SH-SY5Y Human Neuroblastoma Cell Line, a Relevant in Vitro Cell Model for Investigating Neurotoxicology in Human: Focus on Organic Pollutants. *Neurotoxicology* **2022**, *92* (July), 131–155. https://doi.org/10.1016/j.neuro.2022.07.008.

(124) Biedler, J. L.; Helson, L.; Spengler, B. A. Morphology and Growth, Tumorigenicity, and Cytogenetics of Human Neuroblastoma Cells in Continuous Culture. *Cancer Res.* **1973**, *33* (11), 2643–2652.

(125) de Medeiros, L. M.; De Bastiani, M. A.; Rico, E. P.; Schonhofen, P.; Pfaffenseller, B.; Wollenhaupt-Aguiar, B.; Grun, L.; Barbé-Tuana, F.; Zimmer, E. R.; Castro, M. A. A.; Parsons, R. B.; Klamt, F. Cholinergic Differentiation of Human Neuroblastoma SH-SY5Y Cell Line and Its Potential Use as an In Vitro Model for Alzheimer's Disease Studies. *Mol. Neurobiol.* **2019**, *56* (11), 7355–7367. https://doi.org/10.1007/s12035-019-1605-3.

(126) Kovalevich, J.; Langford, D. Considerations for the Use of SH-SY5Y Neuroblastoma Cells in Neurobiology. **2013**, *1078*, 9–21. https://doi.org/10.1007/978-1-62703-640-5_2.

(127) Cuende, J.; Moreno, S.; Bolaños, J. P.; Almeida, A. Retinoic Acid Downregulates Rae1 Leading to APCCdh1 Activation and Neuroblastoma SH-SY5Y Differentiation. *Oncogene* **2008**, *27* (23), 3339–3344. https://doi.org/10.1038/sj.onc.1210987.

(128) Sarkanen, J. R.; Nykky, J.; Siikanen, J.; Selinummi, J.; Ylikomi, T.; Jalonen, T. O. Cholesterol Supports the Retinoic Acid-Induced Synaptic Vesicle Formation in Differentiating Human SH-SY5Y Neuroblastoma Cells. *J. Neurochem.* **2007**, *102* (6), 1941–1952. https://doi.org/10.1111/j.1471-4159.2007.04676.x.

(129) Scott, I. G.; Åkerman, K. E. O.; Heikkilä, J. E.; Kaila, K.; Andersson, L. C. Development of a Neural Phenotype in Differentiating Ganglion Cell-derived Human Neuroblastoma Cells. *J. Cell. Physiol.* **1986**, *128* (2), 285–292. https://doi.org/10.1002/jcp.1041280221.

(130) Arisi, M. F.; Starker, R. A.; Addya, S.; Huang, Y.; Fernandez, S. V. All Trans-Retinoic Acid (ATRA) Induces Re-Differentiation of Early Transformed Breast Epithelial Cells. *Int. J. Oncol.* **2014**, *45* (6), 1831–1842. https://doi.org/10.3892/ijo.2014.2354.

(131) Adem, A.; Mattsson, M. E. K.; Nordberg, A.; Påhlman, S. Muscarinic Receptors in Human SH-SY5Y Neuroblastoma Cell Line: Regulation by Phorbol Ester and Retinoic Acid-Induced Differentiation. *Dev. Brain Res.* **1987**, *33* (2), 235–242. https://doi.org/10.1016/0165-3806(87)90156-8.

(132) Lotan, R. Retinoids in Cancer Chemoprevention. *FASEB J.* **1996**, *10* (9), 1031–1039. https://doi.org/10.1096/fasebj.10.9.8801164.

(133) López-Carballo, G.; Moreno, L.; Masiá, S.; Pérez, P.; Barettino, D. Activation of the Phosphatidylinositol 3-Kinase/Akt Signaling Pathway by Retinoic Acid Is Required for Neural Differentiation of SH-SY5Y Human Neuroblastoma Cells. *J. Biol. Chem.* **2002**, *277* (28), 25297–25304. https://doi.org/10.1074/jbc.M201869200.

(134) Lopes, F. M.; Schröder, R.; Júnior, M. L. C. da F.; Zanotto-Filho, A.; Müller, C. B.; Pires, A. S.; Meurer, R. T.; Colpo, G. D.; Gelain, D. P.; Kapczinski, F.; Moreira, J. C. F.; Fernandes, M. da C.; Klamt, F. Comparison between Proliferative and Neuron-like SH-SY5Y Cells as an in Vitro Model for Parkinson Disease Studies. *Brain Res.* **2010**, *1337*, 85–94. https://doi.org/10.1016/j.brainres.2010.03.102.

(135) Presgraves, S. P.; Ahmed, T.; Borwege, S.; Joyce, J. N. Terminally Differentiated SH-SY5Y Cells Provide a Model System for Studying Neuroprotective Effects of Dopamine Agonists. *Neurotox. Res.* **2003**, *5* (8), 579–598. https://doi.org/10.1007/BF03033178.

(136) Shipley, M. M.; Mangold, C. A.; Szpara, M. L. Differentiation of the SH-SY5Y Human Neuroblastoma Cell Line. *J. Vis. Exp.* **2016**, *2016* (108), 1–11. https://doi.org/10.3791/53193.

(137) Lauzon, M. A.; Drevelle, O.; Faucheux, N. Peptides Derived from the Knuckle Epitope of

BMP-9 Induce the Cholinergic Differentiation and Inactivate GSk3beta in Human SH-SY5Y Neuroblastoma Cells. *Sci. Rep.* **2017**, *7* (1), 1–14. https://doi.org/10.1038/s41598-017-04835-x.

(138) Jauhari, A.; Singh, T.; Pandey, A.; Singh, P.; Singh, N.; Srivastava, A. K.; Pant, A. B.; Parmar, D.; Yadav, S. Differentiation Induces Dramatic Changes in MiRNA Profile, Where Loss of Dicer Diverts Differentiating SH-SY5Y Cells Toward Senescence. *Mol. Neurobiol.* **2017**, *54* (7), 4986–4995. https://doi.org/10.1007/s12035-016-0042-9.

(139) Maurer, L. L.; Ryde, I. T.; Yang, X.; Meyer, J. N. Caenorhabditis Elegans as a Model for Toxic Effects of Nanoparticles: Lethality, Growth, and Reproduction. *Curr. Protoc. Toxicol.* **2015**, *66* (1), 20.10.1-20.10.25. https://doi.org/10.1002/0471140856.tx2010s66.

(140) Piechulek, A.; Berwanger, L. C.; von Mikecz, A. Silica Nanoparticles Disrupt OPT-2/PEP-2-Dependent Trafficking of Nutrient Peptides in the Intestinal Epithelium. *Nanotoxicology* **2019**, *13* (8), 1133–1148. https://doi.org/10.1080/17435390.2019.1643048.

(141) Maglioni, S.; Schiavi, A.; Melcher, M.; Brinkmann, V.; Luo, Z.; Laromaine, A.; Raimundo, N.; Meyer, J. N.; Distelmaier, F.; Ventura, N. Neuroligin-Mediated Neurodevelopmental Defects Are Induced by Mitochondrial Dysfunction and Prevented by Lutein in C. Elegans. *Nat. Commun.* **2022**, *13* (1). https://doi.org/10.1038/s41467-022-29972-4.

(142) Honnen, S. Caenorhabditis Elegans as a Powerful Alternative Model Organism to Promote Research in Genetic Toxicology and Biomedicine. *Arch. Toxicol.* **2017**, *91* (5), 2029–2044. https://doi.org/10.1007/s00204-017-1944-7.

(143) Chisholm, A. D.; Hutter, H.; Jin, Y.; Wadsworth, W. G. The Genetics of Axon Guidance and Axon Regeneration in Caenorhabditis Elegans. *Genetics* **2016**, *204* (3), 849–882. https://doi.org/10.1534/genetics.115.186262.

(144) Mccoll, G.; Roberts, B. R.; Pukala, T. L.; Kenche, V. B.; Roberts, C. M.; Link, C. D.; Ryan, T. M.; Masters, C. L.; Barnham, K. J.; Bush, A. I.; Cherny, R. A. Utility of an Improved Model of Amyloid-Beta (Aβ1-42) Toxicity in Caenorhabditis Elegans for Drug Screening for Alzheimer's Disease. *Mol. Neurodegener.* **2012**, *7* (1), 1–9. https://doi.org/10.1186/1750-1326-7-57.

(145) Fong, S.; Teo, E.; Ng, L. F.; Chen, C. B.; Lakshmanan, L. N.; Tsoi, S. Y.; Moore, P. K.; Inoue, T.; Halliwell, B.; Gruber, J. Energy Crisis Precedes Global Metabolic Failure in a Novel Caenorhabditis Elegans Alzheimer Disease Model. *Sci. Rep.* **2016**, *6* (September), 1–9. https://doi.org/10.1038/srep33781.

(146) Busch, M.; Bredeck, G.; Kämpfer, A. A. M.; Schins, R. P. F. Investigations of Acute Effects of Polystyrene and Polyvinyl Chloride Micro- and Nanoplastics in an Advanced in Vitro Triple Culture Model of the Healthy and Inflamed Intestine. *Environ. Res.* **2021**, *193* (November 2020). https://doi.org/10.1016/j.envres.2020.110536.

(147) Wahle, T.; Thal, D. R.; Sastre, M.; Rentmeister, A.; Bogdanovic, N.; Famulok, M.; Heneka, M. T.; Walter, J. GGA1 Is Expressed in the Human Brain and Affects the Generation of Amyloid β-Peptide. *J. Neurosci.* **2006**, *26* (49), 12838–12846. https://doi.org/10.1523/JNEUROSCI.1982-06.2006.

(148) Sherley, J. L.; Stadler, P. B.; Stadler, J. S. A Quantitative Method for the Analysis of Mammalian Cell Proliferation in Culture in Terms of Dividing and Non-dividing Cells. *Cell Prolif.* **1995**, *28* (3), 137–144. https://doi.org/10.1111/j.1365-2184.1995.tb00062.x.

(149) Kolling, J.; Tigges, J.; Hellack, B.; Albrecht, C.; Schins, R. P. F. Evaluation of the Nlrp3 Inflammasome Activating Effects of a Large Panel of Tio2 Nanomaterials in Macrophages. *Nanomaterials* **2020**, *10* (9), 1–18. https://doi.org/10.3390/nano10091876.

(150) Alboni, S.; Gibellini, L.; Montanari, C.; Benatti, C.; Benatti, S.; Tascedda, F.; Brunello, N.; Cossarizza, A.; Pariante, C. M. N-Acetyl-Cysteine Prevents Toxic Oxidative Effects Induced by IFN-α in Human Neurons. *Int. J. Neuropsychopharmacol.* **2013**, *16* (8), 1849–1865. https://doi.org/10.1017/S1461145713000266.

(151) Pool, M.; Thiemann, J.; Bar-Or, A.; Fournier, A. E. NeuriteTracer: A Novel ImageJ Plugin for Automated Quantification of Neurite Outgrowth. *J. Neurosci. Methods* **2008**, *168* (1), 134–139. https://doi.org/10.1016/j.jneumeth.2007.08.029.

(152) Maglioni, S.; Schiavi, A.; Runci, A.; Shaik, A.; Ventura, N. Mitochondrial Stress Extends Lifespan in C. Elegans through Neuronal Hormesis. *Exp. Gerontol.* **2014**, *56*, 89–98. https://doi.org/10.1016/j.exger.2014.03.026.

(153) *Caenorhabditis Genetics Center (CGC)*. https://cgc.umn.edu/ (accessed 2023-08-03).

(154) Mao, K.; Ji, F.; Breen, P.; Sewell, A.; Han, M.; Sadreyev, R.; Ruvkun, G. Mitochondrial Dysfunction in C. Elegans Activates Mitochondrial Relocalization and Nuclear Hormone Receptor-Dependent Detoxification Genes. *Cell Metab.* **2019**, *29* (5), 1182-1191.e4. https://doi.org/10.1016/j.cmet.2019.01.022.

(155) Stiernagle, T. *Maintenance of C. elegans*. WormBook. https://doi.org/10.1895/wormbook.1.101.1.

(156) Petrascheck, M.; Ye, X.; Buck, L. B. An Antidepressant That Extends Lifespan in Adult Caenorhabditis Elegans. *Nature* **2007**, *450* (7169), 553–556. https://doi.org/10.1038/nature05991.

(157) *MagnitudeBiosciences*. https://magnitudebiosciences.com/ (accessed 2023-04-01).

(158) Maynard, C.; Cummins, I.; Green, J.; Weinkove, D. A Bacterial Route for Folic Acid Supplementation. *BMC Biol.* **2018**, *16* (1), 1–10. https://doi.org/10.1186/s12915-018-0534-3.

(159) Piechulek, A.; von Mikecz, A. Life Span-Resolved Nanotoxicology Enables Identification of Age-Associated Neuromuscular Vulnerabilities in the Nematode Caenorhabditis Elegans. *Environ. Pollut.* **2018**, *233*, 1095–1103. https://doi.org/10.1016/j.envpol.2017.10.012.

(160) Scharf, A.; Limke, A.; Guehrs, K. H.; von Mikecz, A. Pollutants Corrupt Resilience Pathways of Aging in the Nematode C. Elegans. *iScience* **2022**, *25* (9), 105027. https://doi.org/10.1016/j.isci.2022.105027.

(161) Schiavi, A.; Runci, A.; Maiorino, T.; Naso, F. D.; Barenys, M.; Fritsche, E.; Strappazzon, F.; Ventura, N. Cobalt Chloride Has Beneficial Effects across Species through a Hormetic Mechanism. *Front. Cell Dev. Biol.* **2022**, *10* (October), 1–12. https://doi.org/10.3389/fcell.2022.986835.

(162) Chaudhari, S. N.; Kipreos, E. T. Increased Mitochondrial Fusion Allows the Survival of Older Animals in Diverse C. Elegans Longevity Pathways. *Nat. Commun.* **2017**, *8* (1). https://doi.org/10.1038/s41467-017-00274-4.

(163) Schindelin, J.; Arganda-Carreras, I.; Frise, E.; Kaynig, V.; Longair, M.; Pietzsch, T.; Preibisch, S.; Rueden, C.; Saalfeld, S.; Schmid, B.; Tinevez, J. Y.; White, D. J.; Hartenstein, V.; Eliceiri, K.; Tomancak, P.; Cardona, A. Fiji: An Open-Source Platform for Biological-Image Analysis. *Nat. Methods* **2012**, *9* (7), 676–682. https://doi.org/10.1038/nmeth.2019.

(164) Kropp, P. A.; Wu, J.; Reidy, M.; Shrestha, S.; Rhodehouse, K.; Rogers, P.; Sack, M. N.; Golden, A. Allele-Specific Mitochondrial Stress Induced by Multiple Mitochondrial Dysfunctions Syndrome 1 Pathogenic Mutations Modeled in Caenorhabditis Elegans. *PLoS Genet.* **2021**, *17* (8), 1–34. https://doi.org/10.1371/journal.pgen.1009771.

(165) Wählby, C.; Kamentsky, L.; Liu, Z. H.; Riklin-Raviv, T.; Conery, A. L.; O'Rourke, E. J.; Sokolnicki, K. L.; Visvikis, O.; Ljosa, V.; Irazoqui, J. E.; Golland, P.; Ruvkun, G.; Ausubel, F. M.; Carpenter, A. E. An Image Analysis Toolbox for High-Throughput C. Elegans Assays. *Nat. Methods* **2012**, *9* (7), 714–716. https://doi.org/10.1038/nmeth.1984.

(166) Mahoney, T. R.; Luo, S.; Nonet, M. L. Analysis of Synaptic Transmission in Caenorhabditis Elegans Using an Aldicarb-Sensitivity Assay. *Nat. Protoc.* **2006**, *1* (4), 1772–1777. https://doi.org/10.1038/nprot.2006.281.

(167) Han, S. K.; Lee, D.; Lee, H.; Kim, D.; Son, H. G.; Yang, J. S.; Lee, S. J. V.; Kim, S. OASIS 2: Online Application for Survival Analysis 2 with Features for the Analysis of Maximal Lifespan and Healthspan in Aging Research. *Oncotarget* **2016**, *7* (35), 56147–56152. https://doi.org/10.18632/oncotarget.11269.

(168) Yan, Y.; Gause, K. T.; Kamphuis, M. M. J.; Ang, C. S.; O'Brien-Simpson, N. M.; Lenzo, J. C.; Reynolds, E. C.; Nice, E. C.; Caruso, F. Differential Roles of the Protein Corona in the

Cellular Uptake of Nanoporous Polymer Particles by Monocyte and Macrophage Cell Lines. *ACS Nano* **2013**, *7* (12), 10960–10970. https://doi.org/10.1021/nn404481f.

(169) Gopinath, P. M.; Saranya, V.; Vijayakumar, S.; Mythili Meera, M.; Ruprekha, S.; Kunal, R.; Pranay, A.; Thomas, J.; Mukherjee, A.; Chandrasekaran, N. Assessment on Interactive Prospectives of Nanoplastics with Plasma Proteins and the Toxicological Impacts of Virgin, Coronated and Environmentally Released-Nanoplastics. *Sci. Rep.* **2019**, *9* (1), 1–15. https://doi.org/10.1038/s41598-019-45139-6.

(170) Sun, T.; Wu, Z.; Zhuo, Q.; Liu, X.; Wang, Z.; Fan, H. Microstructure and Mechanical Properties of Aminated Polystyrene Spheres/Epoxy Polymer Blends. *Compos. Part A Appl. Sci. Manuf.* **2014**, *66*, 58–64. https://doi.org/10.1016/j.compositesa.2014.06.015.

(171) Parmar Komal, R.; Satapara Vijay, P.; Shah Sunny, R.; Sheth Navin, R. Improvement of Dissolution Properties of Lamotrigine by Inclusion Complexation and Solid Dispersion Technique. *Pharmazie* **2011**, *66* (2), 119–123. https://doi.org/10.1691/ph.2011.0266.

(172) Covolan, V. L.; D'Antone, S.; Ruggeri, G.; Chiellini, E. Preparation of Aminated Polystyrene Latexes by Dispersion Polymerization. *Macromolecules* **2000**, *33* (18), 6685–6692. https://doi.org/10.1021/ma0000430.

(173) Qu, M.; Wang, D. Toxicity Comparison between Pristine and Sulfonate Modified Nanopolystyrene Particles in Affecting Locomotion Behavior, Sensory Perception, and Neuronal Development in Caenorhabditis Elegans. *Sci. Total Environ.* **2020**, *703*, 134817. https://doi.org/10.1016/j.scitotenv.2019.134817.

(174) Fayazfar, H.; Afshar, A.; Dolati, A. Controlled Growth of Well-Aligned Carbon Nanotubes, Electrochemical Modification and Electrodeposition of Multiple Shapes of Gold Nanostructures. *Mater. Sci. Appl.* **2013**, *04* (11), 667–678. https://doi.org/10.4236/msa.2013.411083.

(175) Xu, J.; Long, L.; Hu, H. Preparation of Starch-Based Styrene Acrylate Emulsion Used as Surface-Treatment Agent for Decorative Base Paper. *J. Polym. Eng.* **2013**, *33* (4), 323–330. https://doi.org/10.1515/polyeng-2012-0168.

(176) Michaki, V.; Guix, F. X.; Vennekens, K.; Munck, S.; Dingwall, C.; Davis, J. B.; Townsend, D. M.; Tew, K. D.; Feiguin, F.; Strooper, B. De; Dotti, C. G.; Wahle, T. Down-Regulation of the ATP-Binding Cassette Transporter 2 (Abca2) Reduces Amyloid- □ Production by Altering Nicastrin Maturation and Intracellular Localization *. *J. Biol. Chem.* **2012**, *287* (2), 1100–1111. https://doi.org/10.1074/jbc.M111.288258.

(177) Tominaga, H.; Ishiyama, M.; Ohseto, F.; Sasamoto, K.; Hamamoto, T.; Suzuki, K.; Watanabe, M. A Water-Soluble Tetrazolium Salt Useful for Colorimetric Cell Viability Assay. *Anal. Commun.* **1999**, *36* (2), 47–50. https://doi.org/10.1039/a809656b.

(178) Breijyeh, Z.; Karaman, R. Comprehensive Review on Alzheimer's Disease: Causes and Treatment. *Molecules* **2020**, *25* (24), 5789. https://doi.org/10.3390/molecules25245789.

(179) Belyaev, N. D.; Kellett, K. A. B.; Beckett, C.; Makova, N. Z.; Revett, T. J.; Nalivaeva, N. N.; Hooper, N. M.; Turner, A. J. The Transcriptionally Active Amyloid Precursor Protein (APP) Intracellular Domain Is Preferentially Produced from the 695 Isoform of APP in a β-Secretase-Dependent Pathway. *J. Biol. Chem.* **2010**, *285* (53), 41443–41454. https://doi.org/10.1074/jbc.M110.141390.

(180) Tait, J. F.; Gibson, D. Phospholipid Binding of Annexin V: Effects of Calcium and Membrane Phosphatidylserine Content. *Arch. Biochem. Biophys.* **1992**, *298* (1), 187–191. https://doi.org/10.1016/0003-9861(92)90111-9.

(181) Xiang, J.; Wan, C.; Guo, R.; Guo, D. Is Hydrogen Peroxide a Suitable Apoptosis Inducer for All Cell Types? *Biomed Res. Int.* **2016**, *2016*. https://doi.org/10.1155/2016/7343965.

(182) Moon, Y.; Kwon, Y.; Yu, S. How Does Ethanol Induce Apoptotic Cell Death of SK-N-SH Neuroblastoma Cells? *Neural Regen. Res.* **2013**, *8* (20), 1853–1862. https://doi.org/10.3969/j.issn.1673-5374.2013.20.004.

(183) López, E.; Ferrer, I. Staurosporine- and H-7-Induced Cell Death in SH-SY5Y Neuroblastoma Cells Is Associated with Caspase-2 and Caspase-3 Activation, but Not with Activation of the FAS/FAS-L-Caspase-8 Signaling Pathway. *Mol. Brain Res.* **2000**, *85*

(1–2), 61–67. https://doi.org/10.1016/S0169-328X(00)00235-7.

(184) Villalpando-Rodriguez, G. E.; Gibson, S. B. Reactive Oxygen Species (ROS) Regulates Different Types of Cell Death by Acting as a Rheostat. *Oxid. Med. Cell. Longev.* **2021**, *2021*. https://doi.org/10.1155/2021/9912436.

(185) Kim, H.; Xue, X. Detection of Total Reactive Oxygen Species in Adherent Cells by 2',7'-Dichlorodihydrofluorescein Diacetate Staining. *J. Vis. Exp.* **2020**, *2020* (160), 1–5. https://doi.org/10.3791/60682.

(186) Kim, G. H.; Kim, J. E.; Rhie, S. J.; Yoon, S. The Role of Oxidative Stress in Neurodegenerative Diseases. *Exp. Neurobiol.* **2015**, *24* (4), 325–340. https://doi.org/10.5607/en.2015.24.4.325.

(187) Polster, B. M.; Nicholls, D. G.; Ge, S. X.; Roelofs, B. A. Use of Potentiometric Fluorophores in the Measurement of Mitochondrial Reactive Oxygen Species. *Physiol. Behav.* **2014**, *176* (1), 225–250. https://doi.org/10.1016/B978-0-12-801415-8.00013-8.

(188) Robinson, K. M.; Janes, M. S.; Pehar, M.; Monette, J. S.; Ross, M. F.; Hagen, T. M.; Murphy, M. P.; Beckman, J. S. Selective Fluorescent Imaging of Superoxide in Vivo Using Ethidium-Based Probes. *Proc. Natl. Acad. Sci. U. S. A.* **2006**, *103* (41), 15038–15043. https://doi.org/10.1073/pnas.0601945103.

(189) Stanford, K. R.; Taylor-Clark, T. E. Mitochondrial Modulation-Induced Activation of Vagal Sensory Neuronal Subsets by Antimycin A, but Not CCCP or Rotenone, Correlates with Mitochondrial Superoxide Production. *PLoS One* **2018**, *13* (5), e0197106. https://doi.org/10.1371/journal.pone.0197106.

(190) Tang, Q.; Li, T.; Chen, K.; Deng, X.; Zhang, Q.; Tang, H.; Shi, Z.; Zhu, T.; Zhu, J. PS-NPs Induced Neurotoxic Effects in SHSY-5Y Cells via Autophagy Activation and Mitochondrial Dysfunction. *Brain Sci.* **2022**, *12* (7). https://doi.org/10.3390/brainsci12070952.

(191) Lopez-Suarez, L.; Awabdh, S. Al; Coumoul, X.; Chauvet, C. The SH-SY5Y Human Neuroblastoma Cell Line, a Relevant in Vitro Cell Model for Investigating Neurotoxicology in Human: Focus on Organic Pollutants. *Neurotoxicology* **2022**, *92* (February), 131–155. https://doi.org/10.1016/j.neuro.2022.07.008.

(192) Cheung, Y. T.; Lau, W. K. W.; Yu, M. S.; Lai, C. S. W.; Yeung, S. C.; So, K. F.; Chang, R. C. C. Effects of All-Trans-Retinoic Acid on Human SH-SY5Y Neuroblastoma as in Vitro Model in Neurotoxicity Research. *Neurotoxicology* **2009**, *30* (1), 127–135. https://doi.org/10.1016/j.neuro.2008.11.001.

(193) Lv, M.; Zhang, Y.; Liang, L.; Wei, M.; Hu, W.; Li, X.; Huang, Q. Effect of Graphene Oxide on Undifferentiated and Retinoic Acid-Differentiated SH-SY5Y Cells Line. *Nanoscale* **2012**, *4* (13), 3861–3866. https://doi.org/10.1039/c2nr30407d.

(194) Gibb, S. L.; Jeanblanc, J.; Barak, S.; Yowell, Q. V.; Yaka, R.; Ron, D. Lyn Kinase Regulates Mesolimbic Dopamine Release: Implication for Alcohol Reward. *J. Neurosci.* **2011**, *31* (6), 2180–2187. https://doi.org/10.1523/JNEUROSCI.5540-10.2011.

(195) Isgrò, M. A.; Bottoni, P.; Scatena, R. Neuron-Specific Enolase as a Biomarker: Biochemical and Clinical Aspects. *Adv. Exp. Med. Biol.* **2015**, *867*, 125–143. https://doi.org/10.1007/978-94-017-7215-0_9.

(196) Meyer, J. N.; Lord, C. A.; Yang, X. Y.; Turner, E. A.; Badireddy, A. R.; Marinakos, S. M.; Chilkoti, A.; Wiesner, M. R.; Auffan, M. Intracellular Uptake and Associated Toxicity of Silver Nanoparticles in Caenorhabditis Elegans. *Aquat. Toxicol.* **2010**, *100* (2), 140–150. https://doi.org/10.1016/j.aquatox.2010.07.016.

(197) Rea, S. L.; Ventura, N.; Johnson, T. E. Relationship between Mitochondrial Electron Transport Chain Dysfunction, Development, and Life Extension in Caenorhabditis Elegans. *PLoS Biol.* **2007**, *5* (10), 2312–2329. https://doi.org/10.1371/journal.pbio.0050259.

(198) Ventura, N.; Rea, S. L. Caenorhabditis Elegans Mitochondrial Mutants as an Investigative Tool to Study Human Neurodegenerative Diseases Associated with Mitochondrial Dysfunction. *Biotechnol. J.* **2007**, *2* (5), 584–595. https://doi.org/10.1002/biot.200600248.

(199) Ventura, N.; Rea, S. L.; Schiavi, A.; Torgovnick, A.; Testi, R.; Johnson, T. E. P53/CEP-1

Increases or Decreases Lifespan, Depending on Level of Mitochondrial Bioenergetic Stress. *Aging Cell* **2009**, *8* (4), 380–393. https://doi.org/10.1111/j.1474-9726.2009.00482.x.

(200) Liu, P.; Li, D.; Li, W.; Wang, D. Mitochondrial Unfolded Protein Response to Microgravity Stress in Nematode Caenorhabditis Elegans. *Sci. Rep.* **2019**, *9* (1), 1–9. https://doi.org/10.1038/s41598-019-53004-9.

(201) Cochemé, H. M.; Murphy, M. P. Complex I Is the Major Site of Mitochondrial Superoxide Production by Paraquat. *J. Biol. Chem.* **2008**, *283* (4), 1786–1798. https://doi.org/10.1074/jbc.M708597200.

(202) Tatjana, V.; Domitille, S.; Jean-Charles, S. Paraquat-Induced Cholesterol Biosynthesis Proteins Dysregulation in Human Brain Microvascular Endothelial Cells. *Sci. Rep.* **2021**, *11* (1), 1–10. https://doi.org/10.1038/s41598-021-97175-w.

(203) Heo, G.; Sun, M. H.; Jiang, W. J.; Li, X. H.; Lee, S. H.; Guo, J.; Zhou, D.; Cui, X. S. Rotenone Causes Mitochondrial Dysfunction and Prevents Maturation in Porcine Oocytes. *PLoS One* **2022**, *17* (11 November), 1–18. https://doi.org/10.1371/journal.pone.0277477.

(204) Nel, A. E.; Mädler, L.; Velegol, D.; Xia, T.; Hoek, E. M. V.; Somasundaran, P.; Klaessig, F.; Castranova, V.; Thompson, M. Understanding Biophysicochemical Interactions at the Nano-Bio Interface. *Nat. Mater.* **2009**, *8* (7), 543–557. https://doi.org/10.1038/nmat2442.

(205) Lundqvist, M.; Stigler, J.; Elia, G.; Lynch, I.; Cedervall, T.; Dawson, K. A. Nanoparticle Size and Surface Properties Determine the Protein Corona with Possible Implications for Biological Impacts. *Proc. Natl. Acad. Sci. U. S. A.* **2008**, *105* (38), 14265–14270. https://doi.org/10.1073/pnas.0805135105.

(206) Cedervall, T.; Lynch, I.; Lindman, S.; Berggård, T.; Thulin, E.; Nilsson, H.; Dawson, K. A.; Linse, S. Understanding the Nanoparticle-Protein Corona Using Methods to Quntify Exchange Rates and Affinities of Proteins for Nanoparticles. *Proc. Natl. Acad. Sci. U. S. A.* **2007**, *104* (7), 2050–2055. https://doi.org/10.1073/pnas.0608582104.

(207) Ruenraroengsak, P.; Tetley, T. D. Differential Bioreactivity of Neutral, Cationic and Anionic Polystyrene Nanoparticles with Cells from the Human Alveolar Compartment: Robust Response of Alveolar Type 1 Epithelial Cells. *Part. Fibre Toxicol.* **2015**, *12* (1), 1–20. https://doi.org/10.1186/s12989-015-0091-7.

(208) Shiomi, D.; Sakai, M.; Niki, H. Determination of Bacterial Rod Shape by a Novel Cytoskeletal Membrane Protein. *EMBO J.* **2008**, *27* (23), 3081–3091. https://doi.org/10.1038/emboj.2008.234.

(209) Danaei, M.; Dehghankhold, M.; Ataei, S.; Hasanzadeh Davarani, F.; Javanmard, R.; Dokhani, A.; Khorasani, S.; Mozafari, M. R. Impact of Particle Size and Polydispersity Index on the Clinical Applications of Lipidic Nanocarrier Systems. *Pharmaceutics* **2018**, *10* (2), 1–17. https://doi.org/10.3390/pharmaceutics10020057.

(210) Lesniak, A.; Kilinc, D.; Blasiak, A.; Galea, G.; Simpson, J. C.; Lee, G. U. Rapid Growth Cone Uptake and Dynein-Mediated Axonal Retrograde Transport of Negatively Charged Nanoparticles in Neurons Is Dependent on Size and Cell Type. *Small* **2019**, *15* (2), 1–10. https://doi.org/10.1002/smll.201803758.

(211) Anguissola, S.; Garry, D.; Salvati, A.; O'Brien, P. J.; Dawson, K. A. High Content Analysis Provides Mechanistic Insights on the Pathways of Toxicity Induced by Amine-Modified Polystyrene Nanoparticles. *PLoS One* **2014**, *9* (9). https://doi.org/10.1371/journal.pone.0108025.

(212) Ban, M.; Shimoda, R.; Chen, J. Investigation of Nanoplastic Cytotoxicity Using SH-SY5Y Human Neuroblastoma Cells and Polystyrene Nanoparticles. *Toxicol. Vitr.* **2021**, *76* (July), 105225. https://doi.org/10.1016/j.tiv.2021.105225.

(213) Waetzig, V.; Haeusgen, W.; Andres, C.; Frehse, S.; Reinecke, K.; Bruckmueller, H.; Boehm, R.; Herdegen, T.; Cascorbi, I. Retinoic Acid–Induced Survival Effects in SH-SY5Y Neuroblastoma Cells. *J. Cell. Biochem.* **2019**, *120* (4), 5974–5986. https://doi.org/10.1002/jcb.27885.

(214) Shang, Y.; Wang, S.; Jin, Y.; Xue, W.; Zhong, Y.; Wang, H.; An, J.; Li, H. Polystyrene

Nanoparticles Induced Neurodevelopmental Toxicity in Caenorhabditis Elegans through Regulation of Dpy-5 and Rol-6. *Ecotoxicol. Environ. Saf.* **2021**, *222*, 112523. https://doi.org/10.1016/j.ecoenv.2021.112523.

(215) Qu, M.; Qiu, Y.; Kong, Y.; Wang, D. Amino Modification Enhances Reproductive Toxicity of Nanopolystyrene on Gonad Development and Reproductive Capacity in Nematode Caenorhabditis Elegans. *Environ. Pollut.* **2019**, *254*, 112978. https://doi.org/10.1016/j.envpol.2019.112978.

(216) Qu, M.; Nida, A.; Kong, Y.; Du, H.; Xiao, G.; Wang, D. Nanopolystyrene at Predicted Environmental Concentration Enhances Microcystin-LR Toxicity by Inducing Intestinal Damage in Caenorhabditis Elegans. *Ecotoxicol. Environ. Saf.* **2019**, *183* (March), 109568. https://doi.org/10.1016/j.ecoenv.2019.109568.

(217) Nie, J. hui; Shen, Y.; Roshdy, M.; Cheng, X.; Wang, G.; Yang, X. Polystyrene Nanoplastics Exposure Caused Defective Neural Tube Morphogenesis through Caveolae-Mediated Endocytosis and Faulty Apoptosis. *Nanotoxicology* **2021**, *15* (7), 885–904. https://doi.org/10.1080/17435390.2021.1930228.

(218) Schirinzi, G. F.; Pérez-Pomeda, I.; Sanchís, J.; Rossini, C.; Farré, M.; Barceló, D. Cytotoxic Effects of Commonly Used Nanomaterials and Microplastics on Cerebral and Epithelial Human Cells. *Environ. Res.* **2017**, *159* (June), 579–587. https://doi.org/10.1016/j.envres.2017.08.043.

(219) Polysciences. *Polybead® Microspheres 0.05µm*. https://www.polysciences.com/default/polybead-microspheres-005956m (accessed 2023-06-01).

(220) Yacobi, N. R.; Malmstadt, N.; Fazlollahi, F.; DeMaio, L.; Marchelletta, R.; Hamm-Alvarez, S. F.; Borok, Z.; Kim, K. J.; Crandall, E. D. Mechanisms of Alveolar Epithelial Translocation of a Defined Population of Nanoparticles. *Am. J. Respir. Cell Mol. Biol.* **2010**, *42* (5), 604–614. https://doi.org/10.1165/rcmb.2009-0138OC.

(221) Jiang, X.; Musyanovych, A.; Röcker, C.; Landfester, K.; Mailänder, V.; Nienhaus, G. U. Specific Effects of Surface Carboxyl Groups on Anionic Polystyrene Particles in Their Interactions with Mesenchymal Stem Cells. *Nanoscale* **2011**, *3* (5), 2028–2035. https://doi.org/10.1039/c0nr00944j.

(222) Jiang, X.; Dausend, J.; Hafner, M.; Musyanovych, A.; Röcker, C.; Landfester, K.; Mailänder, V.; Nienhaus, G. U. Specific Effects of Surface Amines on Polystyrene Nanoparticles in Their Interactions with Mesenchymal Stem Cells. *Biomacromolecules* **2010**, *11* (3), 748–753. https://doi.org/10.1021/bm901348z.

(223) Walczak, A. P.; Kramer, E.; Hendriksen, P. J. M.; Tromp, P.; Helsper, J. P. F. G.; Van Der Zande, M.; Rietjens, I. M. C. M.; Bouwmeester, H. Translocation of Differently Sized and Charged Polystyrene Nanoparticles in in Vitro Intestinal Cell Models of Increasing Complexity. *Nanotoxicology* **2015**, *9* (4), 453–461. https://doi.org/10.3109/17435390.2014.944599.

(224) Leroueil, P. R.; Hong, S.; Mecke, A.; Baker, J. R.; Orr, B. G.; Banaszak Holl, M. M. Nanoparticle Interaction with Biological Membranes: Does Nanotechnology Present a Janus Face? *Acc. Chem. Res.* **2007**, *40* (5), 335–342. https://doi.org/10.1021/ar600012y.

(225) Hong, S.; Leroueil, P. R.; Janus, E. K.; Peters, J. L.; Kober, M. M.; Islam, M. T.; Orr, B. G.; Baker, J. R.; Banaszak Holl, M. M. Interaction of Polycationic Polymers with Supported Lipid Bilayers and Cells: Nanoscale Hole Formation and Enhanced Membrane Permeability. *Bioconjug. Chem.* **2006**, *17* (3), 728–734. https://doi.org/10.1021/bc060077y.

(226) Ruenraroengsak, P.; Novak, P.; Berhanu, D.; Thorley, A. J.; Valsami-jones, E.; Gorelik, J.; Korchev, Y. E.; Tetley, T. D. Respiratory Epithelial Cytotoxicity and Membrane Damage (Holes) Caused by Amine-Modi Fi Ed Nanoparticles. **2012**, *6* (February), 94–108. https://doi.org/10.3109/17435390.2011.558643.

(227) Mann, D. M.; Iwatsubo, T.; Ihara, Y.; Cairns, N. J.; Lantos, P. L.; Bogdanovic, N.; Lannfelt, L.; Winblad, B.; Maat-Schieman, M. L.; Rossor, M. N. Predominant Deposition of Amyloid-Beta 42(43) in Plaques in Cases of Alzheimer's Disease and Hereditary Cerebral Hemorrhage Associated with Mutations in the Amyloid Precursor Protein Gene. *Am. J.*

Pathol. **1996**, *148* (4), 1257–1266.

(228) Haque, A.; Polcyn, R.; Matzelle, D.; Banik, N. L. New Insights into the Role of Neuron-Specific Enolase in Neuro-Inflammation, Neurodegeneration, and Neuroprotection. *Brain Sci.* **2018**, *8* (2), 8020033. https://doi.org/10.3390/brainsci8020033.

(229) Yan, T.; Skaftnesmo, K. O.; Leiss, L.; Sleire, L.; Wang, J.; Li, X.; Enger, P. T. Neuronal Markers Are Expressed in Human Gliomas and NSE Knockdown Sensitizes Glioblastoma Cells to Radiotherapy and Temozolomide. *BMC Cancer* **2011**, *11*. https://doi.org/10.1186/1471-2407-11-524.

(230) Gudi, V.; Gai, L.; Herder, V.; Tejedor, L. S.; Kipp, M.; Amor, S.; Sühs, K. W.; Hansmann, F.; Beineke, A.; Baumgärtner, W.; Stangel, M.; Skripuletz, T. Synaptophysin Is a Reliable Marker for Axonal Damage. *J. Neuropathol. Exp. Neurol.* **2017**, *76* (2), 109–125. https://doi.org/10.1093/jnen/nlw114.

(231) Wiedenmann, B.; Franke, W. W.; Kuhn, C.; Moll, R.; Gould, V. E. Synaptophysin: A Marker Protein for Neuroendocrine Cells and Neoplasms. *Proc. Natl. Acad. Sci. U. S. A.* **1986**, *83* (10), 3500–3504. https://doi.org/10.1073/pnas.83.10.3500.

(232) Zhang, Z.; Yu, H.; Jiang, S.; Liao, J.; Lu, T.; Wang, L.; Zhang, D.; Yue, W. Evidence for Association of Cell Adhesion Molecules Pathway and NLGN1 Polymorphisms with Schizophrenia in Chinese Han Population. *PLoS One* **2015**, *10* (12), 1–16. https://doi.org/10.1371/journal.pone.0144719.

(233) Cuttler, K.; Hassan, M.; Carr, J.; Cloete, R.; Bardien, S. Emerging Evidence Implicating a Role for Neurexins in Neurodegenerative and Neuropsychiatric Disorders. *Open Biol.* **2021**, *11* (10). https://doi.org/10.1098/rsob.210091.

(234) Brown, M. K.; Luo, Y. Bilobalide Modulates Serotonin-Controlled Behaviors in the Nematode Caenorhabditis Elegans. *BMC Neurosci.* **2009**, *10*. https://doi.org/10.1186/1471-2202-10-62.

(235) Lei, K.; Qiao, F.; Liu, Q.; Wei, Z.; Qi, H.; Cui, S.; Yue, X.; Deng, Y.; An, L. Microplastics Releasing from Personal Care and Cosmetic Products in China. *Mar. Pollut. Bull.* **2017**, *123* (1–2), 122–126. https://doi.org/10.1016/j.marpolbul.2017.09.016.

(236) Patel, M. M.; Goyal, B. R.; Bhadada, S. V.; Bhatt, J. S.; Amin, A. F. Getting into the Brain: Approaches to Enhance Brain Drug Delivery. *CNS Drugs* **2009**, *23* (1), 35–58. https://doi.org/10.2165/0023210-200923010-00003.

(237) Campanale, C.; Massarelli, C.; Savino, I.; Locaputo, V.; Uricchio, V. F. A Detailed Review Study on Potential Effects of Microplastics and Additives of Concern on Human Health. *Int. J. Environ. Res. Public Health* **2020**, *17* (4). https://doi.org/10.3390/ijerph17041212.

(238) Magrì, D.; Sánchez-Moreno, P.; Caputo, G.; Gatto, F.; Veronesi, M.; Bardi, G.; Catelani, T.; Guarnieri, D.; Athanassiou, A.; Pompa, P. P.; Fragouli, D. Laser Ablation as a Versatile Tool to Mimic Polyethylene Terephthalate Nanoplastic Pollutants: Characterization and Toxicology Assessment. *ACS Nano* **2018**, *12* (8), 7690–7700. https://doi.org/10.1021/acsnano.8b01331.

(239) Chiu, H.; Xia, T.; Lee, Y.; Chen, C.; Tsai, J.; Wang, Y. Cationic Polystyrene Nanospheres Induce Autophagic Cell Death through the Induction of Endoplasmic Reticulum Stress †. **2014**. https://doi.org/10.1039/c4nr05509h.

(240) Koelmans, A. A.; Mohamed Nor, N. H.; Hermsen, E.; Kooi, M.; Mintenig, S. M.; De France, J. Microplastics in Freshwaters and Drinking Water: Critical Review and Assessment of Data Quality. *Water Res.* **2019**, *155*, 410–422. https://doi.org/10.1016/j.watres.2019.02.054.

(241) Song, Y. K.; Hong, S. H.; Jang, M.; Han, G. M.; Rani, M.; Lee, J.; Shim, W. J. A Comparison of Microscopic and Spectroscopic Identification Methods for Analysis of Microplastics in Environmental Samples. *Mar. Pollut. Bull.* **2015**, *93* (1–2), 202–209. https://doi.org/10.1016/j.marpolbul.2015.01.015.

(242) Tagg, A. S.; Sapp, M.; Harrison, J. P.; Ojeda, J. J. Identification and Quantification of Microplastics in Wastewater Using Focal Plane Array-Based Reflectance Micro-FT-IR Imaging. *Anal. Chem.* **2015**, *87* (12), 6032–6040.

https://doi.org/10.1021/acs.analchem.5b00495.

(243) Hernandez, L. M.; Xu, E. G.; Larsson, H. C. E.; Tahara, R.; Maisuria, V. B.; Tufenkji, N. Plastic Teabags Release Billions of Microparticles and Nanoparticles into Tea. *Environ. Sci. Technol.* **2019**, *53* (21), 12300–12310. https://doi.org/10.1021/acs.est.9b02540.

(244) Schymanski, D.; Goldbeck, C.; Humpf, H. U.; Fürst, P. Analysis of Microplastics in Water by Micro-Raman Spectroscopy: Release of Plastic Particles from Different Packaging into Mineral Water. *Water Res.* **2018**, *129*, 154–162. https://doi.org/10.1016/j.watres.2017.11.011.

(245) Qu, M.; Nida, A.; Kong, Y.; Du, H.; Xiao, G.; Wang, D. Nanopolystyrene at Predicted Environmental Concentration Enhances Microcystin-LR Toxicity by Inducing Intestinal Damage in Caenorhabditis Elegans. *Ecotoxicol. Environ. Saf.* **2019**, *183* (August), 109568. https://doi.org/10.1016/j.ecoenv.2019.109568.

(246) Lenz, R.; Enders, K.; Nielsen, T. G. Microplastic Exposure Studies Should Be Environmentally Realistic. *Proc. Natl. Acad. Sci. U. S. A.* **2016**, *113* (29), E4121–E4122. https://doi.org/10.1073/pnas.1606615113.

(247) Shao, H.; Han, Z.; Krasteva, N.; Wang, D. Identification of Signaling Cascade in the Insulin Signaling Pathway in Response to Nanopolystyrene Particles. *Nanotoxicology* **2019**, *13* (2), 174–188. https://doi.org/10.1080/17435390.2018.1530395.

(248) Cox, K. D.; Covernton, G. A.; Davies, H. L.; Dower, J. F.; Juanes, F.; Dudas, S. E. Erratum: Human Consumption of Microplastics (Environmental Science & Technology (2019) 53:12 (7068−7074) DOI: 10.1021/Acs.Est.9b01517). *Environ. Sci. Technol.* **2020**, *54* (17), 10974. https://doi.org/10.1021/acs.est.0c04032.

(249) WWF. *Revealed: plastic ingestion by people could be equating to a credit card a week*. https://wwf.panda.org/wwf_news/?348337/Revealed-plastic-ingestion-by-people-could-be-equating-to-a-credit-card-a-week (accessed 2022-01-26).

(250) ACS. *Methods for microplastics, nanoplastics and plastic monomer detection and reporting in human tissues*. https://www.acs.org/content/acs/en/pressroom/newsreleases/2020/august/micro-and-nanoplastics-detectable-in-human-tissues.html (accessed 2021-11-22).

8 Appendix

Chemicals and Detergents

Table S1. Chemicals and detergents used in this work

Material	Cat. Number	Manufacturer
Accutase®	00-4555-56	Thermo Scientific™
Aldicarb	33386	Merck
All-trans retinoic acid	R2625	Merck
Amersham™ ECL™ Prime Western Blotting Detection Reagent	RPN2232	Cytiva
Ammonium Persulfate	17874	Thermo Scientific™
Antimycin A (AMA)	A8674	Merck
Bovine Serum Albumin	BP9705	Thermo Scientific™
$CaCl_2 \cdot 2\ H_2O$	C-3881	Merck
citric acid monohydrate	C1909	Merck
cOmplete Protease Inhibitor Cocktail	11836170001	Merck
$CuSO_4 \cdot 5\ H_2O$	469130	Merck
Dimethyl sulfoxide	D2650-5	Merck
Disodium EDTA	8043.2	Roth
DL-dithiothreitol	646563	Merck
Dulbeccos modified Eagle Media/F12, GlutaMAX	31331093	Thermo Scientific™
FCS Gold	A11-151	PAA
$FeSO_4 \cdot 7\ H_2O$	450278	Merck
Fetal calf serum, heat inactivated	10082147	Thermo Scientific™
Fluoresbrite® YG Microspheres	17149-10	Polysciences
Geneticin (G418)	G1279	Merck
Glycine	T145.3	Roth
Hydrogen Peroxide	31642	Merck
Hypochlorite	9062.3	Roth
Laemmli sample buffer 4x	161-0747	BioRAD
Latex beads, amine modified polystyrene	L0780	Merck
L-glutamine	M11-004	PAA

MaxGel™ ECM	31331093	Merck
Methanol	4627.6	Roth
Milk powder	T145.3	Roth
$MnCL_2 \cdot 4\ H_2O$	M-3634	Merck
N-acetyl cysteine (NAC)	A0150000	Merck
PageRuler™ Prestained Protein Ladder, 10 to 180 kDa	26617	Thermo Scientific™
Penicillin-Streptomycin	P0781	Merck
Phosphatase Inhibitor Cocktail 2	P5726	Merck
Phosphate buffered saline	D8537	Merck
Pierce™ formaldehyde (w/v) solution	28908	Thermo Scientific™
Polybead® Microspheres 0.05 µm	08691-10	Polysciences
Polyvinylchloride		Werth-Metall
Protease Inhibitor Cocktail cOmplete	11836170001	Merck
PVDF membrane	10600100	Amersham
Resolving gel buffer	161-0798	BioRAD
Restore Western Blot Stripping Buffer	21059	Themo Scientific
RIPA buffer 10 x	20-188	Merck
Rotiphorese Gel30 37,5:1	3957.2	Roth
RPMI 1640	31870-025	Thermo Scientific™
Sodium chloride	3957.2	Roth
Sodium dodecyl sulfate	1156.1	Roth
Sodium dodecyl sulfate pellets	8029.3	Roth
Stacking gel buffer	161-0799	BioRAD
Streptomycin	21211	Cayman Chemical
Tetramethylethylene diamine	T9281	Merck
tri-potassium citrate	1049561000	Merck
Tris	4855.3	Roth
Tris-Glycine SDS running buffer	1610772	BioRAD
Triton X® 100	3051.3	Roth

Trypsin-EDTA solution 0.25%	P0781	Merck
Tween 20	P1379	Merck
$ZnSO_4 \cdot 7\ H_2O$	Z0251	Merck

Antibodies and dyes

Table S2. Unconjugated primary antibodies

Antibody	Cat. Number	Application	Dilution	Manufacturer
NSE (Neuron Specific enolase), monoclonal	MAB324	Western Blot	1:500	Merck
NSE (Neuron Specific enolase), monoclonal	MAB324	Immuno-fluorescence	1:200	Merck
βIIITUB (βIII Tubulin), monoclonal	T8578	Western Blot	1:2000	Thermo Scientific™
βIIITUB (βIII Tubulin), monoclonal	T8578	Immuno-fluorescence	1:500	Thermo Scientific™
SYN (Synaptophysin), monoclonal	ab8049	Immuno-fluorescence	1:50	Abcam
NLGN1 (Neuroligin 1), polyclonal	PA5-786548	Immuno-fluorescence	1:250	Thermo Scientific™
NLGN3 (Neuroligin 3), polyclonal	PA5-78508	Immuno-fluorescence	1:100	Thermo Scientific™
APP (Amyloid Precursor Protein, Amyloid β), polyclonal	25524-1AP	Immuno-fluorescence	1:100	Thermo Scientific™

Table S3. Conjugated secondary antibodies

Antibody	Cat. Number	Application	Dilution	Manufacturer
Mouse IgG HRP Linked	GENA931	Western Blot	1:15000	Merck
Goat anti-Rabbit IgG Alexa Fluor™ Plus 488	A11008	Immuno-fluorescence	1:10000	Thermo Scientific™
Goat anti-Mouse IgG Alexa Fluor™ Plus 594	A32742	Immuno-fluorescence	1:10000	Thermo Scientific™

Table S4. Dyes used in this work

Dye	Cat. Number	Manufacturer
4',6-diamidino-2-phenylindole, DAPI	MBD0015	Merck
Fluoroshield™ DAPI	F6057	Merck
H_2DCF-DA (2´,7´-Dichlorofluorescin diacetate)	287810	Merck
Hoechst 33342, trihydrochloride, Trihydrate	H3570	Thermo Scientific™
JC-1	T3168	Thermo Scientific™
MitoSOX™	M36008	Thermo Scientific™
Tetramethyl rhodamine ethyl ester (TMRE)	T669	Thermo Scientific™
Trypan blue solution	T8154	Merck

Kits

Table S5. Kits used for *in vitro* experiments

Kit	Cat. Number	Manufacturer
Amyloid ELISA Kit Wako Aβ 1 – 40	294-62501	Fujifilm
Amyloid ELISA Kit Wako Aβ 1 – 42	292-64501	Fujifilm
Annexin V-FITC Apoptosis Kit	K101-400	BioVision
BCA Protein Assay Kit	23227	Thermo Scientific™
Resazuirn salt (Cytotox Assay)	37017	Merck
WST-1 Reagent (Cytotox Assay)	11644807001	Merck

Devices and Equipment

Table S6. Devices and equipment used in this study

Equipment	Name	Manufacturer
Autoclave	VX-65	Systec
Blotter	novex® XCell Sure Lock System	Thermo Scientific™
Centrifuge	Mikro 200	Hettich
Centrifuge	Rotina 420R	Hettich
Centrifuge	Fresco 17, Centrifuge	Thermo Scientific™
Flow cytometer	FACSCanto(TM) II	BD Biosciences

Freezer (-20 °C)	economic	Bosch
Freezer (-80 °C)	HeraFreeze Basic	Thermo Scientific™
Fridge (+4 °C)	Liebherr Comfort	Liebherr
Gel cassettes	novex® Casettes 1.5 mm	Thermo Scientific™
Gel electrophoresis power supply	EV265	Consort
Gel electrophoresis tank	novex® XCell Sure Lock System	Thermo Scientific™
Heating block	Labnet	Labnet
Incubator	Hera cell 240	Thermo Scientific™
Incubator	Multitron	Infors HT
Laminar flow hood	MSC-Advantage	Thermo Scientific™
Magnetic stirrer	COMBIMAG RCH	IKA
Micro scale	TE124S	Sartorius
Microscope	Axio Vert A1	Zeiss
Microscope	DMi1	Leica
Microscope	120 KV JOEL 1210	JOEL
Microscope	Axio Imager M1	Zeiss
Pipette (2.5, 10, 20, 100, 1000 µL)	BioPette Plus	Labnet
Pipette (2.5, 10, 20, 100, 1000 µL)	Pipetman	Gilson
Pipette boy	Pipetus	Hirschmann Laborgeräte
Plate reader	Infinite® 200 PRO	Tecan
Plate reader	Multiskan™ GO	Thermo Scientific™
Scale	PC 440	Mettler Toledo
Sonifier	Sonorex Digitec	Bandelin
Spectrometer	FT/IR-4700	Jasco
Turbiscan	TURBISCAN LAB	Formulaction France
UV Light 0	UV 236	Waldmann
Vortexer	Grant-bio PV-1	Fisher Scientific
Water purification	Mili-Q Water Biocel	Merck Milipore
Zetasizer	Zetasizer Nano ZS	Malvern Instuments Ltd

Size measurement of OP50 bacteria (without particles)

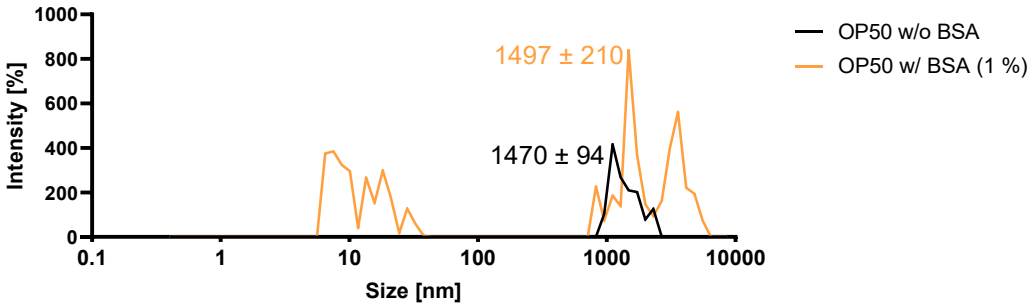

Figure S1 related to Figure 13. Physicochemical characterization of OP50 bacteria via DLS in *C. elegans* liquid culture conditions to identify the Z-Average and PDI. Data shows the average of three measurements per treatment (N=3) and mean Z-Average ± SEM.

Western Blot Raw Data

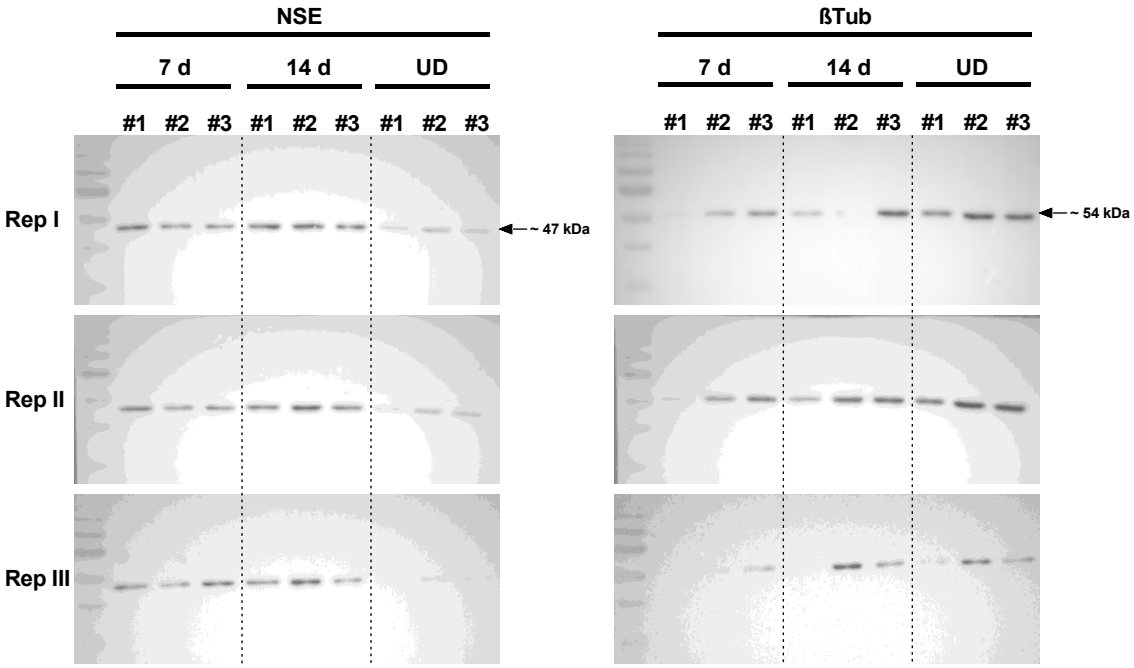

Figure S2 related to Figure 39. Differentiation of SH-SY5Y cells for 7 and 14 days with ATRA dissolved in EtOH. Three biological replicates (#1 - #3) were analyzed via western Blot in three technical replicates (Rep I - III), stained and analyzed with NSE prior stripping and staining with ß Tubulin. NSE is detected at ~ 47 kDa, ßTub is detected at ~ 54 kDa.

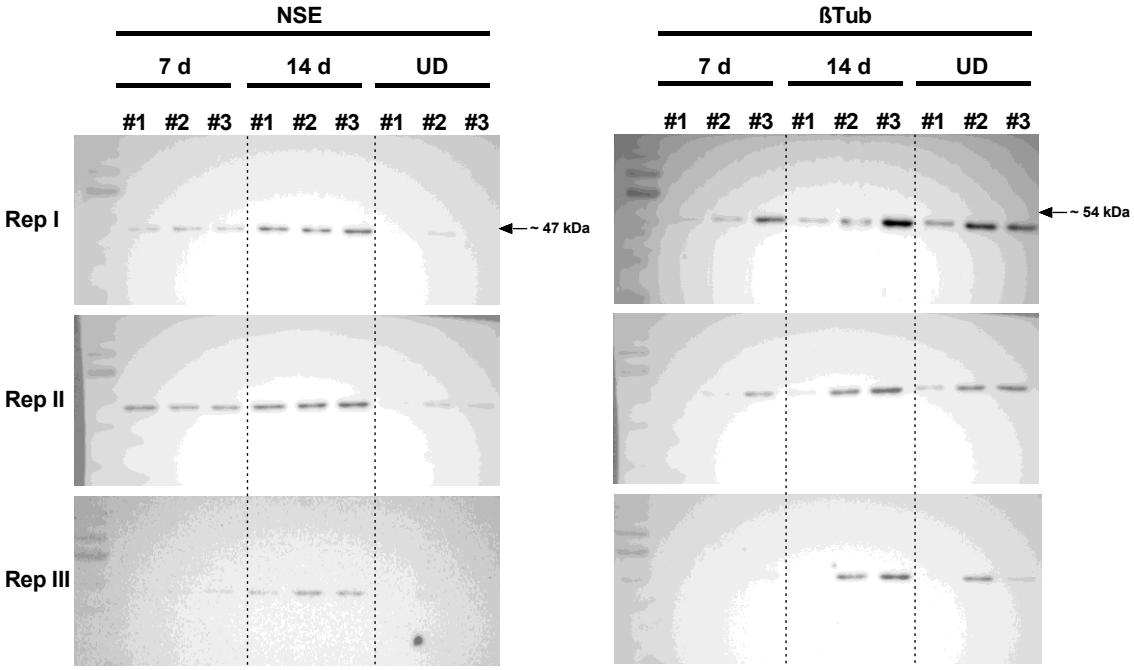

Figure S3 related to Figure 39. Differentiation of SH-SY5Y cells for 7 and 14 days with ATRA dissolved in DMSO. Three biological replicates (#1 - #3) were analyzed via western Blot in three technical replicates (Rep I - III), stained and analyzed with NSE prior stripping and staining with ß Tubulin. NSE is detected at ~ 47 kDa, ßTub is detected at ~ 54 kDa.

Script

Table S7 related to Figure 44. Code for analyzing immunofluorescence data

Application	Macro

Unpack data from different channels into single images	`dir = getDirectory("Select A folder");`
	`fileList = getFileList(dir);`
	`output_dir = dir + File.separator + "output" + File.separator ;`
	`File.makeDirectory(output_dir);`
	
	`setBatchMode(true);`
	
	`// LOOP to process the list of files`
	`for (i = 0; i < lengthOf(fileList); i++) {`
	`  current_imagePath = dir+fileList[i];`
	`  if (!File.isDirectory(current_imagePath)){`
	`  s = "open=["+current_imagePath+"] autoscale color_mode=Grayscale rois_import=[ROI manager] view=Hyperstack stack_order=XYCZT";`
	`run("Bio-Formats Importer", s);`
	
	`  // get some info about the image`
	`  getDimensions(width, height, channels, slices, frames);`
	`  if ((channels > 1)||( bitDepth() == 24 )) run("Split Channels");`
	
	`  // saving as png`
	`  ch_nbr = nImages ;`
	`  for ( c = 1 ; c <= ch_nbr ; c++){`
	`  selectImage(c);`
	`  currentImage_name = getTitle();`
	`  saveAs("png", output_dir+currentImage_name);`
	`  }`
	`  // make sure to close every images before opening the next one`
	`  run("Close All");`
	`  }`
	`}`
	`setBatchMode(false);`

Counting of nuclei	`//Fiji setup`
	`run("Options...", "iterations=1 count=1 black do=Nothing");`
	`run("Set Measurements...", "area mean standard centroid perimeter bounding fit shape feret's integrated median area_fraction display redirect=None decimal=3");`
	
	`//image preperation`
	`original_image=getTitle();`
	`input_dir = getDirectory("image");`
	
	`//pre-processing`
	`run("Unsharp Mask...", "radius=10 mask=0.90");`
	`setOption("ScaleConversions", true);`
	`run("8-bit");`
	`run("Auto Threshold", "method=Huang2 white");`
	`run("Adjustable Watershed", "tolerance=1");`
	`//nuclei analysis`

```
run("Analyze Particles...", "size=100-Infinity show=Outlines
display exclude summarize");

Table.save(input_dir + "Results.tsv", "Results");
Table.save(input_dir + "Results.tsv", "Summary");
```

Comparison of particle concentrations used in vitro and in vivo

Table S8. Treatment concentrations of particles in "*in vitro* concentrations" (µg cm^{-2}) used for *in vivo* (µg mL^{-1}). Frequently used concentrations *in vitro* are 1, 10, 50 and 100 µg mL^{-1}.

Experiment	Well	Surface area [cm^2]	Volume [µL]	"*in vitro* concentration" [µg cm^{-2}]	"*in vivo* concentration" [µg mL^{-1}]	Particles in total [µg]
Cell viability assay	96	0.32	100	1	3.2	0.32
				5	16	1.6
				10	32	3.2
				50	160	16
Cell viability assay	6	9.6	2000	1	4.8	9.6
				5	24	48
				10	48	96
				50	240	480
ELISA Aβ	6	9.6	2000	0.5	2.4	4.8
				1	4.8	9.6
				5	24	48
Neurite Outgrowth Assay	6	9.6	2000	0.1	0.48	0.96
				0.5	2.4	4.8
				1	4.8	9.6
				2	9.6	19.2
				5	24	48
Immuno-fluores-cence	glass slide with chambers	0.7	200	0.25	0.875	0.175
				0.5	1.75	0.35
				1	3.5	0.7

Flow cytometry	24	1.9	500	5	19	9.5
				10	38	19
				25	95	47.5

Lifespan Statistics

Table S9 related to Figure 49. Lifespan summary statistics of PS and PS-NH2 treatment.

condition	Mean lifespan ± SE (Days)	P value vs control	Sample size / N trials
Control	27.09 ± 0.43		229 / 3
PS 1 µg ml^{-1}	26.34 ± 0.47	1	225 / 3
PS 10 µg mL^{-1}	26.85 ± 0.45	1	219 / 3
PS 100 µg mL^{-1}	25.50 ± 0.46	0.011	234 / 3
PS-NH2 1 µg mL^{-1}	26.30 ± 0.47	0.824	245 / 3
PS-NH2 10 µg mL^{-1}	26.38 ± 0.52	0.5476	230 / 3
PS-NH2 50 µg mL^{-1}	23.34 ± 0.48	< 0.0001	244 / 3
PS-NH2 100 µg mL^{-1}	21.86 ± 0.45	< 0.0001	221 / 3

Eidesstattliche Erklärung

Ich versichere an Eides Statt, dass die Dissertation von mir selbständig und ohne unzulässige fremde Hilfe unter Beachtung der „Grundsätze zur Sicherung guter wissenschaftlicher Praxis an der Heinrich-Heine-Universität Düsseldorf“ erstellt worden ist.

Düsseldorf, …….

(Laura Schröter)